Investigations on the Pincer-Ruthenium and Pincer-Nickel Catalyzed Organic Transformations

A Dissertation

Submitted in partial fulfilment for the degree of

Doctor of Philosophy

by

Moumita Dutta
(Roll No: 156122031)

Thesis Supervisor: Dr. Akshai Kumar A S

Department of Chemistry
Indian Institute of Technology Guwahati
Guwahati-781039, Assam, INDIA

September 2020

Dedicated To My Parents

~Acknowledgements~

I would like to appreciate all the people around me who have assisted and guided me throughout my academic journey. Without their contributions, this thesis would not have been a reality.

First of all, I would like to express my sincere gratitude to my supervisor **Dr. Akshai Kumar A S** for his constant guidance, support and insightful advises throughout my research work. I am deeply indebted to him for inspiring me towards scientific research and also thankful for giving me the opportunity to work under his guidance.

I would also like to thank Dr. Hemant Kumar Srivastava for his inspiration and the constant guidance during my research period. I would like to acknowledge my doctoral committee members Prof. Bhisma Kumar Patel (Chairman), Prof. Gopal Das, Prof. A S Achalkumar for their valuable suggestions and encouragement which helped a lot to improve my thesis.

I am thankful to IIT Guwahati for the fellowship and also thankful to IIT Guwahati, Department of Chemistry and Central Instruments Facilities (CIF) for providing research and instrumental facilities. I will always remain thankful to the staff members of CIF and the department of chemistry.

My deepest gratitude to my dear lab mates Kanu Das, Khadimul Islam, Pran Gobinda Nandi, Vinay Arora, Himani Narjinari, and Eileen Yasmin for their great support during my Ph.D. period. Their constant help definitely smoothened this journey. I sincerely thank the project students for their contribution to my works.

I would also like to thank my BSc. and MSc. friends. I would like to thank all my Ph.D. batchmates, seniors and juniors who helped me during my work and for creating a friendly environment during my stay at IITG.

Finally, my Ph.D. endeavor could not have been completed without the endless love, support and blessings from my parents. I thank them for their faith in me, which has always been a constant source of motivation. I am always thankful to the almighty God for everything in my life.

Sincerely,
Moumita Dutta

INDIAN INSTITUTE OF TECHNOLOGY GUWAHATI

Department of Chemistry

STATEMENT

I hereby declare that the research work embodied in the thesis entitled "***Investigations on the Pincer-Ruthenium and Pincer-Nickel Catalyzed Organic Transformations***" is the outcome of the investigations carried out by me in the Department of Chemistry, Indian Institute of Technology Guwahati, India, under the supervision of **Dr. Akshai Kumar A S**, for the award of the degree of Doctor of Philosophy and it has not been submitted elsewhere for the award of any degree or diploma.

In harmony with the general practice in reporting the scientific observations, due acknowledgments have been made whenever the work described is based on the findings of other investigators.

Moumita Dutta.

Guwahati

September 2020

29/9/2020

Moumita Dutta

Roll No: 156122031

Department of Chemistry,.

IIT Guwahati, Assam,

India-781039

भारतीय प्रौद्योगिकी संस्थान गुवाहाटी
Indian Institute of Technology Guwahati

Dr. Akshai Kumar Alape Seetharam
Assistant Professor, Department of Chemistry, Guwahati – 781039, Assam, INDIA
Tel: +91-3612583479 (O), Mobile: +91-8133036890, Fax: +91-3612582349
Email: akshaikumar@iitg.ac.in, akshaikumara@gmail.com

CERTIFICATE

I hereby certify that the entire work embodied in the thesis entitled "***Investigations on the Pincer-Ruthenium and Pincer-Nickel Catalyzed Organic Transformations***" is the result of investigations carried out by **Ms. Moumita Dutta** (Roll No: 156122031) at the Department of Chemistry, Indian Institute of Technology Guwahati, India under my guidance and the same has not been submitted elsewhere for the award of any degree or diploma.

Guwahati

29 September, 2020

Dr. Akshai Kumar A. S.

Supervisor

CONTENTS

CONTENTS

Abstract

The contents of the present thesis entitled "***Investigations on the Pincer-Ruthenium and Pincer-Nickel Catalyzed Organic Transformations***" have been divided into five chapters based on the results achieved from the experimental and computational work carried out during the entire course of the PhD research programme.

Chapter 1 contains a brief introduction and the literature review on the chemistry of pincer-metal complexes and their versatile applications in catalytic organic transformations. The chapter winds up with a discussion on the scope of the current thesis.

Chapter 2 demonstrates an efficient and atom-economical Kharasch addition of CCl_4 to styrene that is catalyzed by a series of pincer-ruthenium complexes (^{R2}NNN)$RuCl_2(PPh_3)$ (R = Cy, ^{t}Bu, ^{i}Pr, and Ph). Gratifyingly, very high turnovers (ca. 5670) have been observed for the (^{Cy2}NNN)$RuCl_2(PPh_3)$ catalyzed Kharasch addition of CCl_4 to styrene. The reaction has also been probed to obtain a detailed mechanistic understanding.

Chapter 3 sheds light on the utility of NNN pincer-ruthenium complexes based on sterically less hindered 2,6-*bis*(benzimidazole-2-yl) pyridine ligands in catalyzing high yield (92%) transformation of glycerol selectively (98%) to lactic acid. Systematic mechanistic studies provide a clear understanding to the role of Ru–P bond and steric crowding around the Ru centre in favoring catalysis.

Chapter 4 illustrates the application of a new and well-defined pincer-nickel complex (^{iPr2}NNN)$NiCl_2(NCCH_3)$ for catalytic *N*-alkylation that proceeds with very high turnovers (34000 TONs). Detailed insight on the operative mechanism points to the involvement of both hydrogenation and alcoholysis steps in the *N*-alkylation reaction. The (^{iPr2}NNN)$NiCl_2(NCCH_3)$ catalyzed reactions have been extended to the dehydrogenative coupling of benzene-1,2-diamines with alcohols to yield the corresponding benzimidazoles.

Chapter 5 reports a computational study on cyanomethylation reaction. Here the energetics of the cyanomethylation catalytic cycle for a series of ten pincer-nickel systems with varying electronic demands have been compared with the corresponding Miller's catalyst (^{iPr2}POCCN^{Et2})NiO^tBu that is reported to be active at room temperature. The study culminates with the identification of imine based pincers with C central atom as potential contenders for the Miller's catalyst. Presence of strong σ-donors in the flanking groups and weak *trans* influencing pincer central atoms were found to lead to unfavorable energetics in the cyanomethylation catalysis.

Chapter 1

Introduction to the Chemistry of Pincer Complexes

1.1 Organometallic complex

Organometallic compounds have at least one bond between a metal and carbon atom which is part of an organic framework and very often, they are highly covalent in nature. Compounds having CO and CN^- ligands, though not derived from organic frameworks, qualify as organometallic. Also, complexes based on phosphines (PR_3; R=H, alkyl) and metal hydrides, though lacking the pre-defined metal-carbon bond, exhibit properties so similar to that of organometallic compounds, that these can be included in the same category. Some of the early organometallic compounds that have found extensive utility include tetraethyllead (antiknock reagent for gasoline) and Grignard reagents. One of the first organometallic compounds was reported by William Zeise in 1827. Zeise's salt $K[PtCl_3(C_2H_4)].H_2O$ was prepared by the reaction between ethanol and platinum(II) chloride.[1] In the mid-1800s Edward C. Frankland synthesized a variety of air-sensitive metal alkyl complexes such as $ZnEt_2$ (1849), $HgEt_2$ (1852) and $SnEt_4$ (1860). In the history of organometallic complexes, the first binary metal carbonyl complex was reported in 1890 by Ludwig Mond.[2] He prepared tetrahedral complex $Ni(CO)_4$, by direct reaction of nickel metal with CO. A year later (1891), Mond and Barthelot synthesized $Fe(CO)_5$.[3] In 1899, Victor Grignard provided a protocol for the generation of Grignard reagent (RMgX) by the reaction of magnesium with organic halides RX (R= alkyl and X= halogen). This discovery is believed to have brought about a renaissance in synthetic organic chemistry as it paved the way for a plethora of valuable reactions of carbonyl compounds with alkyl/aryl halides that were mediated by magnesium. In 1938, Roelen demonstrated the use of $Co_2(CO)_8$ in catalytic oxo process for the hydroformylation of olefin by CO and H_2.[4] Later Karl Ziegler[5] and Giulio Natta[6] independently discovered a catalytic system based on early transition metals such as Ti, Zr or Hf in combination with organoaluminium compounds to polymerize α-olefin with high regio- and stereo-selectivity. Owing to the versatile applications that were offered by the Ziegler Natta catalyst ($Et_3Al+TiCl_4$), Ziegler and Natta were awarded the Nobel Prize in 1963. In 1951, the discovery of first sandwich compound ferrocene exposed a new area of research and numerous cyclopentadienyl derivative of various metal and metalloids have been reported since then. Organometallic chemistry has seen rapid development in the decades that followed and have significantly influenced several branches of chemistry that includes but not limited to organic chemistry, catalysis, bio-inorganic chemistry, medicinal chemistry and bio-organometallic chemistry. In 2001 W. S. Knowles, R. Noyori, and Karl Barry Sharpless received the Nobel Prize in chemistry for transition metal catalyzed asymmetric

hydrogenation. In 2005, Robert H. Grubbs, Yves Chauvin and Richard R. Schrock were awarded the Nobel Prize in chemistry for metal catalyzed alkene metathesis. Richard F. Heck, Ei-ichi Negishi, Akira Suzuki won the Nobel Prize for Pd catalyzed cross coupling reactions in 2010.

The transition metal elements typically have incomplete *d*-orbitals. These transition metal elements have a tendency to achieve stability with the electrons given or shared by ligands. In an organometallic complex, the electrons provided by the ligands permit the metal to achieve the 18-electron stable electronic configuration. A ligand is an ion or a neutral molecule that usually donates electrons to the metal to form a coordination complex. According to the number of donating atoms, ligands are categorized as monodentate, bidentate, tridentate, and so on. Monodentate ligands have only one site coordinated to a metal, and only one pair of electrons is capable of binding to the central atom or ion. H^-, F^-, Cl^-, I^-, H_2O, NH_3 are some examples of monodentate ligands. Bidentate ligands such as ethane 1, 2-diamine have two ligating atoms and tridenatate ligands have three ligating atoms e.g. diethylenetriamine, which has three lone pairs of electrons that can be donated to a metal centre. Ligands that can bind as bidentate, tridentate or polydentate are called chelating ligands. Typically monodentate ligands lead to less stable complexes than bidentate ligands which in turn form less stable complexes than tridentate ligands and so on. However, the stability comes at the cost of reactivity and it has been widely observed that tridentate pincer ligands form complexes with optimal stability and reactivity.[7]

A pincer ligand is a chelating agent that grasps mainly a transition metal tightly via three adjacent ligating atoms in a meridional configuration.[8] While the first report on such tridentate ligands came by pioneering work of Moulton and Shaw in 1976,[9] the term "Pincer" for these type of tridentate ligands was coined by van-Koten in 1989.[10] Prototypical pincer ligands can either have an aryl ring σ-bonded to a given metal or metalloid (M) or could involve chains or rings incorporating donor atoms flanking the C–M bond.[11] Regardless of the type, the pincer framework imparts sufficient stability to the metal complex. The high thermal stability can be mainly attributed to the inflexibility of the pincer-metal interaction. As a result, most of these complexes have proven to be successful in accomplishing highly endothermic reaction such as alkane dehydrogenation.[12-14] Pincer ligands based on aryl backbone could either be anionic with a carbanion as the central donor site or could have neutral donor atoms (Figure 1.1).[12-14] The modular nature of pincer ligands

allows the electronic and steric properties of the complex to be fine-tuned without significant modification of the coordination geometry.

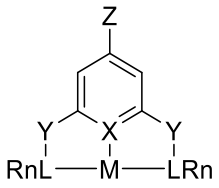

Typical groups

X = C, N, B (Electronic tuning, *trans* influence in particular)

Y= $(CH_2)_n$, O, NH (Indirct steric control and better control of eletron density)

L= P, N, O (Hard/soft variability, lability, steric and electronic control)

Z= Halogen, -OMe, -NMe_2, -CO_2Me (Solubilty and electronic control, ability to heterogenize)

R= ^{t}Bu,^{i}Pr, Et, Me, Ph, Cy (steric and electronic control)

Figure 1.1: Representation of a pincer metal complex depicting the variable parameters for steric and electronic control.

1.2 Types of pincer ligands

1.2.1 ECE (E = N, P) and ENE (E = C, S, Se, P) type pincers

Most of the tridentate pincer ligand systems are planar frameworks consisting of an anionic or neutral atom in the central aromatic backbone attached with flanking two-electron donor substituents. For instance, the terdentate η^3-"ECE" type of pincer complexes contains a central aryl anionic carbon which binds to the metal centre via one metal-carbon σ-bond and the ortho substituents bearing sidearm 'E' that bind via the coordinate bond. In this "ECE" type of pincer complex, 'E' represents neutral two-electron donors such as -PR_2, -SR or -NR_2, which leads to the formation of PCP, SCS or NCN type of pincer systems respectively (Figure 1.2). In 1976 Moulton and Shaw reported the first tridentate chelating system, 2,6-*bis*[(di-*t*-butylphosphino)methyl]phenyl (PCP)H and made it to react with salts of Ni, Pd and Pt to generate the corresponding PCP metal-pincer complexes **1.7** (Figure 1.4). In general, most of the reported pincer systems are co-planar with the metal center, due to the presence of the aromatic backbone in their structure.[15]

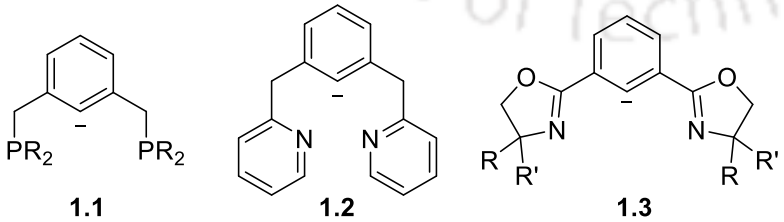

Figure 1.2: PCP and NCN type of pincer ligands.[7]

On the other hand, the "ENE" pincers have a central nitrogen donor atom, with donor atom E on the side arm, which can either be N,[16]C,[17] S,[18] Se[19] or P[20] (Figure 1.3).

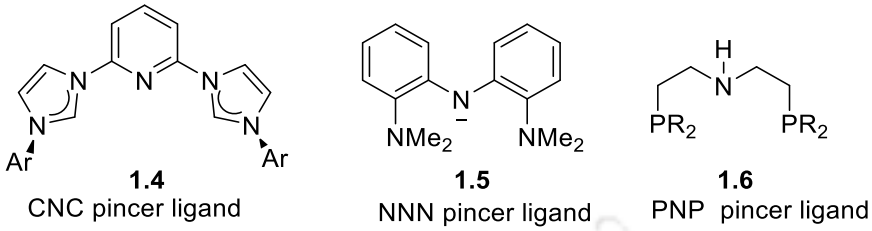

1.4 CNC pincer ligand **1.5** NNN pincer ligand **1.6** PNP pincer ligand

Figure 1.3: Examples of architecture of CNC,[21] NNN[7] and PNP[7] pincer ligands

In tridentate CNC type pincer ligands, there are two M-C σ- bonds, whereas in case of NCN type variation one M-C σ-bond is present. Due to the strong M-C σ-bond, it possesses enhanced stability, thus avoiding dissociation of the metal from the ligand that leads to decomposition of the complex. The donor atoms and their corresponding substituents allow the fine tuning of the steric and electronic properties.

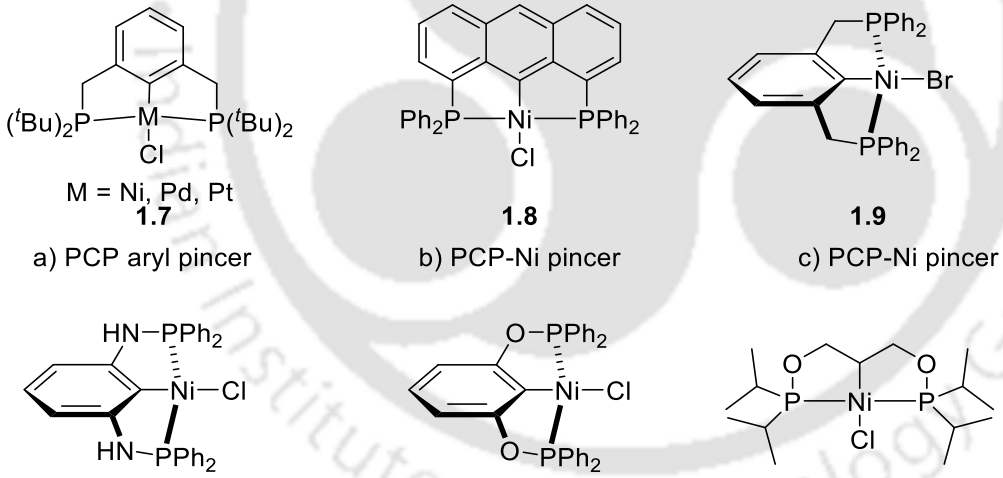

1.7 a) PCP aryl pincer **1.8** b) PCP-Ni pincer **1.9** c) PCP-Ni pincer

1.10 d) PNCNP-Ni pincer **1.11** e) POCOP-Ni pincer **1.12** f) POCOP-Ni pincer

Figure 1.4: Various reports of pincer systems. a) PCP aryl pincer (**1.7**),[22] b) PCP anthraphos Ni complex by Betz (**1.8**),[23] c) PCP pincer-Ni complex by Bubnov (**1.9**),[24] d) PNCNP pincer-Ni complex (**1.10**),[25] e) POCOP pincer-Ni complex (**1.11**) by Morales-Morales,[26] f) POCOP pincer-Ni complex (**1.12**) by Zargarian.[27]

Phosphorous has ability to stabilize the metal centres in both high and low oxidation state. It has been observed that, phosphorous when attached to metal in low oxidation states, exhibits strong

nucleophilicity and reducing character. However, it also requires bulky groups to achieve air stability.[28] Phosphinito PCP pincer ligands with oxygen spacers are commonly represented as POCOP type pincer ligands (Figure 1.4; **1.11** and **1.12**).[26]

Sulfur donor atoms can act as σ-donor, π-acceptor and even π-donor ligands. They have been used to tune the electronic properties of numerous metal centers due to their ability to accommodate both hard and soft auxiliary ligands and metal centers.[29] In general, selenium shows some similarity in its chemistry with sulfur, however, selenium containing compounds are reported to a lesser range than its sulfur counterpart.[28] Figure 1.5 depicts a variety of pincer-metal complexes having symmetrical donor atoms.

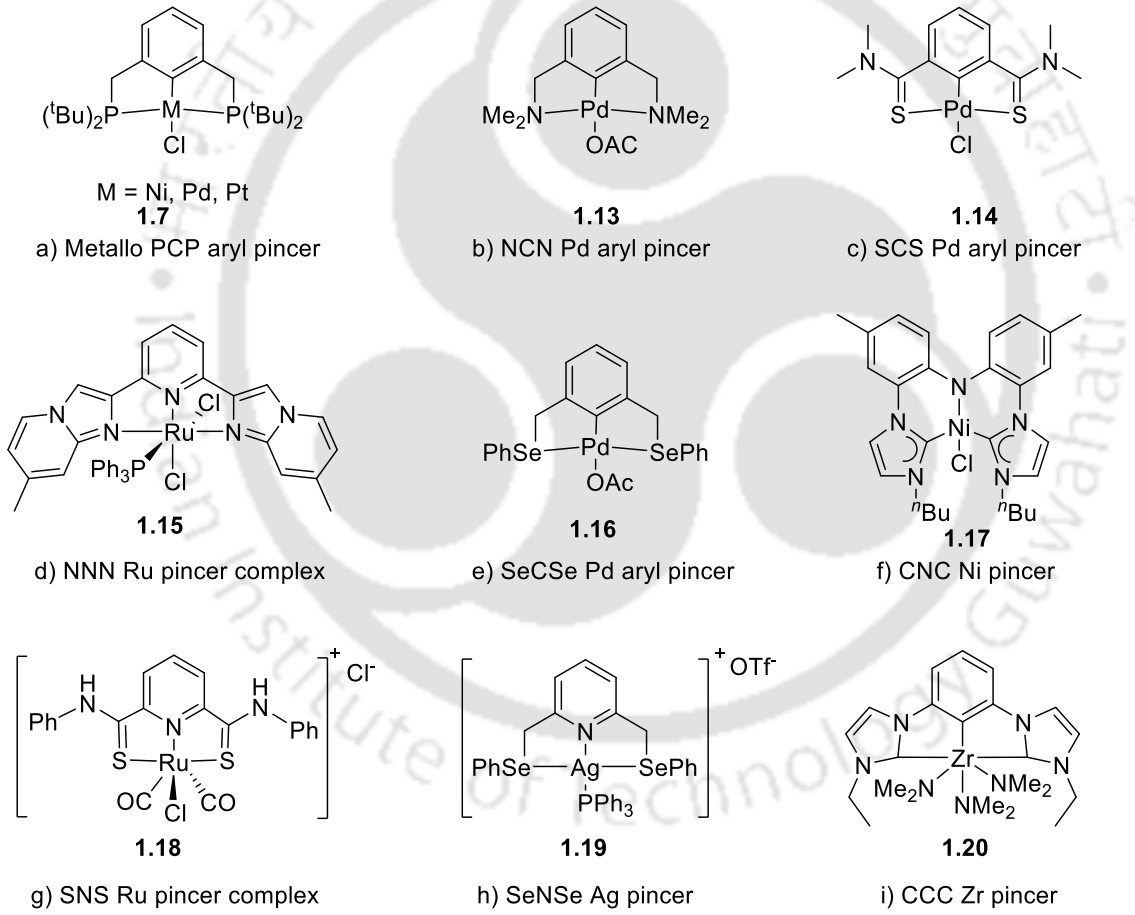

Figure 1.5: Examples of symmetrical pincer complexes. a) PCP aryl pincer (**1.7**),[22] b) NCN pincer-Pd (**1.13**),[30] c) SCS pincer-Pd complex (**1.14**),[31]d) NNN pincer-Ru complex (**1.15**),[32] e) SeCSe pincer-Pd complex (**1.16**),[33] f) CNC pincer-Ni complex (**1.17**),[34] g) SNS pincer-Ru complex (**1.18**),[35] h) SeNSe pincer-Ag complex (**1.19**),[36] i) CCC pincer-Zr complex (**1.20**).[37]

1.2.2 PCN and YNX (Y = C, N or O; X = N, O or S) pincer systems

Apart from the well-known symmetrical pincer systems that include NCN, CNC, PCP, PNP, NNN, SNS and SCS, asymmetric types of pincer ligands also exist. In the asymmetric type of pincer ligand systems, different or combinations of at least two of the donor atoms are present (Figure 1.6). This non-symmetric approach involving hemi-labile ligands might be beneficial as one of the weakly coordinating moiety can dissociate easily and create a vacant co-ordination site to promote catalysis.[38]

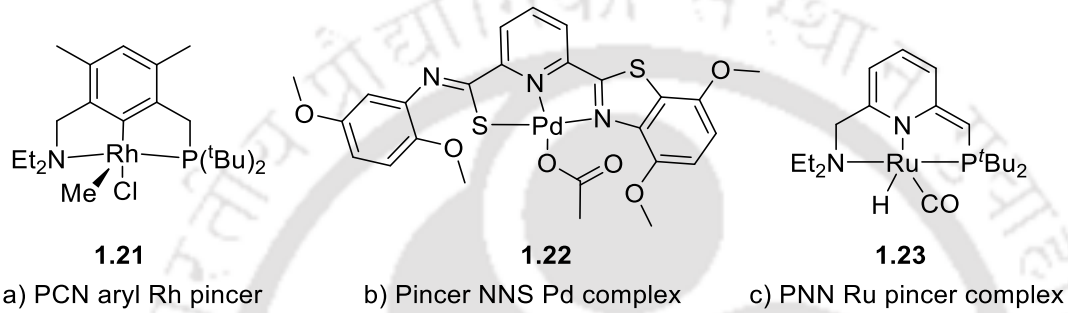

1.21 **1.22** **1.23**

a) PCN aryl Rh pincer b) Pincer NNS Pd complex c) PNN Ru pincer complex

Figure 1.6: a)PCN,[39] b) NNS[40] and c) PNN[38] type of unsymmetrical pincer complex.

1.2.3 Pincer-metal complexes based on NHC

One or more donor sites of the pincer ligands could be *N*-heterocyclic carbenes (NHCs) (Figure 1.7). Monocarbene "ECE" ligands of type **1.26** (Figure 1.7) could have a central carbene with flanking neutral or anionic E groups (E = N, O, S or Se). Alternatively, dicarbene "CEC" pincer ligands of the type **1.25** have a central anionic or neutral E group with two flanking carbene ligands (Figure 1.7).

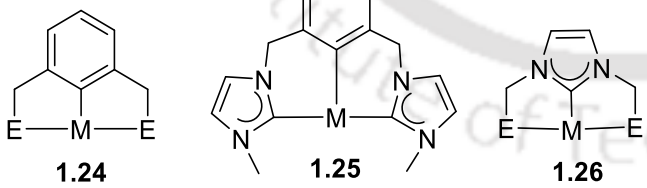

1.24 **1.25** **1.26**

Figure 1.7: Schematic representation of an general "ECE" type of pincer system **1.24**, (E = N, O, S or Se) along with its NHC hybrid systems **1.25** and **1.26** based on dicarbene and monocarbene respectively.[37]

Compared with traditional ligands,[41] NHCs present exciting properties such as σ-donor ability, tailorable structural diversity that includes electronic and steric effects.[42] In 1962, Wanzlick explored the reactivity and stability of *N*-heterocyclc carbenes.[43] In 1991, Arduengo first

established the synthesis of a stable NHC.[44] The electron donating ability of NHCs altered with the nature of azole ring and the order of electron donating power of azole ring follow the trend benzimidazole > imidazole > imidazoline. The first classical donor functionalized *N*-heterocyclic carbene complexes was defined by Lappert.[45] Wanzlick group has shown the first application of NHCs as ligand for metal complexes.[46] NHCs form very strong bond with a majority of metals, and are highly robust to oxidation and hydrolysis. Thus they are stable in presence of air, moisture and even to acidic conditions.

The Marchetti group have reported mono-NHC Ta and Nb complexes.[47-48] There are only a very few reports on tridentate chelating pincers incorporating *N*-heterocyclic carbene of "ECE" type where "ECE" ligands could have a central carbene with flanking neutral or anionic E groups (E = N, O, C, S or Se).[37, 49-50] The first report of CNC pincer-Cr dicarbene complex was reported in 2003.[51] Subsequently, pincer dicarbene complexes of vanadium and titanium were reported.[52] The CCC *N*-heterocyclic dicarbene complex of Zr **1.30** was synthesized by Hollis and co-workers (Figure 1.8).[37]

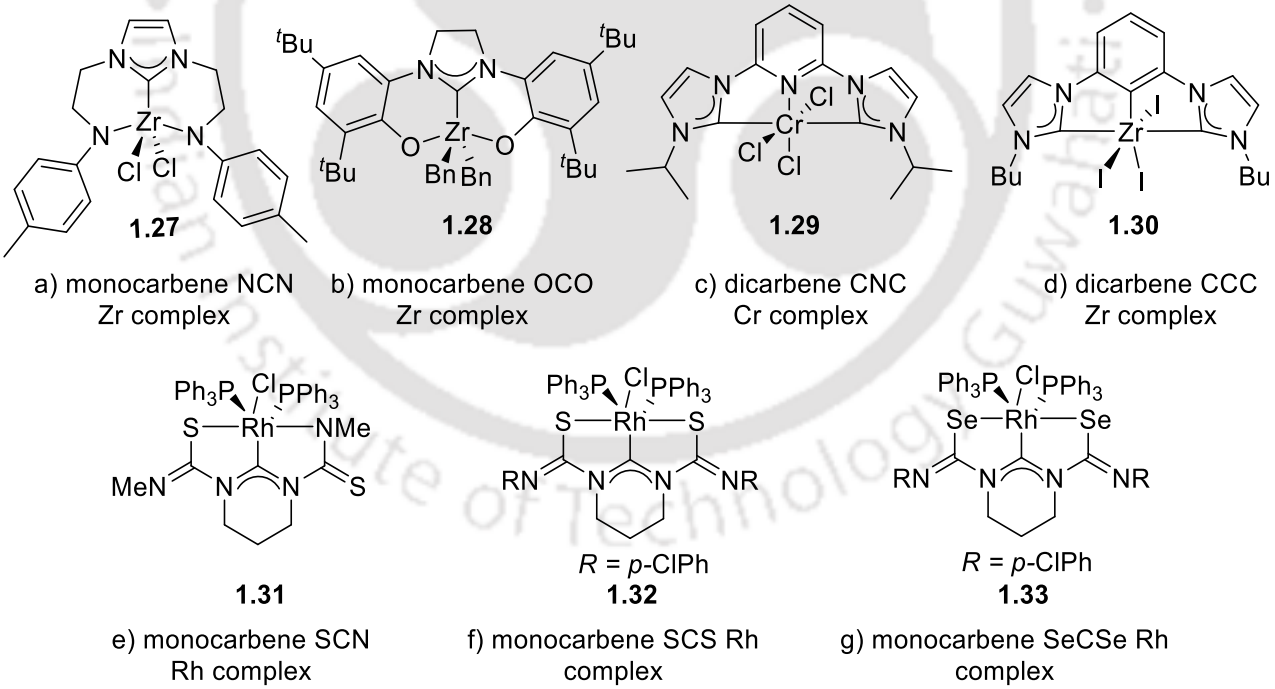

Figure 1.8: Examples of a) mono-carbene NCN pincer-Zr complex,[53] b) monocarbene OCO pincer-Zr complex,[50] c) dicarbene CNC pincer-Cr complex,[51] d) dicarbene CCC pincer-Zr complex,[37] e) monocarbene SCN pincer-Rh complex,[54] f) monocarbene SCS pincer-Rh complex,[54] g) monocarbene SeCSe pincer-Rh complex.[53]

In addition to symmetrical NHC-pincer complexes, there are a few rare examples of NHC-pincer complexes where different donor functionalities are utilized to generate unsymmetrical environment around the metal centre (Figure 1.9).

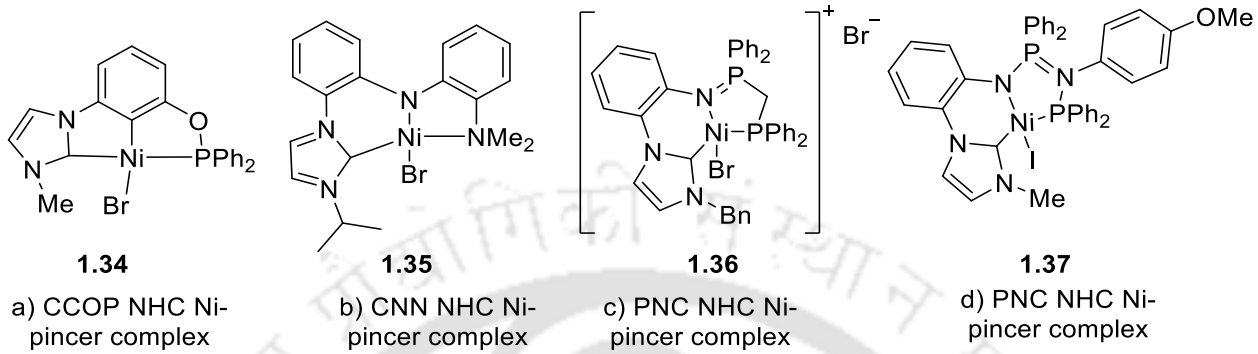

Figure1.9: Examples of unsymmetrical pincer-metal carbene complexes. a) NHCCOP pincer-Ni complex,[55] b) CNN pincer-Ni complex,[56] c) PNC pincer-Ni complex.[57] d) PNC pincer-Ni complex.[58]

1.3 Key factors in pincer ligand design

In pincer architecture (Figure 1.1), bulky R groups have a direct impact on the steric hindrance around the metal, while the size of the linker arms (Y) determines the ring size and therefore influences the bite angle and also affects the reactivity of the complex. The electronic properties of the pincer can be fine-tuned by the nature of Z, a substituent on the *para* position of aromatic ring (Figure 1.1). The donor atom X can be varied to have an important electronic impact, particularly the *trans* influence. In addition to these factors, pincer ligands may introduce chirality in the complex, normally by employing chiral LRn groups (Figure 1.1) and sometimes by having a chiral linker (Y). A few of the salient features associated with the pincer-complexes is discussed below.

1.3.1 Robustness of pincer type complex

The tridentate chelate pincer complexes are highly thermally stable and generally the decomposition of pincer complexes only occur at > 100 °C. For example, diphosphine pincer-Ni(II) complex was thermally stable up to 240 °C in air (Figure 1.10, **1.7**).[22] The thermal stability and presence of strong aromatic backbone allow the pincer complexes to react with otherwise deactivating ligands such as CO,[59] CO_2,[60] CN^-,[61] H_2,[62] di-halide,[63] oxidizing and reducing agents, water[64] and acids,[65] while retaining their coordination geometry (Figure 1.10).

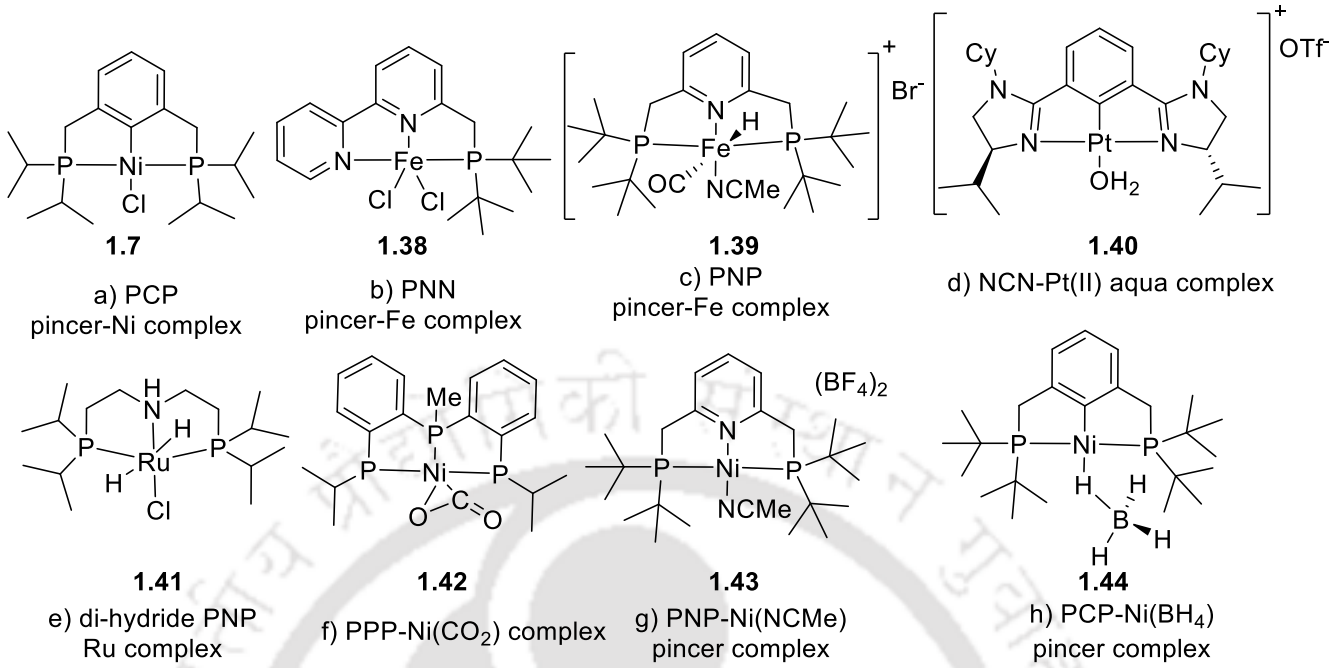

Figure 1.10: Examples of robust pincer-metal complexes a) PCP pincer-Ni complex,[22] b) PNN pincer-Fe complex,[63] c) PNP pincer-Ni carbonyl complex,[59] d) NCN pincer-Pt aqua complex,[64] e) PNP pincer-Ru dihydride complex,[62] f) PNP pincer-Ni CO_2 complex, [60] g) PNP pincer-Ni acetonitrile complex,[61] h) lewis acid BH_3 coordinated with PCP pincer-Ni hydride complex. [65]

Highly endothermic reactions such as the dehydrogenation of organic substrates are successfully carried out with highly robust pincer-Ir catalytic systems (Figure 1.11). Ir pincer complexes shows excellent thermal stability till 300 °C for an extended period of time.[13]

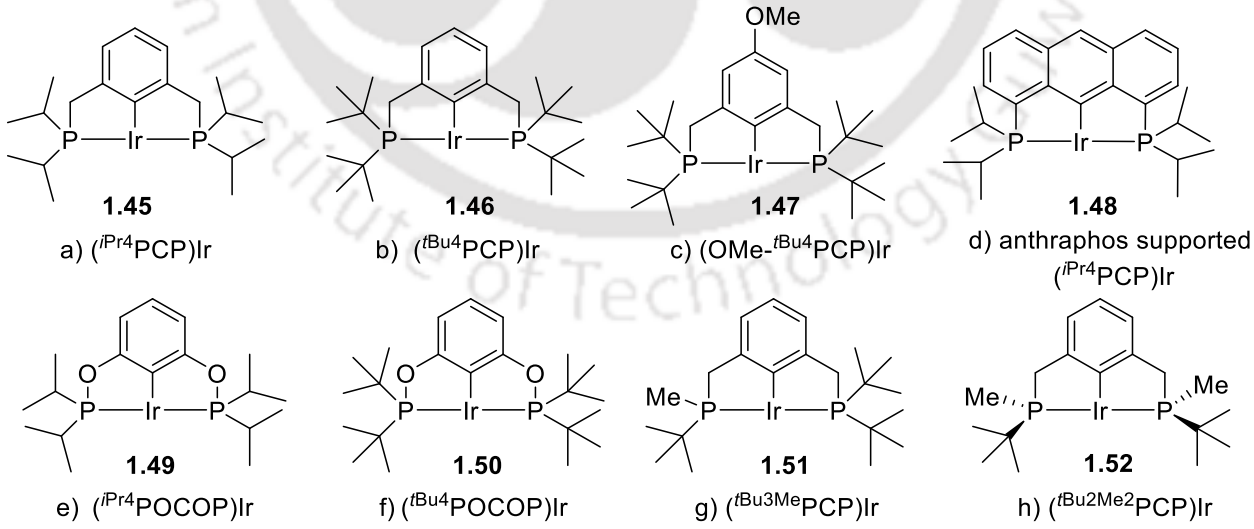

Figure 1.11: A few robust pincer-Ir complexes reported for alkane dehydrogenation.[13] a) (^{i}Pr4PCP)Ir complex,[66] b) (^{t}Bu4PCP)Ir complex,[67] c) (OMe-^{t}Bu4PCP)Ir complex,[68] d) anthraphos supported (^{i}Pr4PCP)Ir complex,[69] e) (^{i}Pr4POCOP)Ir complex,[70] f) (^{t}Bu4POCOP)Ir complex,[71] g) (^{t}Bu3MePCP)Ir complex,[72] h) (^{t}Bu2Me2PCP)Ir complex.[72]

1.3.2 Pincer complexes containing metals in unusal formal oxidation state

The pincer framework sometimes stabilizes the metal in unusual formal oxidation states. While square planar Ni(II) complexes[73] are well known in organometallic chemistry, NCN pincer fragments bound to Ni(III) in species **1.54** have been reported to be stable owing to hard nitrogen donors.[74] Strong σ-donation ability of chelating NMe_2 group assists oxidation of Ni(II) complex to corresponding Ni(III) complex (Scheme 1.2).[75] The subsequent five coordinated, square pyramidal pincer-Ni(III) complex is stabilized by the robustness of tridentate pincer ligand as well as the oxidation state of the metal. These air and moisture stable Ni(III) complexes also have good thermal stability.

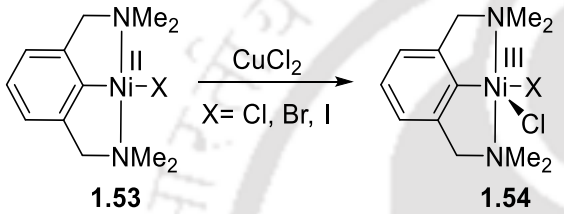

1.53 **1.54**

Scheme 1.2: Formation of Ni(III) from Ni(II) pincer complex.[75]

Similarly, unusual Ni(IV) species **1.56** could be obtained by oxidation of a CCC NHC Ni(II) pincer complex with $PhICl_2$ (Scheme 1.3).[76]

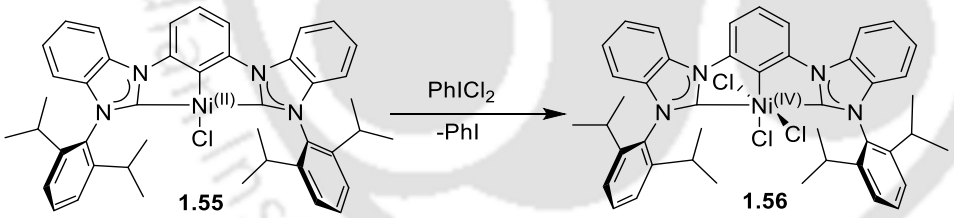

1.55 **1.56**

Scheme 1.3: Formation of unusual Ni(IV) pincer complex.[76]

Pyrrole based PNP pincer-Fe complex could be reduced in presence of CO to afford a low spin carbonyl complex $[Fe^{I}(CO)_2(PNP)]$ **1.59**, which was further reduced to yield an anionic Fe(0) complex **1.60** (Scheme 1.4).[77]

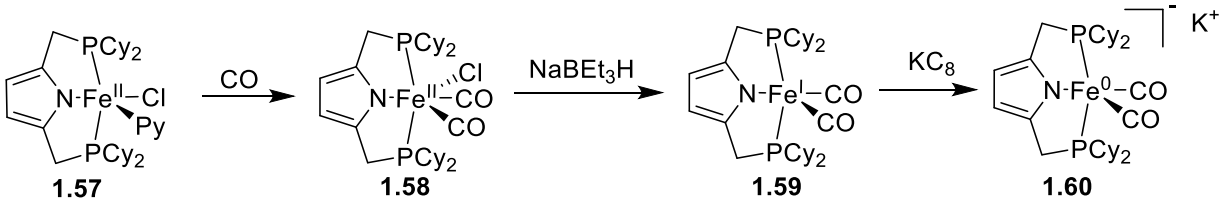

1.57 **1.58** **1.59** **1.60**

Scheme 1.4: Pincer-iron complexes having Fe in different oxidation states.[77]

1.3.3 Hemilability of pincer ligand

Hemilabilty of pincer ligand acts as a key factor for the catalytic efficiency of the corresponding metal complex. In Figure 1.12, the Ni(II) in complex **1.61** (Figure 1.12) binds with a central N donor atom and is coordinated with two asymmetric amine arms. This Ni(II) successfully catalyzed the Sonogashira coupling between terminal alkynes and alkyl halides at room temperature. On the other hand, the symmetric pincer-Ni(II) complex **1.62** (Figure 1.12) showed lower catalytic activity under identical conditions and was active only at elevated temperatures.[78] Here the symmetric rigid pincer ligand of **1.62** does not allow hemilability.

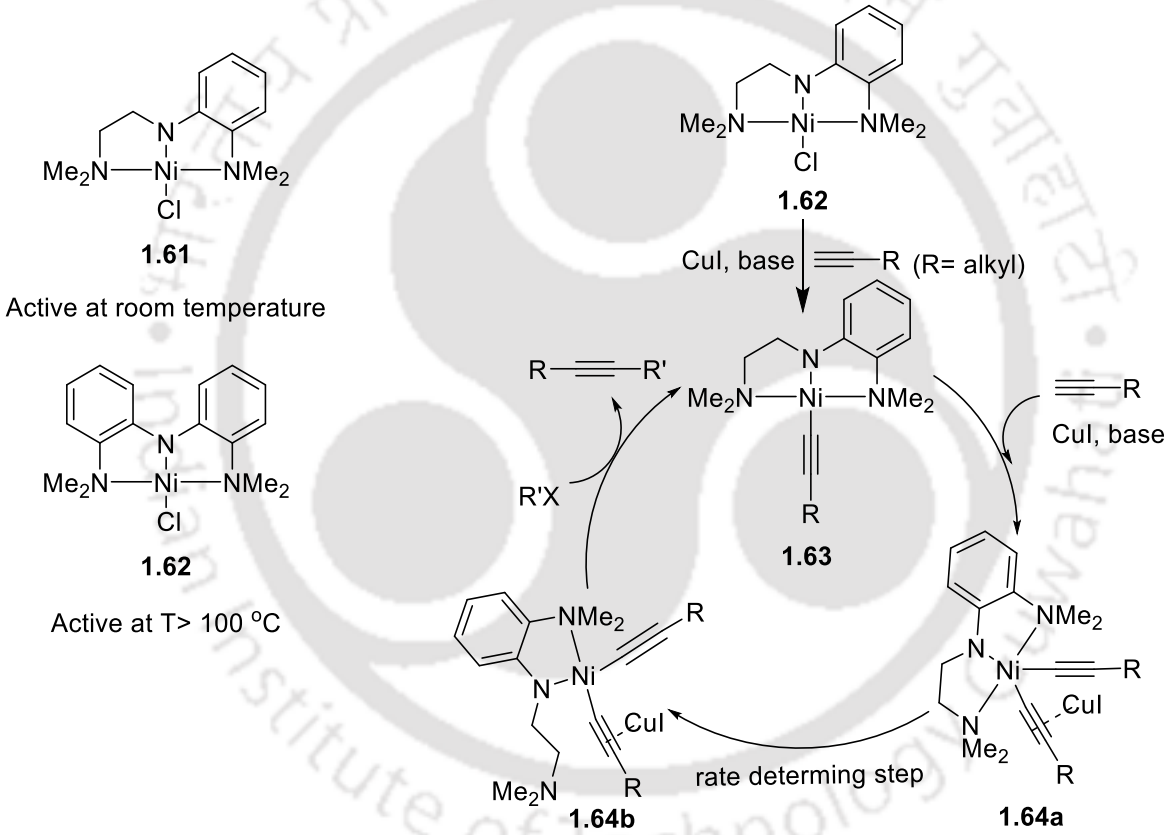

Figure 1.12: Hemilability of Ni-pincer complexes.[78]

In NCN ligand based complexes, the strong σ-donating amine functionalities participated in metal centered reactions and demonstrated good stoichiometric and catalytic properties, whereas PCP ligand based complexes exhibited strong chelation and activated strong bonds. It has been observed that amine arms will be involved in more labile coordination to the low oxidation state of late transition metals in comparison with phosphine arms.[79]

In **1.65** (Figure 1.13) the PCN ligand bears a longer arm with dimethylene unit between aromatic ring and the amine group. This results in loss of planarity and stabilization (arising from a planar 5-membered ring as in the case of **1.66**) which makes the amine arm labile. Hence, **1.65** can react with dihydrogen leading to interesting catalytic properties in stark contrast to unreactive nature of **1.66** (Figure 1.13).[80]

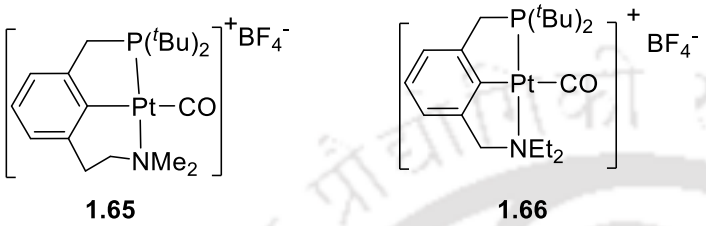

Figure 1.13: Effect of an additional linker atom on the hemilabile nature of a carbonyl pincer-Pt complex.[80]

1.3.4 Pincer complexes; *meridional* Vs. *facial*

Generally, 'pincer' ligand prefers to attain *meridional* tridentate geometry but occasionally we can find very few examples of *facial* tridentate chelates.

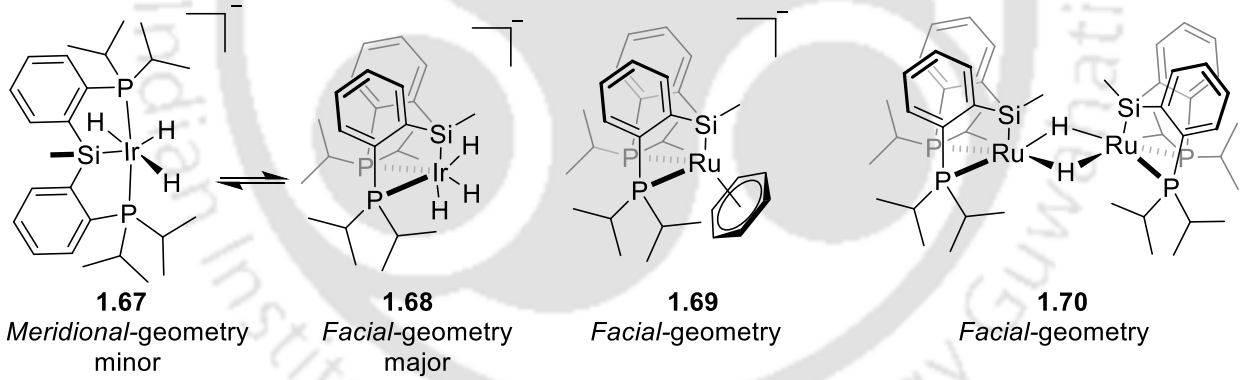

Figure 1.14: Examples of *facial* and *meridional* pincer complexes. Dynamic behavior of Ir with PSiP pincers (**1.67** and **1.68**),[81] Arene complex of Ru with *facial* PSiP pincer ligand (**1.69**),[82] and *facial* complex of PSiP pincer-Ru hydride (**1.70**).[82]

The geometry of the pincer complexes are dependent on the central ligating atom of the tridentate ligand. A sp^2-hybridized central donor atom prefers to attain *meridional* geometrical configuration due to its planar orientation. Steric hindrance or dimerization can enhance the chances of formation of *facial* coordination of the ligand (**1.70**, Figure 1.14). In absence of steric constraints *meridional* coordination is preferred (**1.67**, Figure 1.14). In Figure 1.14 structure **1.69** adopts *facial* geometry to accommodate another facial η^6-arene ligand.

Strongly π- accepting phosphines with -CF_3 groups lead to a pseudo square-planar Ir(I) complex with *meridional* configuration (Scheme 1.5). Addition of another carbonyl ligand to structure **1.71** gives a distorted trigonal bipyramidal complex **1.72**, where the P atoms occupy two equatorial binding sites and give rise to a non-*meridional* pincer co-ordination of PCP ligand to Ir. Oxidative addition of H_2 to Ir(I) in complex **1.71** generates Ir(III) pseudo-octahedral complex **1.74**, where pincer ligands favor *meridional* coordination mode.

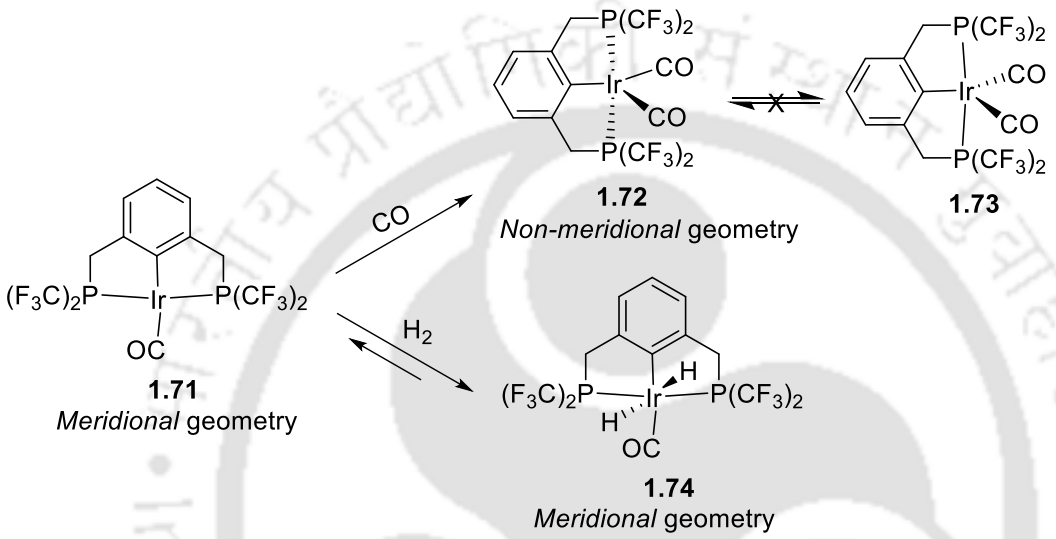

Scheme 1.5: Effect of H_2 and CO on the *meridional* preference of PCP Ir complexes with CF_3 groups.[83]

1.3.5 Ring size effect

In 2003, Yamamoto and coworkers have shown the difference in catalytic activity of allylic alkylation of two identical pincers with different ring size (Scheme 1.6). Symmetrical pincer-Pd complex **1.77a** contains two five membered metallacycles, whereas structure **1.77b** is associated with both the five and six membered ring. With a detailed analysis they have proved that palladium (II) complexes of unsymmetrical PCP' *bis* (phosphinito) ligand (**1.77b**, Scheme 1.6) are much more active towards allylic alkylation due to the greater flexibility of the 6-membered ring than the corresponding five-membered rings in symmetrical complexes based on PCP *bis*(phosphinito) ligand (**1.77a**, Scheme 1.6).[84] Catalyst **1.77a** shows only reasonable activity at high temperature whereas non-symmetrical pincer **1.77b** is highly active at room temperature also.

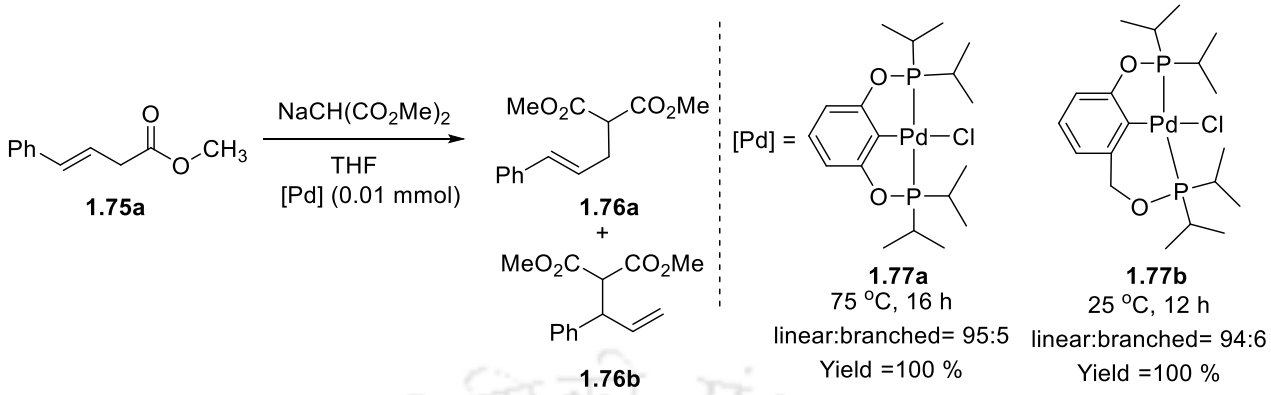

Scheme 1.6: Difference in reactivity of pincer-Pd complexes with varying ring sizes towards allylic alkylation.[84]

Between the symmetrical 6,6 membered pincer-Pd(II) complex **1.78b** and the 5,6 membered selone ligated pincer-Pd(II) complex **1.78a**, the unsymmetrical pincer complex **1.78a** showed better catalytic activity for Heck C-C coupling reaction (Scheme 1.7).[85]

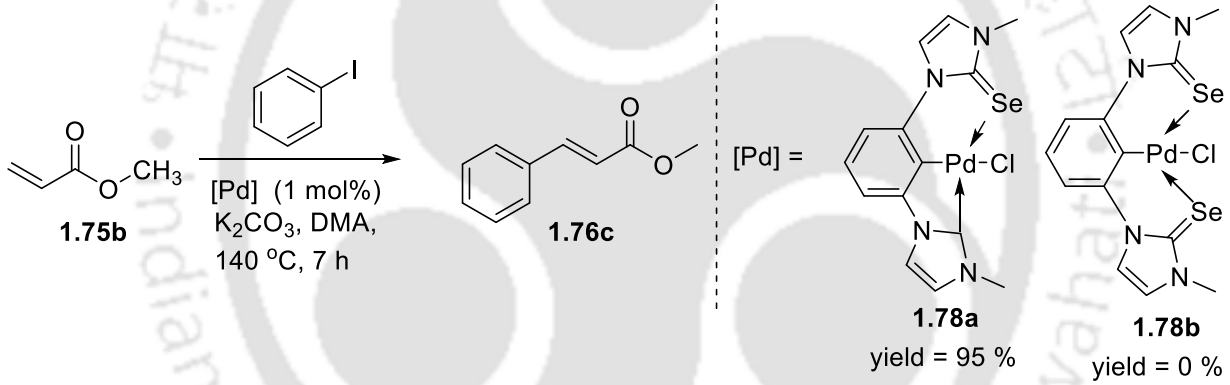

Scheme 1.7: Higher reactivity of pincer-Pd[85] complexes with unsymmetrical pincer ligand.[85]

1.4 Application of pincer complexes in catalysis

In the last four decades, pincer-complexes have been extensively used to efficiently catalyse several reactions, that are either not possible or provide very low yield with classical transition metal complexes. This fascinating chemistry of pincer-complexes have been reviewed several times.[13, 86-91]

1.4.1 Transfer hydrogenation

The variety of factors discussed in section **1.3** imparts versatile reactivity patterns to pincer-metal complexes and rightly a plethora of their applications are realized in catalyzing organic reactions of great synthetic utility. NCN and PCP pincer-Ru complexes efficiently catalyzed the transfer

hydrogenation of ketones to their corresponding alcohols, in presence of isopropanol as a source of sacrificial hydrogen and KOH as a co-catalyst (**1.81** and **1.82**, Scheme 1.8).[92]

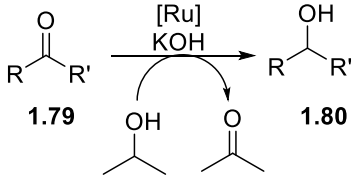

[Ru] =

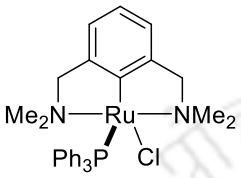

1.81

a) **1.79** = cyclohexanone
[Ru]= 0.1 mol %,
T= 82 °C, 3.3 h
coversion = >98 %,

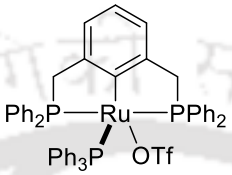

1.82

b) **1.79** = cyclohexanone
[Ru]= 0.01 mol %,
T= 82 °C, 1.3 h
conversion = >98 %,

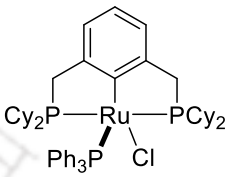

1.83

c) **1.79** = Ph_2CO
[Ru]= 0.1 mol %,
T= 82 °C, 40 h
conversion = 92 %,

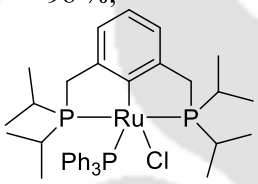

1.84

d) **1.79** = cyclohexanone
[Ru]= 0.1 mol %,
T= 82 °C, 5 h
conversion = 98 %,

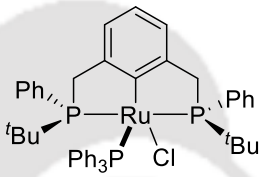

1.85

e) **1.79** = $PhCOCH_3$
[Ru]= 0.01 mmol
T= 82 °C, 17 h
conversion = 40 %,

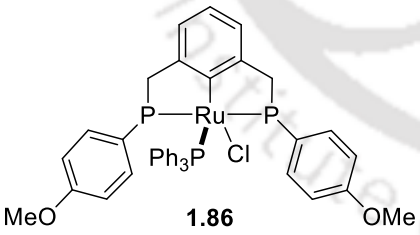

1.86

f) **1.79** = cyclohexanone
[Ru]= 0.1 mol %,
T= 82 °C, 0.5 h
conversion = 96 %,

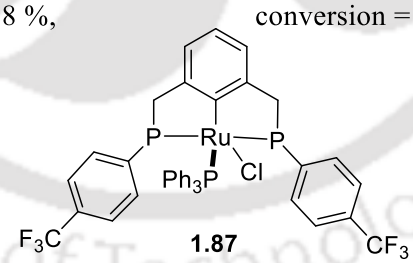

1.87

g) **1.79** = cyclohexanone
[Ru]= 0.1 mol %,
T= 82 °C, 10 min
conversion = 98 %,

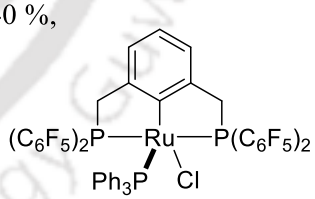

1.88

h) **1.79** = cyclohexanone
[Ru]= 0.1 mol %,
T= 82 °C, 13 h
conversion = 98 %,

Scheme 1.8: Transfer hydrogenation of ketones by a) (^{Me2}NCN)RuCl(PPh_3),[92] b) (^{Ph2}PCP)RuOTf(PPh_3),[92] c) (^{Cy4}PCP)RuCl(PPh_3),[93] d) (^{iPr4}PCP)RuCl(PPh_3),[94] e) (^{Ph2tBu2}PCP)RuCl(PPh_3),[95] f) ($^{p\text{-OMe-C6H4}}$PCP)RuCl(PPh_3),[94] g) ($^{p\text{-CF3-C6H4}}$PCP)RuCl(PPh_3),[94] and h) (^{C24F20}PCP) RuCl(PPh_3)[94]

Even in presence of non-pincer complexes like $RuCl_2(PPh_3)$ or $RuCl(H)(PPh_3)$, hydrogen transfer reactions occurred albeit with lower catalytic efficiency.[96] For example $RuCl_2(PPh_3)$ catalyzed the transfer hydrogenation of cyclohexanone which resulted in only 59% conversion.[97] It has been observed that both NCN pincer-Ru (**1.81**, Scheme 1.8) and PCP pincer-Ru (**1.82**, Scheme 1.8) are active towards transfer hydrogenation. Among the two, the best yield and turnover number were obtained with PCP-Ru (**1.82**, Scheme 1.8) derivatives. For example, in case of cyclohexanone, PCP pincer-Ru (**1.82**, Scheme 1.8) gave 98% yield (27,000 TON).[92] Among several PCP pincer-Ru complexes (Scheme 1.8), ($^{p\text{-CF3-C6H4}}$PCP)Ru (**1.87,** Scheme 1.8) pincer catalyzed transfer dehydrogenation of cyclohexanone resulted in 35,700 TON with 98% yield.

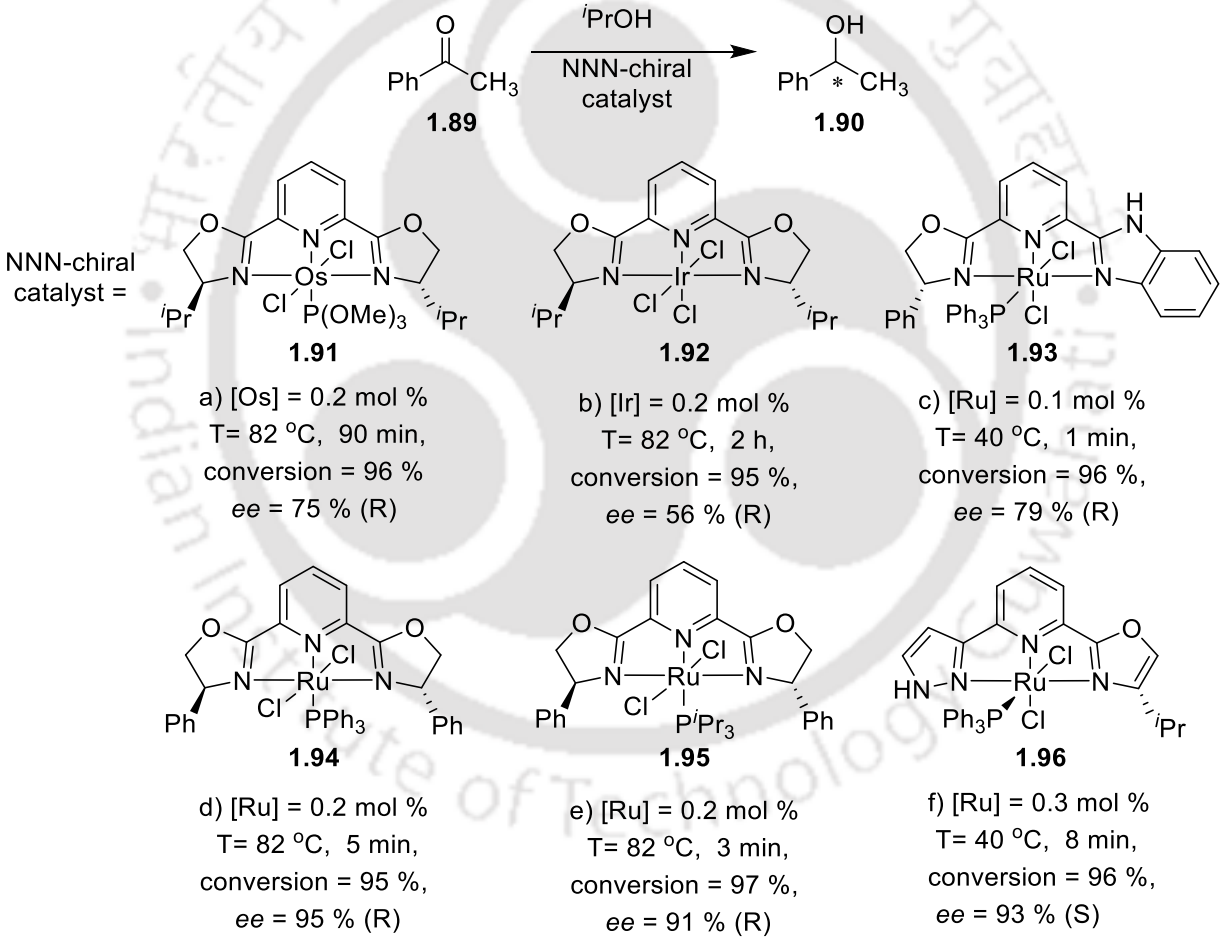

Scheme 1.9: Asymmetric transfer hydrogenation using chiral NNN pincer complexes based on. a) Os,[98] b) Ir,[99] c) oxazolinyl/benzimidazolyl Ru,[100] d) pybox Ru,[101] e) pybox Ru,[101] f) pyrazolyl-pyridyl-oxazolinyl Ru.[102]

Catalytic asymmetric transfer hydrogenation have also been reported by using chiral pincer complexes (Scheme 1.9).[98-102] Among several pincer-metal complexes based on chiral pybox ligand, it has been found that enantioselectivity obtained with Ir (**1.92**, Scheme 1.9) was lower than that of Os and Ru (**1.91**, **1.93** or **1.94**, Scheme 1.9).[103]

Transfer hydrogenation using precious metal-based catalyst such as Ru,[104] Rh,[105] Os[106] or Ir[107] have been well explored. Recently, inexpensive base metal pincer complexes have been developed for transfer dehydrogenation. Among different first row transition metals, base metal pincer complexes utilizing Fe,[108] CO[109] and Mn[110-111] have been used to catalyze transfer hydrogenation of unsaturated compounds such as ketones,[110] aldehydes,[110] nitriles,[110] and esters[111].

1.4.2 Dehydrogenation of alkanes

Saturated hydrocarbons like alkanes or cycloalkanes are most abundant and easily available in nature. However, these compounds have been limited in use due to their lack of reactivity. Selective dehydrogenation of alkanes to produce alkenes have attracted significant attention due to their versatile nature. In one of the first reports, the dehydrogenation of cyclopentane **1.97** and cyclooctane **1.99** was carried out using cationic Ir complex $[Ir(H_2)(acetone)_2(PPh_3)_2][BF_4]$ in presence of *tert*-butylethylene (TBE), which functions as a hydrogen acceptor to produce the corresponding cyclopentadienyl complex **1.98** and cyclooctadienyl complex **1.100** respectively (Scheme 1.10).[112]

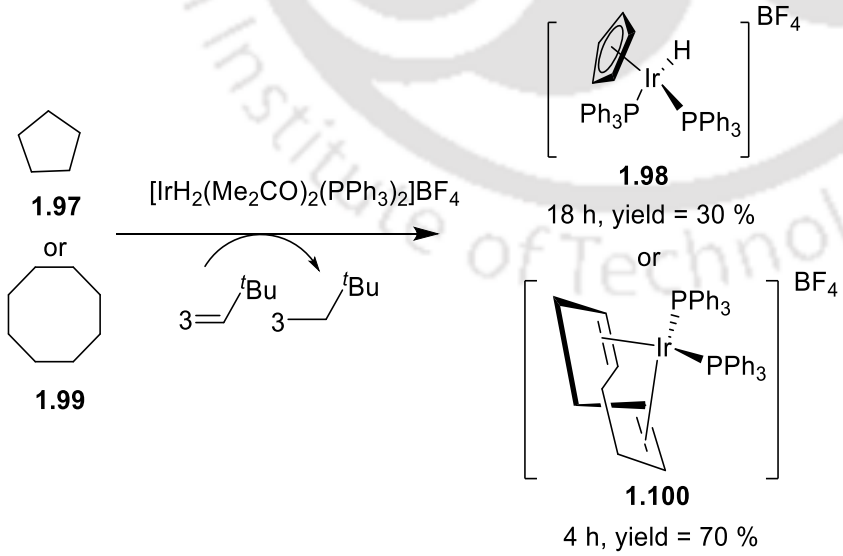

Scheme 1.10: Transfer-dehydrogenation of cycloalkanes using $[Ir(H_2)(acetone)_2(PPh_3)_2][BF_4]$.[112]

Acceptorless dehydrogenation of cyclooctane resulted in cyclooctene in presence of $IrH_2(O_2CR)(PCy_3)_2$ with 36 turnover number (TON) in 48h.[113] Jenson,[114] Goldman[115] and Leitner[116] independently reported the use of derivatives of these complexes for its application in dehydrogenation of alkanes. Classical organometallic complexes catalyze highly endothermic dehydrogenation of alkanes with limited turnover numbers owing to their susceptibility to undergo thermal decomposition under the reaction conditions.

It has been observed that several thermally stable pincer-Ir complexes were active towards dehydrogenation of alkanes. In 1996, Kaska and Jensen reported (^{t}Bu4PCP)IrH$_4$ **1.108** to be a remarkably robust catalyst and obtained 82 turnover/h at 150 ^{o}C for dehydrogenation of cyclooctane.[117] In 1999, Jensen[118] and Goldman[119] have shown that while (^{i}Pr4PCP)IrH$_4$ **1.110** was highly active, the complex (^{t}Bu4PCP)IrH$_4$ **1.108** gave high kinetic selectivity for the formation of α-olefin in the transfer dehydrogenation of *n*-alkanes. For the acceptorless dehydrogenation of both *n*-alkane and cycloalkanes, the sterically less crowded catalyst (^{i}Pr4PCP)IrH$_2$ was found to be more effective than (^{t}Bu4PCP)IrH$_2$.[119]

Successful alkane transfer dehydrogenation were carried out by using 7-6-7 ring-type PCP iridium pincer catalyst **1.102**, which is stable at very harsh reaction conditions and are able to produce the final product with high efficiency and selectivity (Scheme 1.11). [120]

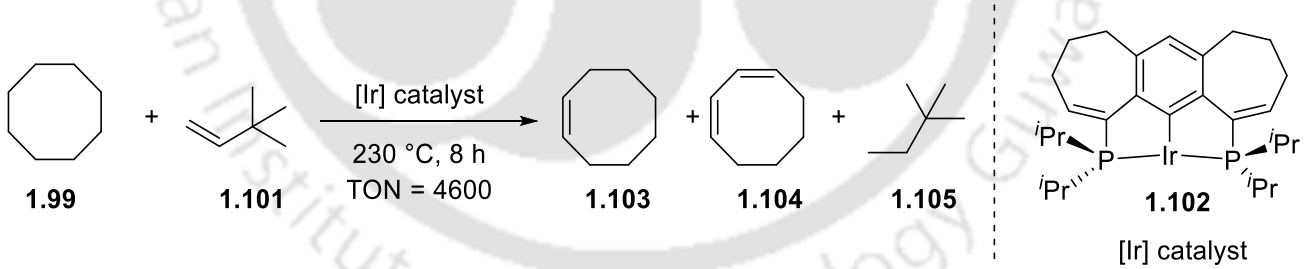

Scheme 1.11: Alkane transfer dehydrogenation by 7-6-7 ring-type PCP iridium catalyst.[120]

In 2009, Goldman and co-workers, investigated the catalytic application of various pincer-Ir complexes by systematic variation of the steric factors. DFT studies indicated that, (^{t}Bu3MePCP)IrH$_4$ complex **1.111** is expected have a favorable barrier than (^{t}Bu4PCP)IrH$_4$ **1.108** for catalytic transfer dehydrogenation owing to lowered steric requirements. However subsequent Me for ^{t}Bu substitution as in (^{t}Bu2Me2PCP)IrH$_4$ complex **1.109** is expected to have negligible effect which has been attributed to the cancellation of favorable steric effects by the inhibition effect due to olefin

binding. Accordingly, (^{t}Bu2Me2PCP)IrH$_4$ complex **1.109** demonstrates lower catalytic activity than (^{t}Bu3MePCP)IrH$_4$ **1.111**(Scheme 1.12).[72] However, as (^{t}Bu2Me2PCP)IrH$_4$ complex **1.109** tends to form dimers, it was difficult to determine if cluster formation rather than intrinsic low reactivity was the source of low TON.

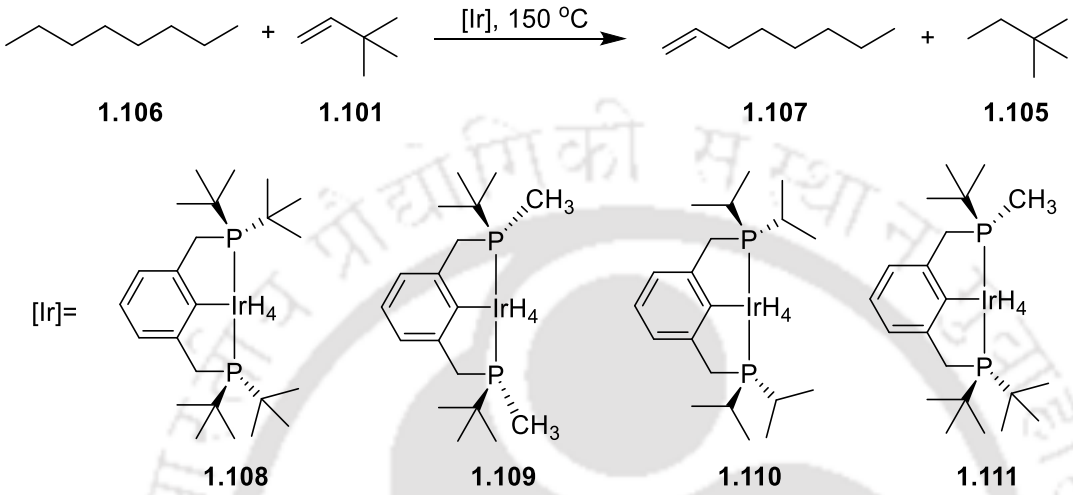

Reactivity after 10 min: **1.111** (TON = 126) >**1.110** (TON = 86) >**1.109**(TON = 76) >**1.108** (TON = 31)

Scheme1.12: Dehydrogenation of *n*-octane using various pincer-Ir systems.[72]

The pincer-Ir catalyzed alkane dehydrogenation has shown great advances in recent times and have lead to conditions that give high turnover number of terminal olefins with good recyclability.[13]

1.4.3 Dehydrogenation of alcohol

Transfer dehydrogenation processes are typically carried out under sealed vessel conditions where the use of sacrificial hydrogen acceptor is mandatory to trap the released hydrogen. On the other hand, acceptorless dehydrogenation reactions are carried out under open-vessel conditions where the molecular hydrogen is free to escape from the system.

The acceptorless dehydrogenation reaction of secondary alcohol **1.112** with evolution of molecular hydrogen to produce ketones is atom-economical and environmentally benign. A library of electron rich PNN and PNP Ru borohydride pincer complexes (Scheme 1.13, **1.114-1.116**) have been reported for dehydrogenation of alcohol under mild conditions, to the corresponding carbonyl compounds with liberation of dihydrogen.[121] Besides dehydrogenation of secondary alcohols, these Ru(II) hydridoborohydride pincer complexes (Scheme 1.13, **1.114-1.116**) effectively catalyze acceptorless dehydrogenative coupling of primary alcohols to esters, and dehydrogenative

cyclisation of diols to lactones.[121] PCP pincer-Ir complex (**1.117**, Scheme 1.13), followed a unique metal-ligand cooperation mechanism in the acceptorless dehydrogenation of alcohol.[122] Apart from precious metal, pincer complexes of inexpensive 3*d* transition metals are also reported for dehydrogenation of alcohols (**1.118**, Scheme 1.13).[109]

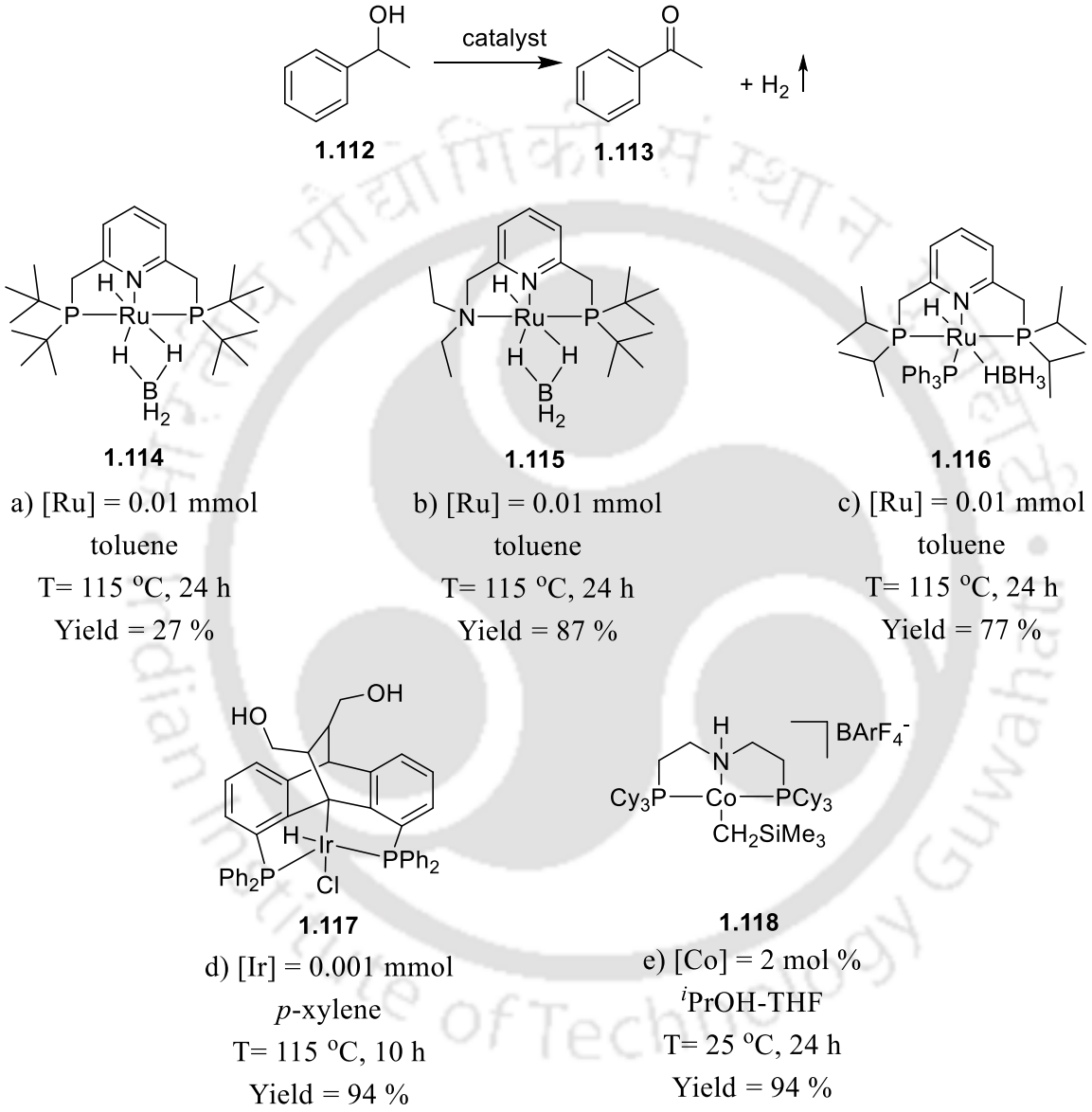

Scheme 1.13: Acceptorless dehydrogenation of 1-phenyl ethanol using pincer-Ru complexes (**1.114-1.116**),[121] PCP pincer-Ir catalyst (**1.117**),[122]and e) PNP pincer-Co catalyst (**1.118**).[109]

Primary alcohols, in addition to being directly converted to aldehydes, can also be converted to acetals **1.120** (Scheme 1.14) which is highly atom-economical. Milstein and co-workers developed

acridine based PNP pincer-Ru complex **1.121** for the conversion of alcohol to acetal (Scheme 1.14).[123-124]

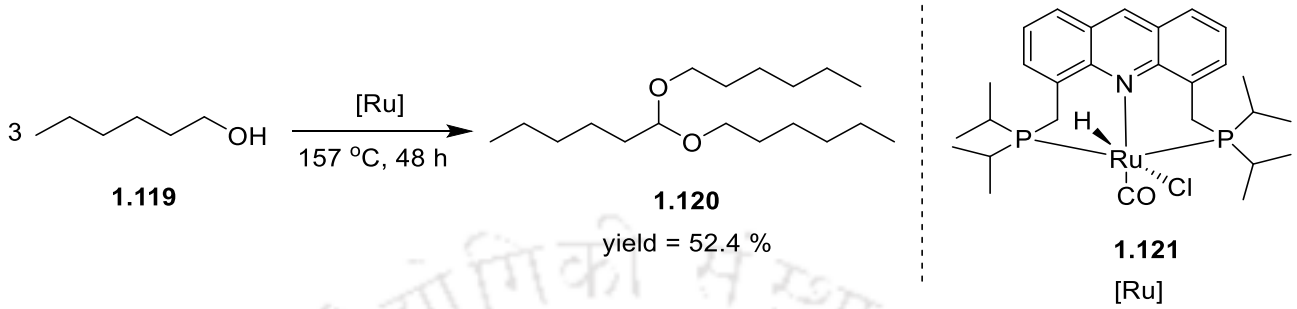

Scheme 1.14: Conversion of primary alcohol to acetal catalyzed by acridine based PNP pincer-Ru catalyst[123, 125]

Methanol can be dehydrogenated to formaldehyde, which can be further dehydrogenated to formic acid and finally to carbon dioxide. During this dehydrogenation, each step releases an equivalent of H_2 gas. The generated hydrogen gas can be utilized as an attractive alternative energy source. PNP supported pincer-Fe complex **1.127** (Scheme 1.15) have been reported to be a highly active catalyst for dehydrogenation of methanol, and in absence of water, methanol is readily converted to methyl formate and H_2. In presence of water and a Lewis acid co-catalyst, the PNP pincer-Fe dehydrogenates methanol to CO_2 and H_2.[126] Non-toxic, easily available pincer-Mn complex **1.129** (Scheme 1.15) has been used to successfully carry out the dehydrogenation of aqueous methanol to carbon dioxide and dihydrogen.[127]

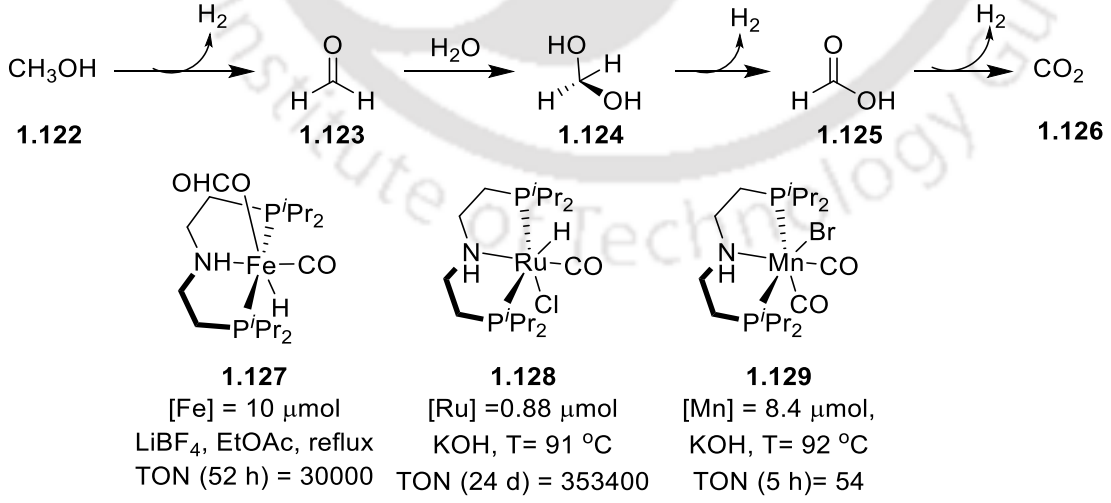

Scheme 1.15: Dehydrogenation of methanol catalyzed by a) pincer-Fe complex,[126] b) pincer-Ru complex,[128] and c) pincer-Mn complex.[127]

1.4.4 Cross-coupling reaction

Cross-coupling reactions represent one of the most important type of catalytic carbon-carbon bond forming reactions between a organic electrophile R_1-X and an organometallic nucleophile R_2-m in presence of a catalyst (Scheme 1.16).[129] Among several transition metals, Pd metal has been widely used for coupling reactions.

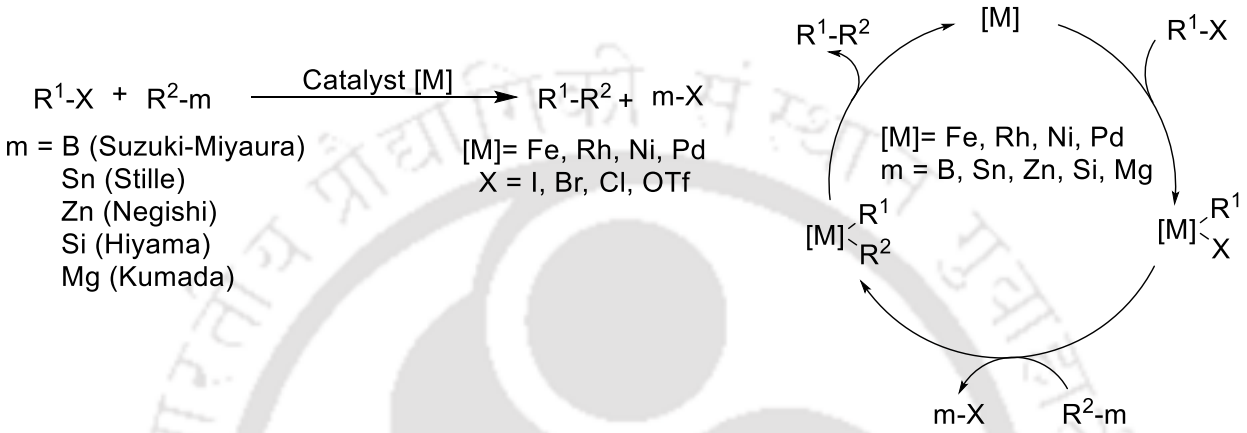

Scheme 1.16: General scheme of C-C cross coupling reaction.[129] [130]

1.4.4.1 Heck-coupling

Heck reaction is the coupling between α-olefin and bromo or iodo derivatives catalyzed by Pd(II) or Pd(0) in presence of PPh_3. Several pincer-Pd complexes containing aryl or pyridine backbone have been reported for catalytic Heck coupling reaction (Scheme 1.17).

Heck reaction is catalyzed by either Pd(II) or Pd(0) derivatives in presence of auxiliary ligands. The reaction intermediates formed during the catalytic cycle are sensitive to oxygen and thermally unstable. To design the ideal catalyst to carry out the process, Milstein and co-workers were the first to employ PCP pincer-Pd(II) complexes (**1.132** and **1.133**, Scheme 1.17) in Heck coupling reaction.[131] Milstein reported that these highly robust pincer-Pd complexes (**1.132** and **1.133**, Scheme 1.17) are stable at a very high temperature (upto 140 °C), over reaction periods of 300 hours or more and act as a catalyst for coupling of iodobenzene with methacrylate with a maximum of 5,00,000 turnover number.[131] Later, several pincer-Pd complexes have been developed. In 2007 Morales-Morales reported that POCOP pincer-Pd complex (**1.134**, Scheme 1.17) displayed better catalytic activity compared to Milstein's PCP-Pd complex.[132] The superior catalytic activity was attributed due to both sterics and electronic factors (better π-donation ability of oxygen atom).

Coupling between bromo benzene and *n*-butyl methacrylate in presence of POCOP-Pd **1.134** lead to quantitative yields (Scheme 1.17).[132] Ahn. *et al.* designed a 6-membered fused metallacycle containing NCN pincer-Pd complex **1.138** (Scheme 1.17) for coupling reaction between halo-benzene and methyl acrylate with turnover number upto 8.4×10^{8}.[133]

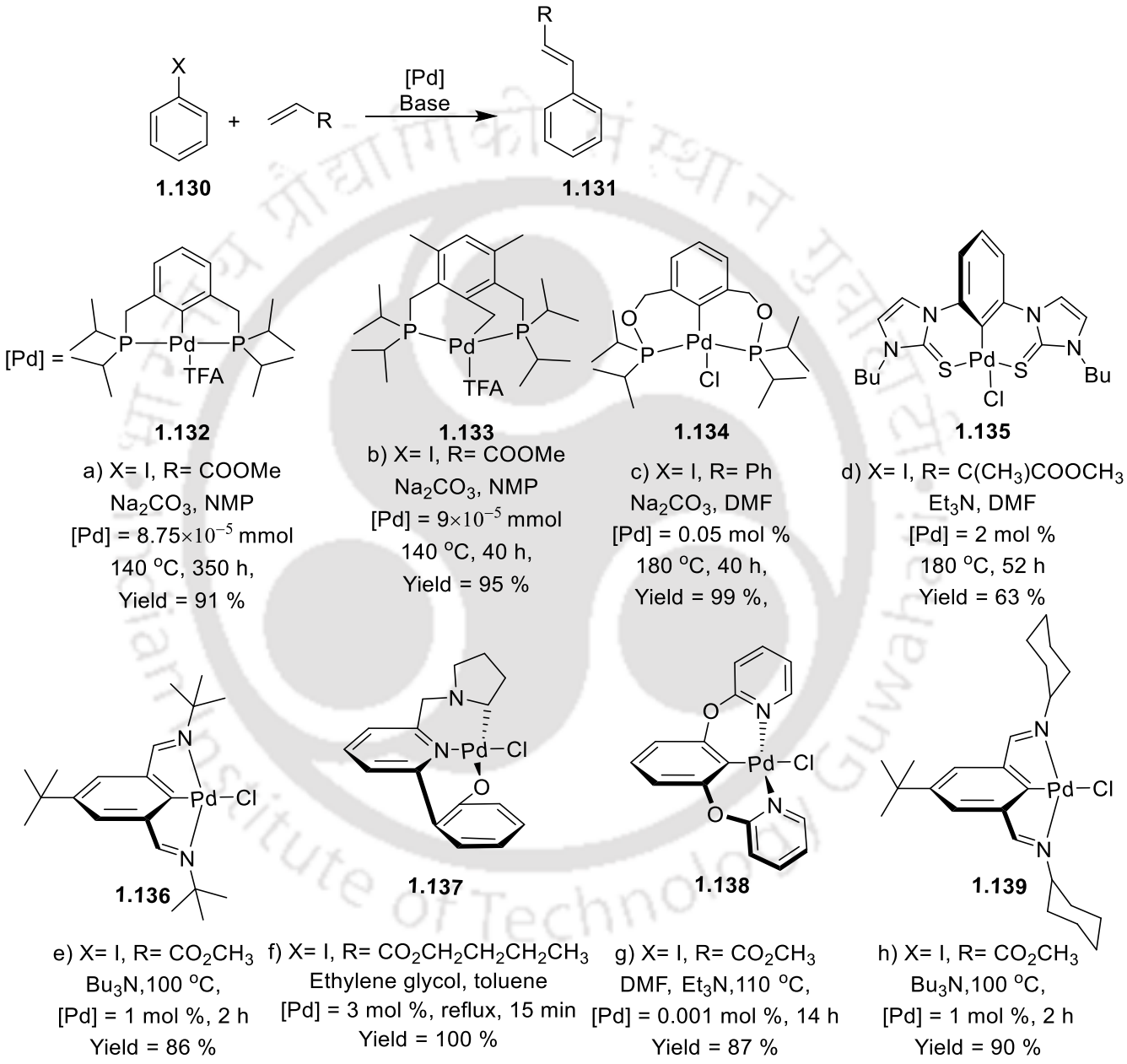

Scheme 1.17: Heck coupling catalyzed by a) PCP pincer-Pd(II) complex[131] b) PC(sp^2)P pincer-Pd(II) complex[131] c) POCOP pincer-Pd(II) complex,[132] d) SCS *bis*(*N*-heterocyclic thione) pincer-Pd(II) complex,[134] e) (^{tBu2}NNN)Pd complex,[135] f) ONN pincer-Pd(II) complex,[136] g) NOCON pincer-Pd(II),[137] h) (^{Cy2}NNN)Pd complex.[135]

1.4.4.2 Suzuki-Miyaura coupling

The Suzuki reaction is an important tool for the construction of biaryl or substituted aromatic moieties. The Suzuki or Suzuki-Miyaura coupling generally occurs between halobenzene with aryl boronic acid in the presence of a base (Scheme 1.18).

POCOP pincer-Pd(II) complex **1.143** has been utilized as a useful catalyst for the coupling between aryl halide and phenyl boronic acid leading to quantitative yield and around 92,000 turnover number (Scheme 1.18).[138] The SCS pincer-Pd(II)complex **1.144** has been reported to be an excellent catalyst for the reaction between *p*-bromo toluene and phenyl boronic acid to generate corresponding biphenyl product with a maximum of 69% yield (Scheme 1.18).[139] The Suzuki coupling reaction of 4-bromo-acetophenone with phenylboronic acid took place in presence of 0.1-0.01 mol % of a POCOP pincer-Pd(II) complex **1.145** to give 5790 TON of 4-acetylbiphenyl (Scheme 1.18).[140] Aryl bromide can couple with phenyl boronic acid within a few minutes in presence of a PNCNP pincer-Pd(II) **1.146** based on amino phosphines (Scheme 1.18).[141] *Bis*(oxazole) coordinated NCN pincer-Pd(II) **1.147** (Scheme 1.18) catalyzed Suzuki-Miyaura coupling for the synthesis of biaryls under aerobic conditions with turnover upto 7,90,000.[142] Unsymmetrical SCS' pincer-Pd(II) complex **1.148** (Scheme 1.18) is shown to be an active catalyst for Suzuki-Miyaura coupling reaction.[143] PNCNN pincer-Pd **1.149** bearing phosphinoamino group (Scheme 1.18) is also effective for Suzuki, Sonogashira and Hiyama coupling reactions.[144] The unsymmetrical NCS pincer-Pd complex **1.150** (Scheme 1.18) demonstrated excellent catalytic activity for Suzuki coupling reaction of aryl halides and phenyl boronic acid.[145]

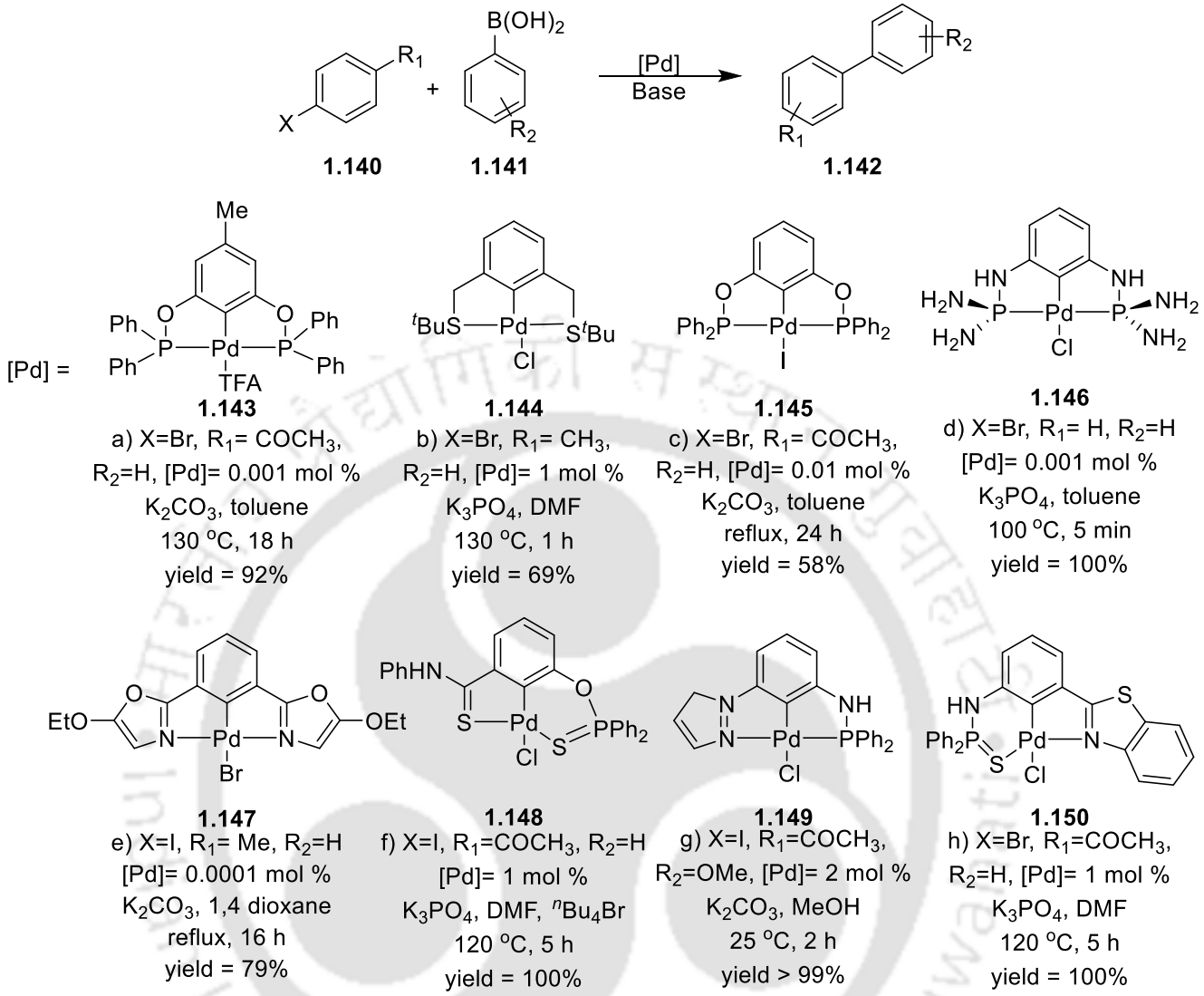

Scheme 1.18: Suzuki cross coupling catalyzed by a) POCOP pincer-Pd(II) complex,[138] b) SCS pincer-Pd(II) pincer,[139] c) POCOP pincer-Pd(II) complex,[140] d) PNCNP pincer-Pd(II) complex.[141] e) *bis*(oxazole) NCN pincer-Pd(II) complex,[142] f) 5- and 6-membered SCS' pincer-Pd(II) complex,[143] g) unsymmetrical PNCNN pincer-Pd(II) complex,[144] h) NCCNPS pincer-Pd(II) complex.[145]

Apart from pincer-Pd, more abundant and bio-compatible metals such as Co[146] and Ni based pincer catalytic systems[147-148] are also known (Scheme 1.19) for catalytic Suzuki-Miyaura cross coupling. Co(II) pincer systems are able to catalyze Suzuki-Miyaura reaction at 80°C under open air. The fine tuning of side arm of the ligand was found to effect the catalytic activity. For instance, increasing the presence of donating nitrogen atoms enhances the catalytic activity. PNNNP Co pincer complex **1.153** thus shows superior catalytic activity than other Co pincer system such as **1.151** and **1.152** (Scheme 1.19).[146]

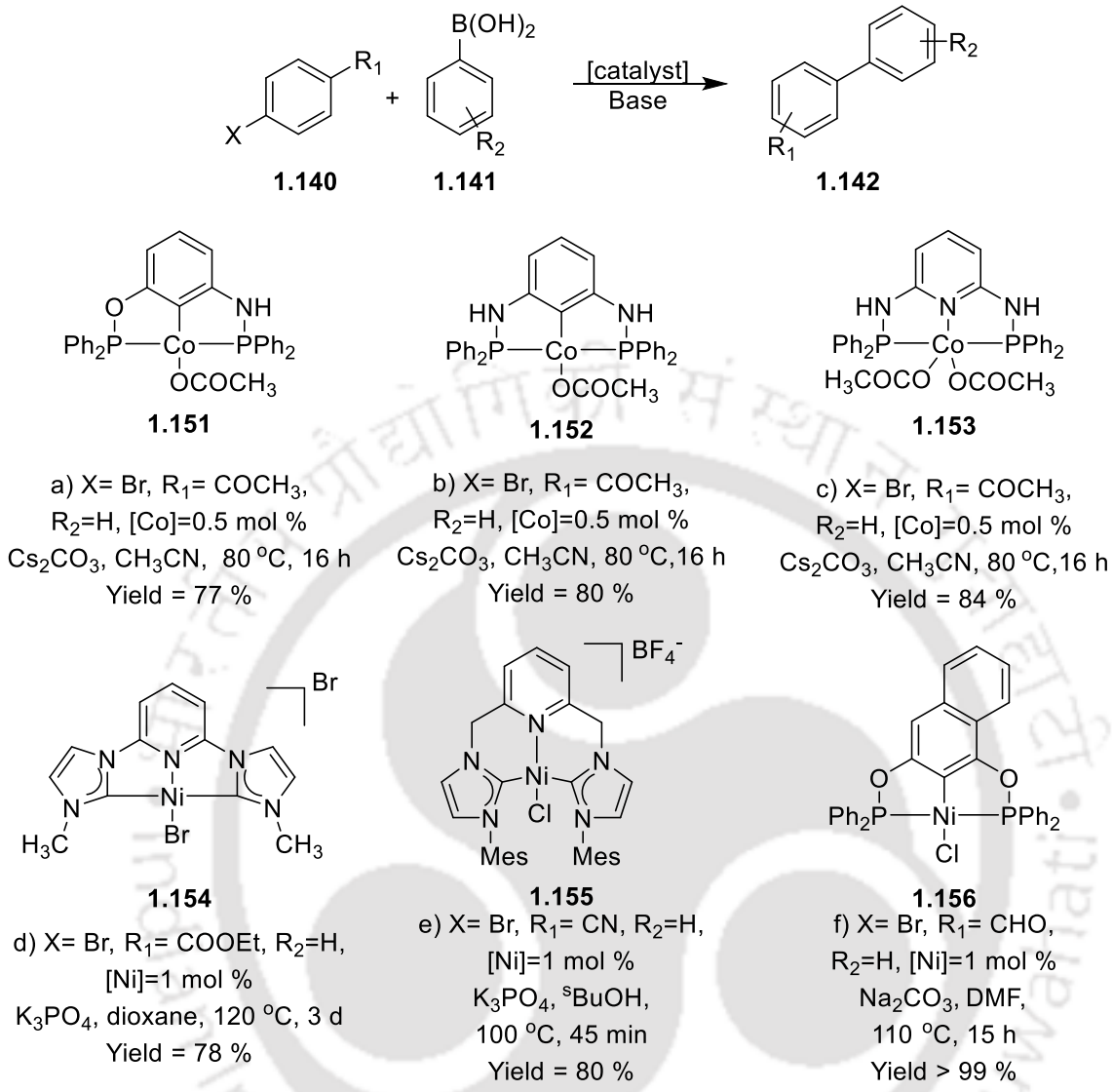

Scheme 1.19: Suzuki-Miyaura cross coupling reaction catalyzed by a) asymmetrical PNCOP pincer-Co,[146] b) symmetrical PNCNP pincer-Co,[146] c) PNNNP pincer-Co,[146] d) *bis*(imidazolin-2-ylidene) pincer-Ni complex,[149] e) *bis*(carbene) derived pincer-Ni complex,[148] f) POCOP pincer-Ni complex,[150]

1.4.4.3 Sonogashira cross-coupling

Sonogashira coupling involves formation of aryl-alkyne or conjugated enyne compounds resulting from the coupling between aryl halide and terminal alkyne moiety (Scheme 1.20).

Unsymmetrical amino phosphine based PCN pincer-Pd complex **1.161** (Scheme 1.20) is effective for coupling of iodo benzene and phenyl acetylene without the use of a typical Cu co-catalyst under mild conditions to obtain 97% of the corresponding product.[144] Furthermore this PCN pincer-Pd complex **1.161** (Scheme 1.20) is shown to be an active catalyst for Suzuki-Miyaura as well as

Heck and Hiyama reaction. Other than Pd, pincer complexes such as **1.162** based on Ni (Scheme 1.20) also catalyzed Sonogashira coupling reaction.[151]

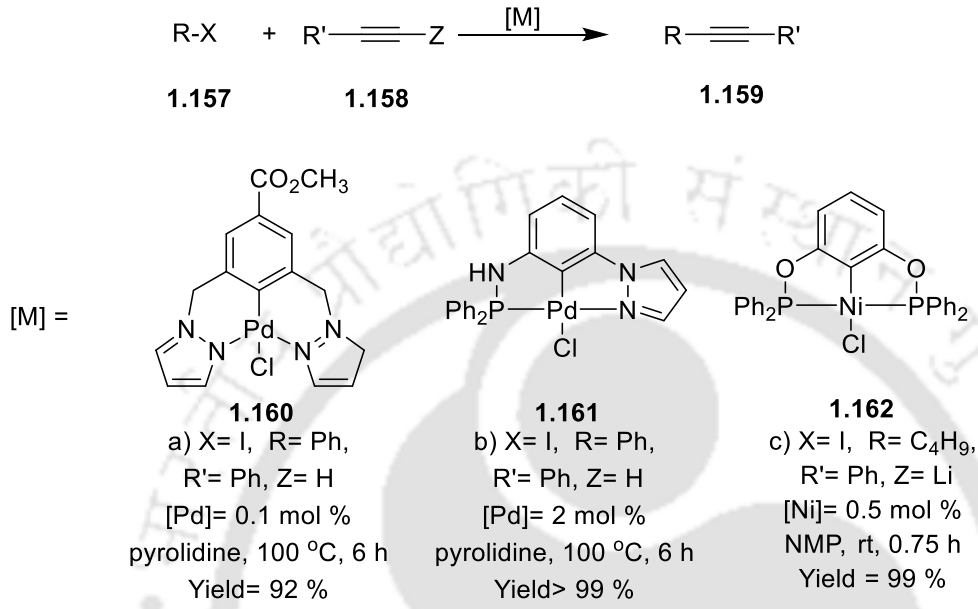

Scheme 1.20: Sonogashira coupling catalyzed by a) *N*-heterocyclic NCN pincer-Pd,[152] b) unsymmetrcal PCN pincer-Pd complex,[144] and c) POCOP pincer-Ni complex.[151]

1.4.4.4 Negishi coupling

The Negishi cross coupling reaction is the coupling between organozinc reagents and aryl halides (Scheme 1.21). Several pincer-Pd and pincer-Ni complexes have been shown to catalyze the Negishi coupling reaction (Scheme 1.21). Lei and co-workers reported high yields in the SNS pincer-Pd **1.166** catalyzed Negishi coupling of aryl iodide and alkyl zinc derivates at very low temperatures (0-20 °C) (Scheme 1.21)[153] and under very low catalyst loading (0.00001 mol %). Other than precious metals, both symmetric and non-symmetric pincer-Ni complexes can effectively catalyze Negishi coupling reaction (Scheme 1.21).[154-155]

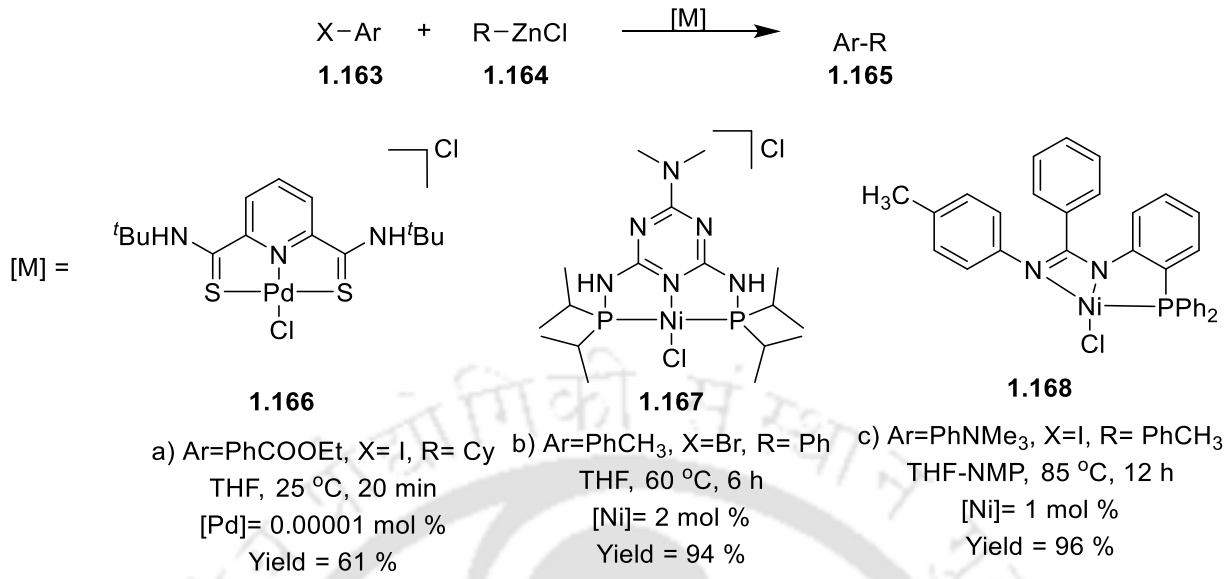

Scheme 1.21: Negishi reaction catalyzed by a) SNS pincer-Pd complex,[153] b) PNP pincer-Ni complex,[154] c) NNP pincer-Ni complex.[155]

1.4.4.5 Kumada-Corriu coupling reaction

The Kumada-Corriu coupling reaction involves the coupling between Grignard reagent and aryl-halide in presence of a catalyst. Nontoxic pincer-metal catalysts based on Ni and Fe were successfully used to carry out Kumada-Corriu coupling reactions (Scheme 1.22). Wang and co-workers reported a series of pincer-Ni catalysts **1.173** which catalyzed Kumada-Corriu coupling reaction under mild conditions (Scheme 1.22).[58] This reaction was successfully carried out to obtain good yields even under very low catalyst loading. Similarly Hu and co-workers demonstrated symmetrical Ni(II) pincer catalytic systems **1.174** for catalyzing the Kumada-Corriu cross coupling of secondary alkyl halides (Scheme 1.22).[156] The same group generated a library of pincer-Fe systems **1.175-1.176** for enantioselective cross-coupling between phenyl magnesium chloride and variety of alkyl chlorides (Scheme 1.22). These pincer-Fe catalyzed Kumada-Corriu coupling reaction is useful for highly chemo-selective synthesis of several natural products in good yields.[157]

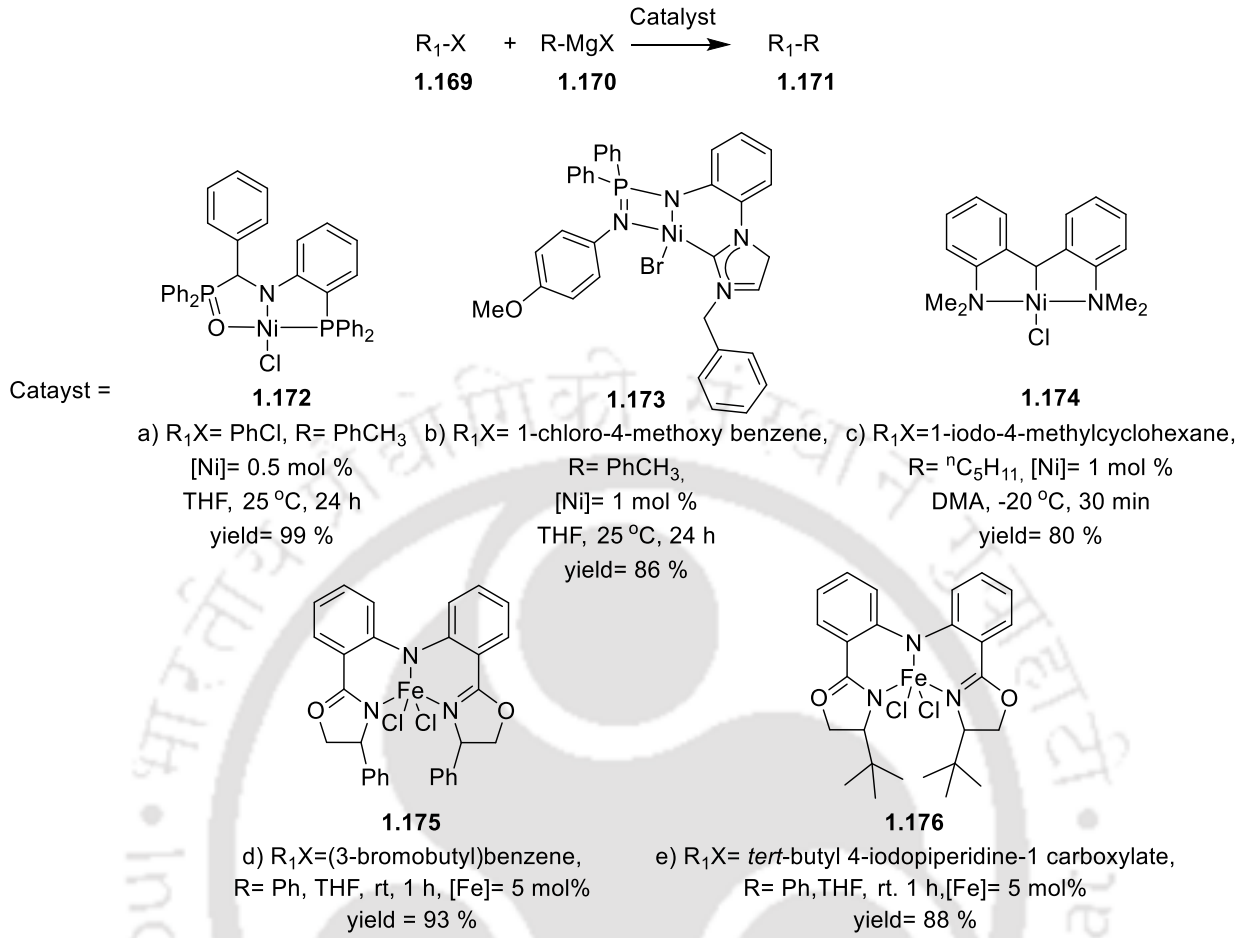

Scheme 1.22: Kumada-Corriu coupling reaction catalyzed by a) unsymmetrical PNO pincer-Ni complex,[158] b) NHC bearing NNC pincer-Ni complex,[58] c) Symmetrical NCN pincer-Ni complex,[156] d) and e) NNN pincer-Fe complex.[157]

1.4.4.6 Allylation of aldehyde

Allylation of aldehyde can be considered as another variety of cross coupling reaction. The SeCSe pincer-Pd complex **1.179** at a low loading (0.02 mol %) gave yields up to 96% in the allylation of benzaldehyde with allyltributyltin (Scheme 1.23). [33] An asymmetric PCN pincer-Pd complex **1.180** when applied for allylation of aldehyde gave a lower yield (67 %) (Scheme 1.23).[159]

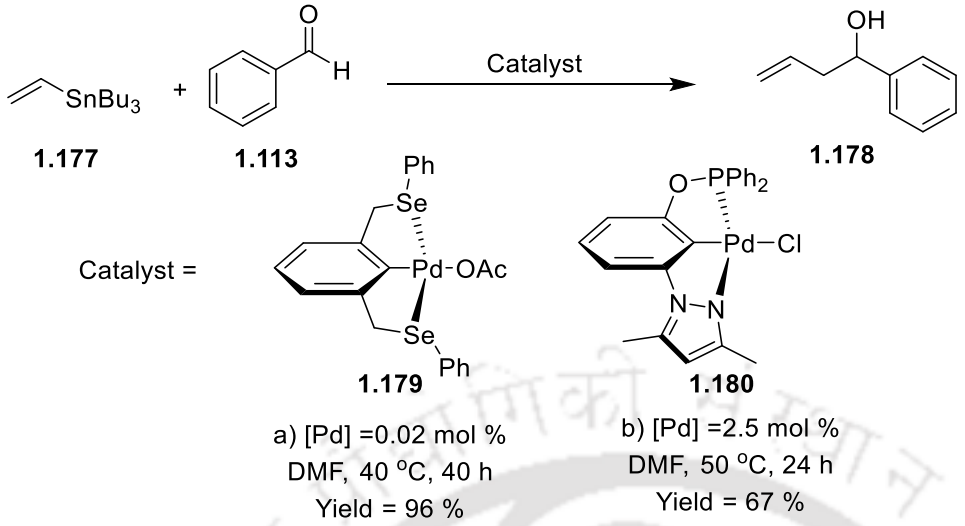

Scheme 1.23: Allylation of benzalehyde with allyltributyltin in presence of a) SeCSe pincer-Pd complex,[33] b) PCN pincer-Pd complex.[159]

1.4.4.7 C-S coupling

Among the cross-coupling reactions, while the C-C coupling reaction is widely explored, the reports on C-S coupling reactions that generate several important natural products are very sparse.

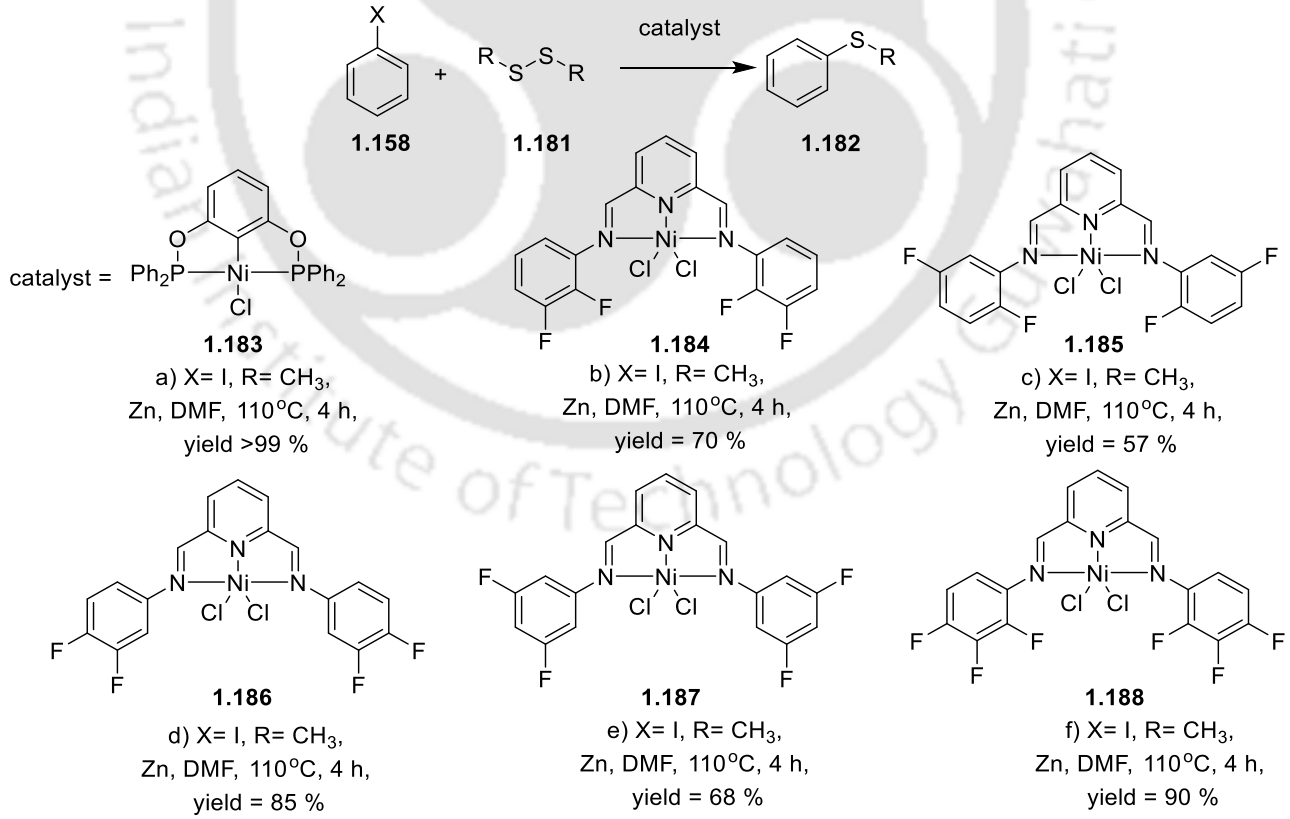

Scheme 1.24: C-S cross coupling using POCOP-Ni pincer complex,[26] and NNN-Ni pincer complex (**1.184-1.188**).[160]

Scheme 1.24 depicts a variety of Ni pincer complexes **1.183-1.188** that have found success in catalyzing C-S couplings. Morales-Morales and co-workers developed a series of Ni(II)-NNN[160] and Ni(II)-POCOP pincer complexes[26] for the cross coupling between halobenzenes and disulphides.

1.4.5 Hydrosilylation of aldehydes and ketones

In 2008, Guan and co-workers studied the utility of Ni-hydride catalyst **1.189** based on pincer ligands for hydrosilylation of aldehydes and ketones (Scheme 1.25).[161]

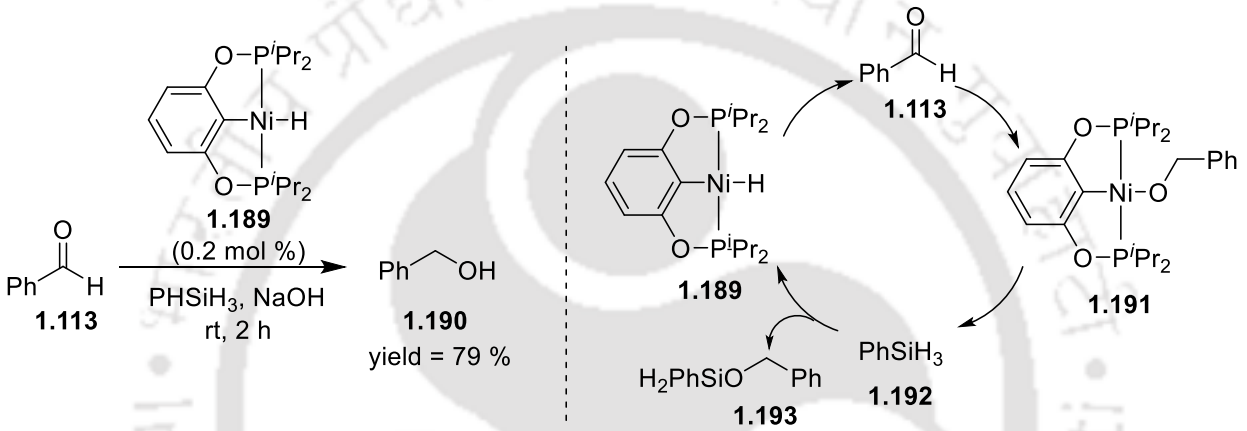

Scheme1.25: Hydrosilylation of aldehydes catalyzed by POCOP-NiH complex.[161]

1.4.6 Hydroamination

Hydroamination reaction involves the addition of hydrogen and an amino group across unsaturated C-C bond. Direct addition of N-H bond to olefin to prepare substituted amine is highly atom-economical, since no by-products are formed. In 2009, Davit Zargarian and co-workers presented a cationic pincer Ni complex **1.197** for hydroamination of cyano-olefins (Scheme 1.26).[162]

In the hydroamination of acetonitrile, reaction proceeds via a mechanism in which the Ni center is acting as Lewis acid for activating olefin towards nucleophilic attack. In 2009, Zargarian proposed a variety of cationic pincer-Ni complexes (**1.198**, **1.199** and **1.200**) and analyzed their structure-activity relationships (Scheme 1.26).[162]

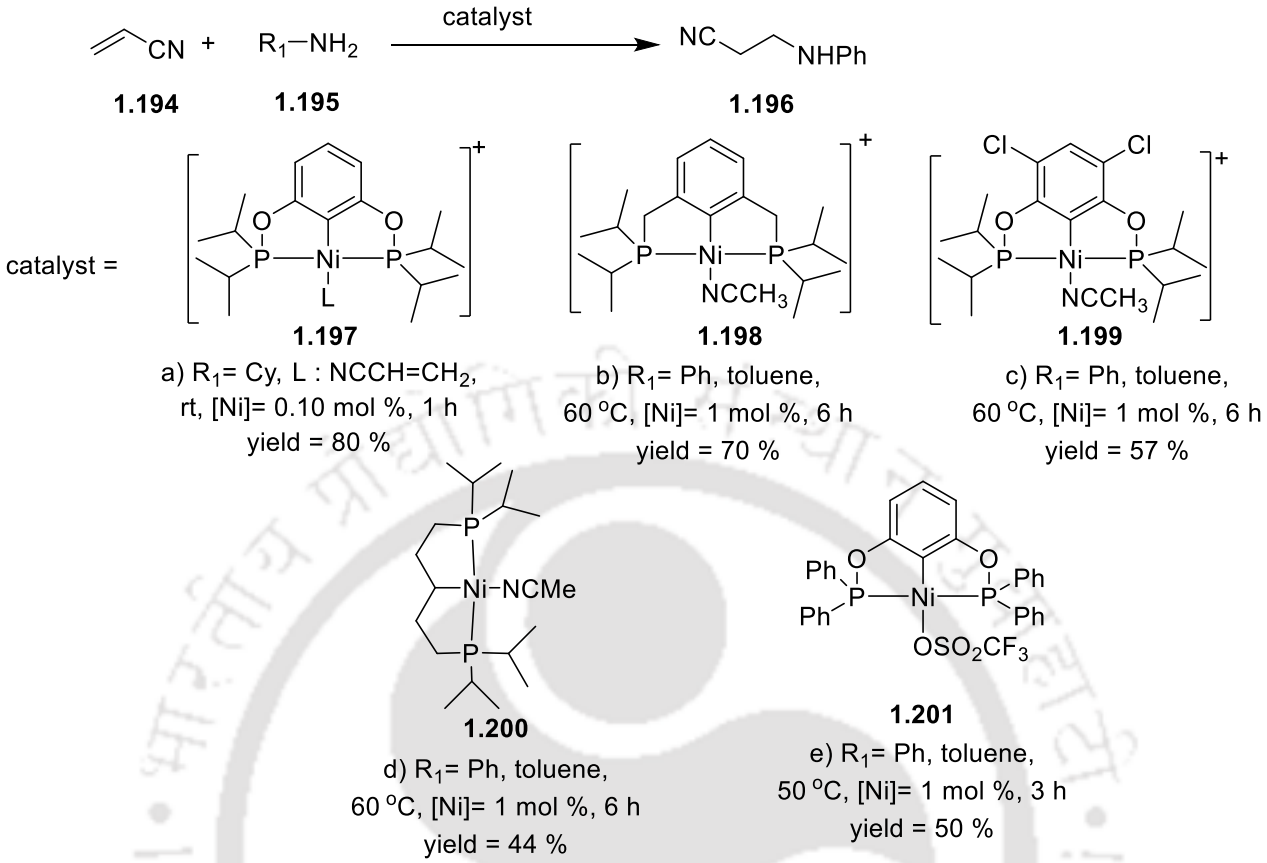

Scheme 1.26: Hydroamination reaction catalyzed by a) cationic (POCOP^{iPr4})Ni(NCMe) pincer complex,[27] b) cationic (PCP^{iPr4})Ni(NCMe) pincer complex,[162] c) cationic (POCOP^{iPr4})Ni(NCMe) pincer complex,[162] d) (PCP^{iPr4})Ni(NCMe) pincer complex,[162] e) (POCOP)Ni(OSO_2CF_3) pincer complex.[163]

1.5 Scope of the present study

The brief review presented above sheds light on the significance of pincer complexes in catalytic organic transformations. The plethora of ligand variations that is available at one's disposal offers promise to create numerous metal-pincer ligand combinations. The rich chemistry of pincer-metal catalysts thus offers several possibilities that are yet to be explored. For instance, while there are several reports on Kharasch addition reactions catalyzed by ruthenium complexes, there are no such studies using a pincer-ruthenium complex. Similarly, the investigations on the catalytic activity of pincer-metal complexes based on environmentally friendly NNN bis(aldimino) pyridine ligands is very sparse. Furthermore, the applicability of phosphine-free pincer complexes based on inexpensive metals in catalysis is still in its infancy.

In the present thesis work, emphasis is laid on testing the catalytic activity of pincer-metal complexes based on less hazardous NNN bis(aldimino) pyridine ligands. The corresponding

pincer-ruthenium complexes have been employed to catalyze radical reactions and reactions that involve tandem dehydrogenation-condensation reactions. With an objective to move away from the use of precious metals and hazardous ligands, phosphine-free pincer-nickel complexes have been utilized to accomplish synthetically useful organic transformations.

The thesis work was taken-up to address the following questions;

1. Can one utilize pincer-ruthenium complexes to bring about the atom transfer radical addition (ATRA) of polyhalogenated methanes to olefins?
2. In addition to reported systems involving phosphine based pincers, is it possible to employ phosphine-free pincer-ruthenium to accomplish the catalytic transformation of glycerol to precious lactic acid?
3. Are phosphine-free pincer-nickel complexes active for catalytic dehydrogenation of alcohols? If so, can we utilize this reactivity to accomplish catalytic *N*-alkylation?
4. How does nickel complexes derived from phosphine-based pincers compare with the corresponding phosphine-free pincer systems towards catalytic cyanomethylation reactions?

1.6 References

1. Hunt, L., *Platin. Met. Rev.* **1984**, *28* (2), 76-83.
2. Mond, L.; Langer, C.; Quincke, F., *J. Chem. Soc., Trans.* **1890**, *57*, 749-753.
3. Español, D. E. F.
4. Shiotsuki, M., *reactions* 9, 26.
5. Ziegler, K.; Holzkamp, E.; Breil, H.; Martin, H., *Angew. Chem.* **1955**, *67* (16), 426-426.
6. Natta, G., *J. Polym. Sci. A Polym. Chem.* **1996**, *34* (3), 321-332.
7. Peris, E.; Crabtree, R. H., *Chem. Soc. Rev.* **2018**, *47* (6), 1959-1968.
8. Lee, D. W.; Jensen, C. M.; Morales-Morales, D., *Organometallics* **2003**, *22* (23), 4744-4749.
9. Moulton, C. J.; Shaw, B. L., *J. Chem. Soc., Dalton Trans.* **1976**, *11*, 1020-1024.
10. Koten, G. v., *Pure Appl. Chem.* **1989**, *61* (10), 1681-1694.
11. Koten, G. v. M. D., **2013**.
12. Choi, J.; Goldman, A., *Top. Organomet. Chem.* **2011**, *34*, 139-167.
13. Choi, J.; MacArthur, A. H. R.; Brookhart, M.; Goldman, A. S., *Chem. Rev.* **2011**, *111* (3), 1761-1779.
14. Kumar, A.; Goldman, A. In *The Privileged Pincer-Metal Platform: Coordination Chemistry & Applications*, van Koten, G., Gossage, R. A., Eds. Springer International Publishing: 2016; Vol. 54, pp 307-334.

15. Bauer, G.; Hu, X., *Inorg. Chem. Front.* **2016**, *3* (6), 741-765.
16. Wang, L.; Pan, H.-R.; Yang, Q.; Fu, H.-Y.; Chen, H.; Li, R.-X., *Inorg. Chem. Commun.* **2011**, *14* (9), 1422-1427.
17. Peris, E.; Loch, J. A.; Mata, J.; Crabtree, R. H., *Chem. Commun.* **2001**, *2*, 201-202.
18. Teratani, T.; Koizumi, T.-a.; Yamamoto, T.; Tanaka, K.; Kanbara, T., *Dalton Trans.* **2011**, *40* (35), 8879-8886.
19. Charette, B. J.; Ritch, J. S., *Inorg. Chem.* **2016**, *55* (12), 6344-6350.
20. Arashiba, K.; Miyake, Y.; Nishibayashi, Y., *Nat. Chem.* **2011**, *3* (2), 120.
21. Danopoulos, A. A.; Tsoureas, N.; Wright, J. A.; Light, M. E., *Organometallics* **2004**, *23* (2), 166-168.
22. Moulton, C. J.; Shaw, B. L., *J. Chem. Soc., Dalton Trans.* **1976**, *11*, 1020-1024.
23. Haenel, M. W.; Jakubik, D.; Krüger, C.; Betz, P., *Chem. Ber.* **1991**, *124* (2), 333-336.
24. Kozhanov, K. A.; Bubnov, M. P.; Cherkasov, V. K.; Fukin, G. K.; Abakumov, G. A., *Dalton Trans.* **2004**, *18*, 2957-2962.
25. Benito-Garagorri, D.; Bocokić, V.; Mereiter, K.; Kirchner, K., *Organometallics* **2006**, *25* (16), 3817-3823.
26. Gómez-Benítez, V.; Baldovino-Pantaleón, O.; Herrera-Alvarez, C.; Toscano, R. A.; Morales-Morales, D., *Tetrahedron Lett.* **2006**, *47* (29), 5059-5062.
27. Pandarus, V.; Zargarian, D., *Organometallics* **2007**, *26* (17), 4321-4334.
28. Lawrence, M. A.; Green, K.-A.; Nelson, P. N.; Lorraine, S. C., *Polyhedron* **2018**, *143*, 11-
29. Artero, V.; Fontecave, M., *Coord. Chem. Rev.* **2005**, *249* (15-16), 1518-1535.
30. Mao, L.; Bertermann, R.; Rachor, S. G.; Szabó, K. J.; Marder, T. B., *Org. Lett.* **2017**, *19* (24), 6590-6593.
31. Takahashi, S.; Nonoyama, M.; Kita, M., *Transit. Met. Chem.* **1995**, *20* (6), 528-532.
32. Cao, X.-N.; Wan, X.-M.; Yang, F.-L.; Li, K.; Hao, X.-Q.; Shao, T.; Zhu, X.; Song, M.-P., *J. Org. Chem.* **2018**, *83* (7), 3657-3668.
33. Yao, Q.; Sheets, M., *J. Org. Chem.* **2006**, *71* (14), 5384-5387.
34. Wang, S.; Ren, F.; Qiu, Y.; Luo, M., *J. Organomet. Chem.* **2015**, *788*, 27-32.
35. Komiyama, Y.; Kuwabara, J.; Kanbara, T., *Organometallics* **2014**, *33* (4), 885-891.
36. Ilie, A.; Laguna, A.; Silvestru, C., *C. R. Chim.* **2012**, *15* (10), 895-903.
37. Rubio, R. J.; Andavan, G. T. S.; Bauer, E. B.; Hollis, T. K.; Cho, J.; Tham, F. S.; Donnadieu, B., *J. Organomet. Chem.* **2005**, *690* (23), 5353-5364.
38. Asay, M.; Morales-Morales, D., *Dalton Trans.* **2015**, *44* (40), 17432-17447.
39. Gandelman, M.; Vigalok, A.; Shimon, L. J. W.; Milstein, D., *Organometallics* **1997**, *16* (18), 3981-3986.
40. Lawrence, M. A.; Jackson, Y. A.; Mulder, W. H.; Björemark, P. M.; Håkansson, M., *Aust. J. Chem.* **2015**, *68* (5), 731-741.
41. Marchetti, F.; Pampaloni, G., *Chem. Commun.* **2012**, *48* (5), 635-653.
42. Thomson, J. E.; Campbell, C. D.; Concellón, C.; Duguet, N.; Rix, K.; Slawin, A. M.; Smith, A. D., *J. Org. Chem.* **2008**, *73* (7), 2784-2791.
43. Wanzlick, H., *Angew. Chem. Int. Ed. in English* **1962**, *1* (2), 75-80.
44. Arduengo III, A. J.; Harlow, R. L.; Kline, M., *J. Am. Chem. Soc.* **1991**, *113* (1), 361-363.
45. Lappert, M. F., *J. Organomet. Chem.* **1988**, *358* (1-3), 185-213.
46. Wanzlick, H. W.; Schönherr, H. J., *Angew. Chem. Int. Ed. in English* **1968**, *7* (2), 141-142.
47. Bortoluzzi, M.; Ferretti, E.; Marchetti, F.; Pampaloni, G.; Zacchini, S., *Chem. Commun.* **2014**, *50* (34), 4472-4474.

48. Bortoluzzi, M.; Ferretti, E.; Marchetti, F.; Pampaloni, G.; Zacchini, S., *Dalton Trans.* **2016**, *45* (16), 6939-6948.
49. Spencer, L. P.; Beddie, C.; Hall, M. B.; Fryzuk, M. D., *J. Am. Chem. Soc.* **2006**, *128* (38), 12531-12543.
50. Dagorne, S.; Bellemin-Laponnaz, S.; Romain, C., *Organometallics* **2013**, *32* (9), 2736-2743.
51. McGuinness, D. S.; Gibson, V. C.; Wass, D. F.; Steed, J. W., *J. Am. Chem. Soc.* **2003**, *125* (42), 12716-12717.
52. McGuinness, D. S.; Gibson, V. C.; Steed, J. W., *Organometallics* **2004**, *23* (26), 6288-6292.
53. Pugh, D.; Danopoulos, A. A., *Coord. Chem. Rev.* **2007**, *251* (5-6), 610-641.
54. Iwasaki, F.; Yasui, M.; Yoshida, S.; Nishiyama, H.; Shimamoto, S.; Matsumura, N., *Bull. Chem. Soc. Jpn.* **1996**, *69* (10), 2759-2770.
55. Vabre, B.; Canac, Y.; Duhayon, C.; Chauvin, R.; Zargarian, D., *Chem. Commun.* **2012**, *48* (84), 10446-10448.
56. Sun, Y.; Li, X.; Sun, H., *Dalton Trans.* **2014**, *43* (25), 9410-9413.
57. Zhang, C.; Wang, Z.-X., *Organometallics* **2009**, *28* (22), 6507-6514.
58. Guo, W.-J.; Wang, Z.-X., *J. Org. Chem.* **2013**, *78* (3), 1054-1061.
59. Langer, R.; Diskin-Posner, Y.; Leitus, G.; Shimon, L. J.; Ben-David, Y.; Milstein, D., *Angew. Chem. Int. Ed.* **2011**, *50* (42), 9948-9952.
60. Kim, Y.-E.; Kim, J.; Lee, Y., *Chem. Commun.* **2014**, *50* (78), 11458-11461.
61. van der Vlugt, J. I.; Lutz, M.; Pidko, E. A.; Vogt, D.; Spek, A. L., *Dalton Trans.* **2009**, *6*, 1016-1023.
62. Clarke, Z. E.; Maragh, P. T.; Dasgupta, T. P.; Gusev, D. G.; Lough, A. J.; Abdur-Rashid, K., *Organometallics* **2006**, *25* (17), 4113-4117.
63. Zell, T.; Langer, R.; Iron, M. A.; Konstantinovski, L.; Shimon, L. J.; Diskin-Posner, Y.; Leitus, G.; Balaraman, E.; Ben-David, Y.; Milstein, D., *Inorg. Chem.* **2013**, *52* (16), 9636-9649.
64. Hao, X.-Q.; Xu, Y.-X.; Yang, M.-J.; Wang, L.; Niu, J.-L.; Gong, J.-F.; Song, M.-P., *Organometallics* **2012**, *31* (3), 835-846.
65. Rossin, A.; Peruzzini, M.; Zanobini, F., *Dalton Trans.* **2011**, *40* (17), 4447-4452.
66. Zheng, Y. Rational design and synthesize sterically less hindered pincer-iridium catalysts for alkane dehydrogenation. Rutgers University-Graduate School-New Brunswick, 2015.
67. Renkema, K. B.; Kissin, Y. V.; Goldman, A. S., *J. Am. Chem. Soc.* **2003**, *125* (26), 7770-7771.
68. Mohammad, H. A. Y.; Grimm, J. C.; Eichele, K.; Mack, H.-G.; Speiser, B.; Novak, F.; Quintanilla, M. G.; Kaska, W. C.; Mayer, H. A., *Organometallics* **2002**, *21* (26), 5775-5784.
69. Romero, P. E.; Whited, M. T.; Grubbs, R. H., *Organometallics* **2008**, *27* (14), 3422-3429.
70. Morales-Morales, D.; Redón, R. o.; Yung, C.; Jensen, C. M., *Inorg. Chim. Acta.* **2004**, *357* (10), 2953-2956.
71. Göttker-Schnetmann, I.; White, P.; Brookhart, M., *J. Am. Chem. Soc.* **2004**, *126* (6), 1804-1811.
72. Kundu, S.; Choliy, Y.; Zhuo, G.; Ahuja, R.; Emge, T. J.; Warmuth, R.; Brookhart, M.; Krogh-Jespersen, K.; Goldman, A. S., *Organometallics* **2009**, *28* (18), 5432-5444.

73. Grove, D.; Van Koten, G.; Ubbels, H.; Zoet, R.; Spek, A., *Organometallics* **1984**, *3* (7), 1003-1009.
74. Grove, D. M.; Van Koten, G.; Louwen, J. N.; Noltes, J. G.; Spek, A. L.; Ubbels, H. J., *J. Am. Chem. Soc.* **1982**, *104* (24), 6609-6616.
75. Grove, D. M.; Van Koten, G.; Mul, P.; Zoet, R.; Van der Linden, J. G.; Legters, J.; Schmitz, J. E.; Murrall, N. W.; Welch, A. J., *Inorg. Chem.* **1988**, *27* (14), 2466-2473.
76. Martinez, G. E.; Ocampo, C.; Park, Y. J.; Fout, A. R., *J. Am. Chem. Soc.* **2016**, *138* (13), 4290-4293.
77. Thompson, C. V.; Arman, H. D.; Tonzetich, Z. J., *Organometallics* **2017**, *36* (9), 1795-1802.
78. Breitenfeld, J.; Ruiz, J.; Wodrich, M. D.; Hu, X., *J. Am. Chem. Soc.* **2013**, *135* (32), 12004-12012.
79. Crabtree, R. H., *The organometallic chemistry of the transition metals*. John Wiley & Sons: 2009.
80. Poverenov, E.; Gandelman, M.; Shimon, L. J. W.; Rozenberg, H.; Ben-David, Y.; Milstein, D., *Organometallics* **2005**, *24* (6), 1082-1090.
81. Suárez, E.; Plou, P.; Gusev, D. G.; Martín, M.; Sola, E., *Inorg. Chem.* **2017**, *56* (12), 7190-7199.
82. Bernal, M. J.; Martín, M.; Sola, E., *Z. Anorg. Allg. Chem.* **2015**, *641* (12-13), 2122-2128.
83. Adams, J. J.; Arulsamy, N.; Roddick, D. M., *Organometallics* **2011**, *30* (4), 697-711.
84. Wang, Z.; Eberhard, M. R.; Jensen, C. M.; Matsukawa, S.; Yamamoto, Y., *J. Organomet. Chem.* **2003**, *681* (1-2), 189-195.
85. Ghavale, N.; Manjare, S. T.; Singh, H. B.; Butcher, R. J., *Dalton Trans.* **2015**, *44* (26), 11893-11900.
86. Kumar, A.; Bhatti, T. M.; Goldman, A. S., *Chem. Rev.* **2017**, *117* (19), 12357-12384.
87. Das, K.; Kumar, A. In *Advances in Organometallic Chemistry*, Elsevier: 2019; Vol. 72, pp 1-57.
88. Burk, M. J.; Crabtree, R. H., *J. Am. Chem. Soc.* **1987**, *109* (26), 8025-8032.
89. Kumar, A.; Goldman, A. S. In *The Privileged Pincer-Metal Platform: Coordination Chemistry & Applications*, Springer: 2015; pp 307-334.
90. Peris, E.; Crabtree, R. H., *Coord. Chem. Rev.* **2004**, *248* (21-24), 2239-2246.
91. Morales-Morales, D.; Jensen, C. G., *The chemistry of pincer compounds*. Elsevier: 2011.
92. Dani, P.; Karlen, T.; Gossage, R. A.; Gladiali, S.; van Koten, G., *Angew. Chem.* **2000**, *112* (4), 759-761.
93. Amoroso, D.; Jabri, A.; Yap, G. P.; Gusev, D. G.; dos Santos, E. N.; Fogg, D. E., *Organometallics* **2004**, *23* (17), 4047-4054.
94. Gagliardo, M.; Chase, P. A.; Brouwer, S.; van Klink, G. P.; van Koten, G., *Organometallics* **2007**, *26* (9), 2219-2227.
95. Medici, S.; Gagliardo, M.; Williams, S. B.; Chase, P. A.; Gladiali, S.; Lutz, M.; Spek, A. L.; van Klink, G. P.; van Koten, G., *Helv. Chim. Acta.* **2005**, *88* (3), 694-705.
96. Naota, T.; Takaya, H.; Murahashi, S.-I., *Chem. Rev.* **1998**, *98* (7), 2599-2660.
97. Spogliarich, R.; Zassinovich, G.; Mestroni, G.; Graziani, M., *J. Organomet. Chem.* **1980**, *198* (1), 81-86.
98. Vega, E.; Lastra, E.; Gamasa, M. P., *Inorg. Chem.* **2013**, *52* (10), 6193-6198.
99. Paredes, P.; Díez, J.; Gamasa, M. P., *Organometallics* **2008**, *27* (11), 2597-2607.

100. Ye, W.; Zhao, M.; Du, W.; Jiang, Q.; Wu, K.; Wu, P.; Yu, Z., *Chem. Eur. J.* **2011**, *17* (17), 4737-4741.
101. Cuervo, D.; Gamasa, M. P.; Gimeno, J., *Chem. Eur. J.* **2004**, *10* (2), 425-432.
102. Ye, W.; Zhao, M.; Yu, Z., *Chem. Eur. J.* **2012**, *18* (35), 10843-10846.
103. Ito, J.-i.; Nishiyama, H., *Tetrahedron Lett.* **2014**, *55* (20), 3133-3146.
104. Noyori, R.; Kitamura, M.; Ohkuma, T., *Acc. Chem. Res.* **1997**, *30*, 97-102.
105. Murata, K.; Ikariya, T.; Noyori, R., *J. Org. Chem.* **1999**, *64* (7), 2186-2187.
106. Baratta, W.; Ballico, M.; Chelucci, G.; Siega, K.; Rigo, P., *Angew. Chem. Int. Ed.* **2008**, *47* (23), 4362-4365.
107. Tanaka, R.; Yamashita, M.; Nozaki, K., *J. Am. Chem. Soc.* **2009**, *131* (40), 14168-14169.
108. Debleds, O.; Zotto, C. D.; Vrancken, E.; Campagne, J. M.; Retailleau, P., *Adv. Synth. Catal.* **2009**, *351* (11-12), 1991-1998.
109. Zhang, G.; Hanson, S. K., *Chem.Commun.* **2013**, *49* (86), 10151-10153.
110. Elangovan, S.; Topf, C.; Fischer, S.; Jiao, H.; Spannenberg, A.; Baumann, W.; Ludwig, R.; Junge, K.; Beller, M., *J. Am. Chem. Soc.* **2016**, *138* (28), 8809-8814.
111. Elangovan, S.; Garbe, M.; Jiao, H.; Spannenberg, A.; Junge, K.; Beller, M., *Angew. Chem. Int. Ed.* **2016**, *55* (49), 15364-15368.
112. Crabtree, R. H.; Mihelcic, J. M.; Quirk, J. M., *J. Am. Chem. Soc.* **1979**, *101* (26), 7738-7740.
113. Aoki, T.; Crabtree, R. H., *Organometallics* **1993**, *12* (2), 294-298.
114. Jensen, C., *Chem. Commun.* **1999**, *24*, 2443-2449.
115. Kanzelberger, M.; Singh, B.; Czerw, M.; Krogh-Jespersen, K.; Goldman, A. S., *J. Am. Chem. Soc.* **2000**, *122* (44), 11017-11018.
116. Six, C.; Gabor, B.; Görls, H.; Mynott, R.; Philipps, P.; Leitner, W., *Organometallics* **1999**, *18* (17), 3316-3326.
117. Gupta, M.; Hagen, C.; Flesher, R. J.; Kaska, W. C.; Jensen, C. M., *Chem. Commun.* **1996**, *17*, 2083-2084.
118. Liu, F.; Pak, E. B.; Singh, B.; Jensen, C. M.; Goldman, A. S., *J. Am. Chem. Soc.* **1999**, *121* (16), 4086-4087.
119. Goldman, A., *Chem. Commun.* **1999**, *7*, 655-656.
120. Shi, Y.; Suguri, T.; Dohi, C.; Yamada, H.; Kojima, S.; Yamamoto, Y., *Chem. Eur. J.* **2013**, *19* (32), 10672-10689.
121. Zhang, J.; Balaraman, E.; Leitus, G.; Milstein, D., *Organometallics* **2011**, *30* (21), 5716-5724.
122. Musa, S.; Shaposhnikov, I.; Cohen, S.; Gelman, D., *Angew. Chem. Int. Ed.* **2011**, *50* (15), 3533-3537.
123. Hallman, P.; Stephenson, T.; Wilkinson, G., *Inorg. Synth.*, **2007**, *12*, 237-240.
124. Gunanathan, C.; Shimon, L. J. W.; Milstein, D., *J. Am. Chem. Soc.* **2009**, *131* (9), 3146-3147.
125. Gunanathan, C.; Shimon, L. J.; Milstein, D., *J. Am. Chem. Soc.* **2009**, *131* (9), 3146-3147.
126. Bielinski, E. A.; Förster, M.; Zhang, Y.; Bernskoetter, W. H.; Hazari, N.; Holthausen, M. C., *ACS Catal.* **2015**, *5* (4), 2404-2415.
127. Andérez-Fernández, M.; Vogt, L. K.; Fischer, S.; Zhou, W.; Jiao, H.; Garbe, M.; Elangovan, S.; Junge, K.; Junge, H.; Ludwig, R., *Angew. Chem. Int. Ed.* **2017**, *56* (2), 559-562.

128. Alberico, E.; Lennox, A. J.; Vogt, L. K.; Jiao, H.; Baumann, W.; Drexler, H.-J.; Nielsen, M.; Spannenberg, A.; Checinski, M. P.; Junge, H., *J. Am. Chem. Soc.* **2016**, *138* (45), 14890-14904.
129. Gonzalez-Sebastian, L.; Morales-Morales, D., *J. Organomet. Chem.* **2019**, *893*, 39-51.
130. Nolan, S.; Navarro, O., *Comprehensive Organometallic Chemistry III* **2007**, *11*, 1-38.
131. Ohff, M.; Ohff, A.; van der Boom, M. E.; Milstein, D., *J. Am. Chem. Soc.* **1997**, *119* (48), 11687-11688.
132. Naghipour, A.; Sabounchei, S.; Morales-Morales, D.; Canseco-González, D.; Jensen, C. M., *Polyhedron* **2007**, *26* (7), 1445-1448.
133. Yoon, M. S.; Ryu, D.; Kim, J.; Ahn, K. H., *Organometallics* **2006**, *25* (10), 2409-2411.
134. Tyson, G. E.; Tokmic, K.; Oian, C. S.; Rabinovich, D.; Valle, H. U.; Hollis, T. K.; Kelly, J. T.; Cuellar, K. A.; McNamara, L. E.; Hammer, N. I., *Dalton Trans.* **2015**, *44* (32), 14475-14482.
135. Takenaka, K.; Minakawa, M.; Uozumi, Y., *J. Am. Chem. Soc.* **2005**, *127* (35), 12273-12281.
136. Debono, N.; Iglesias, a. M.; Sanchez, F., *Adv. Synth. Catal.* **2007**, *349* (16), 2470-2476.
137. Yoon, M. S.; Ryu, D.; Kim, J.; Ahn, K. H., *Organometallics* **2006**, *25* (10), 2409-2411.
138. Bedford, R. B.; Draper, S. M.; Scully, P. N.; Welch, S. L., *New J. Chem.* **2000**, *24* (10), 745-747.
139. Zim, D.; Gruber, A. S.; Ebeling, G.; Dupont, J.; Monteiro, A. L., *Org. Lett.* **2000**, *2* (18), 2881-2884.
140. Kimura, T.; Uozumi, Y., *Organometallics* **2006**, *25* (20), 4883-4887.
141. Bolliger, J. L.; Blacque, O.; Frech, C. M., *Angew. Chem. Int. Ed.* **2007**, *46* (34), 6514-6517.
142. Luo, Q.; Eibauer, S.; Reiser, O., *J. Mol. Catal. A Chem.* **2007**, *268* (1-2), 65-69.
143. Aleksanyan, D.; Kozlov, V.; Nelyubina, Y. V.; Lyssenko, K.; Puntus, L.; Gutsul, E.; Shepel, N.; Vasil'ev, A.; Petrovskii, P.; Odinets, I., *Dalton Trans.* **2011**, *40* (7), 1535-1546.
144. Ines, B.; SanMartin, R.; Churruca, F.; Dominguez, E.; Urtiaga, M. K.; Arriortua, M. I., *Organometallics* **2008**, *27* (12), 2833-2839.
145. Kozlov, V.; Aleksanyan, D.; Nelyubina, Y. V.; Lyssenko, K.; Vasil'ev, A.; Petrovskii, P.; Odinets, I., *Organometallics* **2010**, *29* (9), 2054-2062.
146. Kumar, L. M.; Bhat, B. R., *J. Organomet. Chem.* **2017**, *827*, 41-48.
147. Inamoto, K.; Kuroda, J.-i.; Hiroya, K.; Noda, Y.; Watanabe, M.; Sakamoto, T., *Organometallics* **2006**, *25* (12), 3095-3098.
148. Inamoto, K.; Kuroda, J.-i.; Kwon, E.; Hiroya, K.; Doi, T., *J. Organomet. Chem.* **2009**, *694* (3), 389-396.
149. Inamoto, K.; Kuroda, J.-i.; Hiroya, K.; Noda, Y.; Watanabe, M.; Sakamoto, T., *Organometallics* **2006**, *25* (12), 3095-3098.
150. Estudiante-Negrete, F.; Hernández-Ortega, S.; Morales-Morales, D., *Inorg. Chim. Acta.* **2012**, *387*, 58-63.
151. Xu, G.; Li, X.; Sun, H., *J. Organomet. Chem.* **2011**, *696* (18), 3011-3014.
152. Churruca, F.; SanMartin, R.; Tellitu, I.; Dominguez, E., *Synlett.* **2005**, *2005* (20), 3116-3120.
153. Wang, H.; Liu, J.; Deng, Y.; Min, T.; Yu, G.; Wu, X.; Yang, Z.; Lei, A., *Chem. Eur. J.* **2009**, *15* (6), 1499-1507.

154. Mastalir, M.; Kirchner, K., *Monatsh. Chem.* **2017**, *148* (1), 105-109.
155. Zhang, X.-Q.; Wang, Z.-X., *J. Org. Chem.***2012**, *77* (7), 3658-3663.
156. Perez Garcia, P. M.; Di Franco, T.; Orsino, A.; Ren, P.; Hu, X., *Org. Lett.* **2012**, *14* (16), 4286-4289.
157. Bauer, G.; Wodrich, M. D.; Scopelliti, R.; Hu, X., *Organometallics* **2015**, *34* (1), 289-298.
158. Liu, N.; Wang, Z.-X., *J. Org. Chem.* **2011**, *76* (24), 10031-10038.
159. Hou, A.-T.; Liu, Y.-J.; Hao, X.-Q.; Gong, J.-F.; Song, M.-P., *J. Organomet. Chem.* **2011**, *696* (15-16), 2857-2862.
160. Baldovino-Pantaleon, O.; Hernández-Ortega, S.; Morales-Morales, D., *Adv. Synth. Catal.* **2006**, *348* (1-2), 236-242.
161. Chakraborty, S.; Krause, J. A.; Guan, H., *Organometallics* **2008**, *28* (2), 582-586.
162. Castonguay, A.; Spasyuk, D. M.; Madern, N.; Beauchamp, A. L.; Zargarian, D., *Organometallics* **2009**, *28* (7), 2134-2141.
163. Salah, A. B.; Offenstein, C.; Zargarian, D., *Organometallics* **2011**, *30* (20), 5352-5364.

Chapter 2

Experimental and Computational Studies on Pincer–Ruthenium Catalyzed Atom Transfer Radical Addition of Carbon Tetrachloride to Styrene

2.1 Introduction

Alkanes constitute a major proportion of global hydrocarbon reservoir and are highly unproductive except for a small fraction (C_9–C_{19}) that find utility as fuels. On the other hand, the corresponding olefins are less abundant but versatile intermediates to a plethora of utility chemicals of pharmaceutical, agrochemical and industrial (food, polymers) importance.[1] Routes that accomplish the transformation of either alkanes to alkenes or alkenes to value–added compounds (Figure 2.1) are of high synthetic value.[2] One such transformation involves the addition of polyhalogenated methanes across the double bond of olefins in either thermal or photochemical conditions pioneered by Kharasch in 1947 and hence rightly named as the Kharasch reaction.[3] Since the Kharasch addition involves a free radical chain reaction, it is also called as atom transfer radical addition (ATRA).[4] Notably, the Kharasch addition preferentially gives anti-Markovnikov's product.

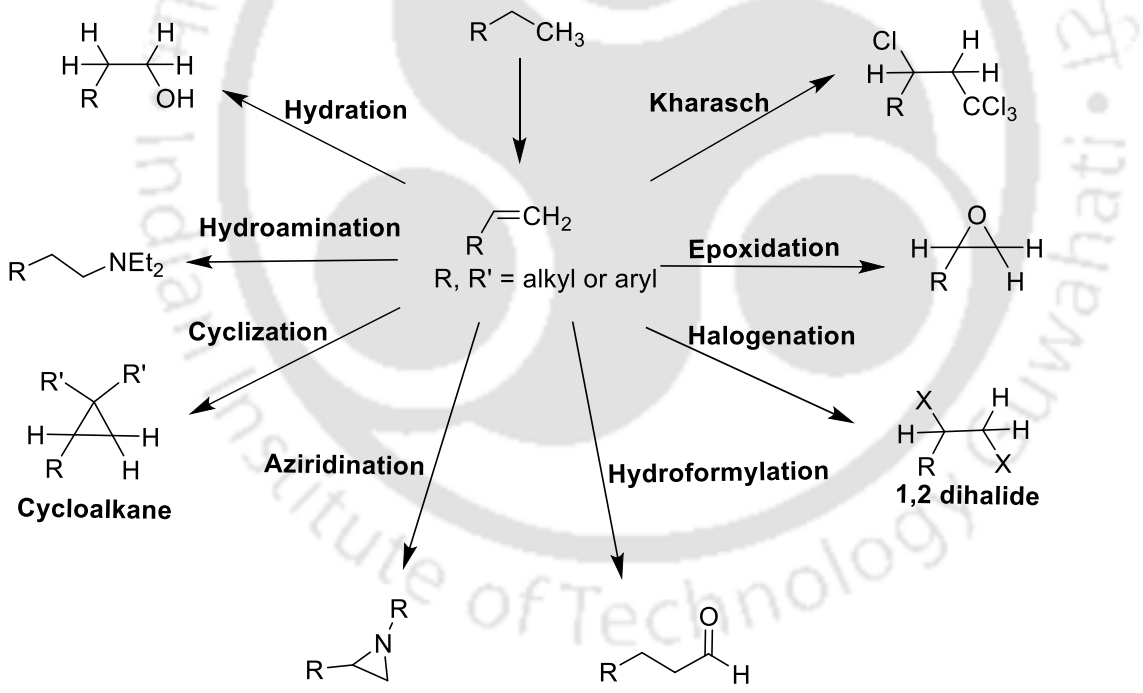

Figure 2.1: Olefins as versatile intermediates to several value-added products.

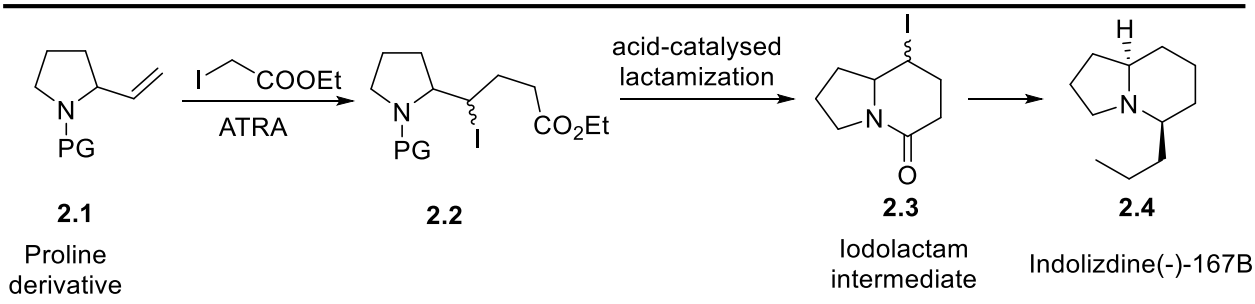

Scheme 2.1: Synthesis of alkaloids involving Kharasch addition as one of the steps.[5]

The ATRA product could be used in further radical or ionic reactions[6] which makes ATRA one of the most powerful tools in organic synthesis. Not surprisingly, ATRA has several applications that include synthesis of natural products[7] with pharmacological properties.[8] For instance, indolizidine alkaloids which belongs to a family of natural products are significantly useful due to their simple structure as well as their activity as moderator of neuromuscular transmission. Cordero-Vargas has shown that indolizidine alkaloids could be obtained starting from ATRA of ethyl iodoacetate to a proline derivative **2.1** followed by acid catalyzed lactamization of the ATRA product **2.2** to give the iodolactam intermediate **2.3**. Subsequently, **2.3** could be easily transformed to the indolizidine **2.4** (Scheme 2.1).[5]

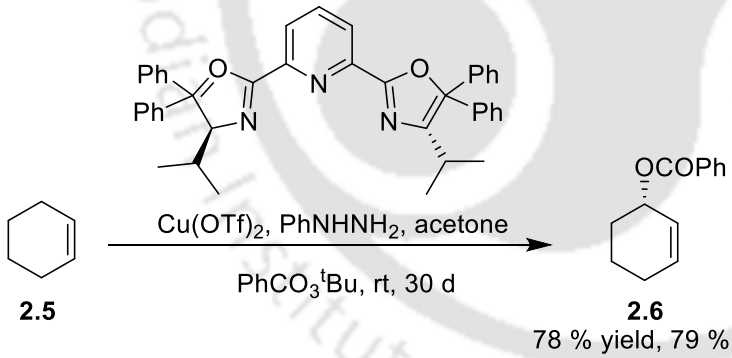

Scheme 2.2: Catalytic enantioselective allylic oxidation of cyclohexene.[9]

Asymmetric allylic ester would eventually generate chiral allylic alcohols which are essential building blocks in organic synthesis.[10-12] In 1998, Singh and co-workers used chiral pyridine *bis*(diphenyloxazoline) ligand coordinated with Cu for the enantioselective allylic oxidation of olefins (Scheme 2.2).[9] In this case, it is assumed that the mechanism followed is a free radical ATRA reaction. The *tert*-butoxy radical abstracts an allylic hydrogen to give *tert*-butyl alcohol

and allylic radical. Next the Cu(II) benzoate adds to the allylic radical to generate allylic benzoate via a six-membered cyclic transition state. The use of $PhNHNH_2$ in the presence of acetone increased the rate of the reaction.

2.2 History of Kharasch reaction

The origin of Kharasch or atom transfer radical addition (ATRA) reaction is associated with the peroxide effect, which was revealed by Kharasch and his co-workers. In 1937, they observed the anti-Markovnikov addition of HBr to unsymmetrical alkenes in the presence of peroxide initiators (Scheme 2.3).[13]

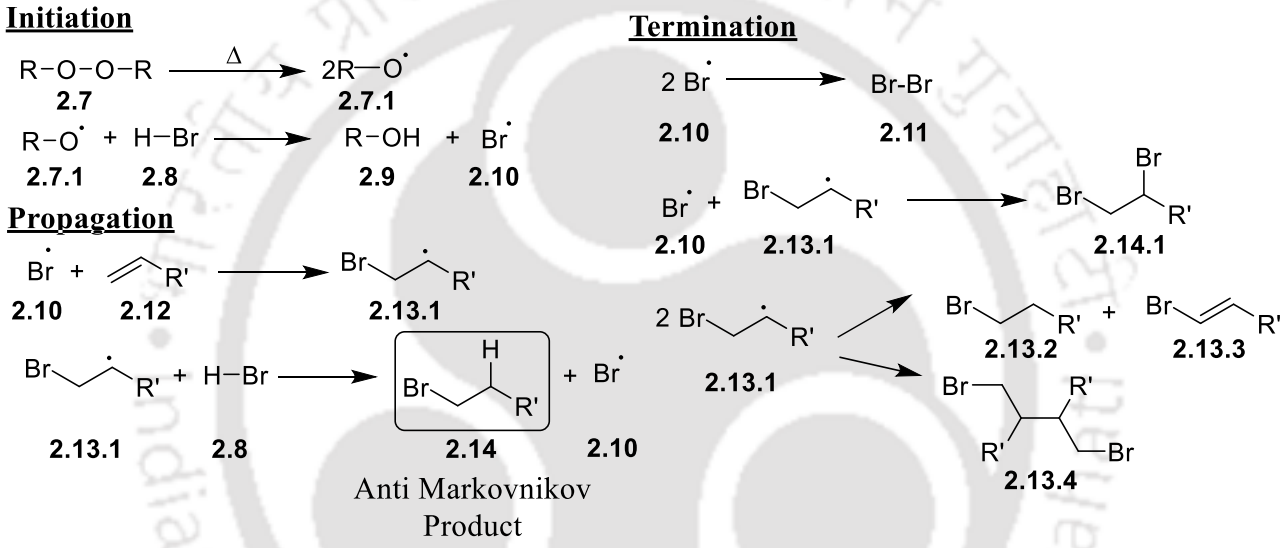

Scheme 2.3: Anti-Markovnikov ATRA of HBr to unsymmetrical alkenes in the presence of peroxide initiators.[13]

Kharasch was the first to discover that CX_4 (X = Cl, Br, I) in the presence of radical initiators generated the organic radicals *in-situ,* which readily added across terminal olefins (Scheme 2.4).[14] He observed that the addition of poly-halogenated alkanes such as CBr_4, CCl_4, CBr_3Cl, and CCl_3Br to alkenes occurred in the presence of free-radical initiators or light with high anti-Markovnikov selectivity and good functional group tolerance.[15] Under thermal conditions, the addition of halogenated hydrocarbons across unsaturated alkenes or alkynes occurs via the activation of halogenated hydrocarbons with a wide variety of radical initiators such as azobisisobutyronitrile (AIBN),[16] BEt_3,[17] sodium dithionate ($Na_2S_2O_4$),[18] and peroxides [diacetyl peroxide $(AcO)_2$, dibenzyl peroxide $(BzO)_2$][19].

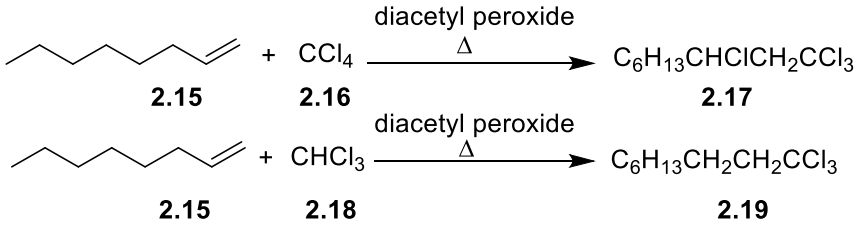

Scheme 2.4: Anti-Markovnikov addition of poly-halomethanes to olefins.[14]

The peroxide effect involves the use of peroxides as radical initiators to generate radicals from a variety of substrates such as hydrocarbons, poly-halogenated substrates,[14] aldehydes,[20] ketones,[21] and esters[22] that could readily add to alkenes in an anti-Markovnikov fashion(Scheme 2.5).

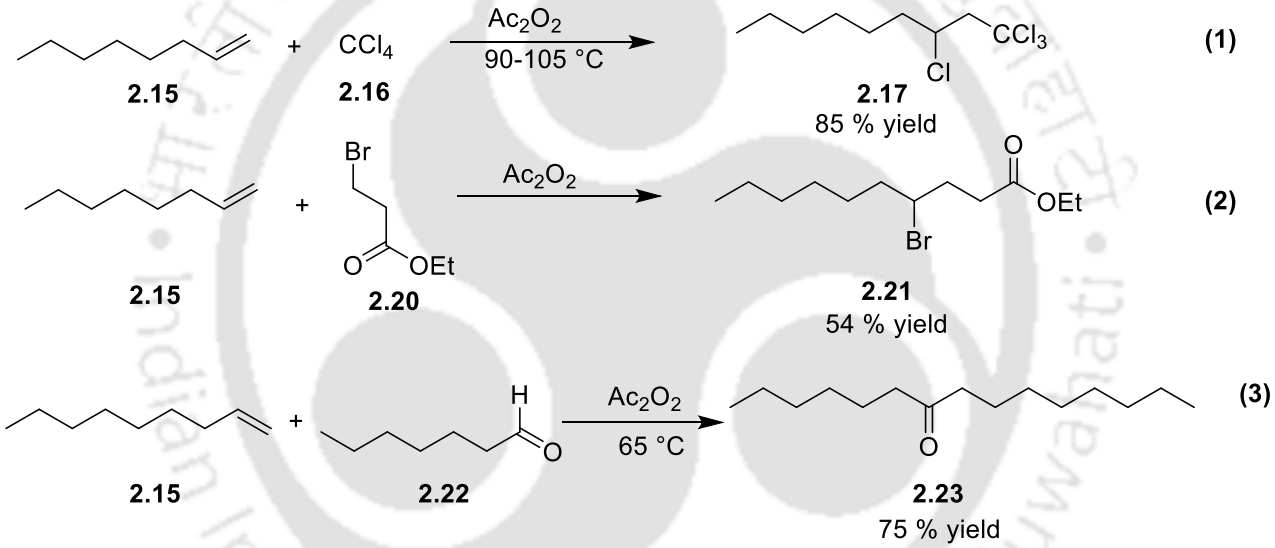

Scheme 2.5: (1) The ATRA of CCl_4 across olefin first reported by Kharasch.[3] (2) The ATRA of bromo-ester to olefins.[22](3) The preparation of ketones by the ATRA of aldehyde to olefin.[20]

This method is widely applicable in the presence of radical initiators or light and high yields are obtained only for α-olefins. One major drawback of Kharasch reaction is that it failed in efficiency with olefins such as styrene and methyl methacrylate. This limitation mainly arises due to the occurrence of side reactions such as radical coupling and telomerization (i.e., the addition of CCl_4 accompanied by alkene coupling to form alkanes).[23] It should also be noted that the radical initiators are typically toxic and hazardous.

In 1956 Minisci and co-workers reported halo-alkylation of acetonitrile in CCl_4 and $CHCl_3$ in a steel autoclave and found a considerable amount of ATRA product.[24] They also noticed that in the case of styrene and MMA, the chain transfer constant of both CCl_4 and $CHCl_3$ were very less and consequently, polymerization would happen. Subsequently, in 1961, the same group repeated the reaction in the presence of $FeCl_2$ and obtained a higher value of chain transfer constant that led to preferential formation of ATRA product. This triggered the exploration of catalysts based on several transition metal complexes including metal oxides,[25-26] zero-valent metal such as Cu(0)[27-28] and Fe(0)[29-30] for ATRA reactions. Transition metal-catalyzed ATRA has now become broadly applicable for synthetic transformations.

In the absence of any transition metal or radical initiator, Sajiki and co-worker reported ATRA of various polyhalo alkanes to terminal olefins in the presence of sodium acetate in good to moderate yields with a broad substrate scope (Scheme 2.6).[31,32] Generally, diacetyl peroxide [$(AcO)_2$], generated the acetyloxyl radical, which is commonly used as radical initiator in Kharasch addition. Wang *et al*. had reported that NaOAc might work as a short-lived radical source.[32] However, due to its potential anionic character, it might not be an efficient acetyloxyl radical source.

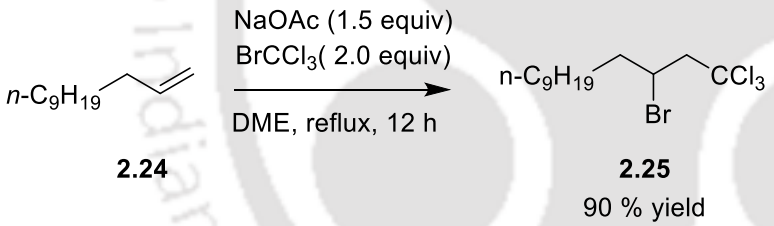

Scheme 2.6: ATRA of polyhaloalkanes to olefins using NaOAc as a radical source. [31]

Over the last seven decades, the emphasis has shifted to the use of transition metal complexes based on Ni,[33-35] Fe,[36] Cu,[37-38] and Nb,[39] to mediate the atom transfer radical addition. Transition-metal-catalyzed ATRA has several applications, and it not only leads to higher yields of highly chemo-selective products but also is extensively applicable for a variety of substrates. It has been shown that one could achieve either ATRA or atom transfer radical polymerization (ATRP) as a significant product by merely varying the ratio of olefin to CCl_4.[40-41] Typically, to reduce the extent of polymerization, excess of CCl_4 or $CHCl_3$ is used with respect to olefin.[14, 40] In 2011, Larbi El Firdoussi and co-workers have shown that among several transition metal acetyl-acetonates, $Fe(acac)_3$ was most reactive in catalyzing the addition of CCl_4 to styrene (Scheme 2.7).[42] They

performed the Kharasch addition of CCl_4 to styrene, under mild condition using $Fe(acac)_3$ (1 mol%) and obtained up to 87 % yield.

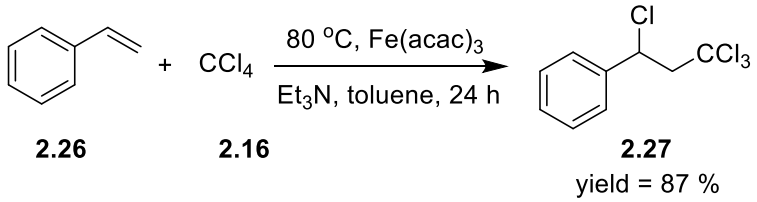

Scheme 2.7: Addition of CCl_4 to styrene using $Fe(acac)_3$ as catalyst.[42]

In the same year, Molina *et al.* carried out the ATRA of CCl_4 to styrene in the presence of $Tp^{tBu,Me}Cu(NCMe)$ (Tp = hydrotrispyrazolyl-borate) (Scheme 2.8).[43] They have obtained a clear mechanistic understanding and have shown that the initial step involves the dissociation of acetonitrile from $Tp^{tBu,Me}Cu(NCMe)$. The resulting $Tp^{tBu,Me}Cu$ subsequently activates CCl_4 to generate CCl_3 radical and Cl radical. The CCl_3 radical then adds to styrene to generate the benzyl radical which subsequently abstracts the Cl radical to yield the corresponding Kharasch product.[43]

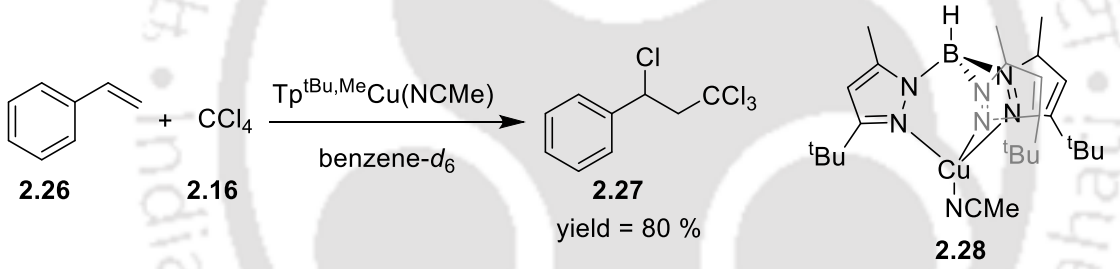

Scheme 2.8: ATRA of CCl_4 to styrene catalyzed by the Cu-homoscorpionate complex **2.28**.[43]

The transition metal-catalyzed ATRA can occur intramolecularly when alkyl halide and olefin functionalities are part of the same substrate. In 2002, Clark reported the Cu mediated atom transfer radical cyclization (ATRC) of mono–, di– and tri–halo olefinic substrates to obtain various ring systems (Scheme 2.9).[44] They have shown that by heating the tri chloro-acetate derivatives with CuCl in acetonitrile, the corresponding γ-lactum would be obtained in 95 % yield.[44]

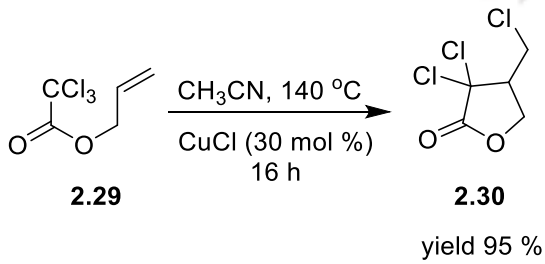

Scheme 2.9: Copper(I) mediated ATRC reported by Clark.[44]

Enantioselective addition of polyhalomethane to terminal olefins provides an optically active secondary halide (Scheme 2.10). Liu and Reddy used [{Rh(COD)$_2$Cl}$_2$] (COD = 1,4-cyclooctadiene) catalyst in the presence of an optically active ligand *p*-tol DIOP (DIOP = 2,3-*O*-isopropylidene-2,3-dihydroxy-1,4-*bis*(diphenylphosphino)butane) with a 1:1 mixture of hexane and toluene.[45] They proposed an asymmetric ATRA where stereo-determining step involves outer-sphere bromine abstraction from a [(bisphosphine)Rh^{II}BrCl] complex via a benzylic radical intermediate.

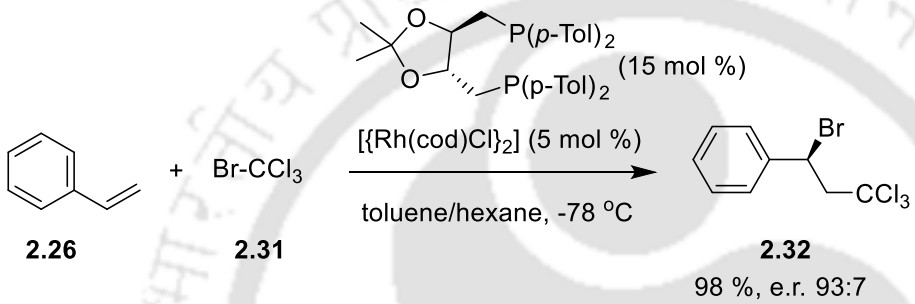

Scheme: 2.10: Rhodium catalyzed enantioselective ATRA of CCl_3Br to styrene.[45]

Among several transition metal catalysts, ruthenium has played a prominent role in the Kharasch chemistry. The first report on ruthenium catalyzed ATRA came in 1973 by Matsumoto, Nakano and Nagai group. Here $RuCl_2(PPh_3)_3$ (0.5 mol %) was utilized as catalyst for the Kharasch addition of CCl_4 to styrene at 80 °C which resulted in 190 turnover number of the ATRA product after 4 hours (Scheme 2.11).[46]

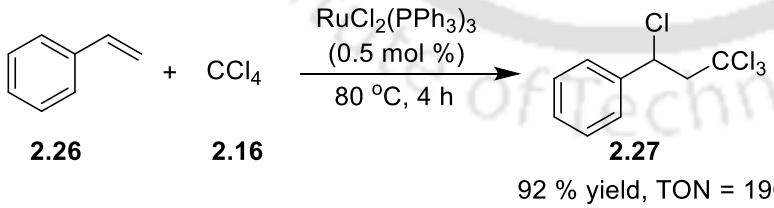

Scheme 2.11: The first report on addition of CCl_4 to styrene catalyzed by Ru(II) complex.[46]

A decade later, the Davis group used $RuCl_2(PPh_3)_3$ for ATRA and proposed that the reaction proceeds through the dissociation of one of the PPh_3 ligands to generate a 14-electron active

species from the 16-electron Ru(II) catalyst precursor.[47] The unsaturated 14-electron species activates the halocarbon towards ATRA. Later in 2007, the Demonceu group extended the $RuCl_2(PPh_3)_3$ catalyzed ATRA by performing the reaction under microwave conditions. These efforts increased turnover number up to 288 (at 135 °C after 30 min) using 0.33 mol % of $RuCl_2(PPh_3)_3$ (Scheme 2.12).[48] Under thermal conditions, the $RuCl_2(PPh_3)_3$ (0.33 mol %) catalyzed ATRA to styrene at 85 °C after 30 h resulted in only 102 turnover number.[48] They have shown that microwave heating has a more beneficial effect on Kharasch addition in comparison to conventional heating.

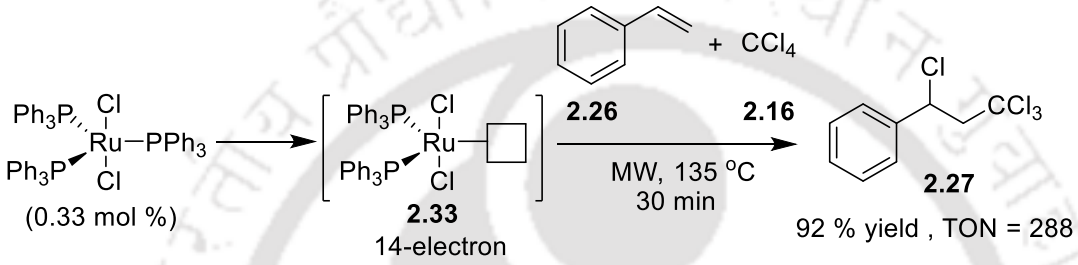

Scheme 2.12: Microwave enhanced Kharasch addition by 16 electron-Ru(II) catalyst precursor.[48]

Under microwave conditions, Demonceu and Gendre studied Kharasch addition of CCl_4 to styrene at 160 °C for 10 min using arene-ruthenium complexes containing phosphane and *N*-heterocyclic carbenes (NHC) groups which gave about 90 and 6 turnovers respectively.[49]

In 2000, Demonceu and co-workers reported stable and well-defined 14-electron ruthenium carborane-phosphine complexes for catalyzing Kharasch addition of CCl_4 to styrene at 60 °C that resulted in 234 turnover number.[40] In 2006, Demonceu demonstrated the prominent role that phosphine ancillary ligands play in generating the active catalyst owing to varying Ru-P bond energy. In these studies Ru(II) *p*-cymene complexes with triarylphosphine ligands with various substituents at the *para*- position were used to catalyze the ATRA of CCl_4 to various olefins.[50] Notably, 12-electron Ru active species **2.34** was involved in the catalytic process, and lower TON (TON = 183) were obtained (Scheme 2.13) as compared to the previous reports where 14-electron Ru species were involved (Scheme 2.12, TON = 288). Here, 12-electron Ru species **2.34** with electron-donating groups in the *para*- position of the aryl group on phosphines showed higher catalytic reactivity than the corresponding phosphines with less electron-donating substituents.[50]

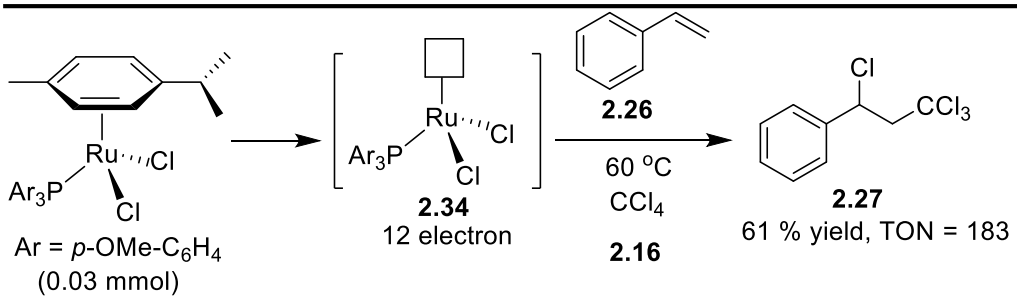

Scheme 2.13: [$RuCl_2$(*p*-cymene)(PAr_3)]-catalyzed Kharasch addition reaction.[50]

To obtain a better understanding of ligand release in ATRA reactions, ruthenium complexes such as [RuCl(arene)$(PR_3)_2$]$^{+}$[40, 51] and [$RuCl_2$(arene)PR_3] were tested for ATRA of CCl_4 to styrene and TON as high as 300 were obtained. While [RuCl(arene)$(PR_3)_2$]$^{+}$ lead to 16-electron [RuCl(arene)(PR_3)]$^{+}$[40, 51] as the active species via loss of PR_3, arene loss lead to 12-electron [$RuCl_2(PR_3)$] as the active species in reactions catalyzed by [$RuCl_2$(arene)PR_3]. Reactivity with systems that generate 16-electron species was found to be better than corresponding systems that generate 12-electron species. When phosphines from $RuCl_2$(arene)PR_3 [48, 50] complex were replaced by *N*-heterocyclic carbenes, comparable catalytic efficiencies (ca. 270 TON) were obtained.[52]

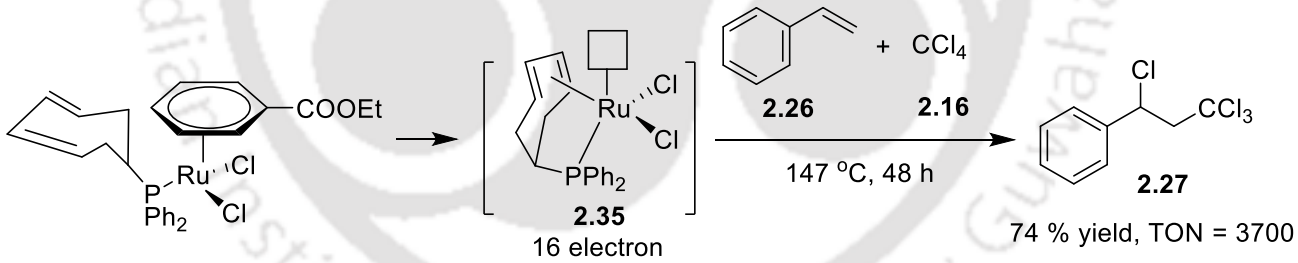

Scheme 2.14: Stabilization of the active species generated from $RuCl_2$(arene)PR_3 by hybrid phosphine−diene ligands during ATRA.[53]

Very recently, the best result for Kharasch addition to styrene was reported by Malacea-Kabbara and Le Gendre.[53] They reported the use of [$RuCl_2$(arene)PR_3] complex where PR_3 is a phosphine diene ligand that could enhance the stability of the arene dissociated 12-electron species by donating additional 4 electrons to yield a 16-electron species. Utilizing this hybrid phosphine-diene ligands at 147ºC in the absence of any co-catalyst, 3700 TON were obtained (Scheme 2.14).[53]

Stradiotto and co-workers have investigated the ATRA activity of a series of neutral, cationic, and zwitterionic (arene)Ru(II) catalysts supported by P, N substituted indene and indenide ligands.[54] This group were the first to discuss the application of ligands which were a combination of both N and P. For the ATRA of CCl_4 to styrene at 60 °C, the Stradiotto group reported 291 turnover number using 0.33 mol % of Cp*Ru(Cl)(κ^2-3-Ph_2P-2-Me_2N-indene).[54] On the other hand under similar conditions, but in the presence of 5 mol% AIBN, 0.02 mol % of [Cp*Ru(Cl) (κ^2-3-Ph_2P-2-Me_2N-indene)]BF_4 resulted in 4450 TON (Scheme 2.15).[54] This is the highest TON (in the presence of co-catalyst radical initiator) reported for the ATRA of CCl_4 to styrene.

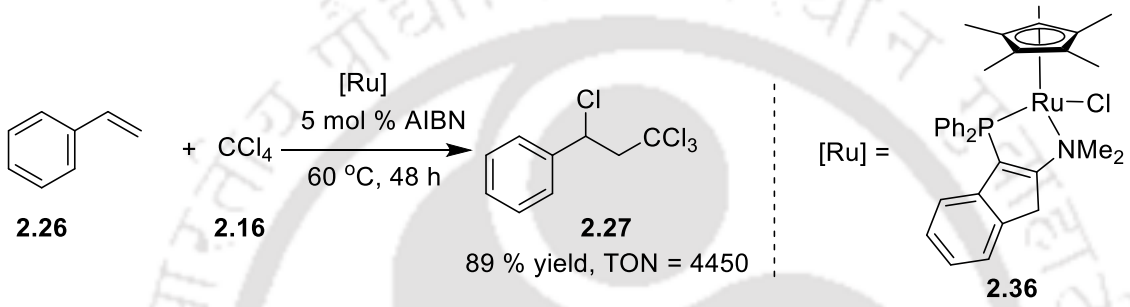

Scheme 2.15: P,N-substituted indene ligands supported by Ru(II) reported for the ATRA reaction.[54]

In 2004, Snapper and co-workers demonstrated $(PCy_3)_2Cl_2Ru$=CHPh catalyzed Kharasch addition of trihaloalkanes across olefin to provide polyhalogenated adducts, which undergo hydrolysis to provide α,β unsaturated ketones, aldehydes or γ-hydroxybutenolides (Scheme 2.16).[55] The overall result of these two consecutive steps was an alternative strategy for direct olefin carbonylation. Olefin carbonylation is an essential developing synthetic methodology which has a lot of applications in natural product synthesis.[7] In addition to examples with Ru,[16] the ATRA has been widely explored with Cu,[56] Ni,[33] Co[57] and Fe[58].

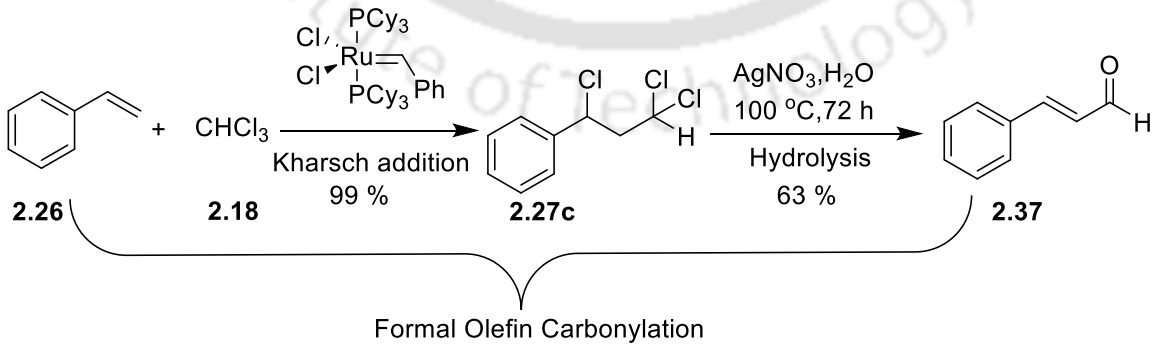

Scheme 2.16: Kharasch addition followed by hydrolysis.[55]

It can be thus said that Ru(II) precursors, which readily produce 16-electron fragments demonstrate better catalytic activity towards ATRA without significant catalyst decomposition in comparison to 14-electron and 12-electron fragments. Generally, pincer complexes are robust in nature and show better catalytic applications due to various factors.[59-60] There have been no reports on the use of pincer-ruthenium complexes in catalytic ATRA reactions. On the other hand, pincer ligated nickel complexes have been well studied towards catalytic ATRA reactions. In his pioneering studies, van Koten reported for the first time the use of a pincer-Ni complex for the Kharasch addition in 1998.[33] They developed Ni(III) NCN type pincer complexes for catalytic additions of poly-halogenated alkanes to olefins to give anti-Markovnikov product. van Koten's group have shown that the addition of CCl_4 to MMA in DCM provides about 200 TON in 1h at room temperature.[33] The van Koten group have several excellent reports and reviews on pincer-nickel catalyzed ATRA reactions.[35] In 2007, Davit Zargarian exhibited Kharasch additions by using a POCOP Ni(III) pincer complex at room temperature to yield 90 and 300 TONs after 8 h and 24 h respectively. The catalytic activity of Ni(III)POCOP is however more efficient in refluxing acetonitrile (300 TON and 1000 TON after 8 h and 24 h respectively, Scheme 2.17).[34]

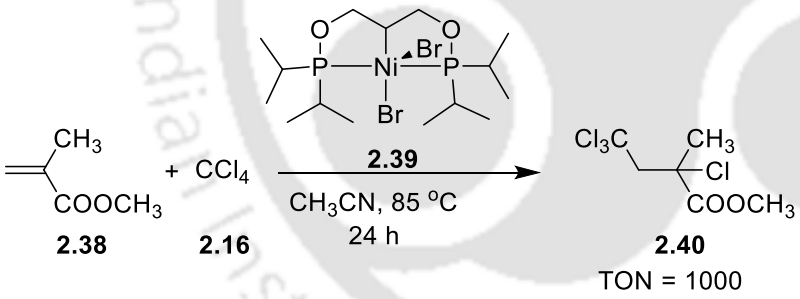

Scheme 2.17: Kharasch addition of CCl_4 to MMA catalyzed by a Ni(III)POCOP pincer complex.[34]

The improved activity of 16–electron Ru(II) species in comparison with the corresponding 14–electron and 12–electron species towards ATRA has already been discussed. It was envisaged that 18-electron NNN pincer–ruthenium complexes (**2.1a-d**, Scheme 2.18) would readily generate the corresponding 16-electron fragment (^{R2}NNN)$RuCl_2$ via the dissociation of the PPh_3 ligand. This would provide access to potential active catalysts for the ATRA of CCl_4 to styrene. Accordingly, the current chapter discusses the catalytic application of a series of four pincer-

ruthenium complexes (^{R2}NNN)RuCl$_2$(PPh$_3$) (**2.1a**; R = Cy, **2.1b**; R = ^{t}Bu, **2.1c**; R = ^{i}Pr, and **2.1d**; R = Ph) chosen from the large library of pincer–ruthenium complexes that were synthesized by Kumar and co-workers[61-63] towards Kharasch addition of CCl_4 to styrene (Scheme 2.18). Prior to this study, the highest reported TON for the ATRA of CCl_4 to styrene was 3700[53] and 4450[54] TONs in the absence and in the presence of co-catalyst radical initiator, respectively. Interestingly, in this study very high turnover number (TON up to 5670) have been observed for the (^{Cy2}NNN)RuCl$_2$(PPh$_3$) **(2.1a)** [0.2 mM] catalyzed Kharasch addition of CCl_4 to styrene at 140 °C.[61]

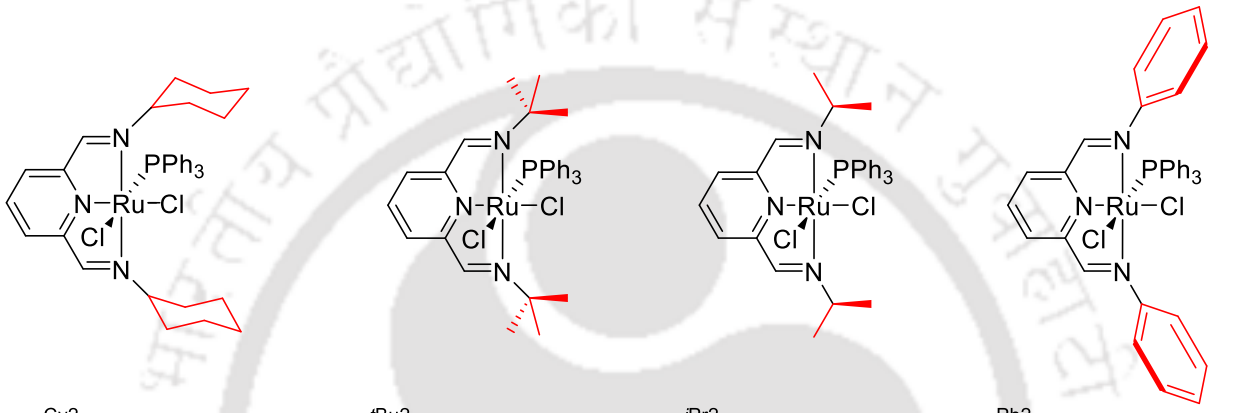

Scheme 2.18: Pincer–ruthenium complexes (^{R2}NNN)RuCl$_2$(PPh$_3$) (R = Cy, ^{t}Bu, ^{i}Pr and Ph) investigated in the current chapter.

2.3 Results & discussions

A typical experiment involved the reaction of styrene [2.17 M] and CCl_4 [7.93 M] that is catalyzed by pincer-ruthenium complex [1 mM] with toluene [0.188 M] as an internal standard at 100 °C. After 48 h, the reaction mixture was cooled to room temperature and an aliquot was subjected to GC analysis. Among the four considered catalysts (**2.1a-d,** Scheme 2.18), while the catalyst **2.1a** demonstrated the highest reactivity (1385 turnover number), the activity of **2.1d** was very poor (350 TON) after 48 h at 100 °C (Table 2.1). Relatively good activity was observed by the use of (^{iPr2}NNN)RuCl$_2$(PPh$_3$) (**2.1c**) (1280 TON) and (^{tBu2}NNN)RuCl$_2$(PPh$_3$) (**2.1b**) (1160 TON).

Table 2.1: ATRA of CCl_4 to styrene catalyzed by pincer–ruthenium complexes (**2.1a-d**)

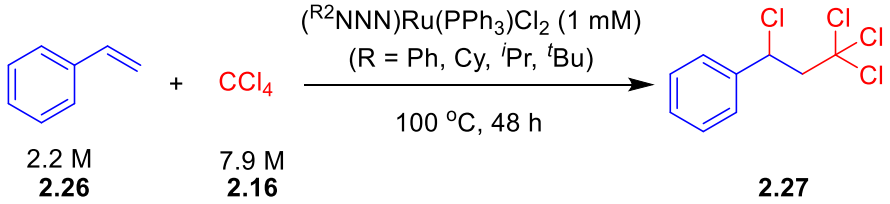

2.2 M **2.26** + 7.9 M **2.16** → **2.27**

Entry	Catalyst [1mM]	Styrene Conversion %	Product 2.27 Yield mM(%)[a]	TON
1.	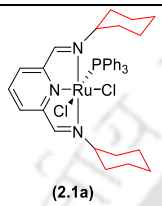 (2.1a)	100	1385 (63)	1385
2.	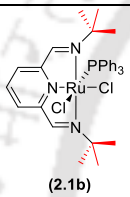 (2.1b)	95	1160 (53)	1160
3.	 (2.1c)	93	1280 (58)	1280
4.	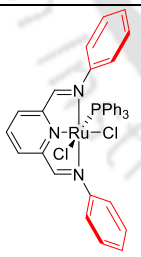 (2.1d)	59	350 (16)	350

Reaction condition: 1 mM of (^{R2}NNN)Ru(PPh_3)Cl_2 (R = Ph, Cy, ^{i}Pr, ^{t}Bu) at 100 °C. [a]Yield determined by GC analysis using toluene as an internal standard.

However, carrying out the ATRA with a mixture of styrene [2.2 M], CCl_4 [7.9 M], and the pincer-ruthenium complex (^{Cy2}NNN)$RuCl_2PPh_3$ [1 mM], it had been observed that along with Kharasch product, a significant portion of styrene was undergoing ATRP as is evident from the broad signals at around 7.5 min and 10 min (Figure 2.2). In the GC spectra of the crude reaction mixture, apart

from the desired product (**2.27**) (30 % yield) observed at 5.21 min and the polymeric products, additional peaks of low intensity were also observed at 7.18 min and 7.27 min (Figure 2.2). These two peaks might correspond to diastereomeric products (**2.41**) or (**2.43**) arising either from the coupling of benzylic radical (**2.40**) or from the coupling of primary (1-chloroethyl) benzene radical (**2.42**) (Scheme 2.19). However, attempts to isolate these trace products were not successful.

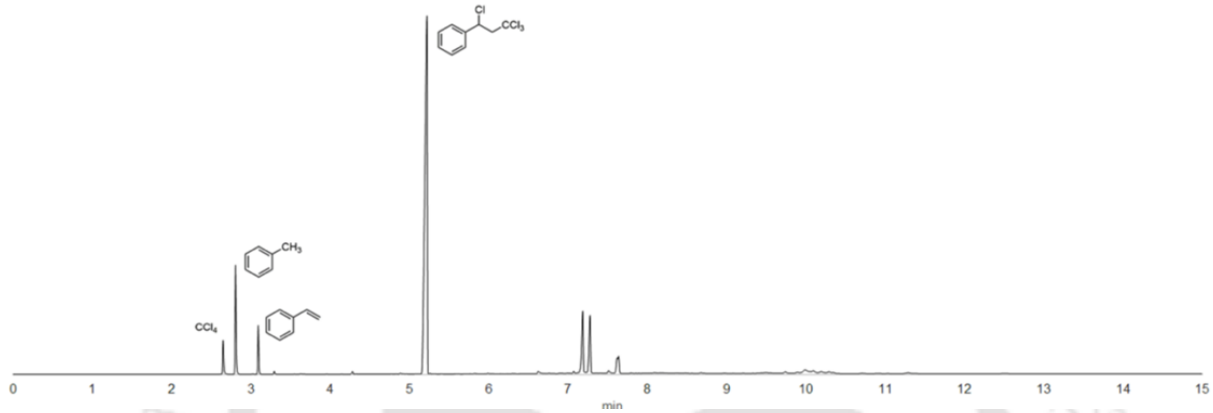

Figure 2.2: GC spectrum of the crude reaction mixture of styrene, CCl_4 and **2.1a** catalyst

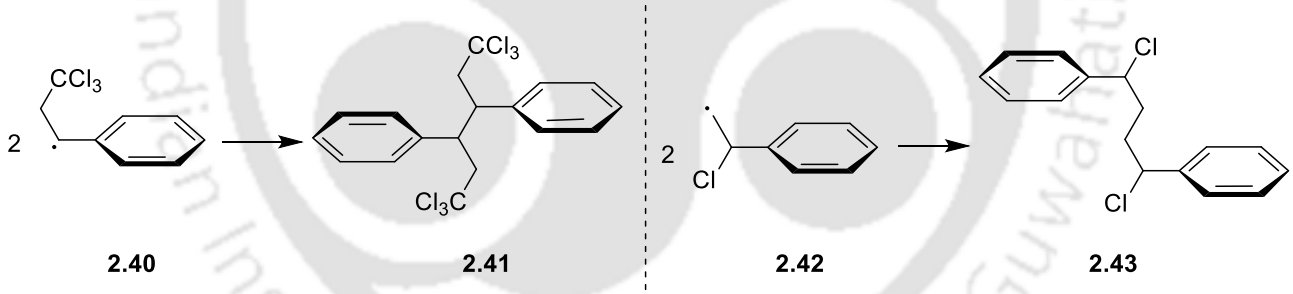

Scheme 2.19: Possible side products formed via radical coupling during ATRA reactions.

The ATRA was then performed by varying the ratio of CCl_4 to styrene while the ratio of styrene to catalyst (**2.1a**) was kept constant at 2170:1. When equimolar amounts of CCl_4 [4.7 M] and styrene [4.7 M] were taken in the presence of (**2.1a**) [2.4 mM], 96 % conversion was observed with only 30 % yield of ATRA product (**2.27**) (Entry 1, Table 2.2). In this case, significant amount of ATRP (atom transfer radical polymerization) products were observed. However, the **2.1a** [1.0 mM] catalyzed reaction of styrene [2.2 M] with 7.9 M CCl_4, resulted in higher yield (63 %) and turnover number (1385 TON) of the ATRA product (**2.27**) (Entry 2, Table 2.2). Further increment

in the concentration of CCl_4 to 8.9 M, gave 92 % of Kharasch product (**2.27**) (ca. 1840 TON) (Entry 3, Table 2.2). It is evident that at a higher ratio of CCl_4 to styrene, the yield of ATRA product increases with a significant reduction in the formation of ATRP as stated in previous reports.[40, 43, 64-67]

2.3.1 Mechanistic studies

The first step of catalysis involves the dissociation of PPh_3 from 18-electron Ru precursors (**2.1a-d,** Scheme 2.18) to generate the corresponding five-coordinate 16-electron species (^{R2}NNN)$RuCl_2$ (**2.45a-d,** Scheme 2.20). As, this step is in equilibrium, it can be expected that in the presence of excess PPh_3, the formation of the product would be reduced. Accordingly, the ATRA activity of 1 mM (^{Cy2}NNN)$RuCl_2(PPh_3)$ (**2.1a**) was inhibited in the presence of excess PPh_3 (Entries 4 and 5, Table 2.2). No reaction was observed in the presence of radical inhibitor TEMPO (2.1 M) (Entry 6, Table 2.2) which points to the involvement of radicals in the process.

Table 2.2: (^{Cy2}NNN)$RuCl_2(PPh_3)$ (**2.1a**) catalyzed ATRA of CCl_4 to styrene under varying conditions at 100 °C.

Entry	Styrene:CCl_4:2.1a M:M:mM	Styrene Conversion (%)	Product (2.27)	
			Yield mM (%)[a]	TON
1	4.7:4.7:2.4	96	1405 (30)	585
2	2.2:7.9:1.0	100	1385(63)	1385
3	1.2:8.9:0.6	100	1104(92)	1840
4[b]	2.2:7.9:1.0	10	115(5)	115
5[c]	2.2:7.9:1.0	30	25 (1)	25
6[d]	2.2:7.9:1.0	0	0 (0)	0

Reaction conditions: [a)] Yield determined by GC analysis using toluene as an internal standard. [b)] Reaction performed in the presence of 100 mM of PPh_3. [c)] Reaction performed in the presence of 500 mM of PPh_3. [d)] Reaction performed in the presence of 2.1 M TEMPO.

Transition-metal catalyzed ATRA reaction between CCl_4 to styrene has been extensively studied and is known to follow a single electron transfer (SET) mechanism.[43, 47] In 1988, van-Koten[68] performed (^{Me2}NCN)NiCl catalyzed ATRA reactions and proposed that the key step involved a SET process that generated Ni(III) species (^{Me2}NCN)$NiCl_2$ and $^{\bullet}CCl_3$. The $^{\bullet}CCl_3$ radical then attacks the alkene to produce the product radical which further attacks on (^{Me2}NCN)$NiCl_2$ leading

to product formation. The reactions involved are in equilibrium with the end result depending on the rate constants. Non-pincer based transition metal complexes are also reported to follow similar mechanism.[43, 47]

In 1998, van Koten's group proposed a catalytic cycle where the first step might be activation of CCl_4 by Ni(II) pincer catalyst through the formation of an inner sphere activated complex.[33] A similar mechanistic cycle can be anticipated (path A) in the pincer-ruthenium catalyzed ATRA of CCl_4 to styrene (Scheme 2.20). However, other possibilities cannot be excluded due to the difference in coordination geometries of the catalytically active species (^{Me2}NCN)NiCl and (^{R2}NNN)$RuCl_2$. Scheme 2.20 portrays four different possible pathways that result in the formation of the observed product in the pincer-ruthenium catalyzed ATRA reactions.

Irrespective of the path, the first step of catalysis involves the dissociation of PPh_3 molecule from the Ru pre-catalyst (**2.1a-d**) to generate the corresponding five-coordinate 16-electron species (^{R2}NNN)$RuCl_2$ (**2.45a-d**) via the transition state (**2.44a-d**). After the formation of catalytically active species 16-electron (^{R2}NNN)$RuCl_2$ (**2.45a-d**), among the four possible pathways it can either undergo a SET process with CCl_4 (path **A** or path **B**) or add to styrene (path **C** or path **D**) prior to the SET process. Irrespective of the path, the 17-electron Ru(III) species (**2.47a–d**, **2.49a–d**, **2.57a–d** and **2.60a–d**) is likely to get stabilized by acting as a trap for the corresponding radicals (**2.40**, **2.42**, $^{\bullet}CCl_3$ and $^{\bullet}Cl$) generated (Scheme 2.20).

Now, if the reaction proceeds through the widely accepted mechanism, i.e. Path **A**, then in the first step CCl_4 (**2.16**) would homolytically cleave to generate $^{\bullet}CCl_3$ and $^{\bullet}Cl$ with a concerted transfer of $^{\bullet}Cl$ to the Ru(II) centre as in transition state (**2.46a-d**). This results in the formation of Ru(III) intermediate (**2.47a-d**) and $^{\bullet}CCl_3$. Subsequent attack of $^{\bullet}CCl_3$ on to styrene would generate the benzylic radical (**2.40**) along TS (**2.51a-d**). Consequently, Ru(III) intermediate (**2.47a-d**) would react with the benzylic radical (**2.40**) via the transition state (**2.53a-d**) to yield the product (**2.27**) along with the regeneration of (**2.45a-d**). During the homolytic radical dissociation of CCl_4, there is a possibility of Path **B** too. Here, $^{\bullet}CCl_3$ gets bound to the Ru(II) centre in (**2.45a-d**) to generate the Ru(III) intermediate (**2.49a-d**) via TS (**2.46'a-d**). The $Cl^{\bullet}$ then attacks styrene to generate a primary (1-chloroethyl)benzene radical (**2.42**) through TS (**2.48**). The active catalyst (**2.45a-d**) is

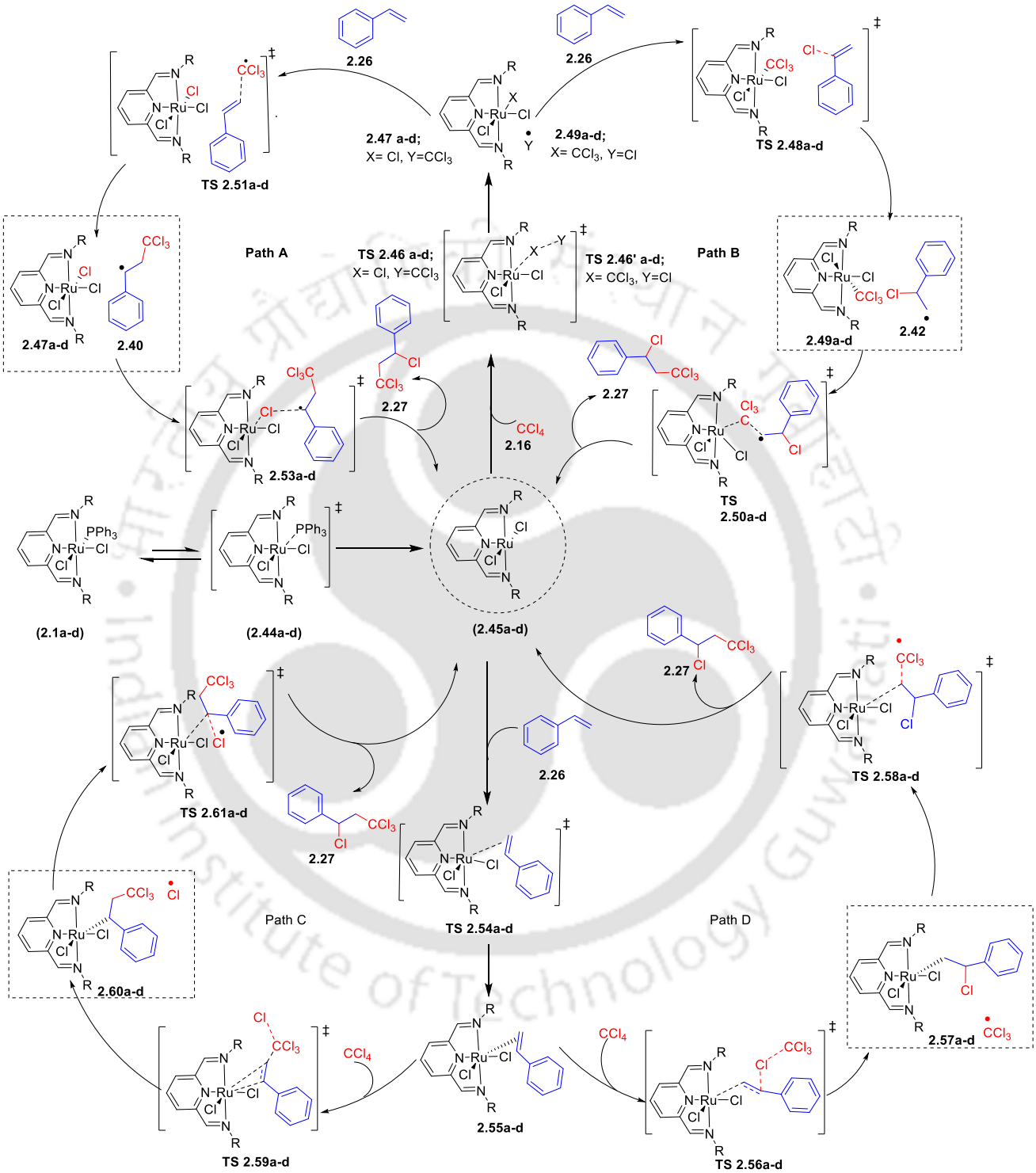

Scheme 2:20: Plausible mechanistic pathways involved in pincer-Ru catalyzed ATRA of CCl_4 to styrene.

then regenerated in the further reaction of (**2.42**) with (**2.49a-d**) via TS (**2.50a-d**) that also leads to the formation of product (**2.27**).

The 5-coordinate 16-electron Ru(II) species (**2.45a-d**) might also prefer to co-ordinate with styrene to produce a relatively stable 18-electron species (**2.55a-d**) through TS (**2.54a-d**). After the generation of 18-electron species (**2.55a-d**), it might undergo either of the two catalytic cycles; path **C** or path **D**. Path **C** consists of the homolytic cleavage of CCl_4, followed by a concerted attack of $^{\bullet}CCl_3$ on coordinated styrene forming (**2.60a-d**) and $Cl^{\bullet}$ via TS (**2.59a-d**). Subsequent attack of $Cl^{\bullet}$ on (**2.60a-d**) via TS (**2.61a-d**) produces the final product (**2.27**) along with the simultaneous regeneration of (**2.45a-d**). Whereas in path **D**, the attack of $Cl^{\bullet}$ on the coordinated styrene in (**2.55a-d**) leads to the formation of (**2.57a-d**) through TS (**2.56a-d**). The complex (**2.57a-d**) could then react with $^{\bullet}CCl_3$ to give the desired product (**2.27**) accompanied by the active catalyst (**2.45a-d**) via TS (**2.58**).

The HRMS analysis of the reaction mixture containing styrene and two equivalents of CCl_4 after stirring at 100 °C for 3 h in the presence of stoichiometric amount of (^{Cy2}NNN)$RuCl_2(PPh_3)$ (**2.1a**) revealed a peak at m/z = 696.1848 that corresponds to $[(^{Cy2}NNN)RuCl(PPh_3)]^+$ (Figure 2.3). With the reaction mixture containing catalytic amounts (10 mM and 40 mM) of (^{Cy2}NNN)$RuCl_2(PPh_3)$ (**2.1a**), similar peaks were observed in the HRMS (ESI) spectrum. This evidently proves that (**2.1a**) is the resting state of catalytic ATRA. The same reaction mixture was also analyzed by ESR experiment before and after heating at 100 °C and no peak was found in the ESR spectrum. Hence, there is no probability of a Ru(III) species as the resting state of the catalytic cycle. Similar results were obtained upon repeating the HRMS (ESI) analysis under identical conditions without styrene. These studies certainly show that the Ru(III) species formed via SET is highly reactive and not isolable.

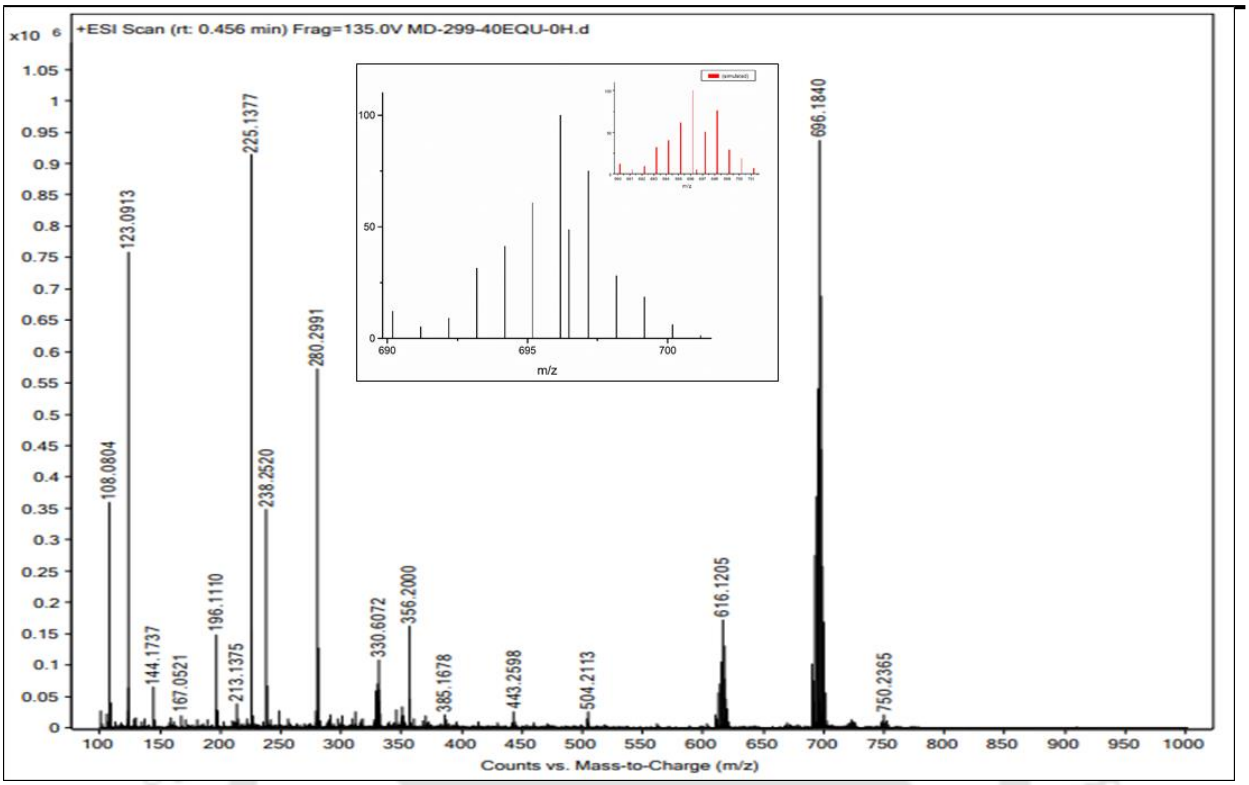

Figure 2.3: HRMS (ESI) spectrum of reaction mixture containing styrene, CCl_4 and equivalent amount of catalyst **2.1a.**

Cyclic voltammetry studies were performed to differentiate the reactivity of the catalysts. Cyclic voltammetry has been reported to be a very useful tool in elucidating the difference in reactivity of several nickel[34-35, 69] and ruthenium[50-51, 67, 70] complexes towards catalytic ATRA which are widely accepted to involve a SET. Cyclic voltammetry analysis of pincer-Ru complexes **2.1a**, **2.1c** and **2.1d** were performed to acquire an understanding on the ease of oxidation of Ru(II) species. The cyclic voltammograms of 1 mM solution of **2.1a**, **2.1c** and **2.1d** in dichloromethane with 0.1 M $^{n}Bu_4NPF_6$ as supporting electrolyte showed reversible redox waves at ca. 0.1-0.4 V vs ferrocene. In Figure 2.4, the representative cyclic voltammograms are given and the corresponding electrochemical data are given in Table 2.3.

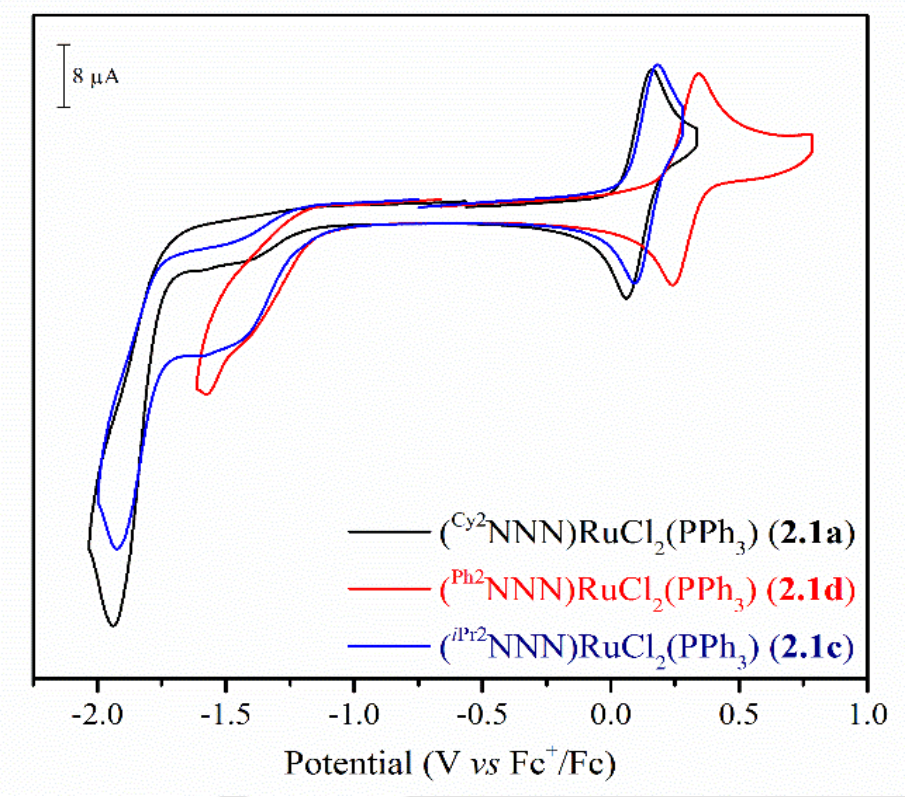

Figure 2.4: Cyclic voltammogram of **2.1a**, **2.1c** and **2.1d** in dichloromethane.

From this cyclic voltammetry data it is evident that (^{Cy2}NNN)RuCl$_2$(PPh$_3$) **2.1a** (E^0 = 0.110 V) and (^{iPr2}NNN)RuCl$_2$(PPh$_3$) **2.1c** (E^0 = 0.137 V) are oxidized at lower potentials as compared to (^{Ph2}NNN)RuCl$_2$(PPh$_3$) **2.1d** (E^0 = 0.293 V). It is clear that irrespective of the path, the SET from Ru(II) should occur more easily with **2.1a** and **2.1c** compared to **2.1d**. In **2.1d** pincer complex, presence of phenyl ring on N atom makes it a poor σ-donor and diminishes electron density on Ru center that makes it harder to oxidize (Table 2.3). The observed trend in potential values of **2.1a**, **2.1c** and **2.1d** are in good agreement with their corresponding catalytic efficiencies.

Table 2.3: Cyclic voltammetry data of pincer Ru complex **2.1a**, **2.1c** and **2.1d**.

Entry	Catalyst 1 mM	E^o (V)[b)]	E^o (V)[c)]	TON[d)]
1.	**2.1a**	0.110	0.100	1385
2.	**2.1c**	0.137	0.090	1280
3.	**2.1d**	0.293	0.102	350

[a)] Pincer Ru complex, 1 mM; ^{n}Bu$_4$NPF$_6$ (0.1 M) in dry and degassed CH$_2$Cl$_2$ under Ar at room temperature; scan rate 100mVs^{-1}; potentials are reported in volts versus ferrocene as internal standard. [b)] $E^o = (E_{pa} + E_{pc})/2$; E_{pa} and E_{pc} are the anodic and cathodic peak potentials respectively. [c)] $\Delta E = | E_{pa} + E_{pc} |$. [d)] Reaction conditions same as in Table 2.1.

2.3.2 Kinetic study

van-Koten[68] and Davis[47] have demonstrated kinetic studies to understand the involvement of the path with radicals bound within the coordination sphere i.e. path **A**. Similar kinetic studies for the ATRA of CCl_4 to styrene catalyzed by **2.1a** at 140 °C were carried out. By employing the initial rate method, it was established that the plot of initial rate vs. [**2.1a**] (Figure 2.5c) and initial rate vs. [CCl_4] was linear (Figure 2.5b). This indicates that rate is first order with respect to concentration of both **2.1a** and CCl_4. However, the dependence on concentration of styrene is non-linear (Figure 2.5a). These observations were very similar to previous reports[68] and they reveal the involvement of either path **A** or path **B** in the catalytic cycle with a rate as given in (Scheme 2.21, equation 1).

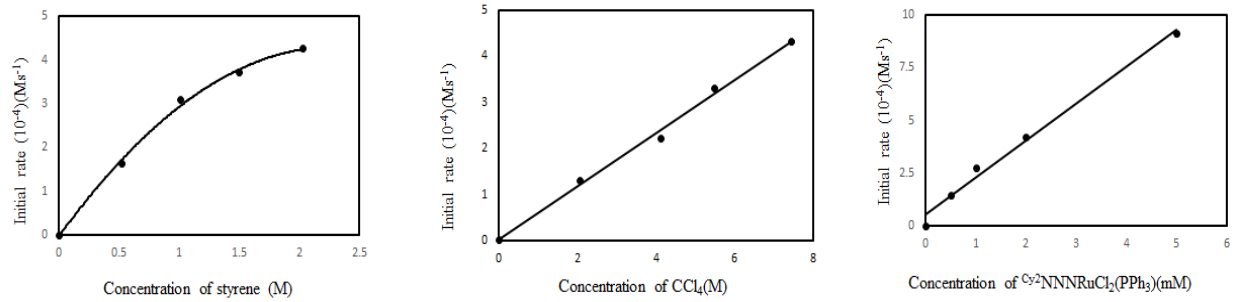

Figure 2.5: Variation of initial rate of ATRA with concentration of (a) Styrene, (b) CCl_4, and (c) (^{Cy2}NNN)$RuCl_2(PPh_3)$.

van Koten has shown that the $^{\bullet}CCl_3$ generated is highly reactive, and for a selective reaction $k_{-2} > k_2$ and $k_4 > k_{-4}$.[68] This corresponds to very low steady state concentration of radicals and the rate of product (**2.27**) formation is given in equation 1 (Scheme 2.21). In contrast, if the reaction follows path **C** or path **D**, then a zero-order dependence on [CCl_4] is expected. In reaction mechanism it has been shown that, after hemolytic cleavage of CCl_4, the corresponding radicals generated were bound to the co-ordination sphere. If the corresponding radicals were outside the coordination sphere then the rate equation would have zero order dependence on styrene concentration.[43, 47] From rate equation 1 (Scheme 2.21) it is clearly observed that free triphenyl phosphine causes a decrease in the rate as concentration of PPh_3 is inversely proportional to rate of the reaction. Experimentally it has been observed that the addition of excess amount of PPh_3 diminishes the rate of the reaction (Entry 4 and 5, Table 2.2).

Path **A**

$(^{Cy2}NNN)RuCl_2(PPh_3) \overset{K_1}{\rightleftharpoons} (^{Cy2}NNN)RuCl_2 + PPh_3$

$(^{Cy2}NNN)RuCl_2 + CCl_4 \overset{K_2}{\rightleftharpoons} \{(^{Cy2}NNN)RuCl_3\}\ \{\dot{C}Cl_3\}$

$\{(^{Cy2}NNN)RuCl_3\}\ \{\dot{C}Cl_3\} + PhCHCH_2 \overset{K_3}{\rightleftharpoons} \{(^{Cy2}NNN)RuCl_3\}\ \{Ph\dot{C}HCH_2CCl_3\}$

$\{(^{Cy2}NNN)RuCl_3\}\ \{Ph\dot{C}HCH_2CCl_3\} \overset{K_4}{\rightleftharpoons} (^{Cy2}NNN)RuCl_2 + PhCHClCH_2CCl_3$

Path **B**

$(^{Cy2}NNN)RuCl_2(PPh_3) \overset{K_1}{\rightleftharpoons} (^{Cy2}NNN)RuCl_2 + PPh_3$

$(^{Cy2}NNN)RuCl_2 + CCl_4 \overset{K_2}{\rightleftharpoons} \{(^{Cy2}NNN)RuCl_2CCl_3\}\ \{\dot{C}l\}$

$\{(^{Cy2}NNN)RuCl_2CCl_3\}\ \{\dot{C}l\} + PhCHCH_2 \overset{K_3}{\rightleftharpoons} \{(^{Cy2}NNN)RuCl_2CCl_3\}\ \{PhCHCl\dot{C}H_2\}$

$\{(^{Cy2}NNN)RuCl_2CCl_3\}\ \{PhCHCl\dot{C}H_2\} \overset{K_4}{\rightleftharpoons} (^{Cy2}NNN)RuCl_2 + PhCHClCH_2CCl_3$

Under a low steady-state concentration of radicals, rate for either path **A** or path **B** $= \dfrac{k_1k_2k_3\,[\mathbf{2.1a}][CCl_4][\text{Styrene}]}{[PPh_3]\,\{k_{-2} + k_3[\text{Styrene}]\}}$ ---------- (1)

Scheme 2.21: Rate equation for the pincer-ruthenium catalyzed ATRA for either path **A** or path **B**.

2.3.3 Computational studies

Quantum mechanical calculations (DFT) were done to get the detailed understanding of the reactivity patterns of (^{Cy2}NNN)RuCl$_2$(PPh$_3$) (**2.1a**), (^{iPr2}NNN)RuCl$_2$(PPh$_3$) (**2.1c**) and (^{Ph2}NNN)RuCl$_2$(PPh$_3$) (**2.1d**). DFT studies offer remarkable understandings of not only the path involved in the ATRA of CCl$_4$ to styrene, but also elucidate the differences in the reactivity of these catalysts. Demonceau had demonstrated that the catalytic efficiency of RuCl(Cp*)(PR$_3$)$_2$ (R = C$_6$H$_5$, *p*-CF$_3$C$_6$H$_4$, *p*-CH$_3$OC$_6$H$_4$) was dependent on the phosphine release with the efficiency increasing with decrease in ruthenium-phosphine bond energy.[40] Similarly, in the current study, the removal of PPh$_3$ is required for the generation of the catalytically active species (**2.45a-d**). The interaction energy (- ΔE_{int}) of the PPh$_3$ fragment with (^{R2}NNN)RuCl$_2$ followed the trend (**2.1a**) (42.15 kcal/mol) < (**2.1c**) (43.24 kcal/mol) < (**2.1d**) (44.35 kcal/mol) (Table 2.4). The Ru-P binding energy (-*BE*) also followed a similar trend, (**2.1a**) (20.86 kcal/mol) < (**2.1c**) (23.86 kcal/mol) < (**2.1d**) (25.21 kcal/mol) (Table 2.4). In accordance with these results, the ^{31}P NMR spectra indicates the P in (**2.1d**) (δ 32.27) is more deshielded than that in (**2.1c**) (δ 29.16) and (**2.1a**) (δ

29.42) (Table 2.4). All these observations prove that the phosphine release is harder with (**2.1d**) as compared to (**2.1a**) and (**2.1c**), thus supporting the trend in catalytic activity (Table 2.4).

Table 2.4: Binding energies, interaction energies and ^{31}P NMR shifts for complexes (**2.1a**), (**2.1c**) and (**2.1d**).

Entry	Catalyst	-BE[a]	-ΔE_{int}[b]	^{31}P shift	TON[c]
1.	2.1a	20.86	42.15	29.42	1385
2.	2.1c	23.86	43.24	29.16	1280
3.	2.1d	25.21	44.35	32.27	350

[a)] Binding energy (kcal/mol) is the difference between the energy of complex (**2.1a-d**) and the energy of the corresponding isolated PPh_3 and (^{R2}NNN)$RuCl_2$ (R = Cy, ^{i}Pr and Ph) in their minima configuration. [b)] Interaction energy (kcal/mol) is the difference between the energy of the complex (**2.1a-d**) and the energy of the corresponding isolated PPh_3 and (^{R2}NNN)$RuCl_2$ (R = Cy, ^{i}Pr and Ph) in the geometry of the complex (**2.1a-d).** [c)] Reaction conditions same as in Table 2.1.

On the other hand, calculations indicate that the Ru-P binding energy (-BE) of (**2.1b**) is very low (ca. 8.90 kcal/mol) presumably due to steric interference between the *t*-Bu groups and PPh_3 ligand. This means that the molecule readily loses PPh_3 to give highly unstable 16-electron species (**2.45 b**), a majority of which may get deactivated via several pathways under the reaction conditions. This high instability in chlorinated solvents also prevents reliable characterization via NMR and cyclic voltammogram studies.[71] The observed reaction (Entry 2, Table 2.1) may be actually catalyzed by a tiny concentration of undecomposed (**2.45b**). However, in the case of **2.1a**, **2.1c** and **2.1d**, there is a better control on the phosphine release. Notably, the catalyst **2.1b** is relatively more stable in alcohol solvents presumably due to the coordinating nature of alcohols (see chapter 3).

To explain the exact path involved in the ATRA, the energetics of all possibilities i.e. path **A**, path **B**, path **C** and path **D** were computed with the most active pincer-ruthenium complex (**2.1a**). The initial formation of active 5-coordinated 16-electron metal catalyst from precursor Ru complex (**2.1a**) is common for all paths.

The formation of catalytically active 5-coordinated 16-electron species (**2.45a**) starting from (**2.1a**) is highly endothermic (ca. 15.17 kcal/mol). The dissociation of PPh_3 molecule from **2.1a** went

through TS **(2.44a)** (ca. 27.60 kcal/mol). The energy barriers involved in the formation of various intermediates through all the four paths (Figure 2.6 and Figure 2.7) are shown in Table 2.5. For both path **A** and path **B**, among all the possible transition states, the highest energy barrier was for the hemolytic cleavage of CCl_4 and generation of corresponding Ru(III) centres **2.47a** (TS:**2.46a** ca. 22.09 kcal/mol) and **2.49a** (TS:**2.46'a** ca. 48.48 kcal/mol) respectively (Entries 1 and 4, Table 2.5).

On the other hand, for both path **C** and path **D** the highest barrier is for the attack of either Cl• or •CCl_3 on coordinated styrene in (**2.55a**) leading to the formation of **2.60a** in path C via TS:**2.59a** (ca. 48.65 kcal/mol) and (**2.57a**) in path D via TS:**2.56a** (ca. 42.08 kcal/mol) (Entries 8 and 10, Table 2.5). Remarkably, the highest barrier via path **A** is approximately half of the energy compared to the highest barrier involved via path **B**, path **C** and path **D** (Compare entry 1 with entries 4, 8 and 10, Table 2.5). It is thus apparent that path **A** is operative during the ATRA reaction which is also in line with findings by van-Koten[68] and Davis.[33, 47]

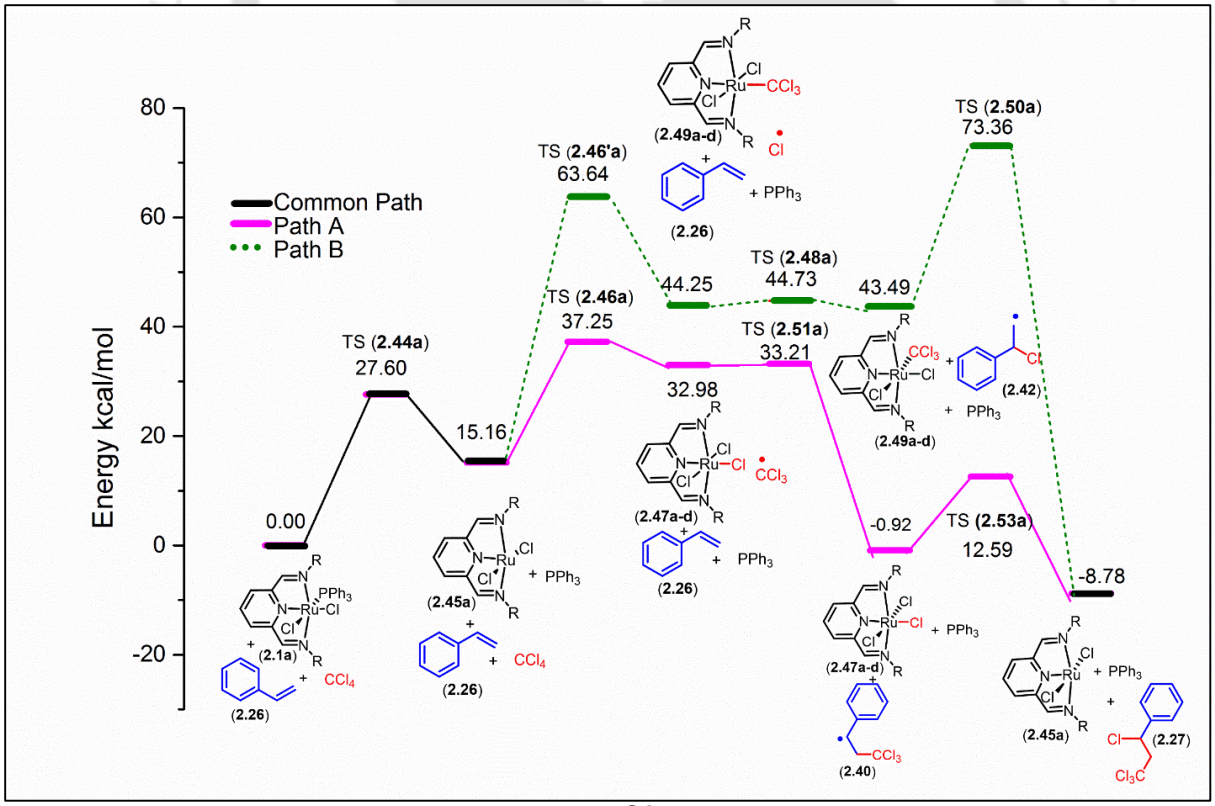

Figure 2.6: Energetics of various species involved in the (^{Cy2}NNN)$RuCl_2(PPh_3)$ catalyzed ATRA via path **A** and **B**. DFT studies were carried out using PBEPBE functional with LANL2DZ basis set for Ru and 6-311G(d,p) for all other atoms.

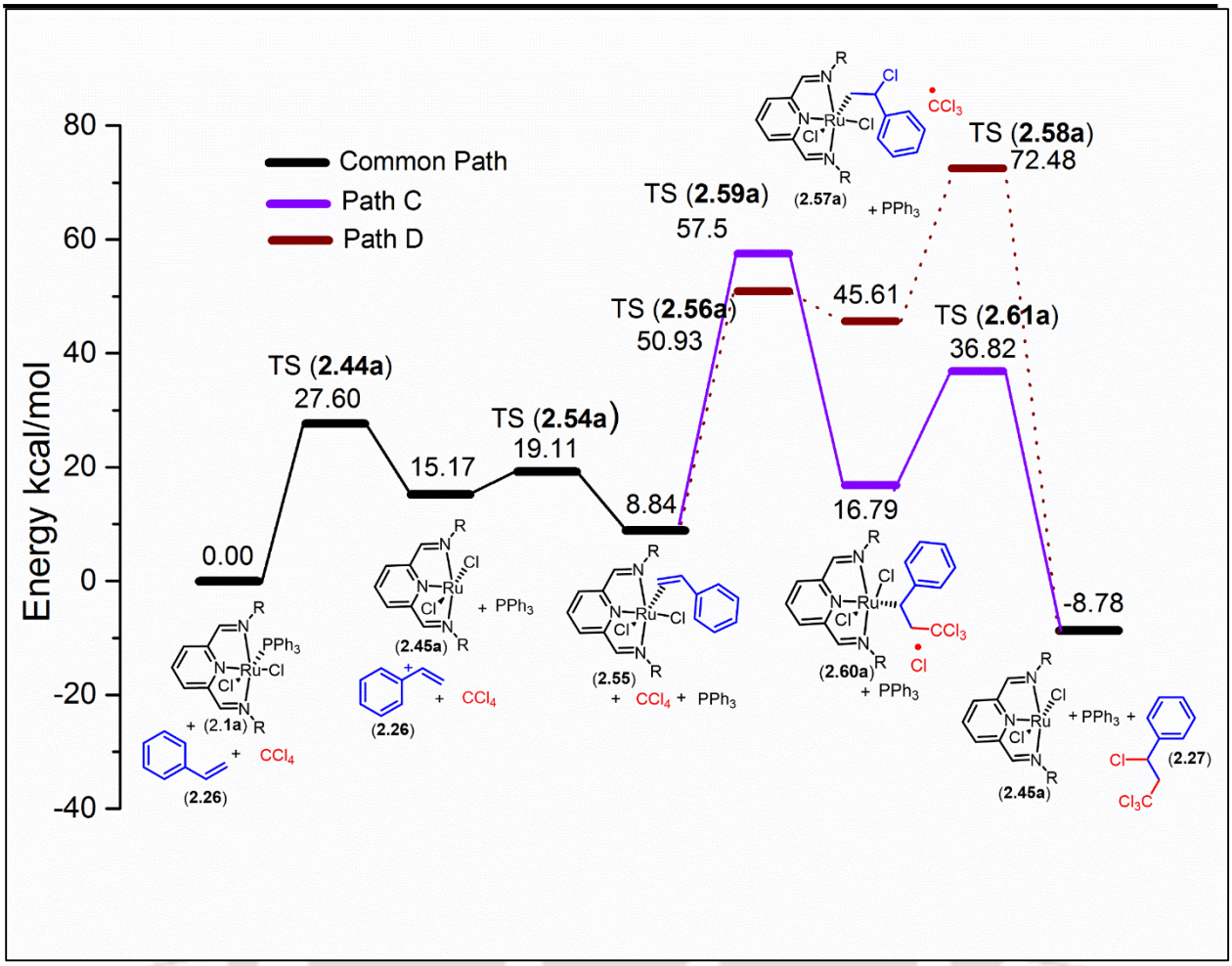

Figure 2.7: Energetics of various species involved in the (^{Cy2}NNN)RuCl$_2$(PPh$_3$) catalyzed ATRA via path **C** and **D**.

DFT studies were carried out using PBEPBE functional with LANL2DZ basis set for Ru and 6-311G(d,p) for all other atoms.

Experimentally, from HRMS studies, it has been proved that **2.1a** is the resting state of the catalyst in the reaction mixture. Thus, it can be conveniently assumed that the transformation of (**2.1a**) to (**2.45a**) is the rate determining step (RDS) and the corresponding barrier (ca. 27.60 kcal/mol) (Figure 2.6 and Figure 2.7) should be energy of the rate-determining transition state RDTS (**2.44a**) (Figure 2.6 and Figure 2.7). This means for the path leading to ATRA, the barrier for all subsequent steps should be lower than 27.60 kcal/mol. So, considering all TS energy barriers among all possible paths, path **A** would be the most favorable as the highest barrier via path **A** is 5.51 kcal/mol lower than the barrier for the generation of (**2.45a**). This observation fits well with the HRMS (ESI) analysis.

Table 2.5: Energy barriers involved in formation of various intermediates via path **A**, path **B**, path **C** and path **D**.

Entry	Path	TS	Barrier kcal/mol
1.	Path **A**	(**2.46a**)	22.09
2.	Path **A**	(**2.51a**)	0.24
3.	Path **A**	(**2.53a**)	13.51
4.	Path **B**	(**2.46'a**)	48.48
5.	Path **B**	(**2.48a**)	0.48
6.	Path **B**	(**2.50a**)	29.87
7.	Path **C** & **D**	(**2.54a**)	3.94
8.	Path **C**	(**2.59a**)	48.65[a]
9.	Path **C**	(**2.61a**)	20.03
10.	Path **D**	(**2.56a**)	42.08
11.	Path **D**	(**2.58a**)	26.87

a) This number is a close approximation as moderedundant was used to freeze the bonds involved in TS.

2.3.4 Varying catalyst loading

The (^{Cy2}NNN)RuCl$_2$(PPh$_3$) (**2.1a**) [1 mM] catalyzed ATRA of CCl_4 to styrene [2.2 M] was then performed with varying catalyst loading. Increasing the catalyst loading to 5 mM and 10 mM in the reaction of CCl_4 [7.9 M] and styrene [2.2 M] at 100 °C resulted in better yields of the ATRA product but with lower turnovers (Entries 1 and 2, Table 2.6). The ATRA of CCl_4 [7.9 M] to styrene [2.2 M] at 100 °C catalyzed by 0.5 mM (**2.1a**) provided 2000 turnover number after 48 h (Entry 4, Table 2.6). Under identical conditions, the use of 0.2 mM (**2.1a**) resulted in 1665 and 2478 TONs (Entry 5 and 6, Table 2.3) after 48 h and 96 h respectively. On increasing the temperature to 140 °C, the ATRA of styrene [2.2 M] with 0.2 mM (**2.1a**) resulted in 5670 turnover number after 48 h (Entry 7, Table 2.6). Presumably, this is the highest turnover reported up till now for the ATRA of CCl_4 to styrene either with or without any radical initiator.

Table 2.6: Catalytic ATRA to styrene with varying loading of (^{Cy2}NNN) $RuCl_2(PPh_3)$

Entry	Catalyst (2.1a) mM	Styrene Conversion (%)	Product (2.27)	
			Yield[a] mM (%)	TON
1.	10.0	100	2100 (95)	210
2.	5.0	100	1605(73)	321
3.	1.0	100	1385 (63)	1385
4.	0.5	98	1000 (45)	2000
5.	0.2	50	334 (15)	1665
6[b].	0.2	57	496[b] (23)	2478
7[c].	0.2	100	1134 (52)	5670

[a)] Yield determined by GC analysis using toluene as an internal standard. [b)] After 96 h of reaction. [c)] Reaction carried out at 140 °C.

2.3.5 Substrate scope

To further explore the catalytic activity, the Kharasch addition catalyzed by (**2.1a**) and (**2.1c**) was screened for two additional substrates 4-methyl styrene **(2.26a**) and 4-fluro-styrene (**2.26b**) (Table 2.7). It is evident that under a given condition, the ATRA is more favorable with styrene substituted by electron-withdrawing -F group compared to electron donating methyl substituent in styrene (entry 2 and 3, table 2.7).

The ATRA was repeated with $CHCl_3$, CH_2Cl_2 and CBr_4 in presence of **2.1a** [1mM]. The catalyst **2.1a** was however very slow towards the ATRA of $CHCl_3$ (Entry 4, Table 2.7), and CBr_4 (Entry 6, Table 2.7). When CH_2Cl_2 was treated with styrene in presence of **2.1a** [1mM], no product was obtained (entry 5, table 2.7). It is observed that CCl_4 is much better towards ATRA compared to CBr_4. Under similar conditions, CCl_4 gave 1385 TON, whereas CBr_4 gave only 400 TON of the corresponding ATRA product.

Table 2.7: ATRA performed with variety of substrates in presence of **2.1a** [1 mM]

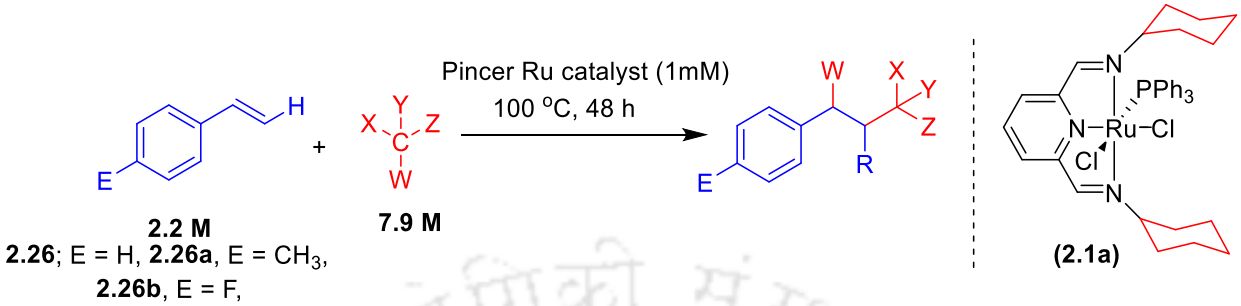

Entry	E	Reactant	Product	TON[a]
1.	H	CCl_4	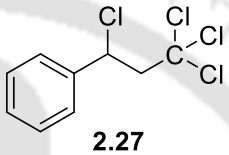 **2.27**	1385
2.	CH_3	CCl_4	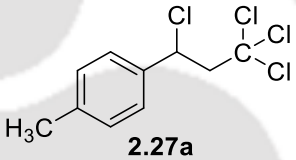 **2.27a**	1141
3.	F	CCl_4	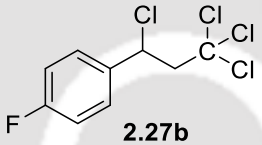 **2.27b**	1540
4.	H	$CHCl_3$	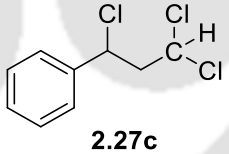 **2.27c**	12
5.	H	CH_2Cl_2	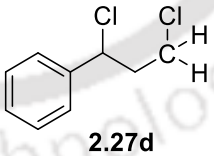 **2.27d**	0
6.	H	CBr_4	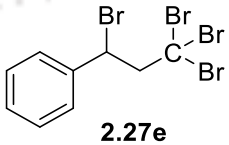 **2.27e**	400

[a]Yield determined by GC analysis using toluene as an internal standard

Table 2.8: ATRA performed with variety of substrate in presence of **2.1a** [0.2 mM]

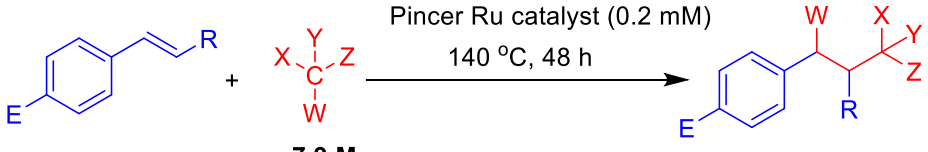

2.26; E = H,R = H
2.26a, E = CH_3, R = H
2.26b, E = F, R = H
2.26f: E = H, R = Me

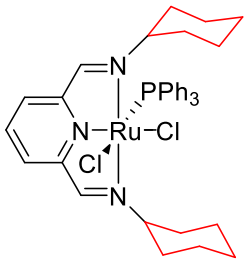

(2.1a)

Entry	E	R	Reactant	Product	TON[a]
1.	H	H	CCl_4	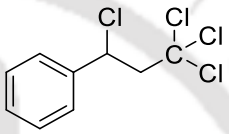 **2.27**	5670
2.	Me	H	CCl_4	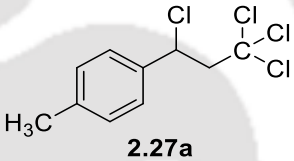 **2.27a**	1747
3.	F	H	CCl_4	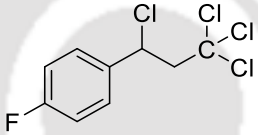 **2.27b**	5920
4.	H	Me	CCl_4	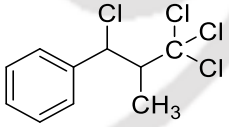 **2.27f**	5873[b]
5[c].	H	H	$CHCl_3$	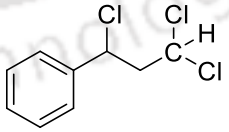 **2.27c**	180

[a]Yield determined by GC analysis using toluene as an internal standard. [b] Syn : Anti = 1 :3.c) Performed with 1 mM of **2.1a**

It is observed that upon decreasing the Cl substituent on the polyhalogenated methane, the rate also decreases. While the polyhalogenated methane with maximum number of Cl as in CCl_4 gave high TON 1385 (entry1, Table 2.7), use of $CHCl_3$ where the Cl substitution is decreased by one unit yielded only 12 TON (entry 4, Table 2.7). The yields obtained from the reaction between styrene and $CHCl_3$ were significantly lowered compared to addition of CCl_4 to styrene, due to the fact that the bond in chloroform is much less susceptible to attack than C-Cl bonds in CCl_4.[3] The ATRA activity was fully diminished in presence of CH_2Cl_2 (entry 5, Table 2.7). The decrease in reactivity of halo-methane with decreasing number of halogen substituents has been previously observed in the addition between α-chlorinated acetic acids to octene.[72] Accordingly, while tricholoroacetyl chloride gave a practically quantitative yield of the addition product, methyl dichloroacetate gave slightly reduced yield (81 %). On the other hand, methyl chloroacetate gave a poor yield (10 %) of addition product.[72]

When the reaction was performed with electron withdrawing F substituent on styrene in presence of **2.1a** [1mM] 1540 TON of the ATRA product was obtained (Entry 3, Table 2.7). On the other hand, electron donating methyl substituent resulted in 1141 TON (Entry 2, Table 2.7). Upon lowering the catalyst loading from 1 mM to 0.2 mM of (^{Cy2}NNN)$RuCl_2(PPh_3)$ (**2.1a**), the TON increased and 1747 TON (entry 2, Table 2.8) were obtained with electron donating methyl substituents on styrene. Under similar condition, with electron withdrawing 4-fluro-styrene, the TON increased to 5920 (entry 3, Table 2.8). In the reactions performed with trans-*β*-methyl styrene, 5873 TON were obtained as a mixture of both *syn* and *anti* in the ratio of 1:3.

2.4 Conclusion

The catalytic application of a series of pincer-ruthenium complexes of the type (^{R2}NNN)$RuCl_2(PPh_3)$ (R = Cy , **2.1a**; ^{t}Bu, **2.1b**; ^{i}Pr, **2.1c**; and Ph, **2.1d**) is reported here. These pincer-ruthenium complexes have been found to be active towards Kharasch addition of CCl_4 to styrene. Among the various complexes, (^{Cy2}NNN)$RuCl_2(PPh_3)$ (**2.1a**) exhibits very high catalytic efficiency (5670 TON) towards Kharasch addition. This is the highest turnover reported yet for the ATRA of CCl_4 to styrene. The catalytic activity follows the order (^{Cy2}NNN)$RuCl_2(PPh_3)$ (**2.1a**) > (^{iPr2}NNN)$RuCl_2(PPh_3)$ (**2.1c**) >> (^{Ph2}NNN)$RuCl_2(PPh_3)$ (**2.1d**). This trend is in line with the cyclic voltammetry data, where it has been observed that **2.1a** and **2.1c** are being oxidized at lower

potentials compared to **2.1d**. Quantum mechanical calculations provide valuable insights into the (^{R2}NNN)$RuCl_2(PPh_3)$ catalyzed Kharasch addition. The Ru-P bond energy is in accordance with the observed trend in corresponding catalytic activity. The generation of catalytically active species (^{Cy2}NNN)$RuCl_2$ (**2.45a**) is more favorable than (^{Ph2}NNN)$RuCl_2$ (**2.45d**). Experimental observations (HRMS analysis) and DFT calculations indicated that (**2.1a-d**) are the resting states of corresponding catalytic cycles. DFT studies also indicate that, the barrier of the path that involves benzyl radical bound within the coordination sphere of the active Ru(III) species is much lower and favorable compared to the barrier of other possible paths.

2.5 Experimental section

General procedure

All manipulations were carried out under purified Ar using a standard double manifold. While tetrahydrofuran (THF) and toluene were dried via double distillation over Na/benzophenone prior to experiment, the solvents ethanol, methanol and CCl_4 were purified and distilled under argon according to a literature procedure.[73] The ruthenium precursor, $RuCl_2(PPh_3)_3$ was prepared following a previous protocol.[61, 74] The pincer-Ru complexes (**2.1a-d**) were synthesized according to literature procedure.[61, 62] All other compounds including styrene and $CDCl_3$ were purchased either from MERCK or from Sigma-Aldrich and used as such.

Physical measurements

^{1}H, ^{13}C, ^{19}F, and ^{31}P{H} NMR were recorded either on a Bruker ASCEND 600 operating at 600 MHz for ^{1}H, 150 MHz for ^{13}C{H}, and 242.85 MHz for ^{31}P{H} or on a Bruker AVANCE 400 operating at 400 MHz for ^{1}H, 100 MHz for ^{13}C{H}, 376 MHz for ^{19}F, and 161.9 MHz for ^{31}P. HRMS measurements were done using an Agilent Accurate-Mass Q-TOF ESI–MS 6520. GC measurements were performed on an Agilent 7820-GC instrument fitted with Agilent Front SS7 enlet N_2 HP5 column (30 m length × 0.32 mm ID). Cyclic voltammograms (CVs) of the Ru complexes (1mM) were carried out on VersaSTST 3 instrument in dry CH_2Cl_2 (25 ^{o}C) solution containing 0.10 M ^{n}Bu$_4$NPF$_6$ as supporting electrolyte. A glassy carbon as working electrode, a platinum wire as counter electrode and Ag/AgCl as reference electrode were used. The experiments were performed with scan rates of 50, 100 and 200 mV/s. Ferrocene was used as an

internal standard and all the potentials were referenced to the ferrocenium (Fc+)/ferrocene (Fc) couple.

General procedure for the pincer-ruthenium catalyzed Kharasch addition of CCl_4 to styrene

In a typical reaction, the complex (^{iPr2}NNN)$RuCl_2(PPh_3)$ (**2.1c**) (0.7 mg, 1µmol) was added to a mixture of styrene (0.25 mL, 2.17 mmol) and CCl_4 (0.77 ml, 7.93 mmol) in a sealable vial under an atmosphere of argon. Toluene (20 µL, 0.188 mmol) was added as an internal standard. The vial was closed under argon and the reaction mixture was refluxed for 48 h. An aliquot of the reaction mixture was subsequently injected into the GC and the TON was measured. The Kharasch addition product was then purified by column chromatography using hexane as eluent.

(1,3,3,3–tetrachloropropyl)benzene (2.27)

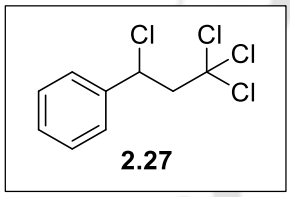

2.27

^{1}H NMR (400 MHz, $CDCl_3$, 25 °C): δ 7.45–7.32 (m, 5H), 5.32–5.29 (m, 1H), 3.58 (qd, J = 15.3, 5.9 Hz, 2H) ^{13}C{H} NMR (100 MHz, $CDCl_3$, 25 °C): δ 140.6, 129.1, 127.5, 96.4, 62.9, 58.4.

1–methyl–4–(1,3,3,3–tetrachloropropyl)benzene (2.27a)

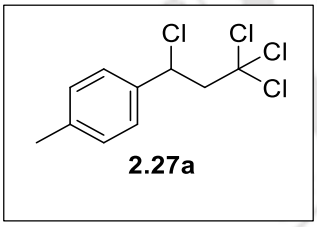

2.27a

^{1}H NMR (400 MHz, $CDCl_3$, 25 °C): δ 7.34 (d, J = 8.1 Hz, 2H), 7.20 (d, J = 8.0 Hz, 2H), 5.32–5.28 (m, 1H), 3.59 (qd, J = 15.3, 5.9 Hz, 2H), 2.37 (s, 3H). ^{13}C{H} NMR (100 MHz, $CDCl_3$, 25 °C): δ 139.0, 137.7, 129.7, 127.4, 96.4, 62.9, 58.4, 21.3.

1–fluro–4–(1,3,3,3–tetrachloropropyl)benzene (2.27b)

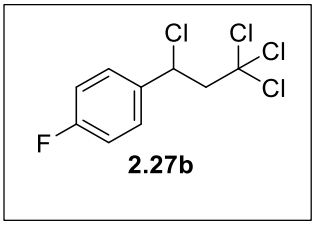

2.27b

^{1}H NMR (400 MHz, $CDCl_3$, 25 °C): δ 7.43 (dd, J = 8.8, 5.2 Hz, 2H), 7.08 (t, J = 8.6 Hz, 2H), 5.31 (dd, J = 6.9, 5.2 Hz, 1H), 3.62 (dd, J = 15.3, 5.2 Hz, 1H), 3.52 (dd, J = 15.3, 7.0 Hz, 1H). ^{13}C{H} NMR (100 MHz, $CDCl_3$, 25 °C): δ 164.1, 161.7, 136.4, 136.3, 129.5, 129.4, 116.1, 115.9, 96.1, 62.8, 57.6. 19F NMR (376 MHz, $CDCl_3$, 25 °C) –112.10.

(1,3,3-trichloropropyl)benzene (2.27c)

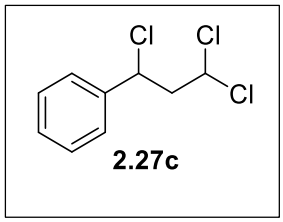

2.27c

^{1}H NMR (400 MHz, $CDCl_3$, 25 °C): δ 7.35 – 7.23 (m, 5H), 5.71 (dd, J = 8.3, 4.9 Hz, 1H), 4.98 (dd, J = 9.5, 5.0 Hz, 1H), 2.99 – 2.54 (m, 2H). ^{13}C{H} NMR (100 MHz, $CDCl_3$, 25 °C): δ 139.56, 129.18, 129.17, 127.13, 70.46, 59.52, 52.89.

(1,3,3,3–tetrabromopropyl)benzene (2.27e)

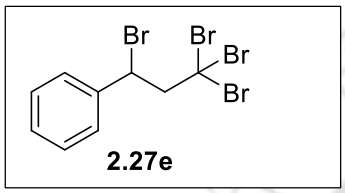

2.27e

^{1}H NMR (400 MHz, $CDCl_3$, 25 °C): δ 7.59 – 7.47 (m, 2H), 7.42 – 7.30 (m, 3H), 5.33 (dd, J = 7.7, 4.1 Hz, 1H), 4.28 – 3.93 (m, 2H). ^{13}C{H} NMR (100 MHz, $CDCl_3$, 25 °C): δ 140.94, 129.09, 129.03, 128.30, 66.61, 50.19, 35.15.

Computational details

Gaussian-09 (revision D.01) program package was used for all the calculations.[75] Geometries of all the considered molecules were fully optimized using generalized gradient corrected exchange and correlation functional PBEPBE.[76] The double-ζ quality LANL2DZ[77-79] basis set with effective core potential (ECP) was used for Ru atom and triple-ζ quality 6-311G basis set with polarization function (d,p) was used for all other atoms. Frequency calculations at the same method and basis set were performed to distinguish the optimized geometries as minima or transition state on the potential energy surface. Intrinsic reaction coordinate (IRC) calculations,[80] with mass weighted coordinates, were also performed to validate the reaction path and to follow the reaction profile.

Supporting information (containing NMR spectra of various compound and Cartesian coordinates of the computed complexes) for chapter 2 is available as appendix 1 and can be found at https://drive.google.com/file/d/1ihehIqPowud_sMY2RUiE8h3ZbLGq1vos/view?usp=sharing

2.6 References

1. Chung, W. j.; Vanderwal, C. D., *Angew. Chem. Int. Ed.* **2016**, *55* (14), 4396-4434.
2. Costa, D. C. S., *Arab. J. Chem.* **2020**, *13* (1), 799-834.
3. Kharasch, M.; Jensen, E. V.; Urry, W., *J. Am. Chem. Soc.* **1947**, *69* (5), 1100-1105.
4. Severin, K., *Curr. Org. Chem.* **2006**, *10* (2), 217-224.
5. Morales-Chamorro, M.; Meza-Gonzalez, J.; Cordero-Vargas, A., *Tetrahedron Lett.* **2015**, *56* (34), 4892-4894.

6. Wallentin, C.-J.; Nguyen, J. D.; Finkbeiner, P.; Stephenson, C. R. J., *J. Am. Chem. Soc.* **2012**, *134* (21), 8875-8884.
7. Arshad, D.; Jantan, I.; Haque, M.; Bukhari, S. N. A., **2017**.
8. Guo, Z., *Acta. Pharm. Sin. B* **2017**, *7* (2), 119-136.
9. Sekar, G.; DattaGupta, A.; Singh, V. K., *J. Org. Chem.* **1998**, *63* (9), 2961-2967.
10. Charette, A. B.; Lemay, J., *Angew. Chem. Int. Ed. in English* **1997**, *36* (10), 1090-1092.
11. Weinreb, S.; Trost, B.; Fleming, I., *Trost, BM; Fleming, I.(eds.)* **1991**, 5.
12. Adam, W.; Corma, A.; Reddy, T. I.; Renz, M., *J. Org. Chem.* **1997**, *62* (11), 3631-3637.
13. Kharasch, M.; ENGELMANN, H.; MAYO, F. R., *J. Org. Chem.* **1937**, *2* (3), 288-302.
14. Kharasch, M.; Jensen, E. V.; Urry, W., *Science* **1945**, *102* (2640), 128-128.
15. Courant, T.; Masson, G. r., *J. Org. Chem.* **2016**, *81* (16), 6945-6952.
16. Nair, R. P.; Kim, T. H.; Frost, B. J., *Organometallics* **2009**, *28* (16), 4681-4688.
17. Yorimitsu, H.; Shinokubo, H.; Matsubara, S.; Oshima, K.; Omoto, K.; Fujimoto, H., *J. Org. Chem.* **2001**, *66* (23), 7776-7785.
18. Wu, F.-H.; Huang, W.-Y., *J. Fluor. Chem.* **2001**, *110* (1), 59-61.
19. Denisov, E. T.; Denisova, T. G.; Pokidova, T. S., *Handbook of free radical initiators*. John Wiley & Sons: 2005.
20. Kharasch, M.; Urry, W.; Kuderna, B., *J. Org. Chem.* **1949**, *14* (2), 248-253.
21. Mayo, P. d.; Stothers, J.; Templeton, W., *Can. J. Chem.* **1961**, *39* (3), 488-497.
22. Kharasch, M.; Skell, P.; Fisher, P., *J. Am. Chem. Soc.* **1948**, *70* (3), 1055-1059.
23. Pintauer, T.; Matyjaszewski, K., *Chem. Soc. Rev.* **2008**, *37* (6), 1087-1097.
24. De Malde, M.; Minisci, F.; Pallini, U.; Volterra, E.; Quilico, A., *Chim.Ind. (Milano)* **1956**, *38*, 371-382.
25. Hájek, M.; Šilhavý, P.; Málek, J., *Collect. Czech. Chem. Commun.* **1980**, *45* (12), 3502-3509.
26. Hájek, M.; Šilhavý, P.; Málek, J., *Collect. Czech. Chem. Commun.* **1980**, *45* (12), 3488-3501.
27. Metzger, J. O.; Mahler, R., *Angew. Chem. Int. Ed. in English* **1995**, *34* (8), 902-904.
28. Steiner, E.; Martin, P.; Belluš, D., *Helv. Chim. Acta* **1982**, *65* (3), 983-985.
29. Forti, L.; Ghelfi, F.; Libertini, E.; Pagnoni, U. M.; Soragni, E., *Tetrahedron* **1997**, *53* (52), 17761-17768.
30. Forti, L.; Ghelfi, F.; Pagnoni, U. M., *Tetrahedron Lett.* **1996**, *37* (12), 2077-2078.
31. Sawama, Y.; Nakatani, R.; Imanishi, T.; Fujiwara, Y.; Monguchi, Y.; Sajiki, H., *RSC Adv.* **2014**, *4* (17), 8657-8660.
32. Wang, X.-B.; Woo, H.-K.; Wang, L.-S.; Minofar, B.; Jungwirth, P., *J. Phy. Chem. A* **2006**, *110* (15), 5047-5050.
33. Gossage, R. A.; van de Kuil, L. A.; van Koten, G., *Acc. Chem. Res.* **1998**, *31* (7), 423-431.
34. Pandarus, V.; Zargarian, D., *Organometallics* **2007**, *26* (17), 4321-4334.
35. van de Kuil, L. A.; Grove, D. M.; Gossage, R. A.; Zwikker, J. W.; Jenneskens, L. W.; Drenth, W.; van Koten, G., *Organometallics* **1997**, *16* (23), 4985-4994.
36. Minisci, F., *Acc. Chem. Res.* **1975**, *8* (5), 165-171.
37. Muñoz-Molina, J. M.; Belderraín, T. R.; Pérez, P. J., *Adv. Synth. Catal.* **2008**, *350* (14-15), 2365-2372.
38. Patten, T. E.; Matyjaszewski, K., *Acc. Chem. Res.* **1999**, *32* (10), 895-903.

39. Nishiyama, H.; Ikeda, H.; Saito, T.; Kriegel, B.; Tsurugi, H.; Arnold, J.; Mashima, K., *J. Am. Chem. Soc.* **2017**, *139* (18), 6494-6505.
40. Simal, F.; Wlodarczak, L.; Demonceau, A.; Noels, A. F., *Tetrahedron Letters* **2000,** 41 (32), 6071-6074.
41. Simal, F.; Demonceau, A.; Noels, A. F., *Tetrahedron Lett.* **1999**, *40* (31), 5689-5693.
42. Boualy, B.; Harrad, M. A.; El Firdoussi, L.; Ali, M. A.; El Houssame, S.; Karim, A., *Catal. Commun.* **2011**, *12* (14), 1295-1297.
43. Muñoz-Molina, J. M.; Sameera, W.; Álvarez, E.; Maseras, F.; Belderrain, T. R.; Pérez, P. J., *Inorg. Chem.* **2011**, *50* (6), 2458-2467.
44. Clark, A. J., *Chem. Soc. Rev.* **2002**, *31* (1), 1-11.
45. Chen, B.; Fang, C.; Liu, P.; Ready, J. M., *Angew. Chem.* **2017**, *129* (30), 8906-8910.
46. Matsumoto, H.; Nakano, T.; Nagai, Y., *Tetrahedron Lett.* **1973**, *14* (51), 5147-5150.
47. Bland, W. J.; Davis, R.; Durrant, J. L., *J. Organomet. Chem.* **1985**, *280* (3), 397-406.
48. Borguet, Y.; Richel, A.; Delfosse, S.; Leclerc, A.; Delaude, L.; Demonceau, A., *Tetrahedron Lett.* **2007**, *48* (36), 6334-6338.
49. Baraut, J.; Massard, A.; Chotard, F.; Bodio, E.; Picquet, M.; Richard, P.; Borguet, Y.; Nicks, F.; Demonceau, A.; Le Gendre, P., *Eur. J. Inorg. Chem.* **2015**, *2015* (16), 2671-2682.
50. Richel, A.; Demonceau, A.; Noels, A. F., *Tetrahedron Lett.***2006**, *47* (13), 2077-2081.
51. Tutusaus, O.; Viñas, C.; Núñez, R.; Teixidor, F.; Demonceau, A.; Delfosse, S.; Noels, A. F.; Mata, I.; Molins, E., *J. Am. Chem. Soc.* **2003**, *125* (39), 11830-11831.
52. Richel, A.; Delfosse, S.; Cremasco, C.; Delaude, L.; Demonceau, A.; Noels, A. F., *Tetrahedron Lett.* **2003**, *44* (32), 6011-6015.
53. Chotard, F.; Malacea-Kabbara, R.; Balan, C.; Bodio, E.; Picquet, M.; Richard, P.; Ponce-Vargas, M.; Fleurat-Lessard, P.; Le Gendre, P., *Organometallics* **2018**, *37* (5), 812-820.
54. Lundgren, R. J.; Rankin, M. A.; McDonald, R.; Stradiotto, M., *Organometallics* **2007**, *27* (2), 254-258.
55. Lee, B. T.; Schrader, T. O.; Martín-Matute, B.; Kauffman, C. R.; Zhang, P.; Snapper, M. L., *Tetrahedron* **2004**, *60* (34), 7391-7396.
56. Eckenhoff, W. T.; Pintauer, T., *Catal. Rev.* **2010**, *52* (1), 1-59.
57. Wu, G.; Börger, J.; Jacobi von Wangelin, A., *Angew. Chem.* **2019**, *131* (48), 17401-17405.
58. Eckenhoff, W. T.; Biernesser, A. B.; Pintauer, T., *Inorg. Chim. Acta.* **2012**, *382*, 84-95.
59. Kumar, A.; Bhatti, T. M.; Goldman, A. S., *Chem. Rev.* **2017**, *117* (19), 12357-12384.
60. Peris, E.; Crabtree, R. H., *Chem. Soc. Rev.* **2018**, *47* (6), 1959-1968.
61. Das, K.; Dutta, M.; Das, B.; Srivastava, H.; Kumar, A., *Adv. Synth. Catal.* **2019**, *361* (12), 2965-2980.
62. Das, K. Ph.D Thesis (On-going), Indian Institute of Technology Guwahati.
63. Das, K.; Nandi, P. G.; Islam, K.; Srivastava, H. K.; Kumar, A., *Eur. J. Org. Chem.* **2019**, *40*, 6855-6866.
64. Chotard, F.; Malacea-Kabbara, R.; Balan, C. d.; Bodio, E.; Picquet, M.; Richard, P.; Ponce-Vargas, M.; Fleurat-Lessard, P.; Le Gendre, P., *Organometallics* **2018**, *37* (5), 812-820.
65. Simal, F.; Demonceau, A.; Noels, A. F., *Angew. Chem. Int. Ed.* **1999**, *38* (4), 538-540.
66. Kato, M.; Kamigaito, M.; Sawamoto, M.; Higashimura, T., *Macromolecules* **1995**, *28* (5), 1721-1723.
67. Takahashi, H.; Ando, T.; Kamigaito, M.; Sawamoto, M., *Macromolecules* **1999**, *32* (11), 3820-3823.

68. Koten, G. v.; Grove, D.; Verschuuren, A. H., *J. Mol. Catal.* **1988**, *45* (2), 169-174.
69. Spasyuk, D. M.; Zargarian, D.; van der Est, A., *Organometallics* **2009**, *28* (22), 6531-6540.
70. Gamasa, M. P.; Gimeno, J.; Gonzalez-Bernardo, C.; Martín-Vaca, B. M.; Monti, D.; Bassetti, M., *Organometallics* **1996**, *15* (1), 302-308.
71. Das, K.; Dutta, M.; Das, B.; Srivastava, H. K.; Kumar, A., *Adv. Synth. Catal.* **2019**, *361* (12), 2965-2980.
72. Kharasch, M. S.; Urry, W. H.; Jensen, E. V., *J. Am. Chem. Soc.* **1945**, *67* (9), 1626-1626.
73. Armarego, W. L., *Purification of laboratory chemicals*. Butterworth-Heinemann: 2017.
74. Samouei, H.; Grushin, V. V., *Organometallics* **2013**, *32* (15), 4440-4443.
75. G.W. T. M. J. Frisch, H. B. Schlegel, G. E. Scuseria, M. A. Robb, J. R. Cheeseman, G. Scalmani, V. Barone, B. Mennucci, G. A. Petersson, H. Nakatsuji, M. Caricato, X. Li, H. P. Hratchian, A. F. Izmaylov, J. Bloino, G. Zheng, J. L. Sonnenberg, M. Hada, M. Ehara, K. Toyota, R. Fukuda, J. Hasegawa, M. Ishida, T. Nakajima, Y. Honda, O. Kitao, H. Nakai, T. Vreven, J. A. Montgomery, Jr., J. E. Peralta, F. Ogliaro, M. Bearpark, J. J. Heyd, E. Brothers, K. N. Kudin, V. N. Staroverov, T. Keith, R. Kobayashi, J. Normand, K. Raghavachari, A. Rendell, J. C. Burant, S. S. Iyengar, J. Tomasi, M. Cossi, N. Rega, J. M. Millam, M. Klene, J. E. Knox, J. B. Cross, V. Bakken, C. Adamo, J. Jaramillo, R. Gomperts, R. E. Stratmann, O. Yazyev, A. J. Austin, R. Cammi, C. Pomelli, J.W. Ochterski, R. L. Martin, K. Morokuma, V. G. Zakrzewski, G. A. Voth, P. Salvador, J. J. Dannenberg, S. Dapprich, A. D. Daniels, O. Farkas, J. B. Foresman, J. V. Ortiz, J. Cioslowski, and D. J. Fox, *Gaussian 09, Revision D.01, Gaussian, Inc., Wallingford CT* **2013**.
76. Perdew, J. P.; Burke, K.; Ernzerhof, M., *Phys. Rev. Lett.* **1996**, *77* (18), 3865.
77. Wadt, W. R.; Hay, P. J., *J. Chem. Phy.* **1985**, *82* (1), 284-298.
78. Hay, P. J.; Wadt, W. R., *J. Chem. Phy.* **1985**, *82* (1), 299-310.
79. Hay, P. J.; Wadt, W. R., *J. Chem. Phy.* **1985**, *82* (1), 270-283.
80. K. Fukui, Acc. Chem. Res. **1981**, *14*, 363–368.

Chapter 3

NNN Pincer-Ruthenium Catalyzed Transformation of Glycerol Selectively to Lactic Acid: An Experimental and Computational Study

3.1 Introduction

In recent years, crude-oil consumption has dramatically increased as a result of the enormous demand for transportation and domestic use, which has caused severe environmental concerns. As crude oil reserves diminish, emphasis has been laid on renewable and alternative energy sources in order to cater to the constantly increasing energy demand.[1] Biodiesel can be one of the prominent renewable fuels which can be made from a variety of resources such as recycled cooking oil, soybean oil and animal fat. In the period of 2000-2012, biodiesel production has significantly increased from 15 to 430 thousand barrels.[2-3] In 2018, global production of biodiesel increased nearly 7% compared to 2017, reaching to 153 billion liters.[4] In the process of producing biodiesel during base-catalyzed transesterification, saponification and hydrolysis of fats/oils, glycerol is one of the major by-products.[5] The last two decades have witnessed enormous use of biodiesel which has to lead to a surge in the production of glycerol. Approximately 0.1 pounds of crude glycerol is produced during the production of every one pound of oil.[6] Worldwide crude glycerol derived from biodiesel conversion increased from 2,00,000 tonnes in 2004[7] to 9,00,000 tonnes in 2005[8] and 1.224 million tonnes in 2008[9] that progressed to > 2 million tonnes in 2012.[10] Now a days, the supply of glycerol is entirely independent of its demand as there is as much glycerol as the amount of vegetable oils and animal fats that are hydrolyzed or trans-esterified to produce biodiesel. Huge formation of crude glycerol from biodiesel has impacted the refined glycerol market and glycerol turns out to be significantly cheap. Glycerol can be converted to several value-added products including food, cosmetics and fine chemicals.[11] Several value-added feedstock for chemicals such as 1,3-propanediol,[12] citric acid,[13] poly-hydroxyalkanoates (PHA),[14] decosahexanoic acid,[15] succinic acid,[16] hydrogen gas[17] and other fuel molecules such as ethanol,[18] methane,[19] butanol[20] can be produced from glycerol via biological conversion. Numerous industrially important intermediates can be derived from glycerol including glyceric acid, glycolic acid, 1,2-propane diol (1,2-PDO), 1,3-propane diol (1,3-PDO) and ethylene glycol. These are essential building blocks for the synthesis of antifreeze, resin, polyester and other bio-gradable materials.[21-24] Dehydrogenation of glycerol also yields lactic acid which is a valuable feedstock for organic synthesis including food, pharmaceuticals, fine chemicals and cosmetics.[25-26]

Selective acceptorless dehydrogenation of glycerol to lactic acid is very attractive. Lactic acid can be beneficial as an environmentally friendly green solvent[27] and as a precursor for poly-lactic acid (PLA)[28]. The acceptorless dehydrogenative transformation of glycerol to precious lactic acid is

atom economical and is not only accompanied by the production of H_2, a good source of clean energy but it also does not lead to waste generation.[29]

H_2 gas can be generated from water,[30] from enzyme fermentation of biomass,[31] from gasification,[32] and from heterogeneous catalytic reforming in super-critical water[33]. Homogeneous methods for hydrogen generation involve acceptorless dehydrogenation of alcohols such as EtOH, MeOH, ^{i}PrOH.[34-37] Besides simple alcohols, polyols like glycerol can also generate H_2 gas.[38-40] Compared to the dehydrogenation of simple alcohols, glycerol dehydrogenation has several advantages since it is non-flammable, relatively non-toxic, has a high boiling point and is readily available via biodiesel production.[41]

Lactic acid is non-volatile, odorless and recognized as safe for the general purpose use as food additive. It is an excellent preserving agent for pickled vegetables and used as an inhibitor of bacterial spoilage in a wide variety of processed food such as bakery products, soft drink, dairy products, candy, jam, jellies and processed eggs. In the leather tanning industry, technical grade lactic acid can be used as an acidulate for deliming hides and in vegetable tanning. Lactic acid is also used in pharmaceuticals, cosmetic and medicinal applications.

3.2 History of lactic acid synthesis

Lactic acid production was around 10,000 pounds in 1894;[42] 400,000 pounds in 1897;[42] 1,000,000 pounds in 1917,[42] and in 1982 it reached approximately 24,000-28,000 metric tonnes per year.[43] By 1990, the worldwide production of lactic acid had significantly increased to approximately 40,000 metric tonnes per year.[44] In 2006, the world wide lactic acid production including polymer uses was estimated to be around 1,20,000 metric tonnes per year.[45] The polymeric form of lactic acid, polylactic acid (PLA) is a valuable feedstock for biodegradable polymer and the market demand of PLA is estimated at 1,50,000 tons by 2017 and 4,00, 000 tons by 2022.[46]

Lactic acid is a naturally occurring organic acid. The boiling point of lactic acid is 122 °C at 2 KPa. In 1780, Swedish chemist Scheele first commercially produced lactic acid through its isolation from sour milk.[47] Lactic acid is synthesized from glycerol via bioconversion involving traditional fermentation or chemical synthesis.

3.2.1 Microbial source of lactic acid :

Bacterial fermentation is well known for lactic acid production. Lactic acid bacteria (LAB) are used in lactic acid production from different carbon sources. The first report of lactic acid

production through fungal fermentation was reported in 1936.[48] Bacterial species[43] such as *Lactobacillus*, *Streptococcus*, *Leuconostoc* and *Enterococcus* as well as fungal strains[49] such as *Mucor*, *Monilia*, *Rhizopus*can efficiently produce lactic acid. The best known fungal source of lactic acid is *Rhizopusoryzae*.[50] Fermentation techniques lead to high yields of desired stereo-selective lactic acid.[51] However, these suffer from several drawbacks such as expensive culture media for a specific lactic acid producing bacteria,[47] product inhibition caused by impurities in crude glycerol [52] uneconomical and environment unfriendly purification processes[47].

3.2.2 Lactic acid production from renewable sources:

Recovery and reuse of waste material are essential from both an environmental and rational utilization of natural resources point of view. Significant amounts of lactic acid are produced from hydrothermal treatment of organic waste *i.e.* domestic sludge, cellulosic and plastic waste with or without using H_2O_2.[53] Lactic acid can also be manufactured by means of anaerobic fermentation of carbohydrates (glucose, sucrose and lactose), sugar-containing materials (molasses and sugarcane bagasse) and starchy materials from potato, tapioca, wheat and barley.[54] Globally, on an approximate, 3.5 billion tons of agricultural residue are produced per annum, and these agro-industrial residues are utilized as a huge source of lactic acid production.[44] Apart from agricultural resources, waste materials from animal origin can also be utilized as the carbon source for lactic acid formation. Different types of LAB under free cell or immobilized conditions enhances the fermentation of lactic acid.[55-56] Hydrolysis of waste fish or meat from subcritical water can produce about 0.03g lactic acid per gram of dry meat and during the process, lactic acid is stable up to the reaction temperature of 240 °C (at 3.35 MPa).[57] Quitain *et al.* have shown that lactic acid can be obtained through deamination and hydroxylation of amino acids such as alanine, aspartic acid.[58]

3.2.3 Lactic acid from chemical synthesis:

Earlier lactic acid was chemically synthesized from lactonitrile intermediate, which is obtained through base-catalyzed addition of hydrogen cyanide to aldehyde. From crude lactonitrile, lactic acid is obtained via hydrolysis by using either concentrated hydrochloric acid or sulfuric acid and then purified by hydrolysis.[59] Along with the formation of crude lactic acid, corresponding ammonium salt is obtained as a byproduct. This crude lactic acid is esterified with methanol to form methyl lactate and further purified (Scheme 3.1, equation 1-3). This method is useful for

large scale synthesis of lactic acid but the limited raw material was a major drawback for this process. The chemical reaction between HCN and acetaldehyde is of less interest due to environmental concerns.

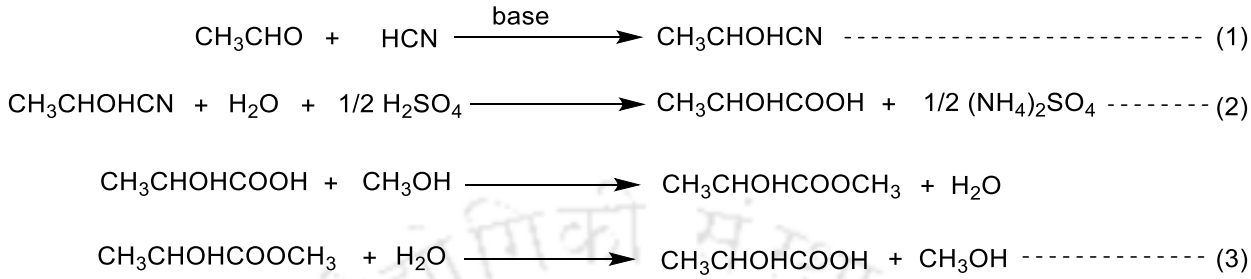

Scheme 3.1: Lactic acid generated from an lactonitrile intermediate.[59]

Kishida *et al.* studied a base-catalyzed conversion of glycerol to lactic acid by hydrothermal treatment at 573K (Scheme 3.2).[60] In this base-catalyzed glycerol dehydrogenation reaction, glycerol is first converted to 2-hydroxypropenal and a molecule of H_2. Then through keto-enol tautomerization, 2-hydroxypropenal leads to pyruvaldehyde, which is followed by Cannizaro reaction of pyruvaldehyde to lactic acid. Here, OH^- group not only reacts as a catalyst but also acts as a base.

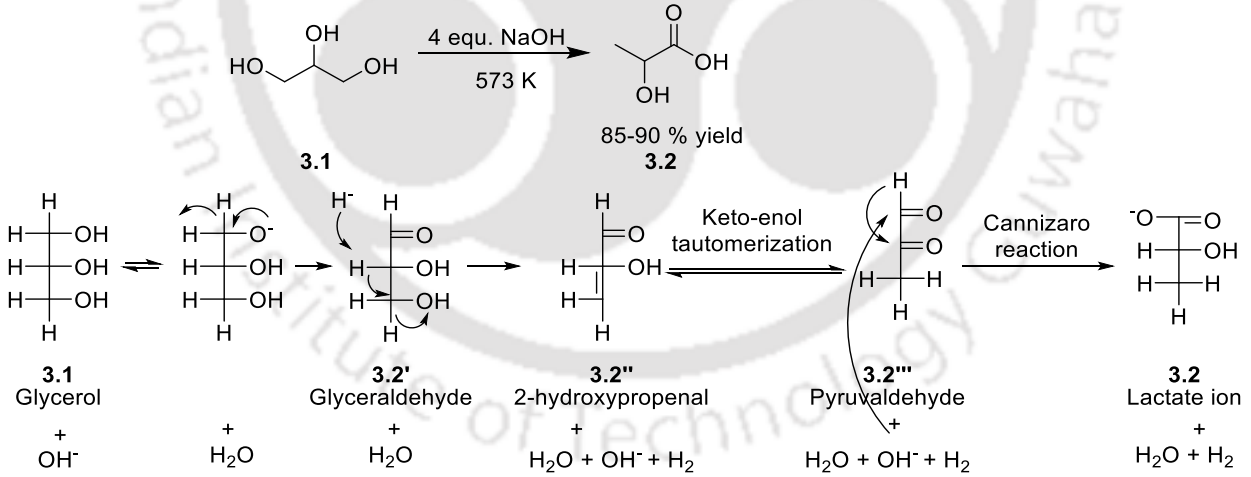

Scheme 3.2: Glycerol dehydrogenation under alkaline conditions.[60]

The concentration of OH^- is vital for the transformation of glycerol. Various metal hydroxides with the same initial concentration gave different results. Alkaline metal hydroxides catalyzed glycerol dehydrogenation reaction followed the sequence KOH > NaOH > LiOH > $Ba(OH)_2$ > $Sr(OH)_2$ > $Ca(OH)_2$ > $Mg(OH)_2$.[61] It was hypothesized that alkaline earth-based hydroxide forms five-

membered ring salt with lactic acid and the ring structure promotes the decomposition of lactic acid which is facilitated by the increase of ionic radius. The major drawback in the base-catalyzed glycerol dehydrogenation reaction is its corrosiveness. The high concentration of OH^- (excess than 1 M) causes major corrosion of the stainless-steel container. High temperature and high pressure will further increase the corrosion.[62] Also, high base concentration limits the initial concentration of glycerol and subsequently decreases the yield of lactic acid.

To reduce the corrosiveness, the reaction was performed under reduced temperature, and the glycerol to glyceraldehyde or dihydroxy acetone conversion was performed in the presence of Au-Pt/TiO_2 and O_2 (Scheme 3.3). In the next steps, the glyceraldehyde or dihydroxyacetone are subjected to Cannizaro reaction in a lower concentration of alkaline medium to obtain lactic acid.[63]

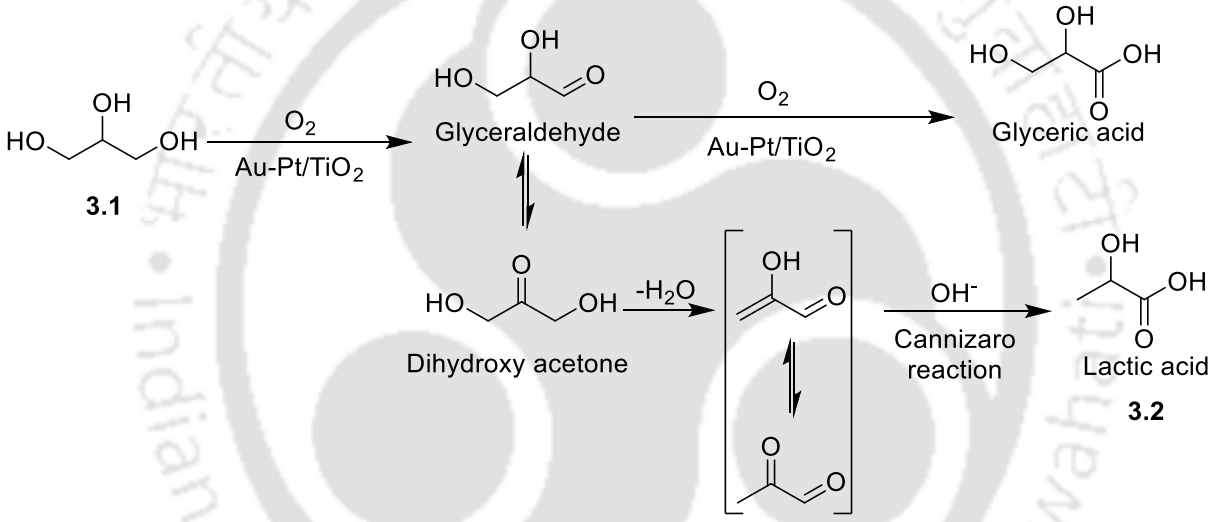

Scheme 3.3: Proposed pathway of glycerol conversion to lactic acid in the presence of Au-Pt/TiO_2.[63]

Other base mediated procedures involving NaOH in combination with either Cu_2O,[64] or Na_2SiO_3[65] produce lactic acid from glycerol. However, alkali mediated reaction procedures suffer from either low productivity or high corrosive nature. Single component metal oxide like Na_2O, K_2O, CaO, MgO can act as Brønsted base for the reaction and is susceptible to CO_2 or H_2O contamination.[66] For such glycerol to lactic acid conversions; the catalyst should be isolated from CO_2 or H_2O by using anhydrous glycerol.

In 2010, Lux *et al.* proposed partial electrochemical oxidation of glycerol to dihydroxy acetone and glyceraldehyde, which can be catalytically converted to lactic acid.[67] Continuously, lactic acid and by-products were separated from the electrolyte by liquid extraction. Regeneration of the

electrolyte and isolation of lactic acid and by-products from the extracting phase was carried out through re-extraction with water at elevated temperature. The remaining unconverted glycerol along with the catalyst were recycled and the glycerol concentration was maintained by addition of crude glycerol to the anodic compartment of the electrolytic cell.

Employing heterogeneous catalysts, the glycerol to lactic acid conversion occurred under both reductive[68-70] and oxidative[63, 71] conditions. Dam *et al.* have reported lactic acid formation with moderate (55%) selectivity by using $Pt/CaCO_3$.[70] Hydrogenolysis of glycerol to lactic acid selectively was performed with up to 62% yield by using Pt/C and 60% yield by using Au-Ru/C.[70] Xu *et al.* have reported the glycerol to lactic acid transformation by using a bimetallic catalyst based on $Au-Pd/TiO_2$ in the presence of Lewis acid $AlCl_3$.[72] Cho *et al.* have reported highly selective lactic acid production with a bifunctional Pt/Sn-MFI catalyst under base-free conditions.[73] Using these tin zeolites in combination with platinum, glycerol oxidation in water led to lactic acid with up to 80% selectivity at 90% conversion. Zhang *et al*. have reported unique bimetallic $Pt-Co/CeO_x$ complex to catalyze glycerol to lactic acid.[74] Kamonoya have reported PVP-stabilized Pt nanoparticles (Pt-PVP) (PVP = polyvinylpyrrolidone) and TiO_2 as a highly active catalyst for glycerol to lactic acid formation.[75] Feng *et al*. proposed a bifunctional catalyst consisting of Pt nanoparticles (Pt NPs) and layered-Nb_2O_5 for glycerol to lactic acid without using any additive.[76] The advantage of base free or Lewis acid-catalyzed reaction is that further purification steps can be avoided for lactic acid generation from the sodium lactate salt. However, these reactions often require intensive harsh conditions and are performed at about >200 °C with more than 2 MPa pressure causing a matter of concern.[73] Non-noble metals can also catalyze glycerol to lactic acid transformation under the inert atmosphere in the presence of a base. Ni/graphite system has been studied for glycerol to lactic acid conversion with a yield of 89%.[24] A 30% CuO/ZrO_2 catalyst can result in lactic acid yielding up to 95%.[77] On the other hand, with 20% Co_3O_4/CeO_2, glycerol conversion of 86% with a selectivity of up to 80% have been achieved towards lactic acid.[78] Bimetallic Ni-Co supported on nanosized CeO_2 catalyzed the glycerol transfer dehydrogenation reaction to selectively produce lactic acid.[79] For effective heterogeneous catalyzed dehydrogenation, extremely harsh reaction conditions are required and the observed selectivity towards lactic acid is very low.[69, 80-83]

Homogeneous catalysis for glycerol to lactic acid conversion demonstrated excellent reactivity and selectivity.[84-86] Crabtree and co-workers have reported the first example of a homogeneous

catalyst for the conversion of glycerol to lactic acid. They have studied the acceptorless dehydrogenation of glycerol by using an Ir(I) NHC complex which provided up to 31,000 turnover number (TON) in about 90% yield with a selectivity of 95% towards lactic acid (Scheme 3.4).[87]

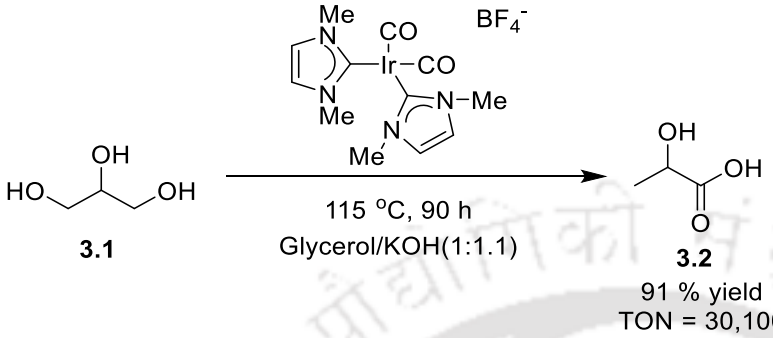

Scheme 3.4: High productivities of lactic acid using Ir(I)NHC complex.[87]

The significant advantage of the reaction reported by Crabtree is that it is carried out under mild reaction conditions under solvent-free conditions using catalyst loading as low as 0.003 mol %. It was proposed that glycerol was catalytically dehydrogenated to lactic acid through dihydroxyacetone and glyceraldehyde intermediates. Consequently, the base-catalyzed dehydration results in the formation of lactate salt. Beller and co-workers have reported numerous ruthenium complexes containing PNP[38], PNN[38] and CNN[38] pincer ligands as capable catalysts for lactic acid and hydrogen production from glycerol. Among several pincer-Ru complexes, the Beller group demonstrated the utility of PNP pincer-Ru complex in obtaining 2,70,000 TON with about 67% yield of lactic acid at 140 °C using NMP as a solvent (Scheme 3.5).[38]

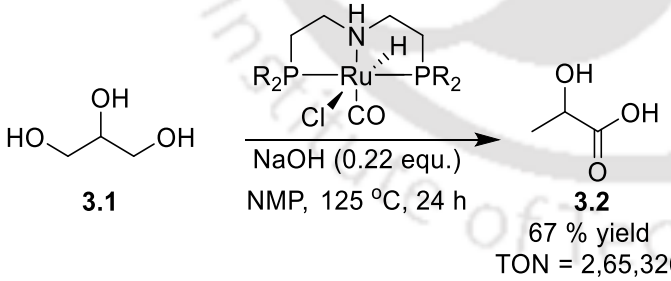

Scheme 3.5: PNP pincer-Ru catalyzed glycerol to lactic acid synthesis.[38]

Hazari and Crabtree have developed a catalyst having a similar PNP ligand coordinated to an inexpensive metal iron. For the first time, they have reported the base metal-catalyzed homogeneous glycerol conversion to lactic acid. In this selective conversion of glycerol to lactic acid catalyzed by PNP pincer-iron, about 880 turnover number were obtained in 3h using NMP as

solvent (Scheme 3.6).[39] Previously, this homogeneous Fe complex with ancillary bifunctional PNP ligand was shown to be active towards dehydrogenation of formic acid,[88] primary and secondary alcohols,[89] methanol[90-91] and nitrogen-containing heterocycles[92]. They have proposed a mechanism which involved metal-catalyzed dehydrogenation of glycerol to glyceraldehyde which is followed by dehydration, tautomerization, and an intra-molecular Cannizzaro reaction. The lactic acid is isolated as lactate salt.

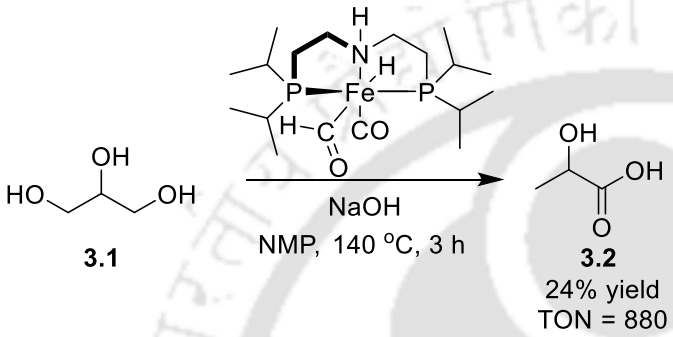

Scheme 3.6: Glycerol to lactic acid formation using Fe-PNP complex.[39]

In 2015, Tao and co-workers have reported a highly selective, efficient and recyclable NHC-Ir co-ordination polymer for the transformation of glycerol to value-added products.[93] Here an NHC Ir coordination polymer was successfully applied as a robust self-supported catalyst in the oxidative dehydrogenation of glycerol to potassium lactate along with the liberation of hydrogen gas (Scheme 3.7).[93]The reaction was carried out under open-air with mild reaction conditions and exhibited high selectivity and productivity for potassium lactate with up to 1.24×10^5 turnover number (TON).

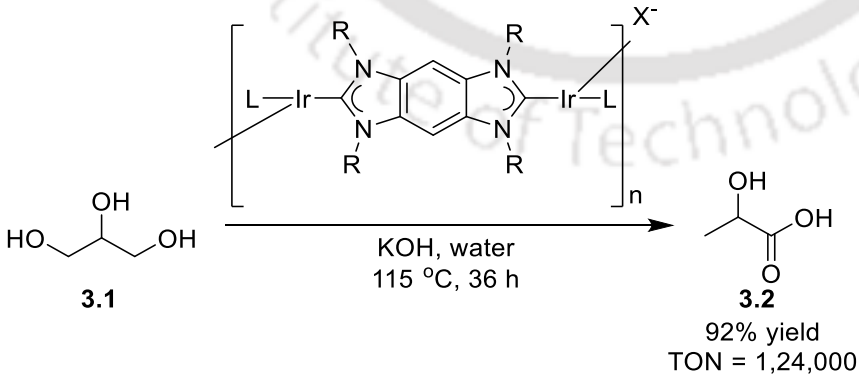

Scheme 3.7: Oxidative dehydrogenation of glycerol catalyzed by NHC-Ir coordination polymer.[93]

Subsequently, William *et al*. have reported a highly robust NHC-pyridine Ir(I) catalyst for glycerol to lactic acid formation and obtained 4.5 million turnover number in 32 days under neat condition (Scheme 3.8).[40] This catalytic system enables comparatively high conversion of neat glycerol to sodium lactate salt with 99% selectivity. They have also isolated lactic acid from the crude reaction mixture.

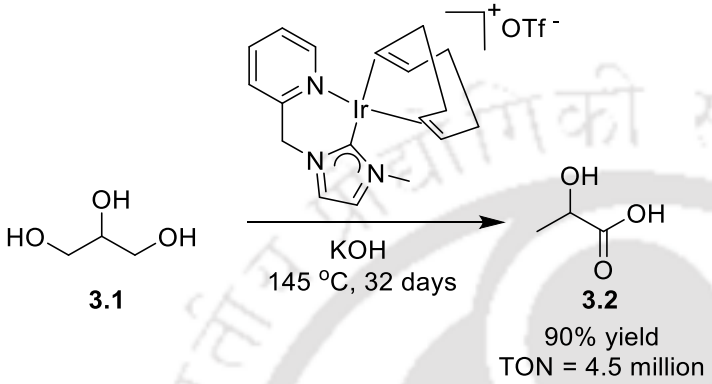

Scheme 3.8: Dehydrogenation of neat glycerol to lactic acid with an Ir complex.[40]

Very recently, Vouthkova-kostal has utilized Ir(I), Ir(III) and Ru(II) NHC complexes with sulfonate functionalized wingtips for efficient transformation of glycerol to lactic acid. The catalytic activity was compared under both conventional heating and microwave condition. The most active $[(NHC\text{-}Ph\text{-}SO_3)_2Ir(CO)_2]^-$complex reaches a TOF of 45,592 h^{-1} under microwave conditions and afforded 2,93,249 TON in 8 h (Scheme 3.9).[94] The significant improvement in the activity of catalyst under microwave condition (11-folds on an average) might be due to more efficient heating at a set temperature and better solubility of base in viscous glycerol medium.

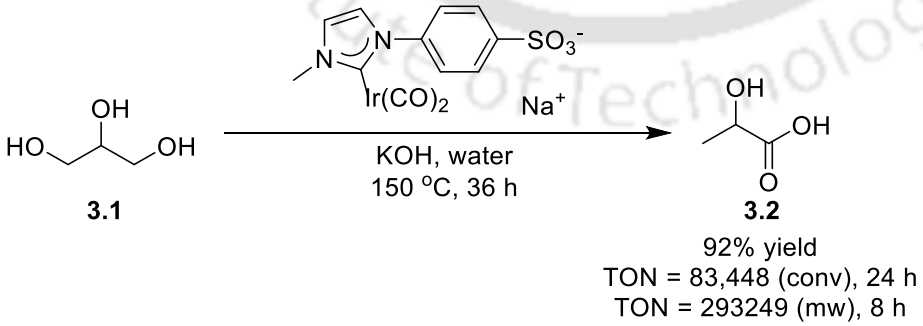

Scheme 3.9: Conversion of glycerol to lactic acid using Ir-NHC complex.[94]

Recently, Kumar and co-workers have reported the synthesis of NNN pincer Ru complexes (**3.3a**, **3.3b** Scheme 3.10)[95] and have successfully applied them for *N*-alkylation reactions[96] which involved the dehydrogenation as the first step with **3.3a** being more efficient than **3.3b**. It was envisaged that these catalysts would find utility in other synthetically useful transformations that rely on dehydrogenation such as glycerol to lactic acid formation. In this chapter, a systematic mechanistic insight has been obtained by comparing the activity of pincer-ruthenium complexes (**3.3a** and **3.3b**) based on *bis*(imino)pyridine with corresponding sterically less hindered 2,6-*bis*(benzimidazole-2-yl) pyridine based complexes (**3.3c** and **3.3d**) towards the synthesis of lactic acid from glycerol.

3.3 Results & discussions

A good dehydrogenation catalyst in combination with a base derived from alkali metal can bring about the conversion of glycerol to lactic acid *via* dihydroxyacetone (DHA) or glyceraldehyde (GAL) (Figure 3.1).

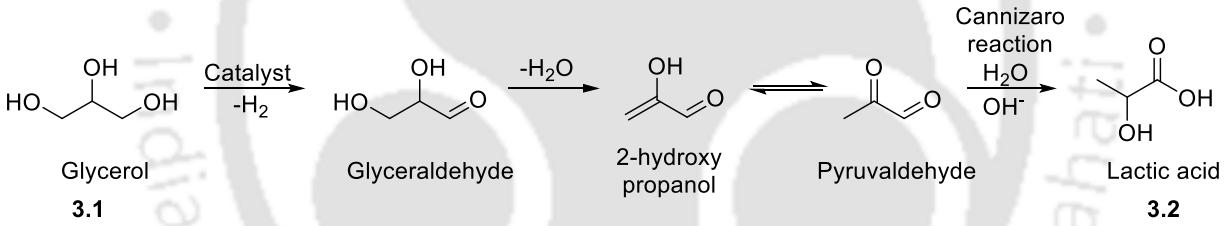

Figure 3.1: Reaction pathway for conversion glycerol to lactic acid

Use of stoichiometric amount of base during dehydrogenation stimulates the dehydration of pyruvaldehyde. In addition, the conversion and selectivity towards lactic acid is enhanced as the lactic acid is trapped as lactate salt. The utility of a variety of pincer-ruthenium complexes (Scheme 3.10) reported by Kumar and co-workers[95, 97] has been tested here for the selective catalytic transformation of glycerol to lactic acid.[98]

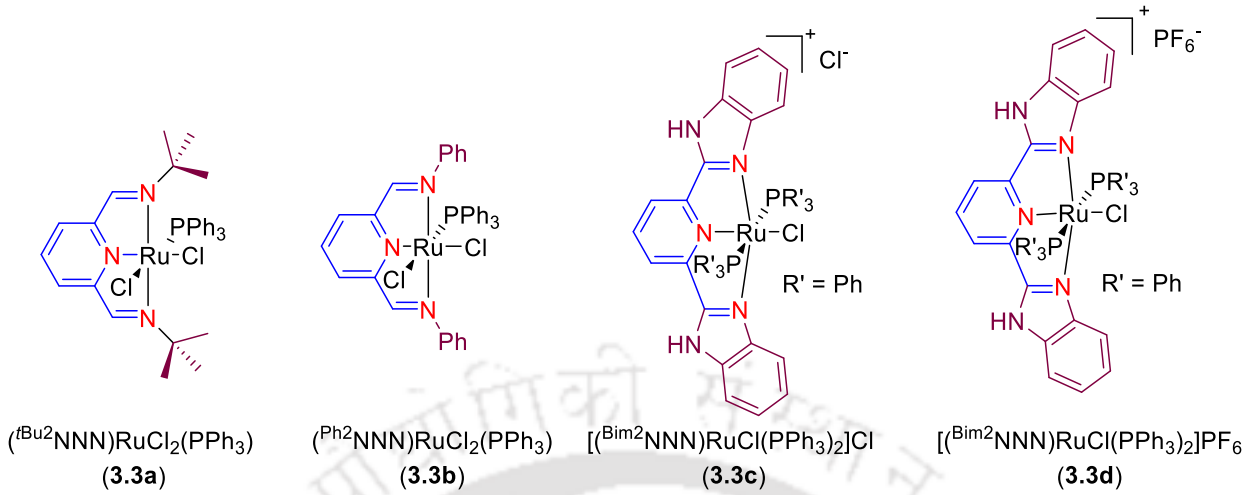

Scheme 3.10: NNN pincer-ruthenium complexes **3.3** screened for the glycerol to lactic acid transformation

In a typical experiment, to a flask containing 0.7 μmol of catalyst **3.3** (Scheme 3.10) in glycerol (2.56 mmol), KOH (1.48 mmol) was added, followed by the addition of 2 ml ethanol (Table 3.1). The reaction mixture was heated at 140 °C, under an argon atmosphere. Ethanol is added to maintain proper homogeneity of the highly viscous reaction medium. Under the reaction conditions, ethanol (boiling point = 78 °C) was fully evaporated as is evident from NMR spectra of the crude products (Appendix 3).

Table 3.1: Comparison of activity of **3.3a-d** towards glycerol to lactic acid conversion

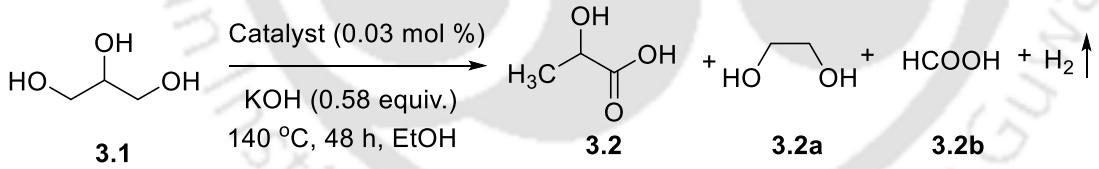

Entry	Catalyst (3.3)	3.2 Yield[a] (TON)	3.2a(3.2b) Yield[a]	Selectivity of 3.2[b]
1.	**3.3a**	53 (1767)	3%(2%)	85%
2.	**3.3b**	26 (867)	1%(1%)	96%
3.	**3.3c**	69±3[c] (2300)	2%(1%)	97%
4.	**3.3d**	66 (2200)	1%(-)	98%

Reaction conditions: 0.7 μmol of **3.3**, 2.56 mmol of **3.1**, 1.48 mmol KOH, 2 mL solvent in an open vessel under Ar at 140 °C. [a)] Yield determined from ^{1}H NMR using sodium acetate as an internal standard. [b)]Selectivity=(yield of **3.2**/ conversion of **3.1**)100. [c)] Reported as an average of two runs.

The reactions catalyzed by **3.3a** (Entry 1, Table 3.1) gave moderate yields of lactic acid, whereas **3.3b** showed very poor activity towards lactic acid formation (Entry 2, Table 3.1). Among the screened catalysts (Scheme 3.10), the ruthenium complex **3.3c** with 2,6-*bis*(1H-benzo[d]imidazol-2-yl) pyridine ligand exhibited the best performance towards the selective formation of lactic acid with good yield (Entry 3, Table 3.1). Its analog **3.3d** with a PF_6 counter ion produced lactic acid with comparable efficiency.

Table 3.2: Glycerol dehydrogenation to lactic acid catalyzed by **3.3c** under varying conditions

Entry	**Catalyst 3.3c (mol %)**	**Base (Equiv.)**	**Solvent (2 ml)**	**Yield[a]**		**3.1 conversion[a] (3.2 selectivity)[b]**
				3.2 (TON)	**3.2a(3.2b)**	
1.	(0.03)	KOH(0.58)	EtOH	69±3 (2367)	2% (1%)	71% (97%)
2.	(0.03)	KOH (0.58)	DMSO	9 (300)	5% (3%)	26% (35%)
3.	(0.03)	KOH (0.58)	DMF	2 (67)	5% (25%)	34% (6%)
4.	(0.03)	KOH (0.58)	*P*-xylene	46 (1533)	2% (-)	73% (63%)
5.	(0.03)	KOH (0.58)	Benzonitrile	2 (67)	1% (-)	3% (67%)
6.	(0.03)	KOH (0.58)	H_2O	40 (1344)	3% (-)	44% (98%)
7.	(0.03)	KOH (1.0)	-	59 (1966)	2% (-)	61 % (97%)
8.	(0.03)	KOH (0.58)	Dioxane	68 (2267)	3% (-)	72% (94%)
9.	(0.03)	KOH (1.0)	EtOH	90±2[c] (3066)	1% (-)	92% (98%)
10.	(0.03)	KOH (1.0)	Dioxane	76 (2557)	1% (1%)	78% (97%)
11.	(0.03)	NaOH (1.0)	EtOH	37±1[c] (1267)	4% (5%)	52 % (71%)
12[d].	(0.003)	KOH (1.0)	EtOH	5 (1667)	1% (1%)	6% (83 %)
13[d,e].	(0.003)	KOH(1.0)	EtOH	45 (15000)	1% (1%)	46% (98%)
14[d,e].	(0.003)	KOH (1.0)	-	44 (14666)	1% (1%)	46% (96%)

Reaction conditions: 0.7 μmol of **3.3c**, 2.56 mmol of **3.1**, 1.48 mmol KOH, 2 mL solvent in an open vessel under Ar at 140 °C. [a)] Yield determined from ^{1}H NMR using sodium acetate as an external standard. [b)]Selectivity=(yield of **3.2**/ conversion of **3.1**)100. [c)] Reported as an average of two runs. [d)] 0.3 μmol (0.003 mol %) of **3.3c**, 10.24 mmol of **3.1**, 10.24 mmol KOH, and 2 mL solvent in an open vessel under Ar at 140 ° C. [e)] Reaction performed in presences of 5.12 mmol of water.

It can be attributed to the fact that both the **3.3c** and **3.3d** give rise to the same active catalyst **3.5c** (Scheme 3.12). Further optimization of the reaction conditions was carried out with **3.3c** (Table 3.2). Under the best reaction conditions, the observed high selectivity (Table 3.1 and 3.2) of lactic acid indicates that the decarbonylation of glycerol and decarboxylation of lactic acid leading to ethylene glycol and formic acid, respectively, is negligible.[38-40, 86-87, 93-94]

The **3.3c** catalyzed transformation of glycerol to lactic acid by using DMSO, DMF, and benzonitrile proceeded with very low yields (entries 2, 3 and 5, Table 3.2). Moderate yield of lactic acid was obtained with either *p*-xylene or water as a solvent (entries 4 and 6, Table 3.2). In the presence of dioxane as a solvent, the reaction yielded 68% of lactic acid. It should be noted that dioxane is quickly lost under the reaction conditions. In the presence of EtOH, the conversion of glycerol to form lactic acid occurred with high yield (72%) (Entry 1, Table 3.2). Upon increasing the base loading, the reaction leads to the highest yield (92%) of lactic acid (Entry 9, Table 3.2). The yield however dropped to 59% under solvent-free conditions indicating the importance of thorough premixing of the contents (Entry 7, Table 3.2). In particular, the use of ethanol may assist in the spontaneous generation of the catalytically active Ru-H species via *β*-hydride elimination from Ru-ethoxide (**3.7a-c**).[99] The yields were drastically reduced with the use of NaOH as a base (entry 11, Table 3.2). Even upon decreasing the loading of **3.3c** to 0.003 mol % (entry 12, Table 3.2), lactic acid formation was reduced. However, in the presence of 0.5 equivalents of water, 45% of lactic acid (TON = 15,000) was obtained with 0.003 mol % of **3.3c** catalyst (Entry 13 and 14, Table 3.2). It is noteworthy that at lower catalyst loading it is easy to homogenize the reaction mixture without the use of ethanol.

Kumar and co-workers have recently demonstrated the ability of catalysts (**3.3a-b**) to generate H_2 when treated with primary alcohols at 140 °C.[99] The plausible mechanism involved in the reaction is provided in Scheme 3.11. The complexes (**3.5a-c**), (**3.6a-c**), (**3.7a-c**) and (**3.8a-c**) depicted in Scheme 3.11 are either the intermediates or the transition states (TSs) involved in the cycle catalyzed by the corresponding complexes (**3.3a-d**). For the sake of simplicity, only the NNN ligating section of the pincer framework is represented (Scheme 3.11). While for (**3.3a-b**), the generation of active species (**3.5a-b**) is fairly straightforward (eq. 1, Scheme 3.12), one could anticipate the loss of two PPh_3 molecules in the corresponding formation of the catalytically active species (**3.5c**) starting from both **3.3c** and **3.3d** (equation 2, Scheme 3.12).

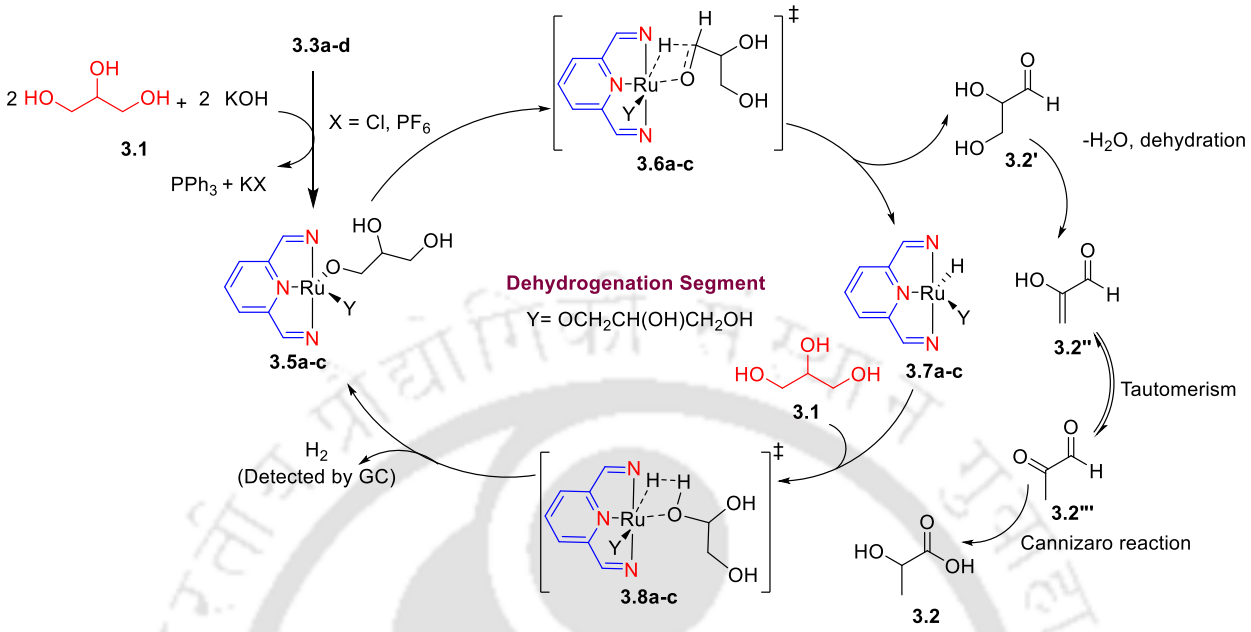

Scheme 3.11: Plausible mechanism involved in the (**3.3a-d**) catalyzed transformation of glycerol to lactic acid

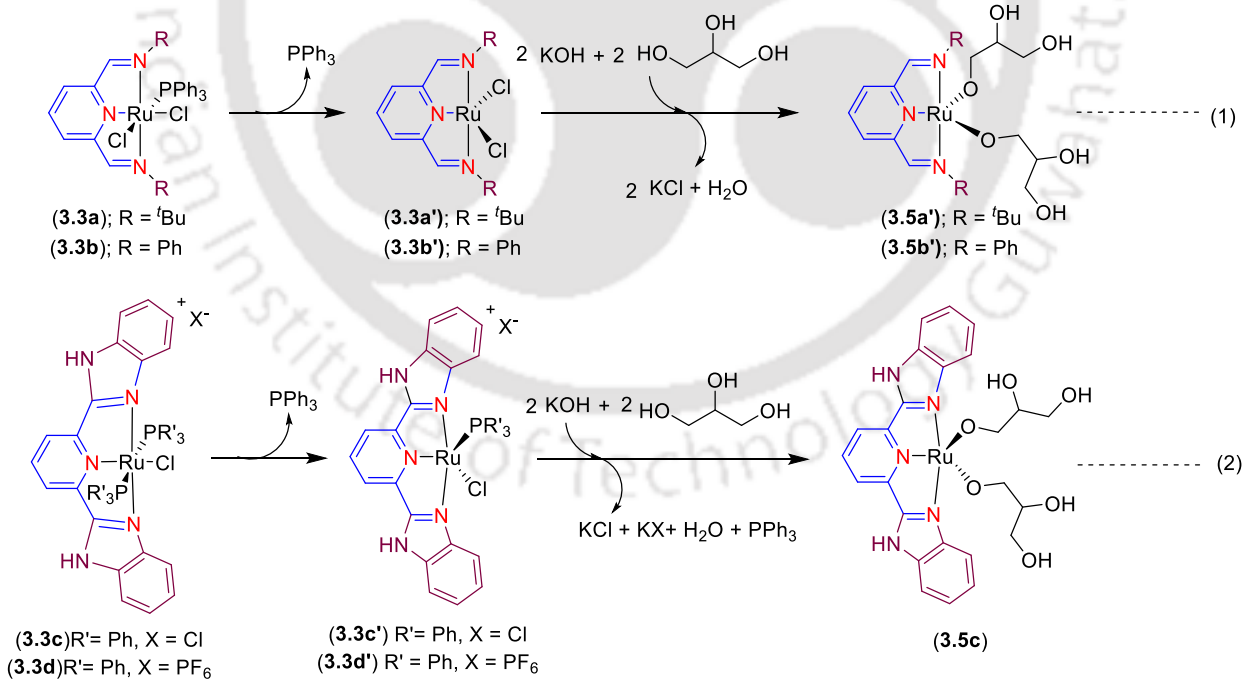

Scheme 3.12: Generation of catalytically active (**3.5a-c**) starting from (**3.3a-d**).

A *β*-hydride elimination from (**3.5a-c**) would result in the formation of (**3.7a-c**) and glyceraldehyde **3.2'** *via* TS (**3.6a-c**) (Scheme 3.11). Next, the catalytic cycle is completed by regeneration of the

active species (**3.5a-c**) via a σ-bond metathesis of O-H of **3.1** with the Ru-H of (**3.7a-c**) while going through TS (**3.8a-c**) (Scheme 3.11). Subsequent dehydration of **3.2'** resulted in *α,β*-unsaturated aldehyde **3.2''** along with its tautomer **3.2.'''**A Cannizaro reaction of **3.2'''** leads to the formation of lactic acid **3.2**.

Table 3.3. Interaction energy, energy of formation and *β*-hydride elimination energy barriers involved in the transformation of glyceraldehyde to lactic acid catalyzed by **3.3a-d.**

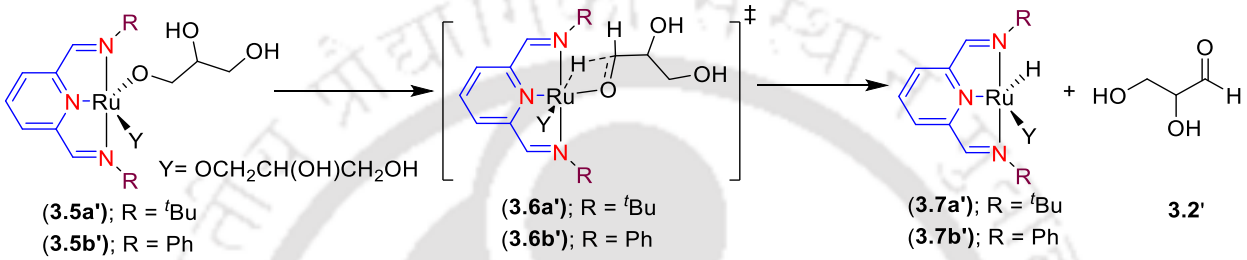

Entry	catalyst	$-\Delta E_{int}$[a] (Ru-P)(kcal/mol)	ΔG_f[b](**3.5→3.7**) (kcal/mol)	TS **3.6** /**TS 3.8** (kcal/mol)	TON[c]
1.	**3.3a**	39.82	8.62	31.78/21.39	1767
2.	**3.3b**	44.35	2.51	21.89/23.90	867
3.	**3.3c**	39.00[d]	2.08[d]	16.17/21.39[d]	2300
4.	**3.3d**	39.00[d]	2.08[d]	16.17/21.39[d]	2200

[a)]Interaction energy is calculated as the difference between the energy of the complex (**3.3a–d**) and the energy of the corresponding isolated PPh_3 and (^{R2}NNN)$RuCl_2$ (R= ^{t}Bu, Ph) or [(^{Bim2}NNN)$RuCl(PPh_3)$]$^+$ in the geometry of the complex (**3.3a–d**). [b)] Free energy of formation for the *β*-hydride elimination step **3.5→3.7**. [C)] Values obtained from Table 3.1. [d)] As Cation was computed, the values are the same for **3.3c** and **3.3d**.

It has been widely accepted that, in the transformation of glycerol to lactic acid, only the dehydrogenation step is metal-catalyzed and the rest of the steps are spontaneous organic processes in basic solution.[39] The observed difference between various catalysts (Table 3.1) can be attributed to the variation in their relative dehydrogenation efficiencies. With an intent to understand the relative ease of dehydrogenation, the Ru-P interaction energy and the relative free energy change (ΔG_{140}) for the species involved in the catalysis were computed. The catalytic efficiency of Ru catalysts with phosphine as ancillary ligands is dependent on the ease of their release to generate the active catalyst (**3.5a-c**).[95, 100]The phosphine release can be quantified as the interaction energy

($-\Delta E_{int}$) of PPh_3 either with (^{R2}NNN)$RuCl_2$ (R= ^{t}Bu, Ph) arising from **3.3a** and **3.3b** or with [(^{Bim2}NNN)RuCl(PPh_3)]$^+$ arising from both **3.3c** and **3.3d** (Table 3.3).The ($-\Delta E_{int}$) followed the trend; **3.3b** (44.35 kcal/mol) > **3.3a** (39.82 kcal/mol)> (**3.3c or 3.3d**) (39.00 kcal/mol). Clearly, the complex **3.3b** where the PPh_3 is the hardest to remove in comparison with **3.3a**, **3.3c** and **3.3d**, exhibited the lowest activity (867 TON).

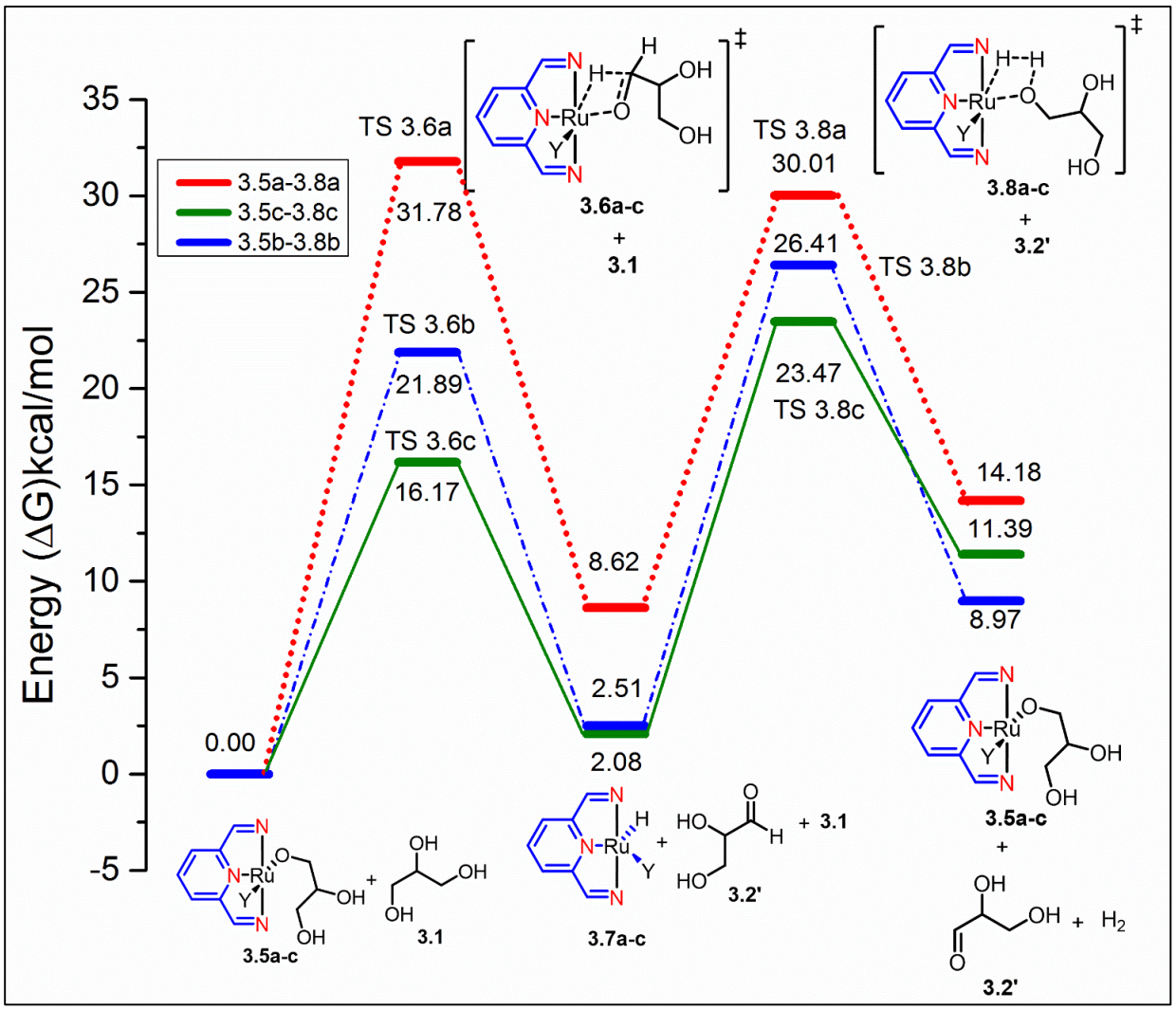

Figure 3.1: Free energy (140 °C) profile of the (**3.3a-d**) catalyzed glycerol dehydrogenation at PBEPBE functional using LANL2DZ basis set for Ru and 6-311G(d,p) for all other atoms.

However, among **3.3a** and **3.3c** or **3.3d** with comparable Ru-P bond energy, contrary to the expected trend, **3.3a** exhibited much lower activity (1767 TON) than **3.3c** (2300 TON) and **3.3d** (2200 TON). This can be satisfactorily explained if one considers the energetics of *β*-hydride elimination and H_2 evolution (Figure 3.1).

While for the reactions catalyzed by **3.3a**, *β*-hydride elimination is the RDS, H_2 evolution is the RDS for corresponding reactions catalyzed by **3.3b** and **3.3c** (Table 3.3, Figure 3.1). The barrier for the RDS followed the trend; **3.3a** (TS **3.6a**; $\Delta G^{\ddagger}140$ = 31.78 kcal/mol) > **3.3b** (TS **3.8b**; $\Delta G^{\ddagger}140$ = 23.90 kcal/mol) > (**3.3c** or **3.3d**) (TS **3.8c**; $\Delta G^{\ddagger}140$ = 21.39 kcal/mol) (Table 3.3, Figure 3.1). Though the energetics of the **3.3b** catalyzed reactions are more favourable than **3.3a** (Table 3.3, Figure 3.1), the reluctance of **3.3b** to easily release the PPh_3 (Entry 2, Table 3.3) contributes to its lower reactivity. On the other hand, the reaction with catalyst **3.3c** and **3.3d** proceeds very efficiently not only because the barrier for the *β*-hydride elimination (TS **3.6c**; $\Delta G^{\ddagger}140$ = 16.17 kcal/mol) is about 1.96 folds (compare TS **3.6** barrier in entries 1 and 3 Table 3.3) lower but also because the *β*-hydride elimination is downhill by 6.54 kcal/mol ($\Delta G^{\ddagger}140$ for entries 1 and 3 Table 3.3) in comparison with **3.3a** (Figure 3.1). This results in a significant build-up of glyceraldehyde in reactions catalyzed by **3.3c**/**3.3d** in stark contrast to **3.3a** where the equilibrium is more towards the left (**3.5a** + **3.1**). The open vessel conditions ensure that the equilibrium for the subsequent step (**3.7c** +**3.1**→**3.5c**+H_2) is more towards the right. Furthermore, among **3.3c**/**3.3d** and **3.3a**, the barrier for the RDS with **3.3c**/**3.3d** is lower by ~10.39 kcal/mol (TS: **3.8c**, TS: **3.6a**, Table 3.3). Despite the fact that the generation of the active catalyst **3.5** starting from **3.3c** and **3.3d** is comparable to **3.3a** (Table 3.3), the favorable energetics that is attributable to a lower steric encumbrance (Figure 3.2) around the Ru center makes the catalysis with **3.3c**/**3.3d** more favorable.

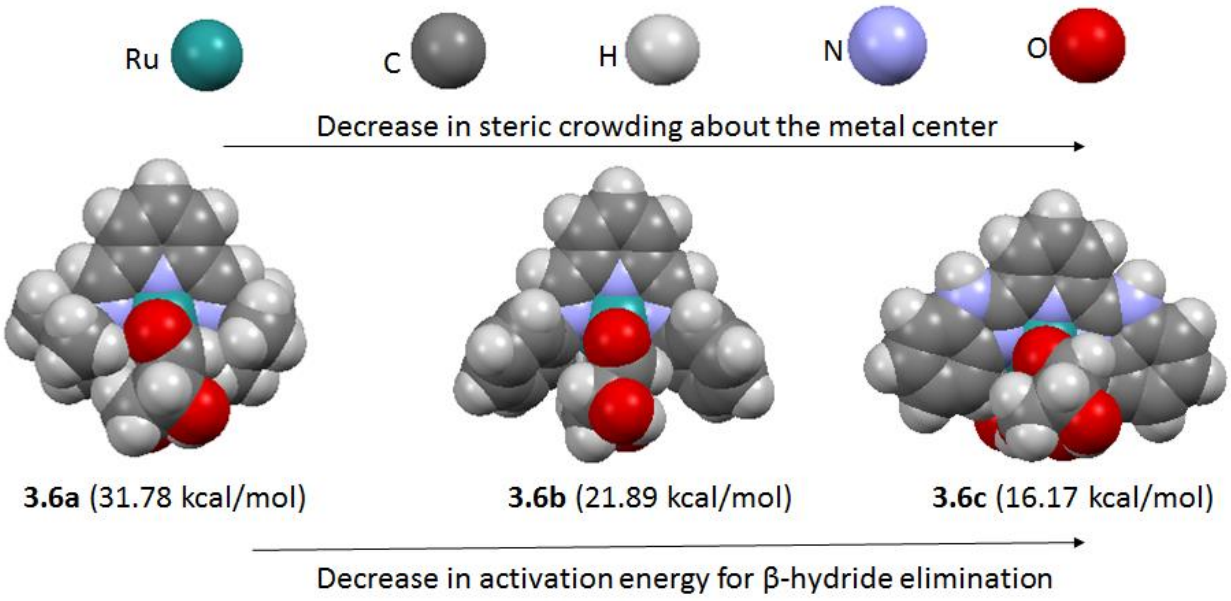

Figure 3.2: Space-filling model of TS **3.6** depicting the steric crowding around ruthenium

3.4 Conclusion

In conclusion, we represent here the dehydrogenation utilizing pincer-Ru catalysts based on 2,6-*bis*(1H-benzo[d]imidazol-2-yl)pyridine and *bis*(imino)pyridine ligands. In the process, we have obtained selective formation of lactic acid with high catalytic efficiency and selectivity. Milder conditions, renewable feedstock, bio-degradable product and low catalyst loadings are the salient features of the current pincer-ruthenium catalyzed transformation of glycerol selectively to lactic acid. Using EtOH as a solvent initially helped to homogenize the catalyst in the highly viscous medium. The initial reaction of ethanol with catalyst would help in generating Ru-H species via *β*-hydride elimination from Ru-ethoxide. Catalysts based on 2,6-*bis*(benzimidazole-2yl) pyridine ligands not only have optimal Ru-P bond energy that facilitates easy generation of active catalyst, but also enjoys less steric crowding around the Ru center that leads to favorable energetics making them highly efficient catalysts.

3.5 Experimental section

General procedure

All manipulations were carried out under purified Ar using a standard double manifold. Anhydrous glycerol was purchased from SRL, and degassed prior to experiment. KOH, NaOH were purchased from Merck and used as such. DMSO, benzonitrile, DMF, dioxane, EtOH were purchased from Spectrochem and dried according to standard literature technique.[101] All catalytic reactions were carried out under argon atmosphere using dried glassware.D_2O was purchased from Sigma-Aldrich and used as such. ^{1}H NMR was recorded either on Bruker ASCEND 600 operating at 600 MHz or on Bruker AVANCE 400 operating at 400 MHz. Pincer complexes (**3.3a**, **3.3b**, **3.3c** and **3.3d**) were synthesized according to the literature procedure.[95, 97, 98]

General procedure for the glycerol (3.1) conversion to lactic acid (3.2): To a 25 ml two neck round bottom flask containing degassed glycerol (**3.1**) (0.235g, 2.56 mmol), the pincer-ruthenium catalyst (**3.3c)** (0.7μmol) was added under Ar atmosphere inside a glove box. The vessel was brought outside the glove box and connected to a Schlenk line through a water-cooled condenser. This was followed by addition of 0.58 equivalents of KOH (0.083 g, 1.48 mmol) under Ar

atmosphere. After addition of 2 mL of appropriate dry solvent (EtOH, DMSO, DMF, *p*-xylene or dioxane), the resulting reaction mixture was heated at 140 ^{o}C for 48 hours. The reaction mixture was then cooled to room temperature. An aliquot (known amount in each case) was withdrawn from the reaction mixture and sodium acetate solution was added as an internal standard. NMR yield was determined by ^{1}H NMR using D_2O (0.4 ml) as the solvent. The yield was calculated by ^{1}H NMR integration versus the internal standard (sodium acetate). The products sodium lactate, ethylene glycol and formic acid were identified by their reported signature peaks.[39, 87, 94]

Computational methodology

All the calculations were performed using Gaussian-16 (revision C.01) program package.[102] PBEPBE level of DFT functional, along with LANL2DZ basis set for Ruthenium atom and 6-311G(d,p) basis set for all other atoms, were selected on the basis of previous reports for geometry optimization of all considered complexes.[103-106] Frequency calculations were performed at the same level of theory to confirm the minimum energy and transition state structures.

Supporting information (containing NMR spectra of various compound and Cartesian coordinates of the computed complexes) for chapter 3 is available as appendix 2 and can be found at https://drive.google.com/file/d/1ihehIqPowud_sMY2RUiE8h3ZbLGq1vos/view?usp=sharing

3.6 References

1. Christopher, K.; Dimitrios, R., *Nature* **2001**, *414*, 338-344.
2. Stelmachowski, M., *Ecol. Chem. Eng. S* **2011**, *18* (1), 9-30.
3. Speight, J. G., *Chemical and process design handbook*. The McGraw-Hill Companies: 2002.
4. Mestre Martínez, M. V., **2017**.
5. Bagnato, G.; Iulianelli, A.; Sanna, A.; Basile, A., *Membranes* **2017**, *7* (2), 17.
6. Dasari, M. A.; Kiatsimkul, P.-P.; Sutterlin, W. R.; Suppes, G. J., *Appl. Catal. A: Gen.* **2005**, *281* (1-2), 225-231.
7. Pagliaro, M.; Rossi, M. In *The future of glycerol: new usages for a versatile raw material, RSC Green Chem*, Ser: 2008.
8. Nilles, D., *Biodiesel Magazine* **2006**, 3.
9. Markets, E., Biodiesel 2020: Global Market Survey, Feedstock Trends and Market Forecasts. 2008.
10. Ciriminna, R.; Pina, C. D.; Rossi, M.; Pagliaro, M., *Eur. J. Lipid. Sci. Tech.* **2014**, *116* (10), 1432-1439.
11. Ayoub, M.; Abdullah, A. Z., *Renew. Sust. Energ. Rev.* **2012**, *16* (5), 2671-2686.
12. Hiremath, A.; Kannabiran, M.; Rangaswamy, V., *New Biotechnol.* **2011**, *28* (1), 19-23.

13. Rywinska, A.; Rymowicz, W.; Zarowska, B.; Wojtatowicz, M., *Food Technol. Biotech.* **2009**, *47* (1), 1-6.
14. Ibrahim, M. H.; Steinbüchel, A., *Appl. Environ. Microbiol.* **2009**, *75* (19), 6222-6231.
15. Ethier, S.; Woisard, K.; Vaughan, D.; Wen, Z., *Bioresour. Technol.* **2011**, *102* (1), 88-93.
16. Scholten, E.; Renz, T.; Thomas, J., *Biotechnol. Lett.* **2009**, *31* (12), 1947.
17. Sabourin-Provost, G.; Hallenbeck, P. C., *Bioresour. Technol.* **2009**, *100* (14), 3513-3517.
18. Choi, W. J.; Hartono, M. R.; Chan, W. H.; Yeo, S. S., *Appl. Microbiol. Biot.* **2011**, *89* (4), 1255-1264.
19. López, J. Á. S.; Santos, M. d. l. Á. M.; Pérez, A. F. C.; Martín, A. M., *Bioresour. Technol.* **200**9, *100* (23), 5609-5615.
20. Taconi, K. A.; Venkataramanan, K. P.; Johnson, D. T., *Environ. Prog. Sustain. Energy.* **2009**, *28* (1), 100-110.
21. D'Hondt, E.; Van de Vyver, S.; Sels, B. F.; Jacobs, P. A., *Chem. Commun.* **2008**, *45*, 6011-6012.
22. Jin, X.; Roy, D.; Thapa, P. S.; Subramaniam, B.; Chaudhari, R. V., *ACS Sustain. Chem. Eng.* **2013**, *1* (11), 1453-1462.
23. Jin, X.; Shen, J.; Yan, W.; Zhao, M.; Thapa, P. S.; Subramaniam, B.; Chaudhari, R. V., *ACS Catal.* **2015**, *5* (11), 6545-6558.
24. Yin, H.; Yin, H.; Wang, A.; Shen, L., *J. Ind. Eng. Chem.* **2018**, *57*, 226-235.
25. Wee, Y.-J.; Kim, J.-N.; Ryu, H.-W., *Food Technol. Biotechnol.* **2006**, *44* (2), 163-172.
26. Dusselier, M.; Van Wouwe, P.; Dewaele, A.; Makshina, E.; Sels, B. F., *Energy Environ. Sci.* **2013**, *6* (5), 1415-1442.
27. Díaz-Álvarez, A. E.; Francos, J.; Croche, P.; Cadierno, V., *Curr. Green Chem.* **2014**, *1* (1), 51-65.
28. Drumright, R. E.; Gruber, P. R.; Henton, D. E., *Adv. Mater.* **2000**, *12* (23), 1841-1846.
29. Armaroli, N.; Balzani, V., *ChemSusChem* **2011**, *4* (1), 21-36.
30. Maschmeyer, T.; Che, M., *Angew. Chem. Int. Ed.* **2010**, *49* (9), 1536-1539.
31. de Barros, R. d. R. O.; de Sousa Paredes, R.; Endo, T.; da Silva Bon, E. P.; Lee, S.-H., *Bioresour. Technol.* **2013**, *136*, 288-294.
32. Azadi, P.; Farnood, R., *Int. J. Hydrogen Energ.* **2011**, *36* (16), 9529-9541.
33. Cortright, R. D.; Davda, R.; Dumesic, J. A. In *Materials For Sustainable Energy: A Collection of Peer-Reviewed Research and Review Articles from Nature Publishing Group*, World Scientific: 2011; pp 289-292.
34. Nielsen, M.; Alberico, E.; Baumann, W.; Drexler, H.-J.; Junge, H.; Gladiali, S.; Beller, M., *Nature* **2013**, *495* (7439), 85-89.
35. Nielsen, M.; Junge, H.; Kammer, A.; Beller, M., *Angew. Chem. Int. Ed.* **2012**, *51* (23), 5711-5713.
36. Nielsen, M.; Kammer, A.; Cozzula, D.; Junge, H.; Gladiali, S.; Beller, M., *Angew. Chem. Int. Ed.* **2011**, *50* (41), 9593-9597.
37. Junge, H.; Loges, B.; Beller, M., *Chem. Commun.* **2007**, *5*, 522-524.
38. Li, Y.; Nielsen, M.; Li, B.; Dixneuf, P. H.; Junge, H.; Beller, M., *Green Chem.* **2015**, *17* (1), 193-198.
39. Sharninghausen, L. S.; Mercado, B. Q.; Crabtree, R. H.; Hazari, N., *Chem.Commun.* **2015**, *51* (90), 16201-16204.
40. Lu, Z.; Demianets, I.; Hamze, R.; Terrile, N. J.; Williams, T. J., *ACS Catal.* **2016**, *6* (3), 2014-2017.

41. Vaidya, P. D.; Rodrigues, A. E., *Chem. Eng. Technol.* **2009**, *32* (10), 1463-1469.
42. Inskeep, G. C.; Taylor, G.; Breitzke, W., *Ind. Eng. Chem.* **1952**, *44* (9), 1955-1966.
43. Naveena, B. J.; Altaf, M.; Bhadrayya, K.; Reddy, G., *Food Technol. Biotechnol.* **2004**, *42* (3), 147-152.
44. John, R. P.; Nampoothiri, K. M.; Pandey, A., *Appl. Microbiol. Biot.* **2007**, *74* (3), 524-534.
45. Datta, R.; Henry, M., *J. Chem. Technol. Biot.* **2006**, *81* (7), 1119-1129.
46. Perlack, R. D., *Biomass as feedstock for a bioenergy and bioproducts industry: the technical feasibility of a billion-ton annual supply*. Oak Ridge National Laboratory: 2005.
47. Datta, R.; Tsai, S.-P. ACS Publications: 1997.
48. Ward, G.; Lockwood, L.; May, O.; Herrick, H., *J. Am. Chem. Soc.* **1936**, *58* (7), 1286-1288.
49. Prescott, S.; Dunn, C., *Industrial Microbiology, 3rd ed. McGraw-Hill Book Co., Inc., New York, NY* **1959**, 304-369.
50. Yu, R.-c.; Hang, Y., *Biotechnol. Lett.* **1989**, *11* (8), 597-600.
51. Yun, J.-S.; Wee, Y.-J.; Kim, J.-N.; Ryu, H.-W., *Biotechnol. Lett.* **2004**, *26* (20), 1613-1616.
52. Singh, S. K.; Ahmed, S. U.; Pandey, A., *Process Biochem.* **2006**, *41* (5), 991-1000.
53. Quitain, A. T.; Faisal, M.; Kang, K.; Daimon, H.; Fujie, K., *J. Hazard. Mater.* **2002**, *93* (2), 209-220.
54. Anuradha, R.; Suresh, A.; Venkatesh, K., *Process Biochem.* **1999**, *35* (3-4), 367-375.
55. Borzani, W.; Luna, M. F.; Podlech, P. S.; Carlos, P. R. J.; de Souza Neto, A.; dos Passos, R. F.; Souza, O., *Biotechnol. Lett.* **1990**, *12* (7), 535-540.
56. Roukas, T.; Kotzekidou, P., *Enzyme Microb. Technol.* **1998**, *22* (3), 199-204.
57. Yoshida, H.; Terashima, M.; Takahashi, Y., *Biotechnol. Prog.* **1999**, *15* (6), 1090-1094.
58. Quitain, A. T.; Sato, N.; Daimon, H.; Fujie, K., *Ind. Eng. Chem. Res.* **2001**, *40* (25), 5885-5888.
59. Narayanan, N.; Roychoudhury, P. K.; Srivastava, A., *Electron. J. Biotechn.* **2004**, *7* (2), 167-178.
60. Kishida, H.; Jin, F.; Zhou, Z.; Moriya, T.; Enomoto, H., *Chem. Lett.* **2005**, *34* (11), 1560-1561.
61. Shen, Z.; Jin, F.; Zhang, Y.; Wu, B.; Kishita, A.; Tohji, K.; Kishida, H., *Ind. Eng. Chem. Res.* **2009**, *48* (19), 8920-8925.
62. Ramírez-López, C. A.; Ochoa-Gómez, J. R.; Fernández-Santos, M. a.; Gómez-Jiménez-Aberasturi, O.; Alonso-Vicario, A.; Torrecilla-Soria, J., *Ind. Eng. Chem. Res.* **2010**, *49* (14), 6270-6278.
63. Shen, Y.; Zhang, S.; Li, H.; Ren, Y.; Liu, H., *Chem. Eur. J.* **2010**, *16* (25), 7368-7371.
64. Roy, D.; Subramaniam, B.; Chaudhari, R. V., *ACS Catal.* **2011**, *1* (5), 548-551.
65. Long, Y.-D.; Guo, F.; Fang, Z.; Tian, X.-F.; Jiang, L.-Q.; Zhang, F., *Bioresour. Technol.* **2011**, *102* (13), 6884-6886.
66. Yan, S.; DiMaggio, C.; Mohan, S.; Kim, M.; Salley, S. O.; Ng, K. S., *Top. Catal.* **2010**, *53* (11-12), 721-736.
67. Lux, S.; Stehring, P.; Siebenhofer, M., *Sep. Sci. Technol.* **2010**, *45* (12-13), 1921-1927.
68. Maris, E. P.; Ketchie, W. C.; Murayama, M.; Davis, R. J., *J. Catal.* **2007**, *251* (2), 281-294.
69. Maris, E. P.; Davis, R. J., *J. Catal.* **2007**, *249* (2), 328-337.
70. ten Dam, J.; Kapteijn, F.; Djanashvili, K.; Hanefeld, U., *Catal. Commun.* **2011**, *13* (1), 1-5.
71. Auneau, F.; No, S., *Catal. Commun.* **2011**, *16*, 144-149.

72. Xu, J.; Zhang, H.; Zhao, Y.; Yu, B.; Chen, S.; Li, Y.; Hao, L.; Liu, Z., *Green Chem.* **2013**, *15* (6), 1520-1525.
73. Cho, H. J.; Chang, C.-C.; Fan, W., *Green Chem.* **2014**, *16* (7), 3428-3433.
74. Zhang, G.; Jin, X.; Guan, Y.; Yin, B.; Chen, X.; Liu, Y.; Feng, X.; Shan, H.; Yang, C., *Ind. Eng. Chem. Res.* **2019**, *58* (31), 14548-14558.
75. Komanoya, T.; Suzuki, A.; Nakajima, K.; Kitano, M.; Kamata, K.; Hara, M., *ChemCatChem* **2016**, *8* (6), 1094-1099.
76. Feng, S.; Takahashi, K.; Miura, H.; Shishido, T., *Fuel Process. Technol.* **2020**, *197*, 106202.
77. Yang, G.-Y.; Ke, Y.-H.; Ren, H.-F.; Liu, C.-L.; Yang, R.-Z.; Dong, W.-S., *Chem. Eng. J.* **2016**, *283*, 759-767.
78. Palacio, R.; Torres, S.; Lopez, D.; Hernandez, D., *Catal. Today* **2018**, *302*, 196-202.
79. Tang, Z.; Cao, H.; Tao, Y.; Heeres, H. J.; Pescarmona, P. P., *Appl. Catal. B* **2020**, 263, 118273.
80. Montassier, C.; Menezo, J.; Hoang, L.; Renaud, C.; Barbier, J., *J. Mol. Catal.* **1991**, *70* (1), 99-110.
81. Auneau, F.; Noël, S.; Aubert, G.; Besson, M.; Djakovitch, L.; Pinel, C., *Catal. Commun.* **2011**, *16* (1), 144-149.
82. Auneau, F.; Arani, L. S.; Besson, M.; Djakovitch, L.; Michel, C.; Delbecq, F.; Sautet, P.; Pinel, C., *Top. Catal.* **2012**, *55* (7-10), 474-479.
83. Dusselier, M.; Van Wouwe, P.; Dewaele, A.; Makshina, E.; Sels, B., *Chem. Rev.* **2014**, *114*, 1909-1971.
84. Sordakis, K.; Tang, C.; Vogt, L. K.; Junge, H.; Dyson, P. J.; Beller, M.; Laurenczy, G., *Chem. Rev.* **2018**, *118* (2), 372-433.
85. Werkmeister, S.; Neumann, J.; Junge, K.; Beller, M., *Chem. Eur. J.* **2015**, *21* (35), 12226-12250.
86. Nguyen, D. H.; Morin, Y.; Zhang, L.; Trivelli, X.; Capet, F.; Paul, S.; Desset, S.; Dumeignil, F.; Gauvin, R. M., *ChemCatChem* **2017**, *9* (14), 2652-2660.
87. Sharninghausen, L. S.; Campos, J.; Manas, M. G.; Crabtree, R. H., *Nature Commun.* **2014**, *5*, 5084.
88. Bielinski, E. A.; Lagaditis, P. O.; Zhang, Y.; Mercado, B. Q.; Würtele, C.; Bernskoetter, W. H.; Hazari, N.; Schneider, S., *J. Am. Chem. Soc.* **2014**, *136* (29), 10234-10237.
89. Chakraborty, S.; Lagaditis, P. O.; Förster, M.; Bielinski, E. A.; Hazari, N.; Holthausen, M. C.; Jones, W. D.; Schneider, S., *ACS Catal.* **2014**, *4* (11), 3994-4003.
90. Bielinski, E. A.; Förster, M.; Zhang, Y.; Bernskoetter, W. H.; Hazari, N.; Holthausen, M. C., *ACS Catal.* **2015**, *5* (4), 2404-2415.
91. Alberico, E.; Sponholz, P.; Cordes, C.; Nielsen, M.; Drexler, H. J.; Baumann, W.; Junge, H.; Beller, M., *Angew. Chem. Int. Ed.* **2013**, *52* (52), 14162-14166.
92. Chakraborty, S.; Brennessel, W. W.; Jones, W. D., *J. Am. Chem. Soc.* **2014**, *136* (24), 8564-8567.
93. Sun, Z.; Liu, Y.; Chen, J.; Huang, C.; Tu, T., *ACS Catal.* **2015**, *5* (11), 6573-6578.
94. Finn, M.; Ridenour, J. A.; Heltzel, J.; Cahill, C.; Voutchkova-Kostal, A., *Organometallics* **2018**, *37* (9), 1400-1409.
95. Das, K.; Dutta, M.; Das, B.; Srivastava, H. K.; Kumar, A., *Adv. Synth. Catal.* **2019**, *361* (12), 2965-2980.

96. Das, K.; Nandi, P. G.; Islam, K.; Srivastava, H. K.; Kumar, A., *Eur. J. Org. Chem.* **2019**, *40*, 6855-6866.
97. Das, K. Ph.D Thesis (On-going), Indian Institute of Technology Guwahati.
98. Dutta, M.; Das, K.; Prathapa, S. J.; Srivastava, H. K.; Kumar, A., *Chem. Commun.* **2020**, *56*, 9886-9889.
99. Das, K.; Nandi, P. G.; Islam, K.; Srivastava, H. K.; Kumar, A., *Eur. J. Org. Chem.* **2019**, *40*, 6855-6866.
100. Dai, Z.; Luo, Q.; Meng, X.; Li, R.; Zhang, J.; Peng, T., *J. Organomet. Chem.* **2017**, *830*, 11-18.
101. Armarego, W. L., *Purification of laboratory chemicals*. Butterworth-Heinemann: 2017.
102. Gaussian 16, R. C., M. J. Frisch, G. W. Trucks, H. B. Schlegel, G. E. Scuseria, M. A. Robb, J. R. Cheeseman, G. Scalmani, V. Barone, G. A. Petersson, H. Nakatsuji, X. Li, M. Caricato, A. V. Marenich, J. Bloino, B. G. Janesko, R. Gomperts, B. Mennucci, H. P. Hratchian, J. V. Ortiz, A. F. Izmaylov, J. L. Sonnenberg, D. Williams-Young, F. Ding, F. Lipparini, F. Egidi, J. Goings, B. Peng, A. Petrone, T. Henderson, D. Ranasinghe, V. G. Zakrzewski, J. Gao, N. Rega, G. Zheng, W. Liang, M. Hada, M. Ehara, K. Toyota, R. Fukuda, J. Hasegawa, M. Ishida, T. Nakajima, Y. Honda, O. Kitao, H. Nakai, T. Vreven, K. Throssell, J. A. Montgomery, Jr., J. E. Peralta, F. Ogliaro, M. J. Bearpark, J. J. Heyd, E. N. Brothers, K. N. Kudin, V. N. Staroverov, T. A. Keith, R. Kobayashi, J. Normand, K. Raghavachari, A. P. Rendell, J. C. Burant, S. S. Iyengar, J. Tomasi, M. Cossi, J. M. Millam, M. Klene, C. Adamo, R. Cammi, J. W. Ochterski, R. L. Martin, K. Morokuma, O. Farkas, J. B. Foresman, and D. J. Fox,, *Gaussian inc., Wallingford CT* **2016**, *2* (3), 4.
103. Perdew, J. P.; Burke, K.; Ernzerhof, M., *Phys. Rev. Lett.* **1996**, *77* (18), 3865.
104. Wadt, W. R.; Hay, P. J., *J. Chem. Phy.* **1985**, *82* (1), 284-298.
105. Hay, P. J.; Wadt, W. R., *J. Chem. Phy.* **1985**, *82* (1), 299-310.
106. Hay, P. J.; Wadt, W. R., *J. Chem. Phy.* **1985**, *82* (1), 270-283.

Chapter 4

Experimental and Computational Studies on Pincer-Nickel Catalyzed N-Alkylation and Dehydrogenative Coupling

4.1 Introduction

The C-N bond formation leads to a variety of nitrogen containing compounds, which are widely used in the synthesis of agrochemicals,[1] dyes[2] and fine chemicals.[3] The *N*-alkylated moiety is also prevalent in bioactive pharmaceuticals as essential building blocks (Figure 4.1).

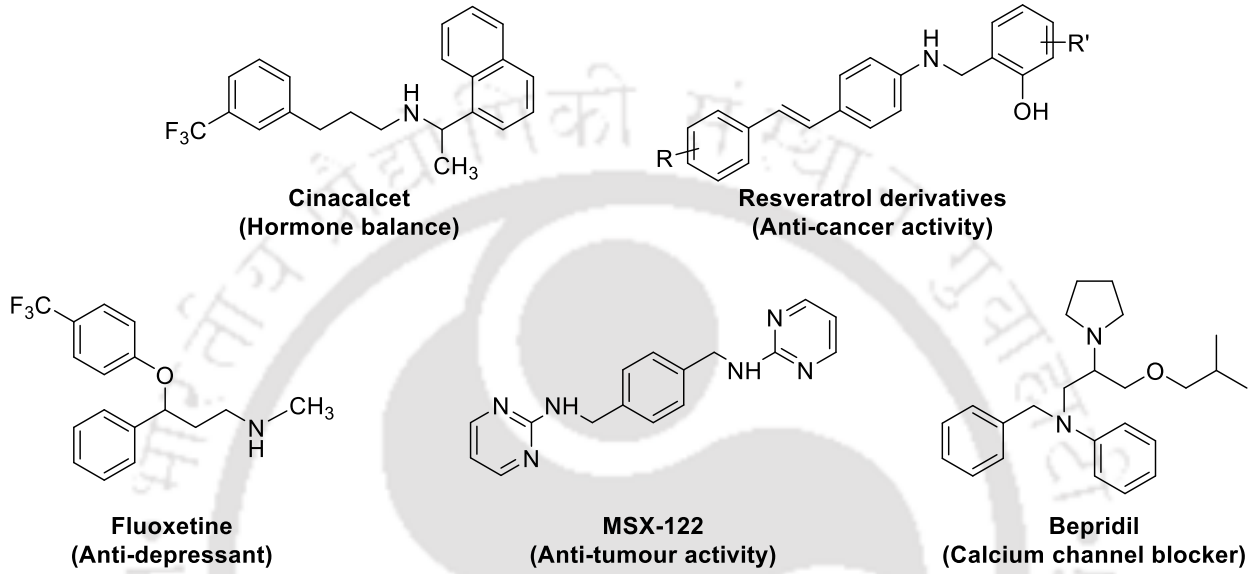

Figure 4.1: Selected examples of nitrogen-containing drugs.

There are a lot of powerful methods available that address the synthesis of amines such as, alkylation of amines by alkyl halides under basic conditions,[4] reductive amination of carbonyl compounds,[5] hydroamination of alkenes,[6] hydroaminomethylation,[7] reduction of nitriles[8] and nitro[9] compounds. Besides these, there are several typical nucleophilic substitutions reactions such as Hoffman alkylation,[10] Ullmann reaction,[11] Buchwald-Hartwig reaction,[12] Gabriel reaction,[13] and Mitsunobu reaction[14] that leads to amines.

C-N bond formation using Pd catalysts is widely known for the synthesis of a variety of amides,[15] aryl amines,[16] and alkyl amines[17]. In the last three decades, the study on C-N bond formation via coupling of amines and aryl halides have been widely studied. In 1983, Migita and co-workers were the first to use palladium to catalyze the formation of C-N bonds (Scheme 4.1).[18] Here they demonstrated the coupling of aryl bromide with *N*,*N*-diethylamino-tributyltin to provide diethylanilines in moderate yield.

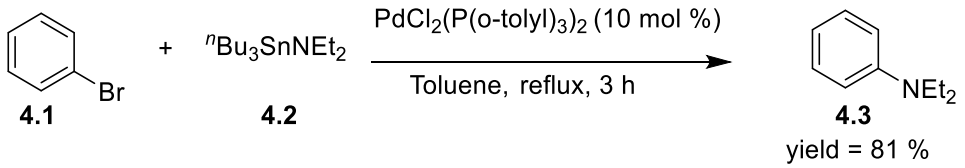

Scheme 4.1: One of the preliminary reports on C-N bond formation by Migita using a Pd complex[18]

Migita's work stimulated a lot of related research activities. In 1984, Dale Boger and James Panek studied the intramolecular cyclization to generate C-N bond using Pd(0) in the absence of hazardous organotin reagent (Scheme 4.2).[19]

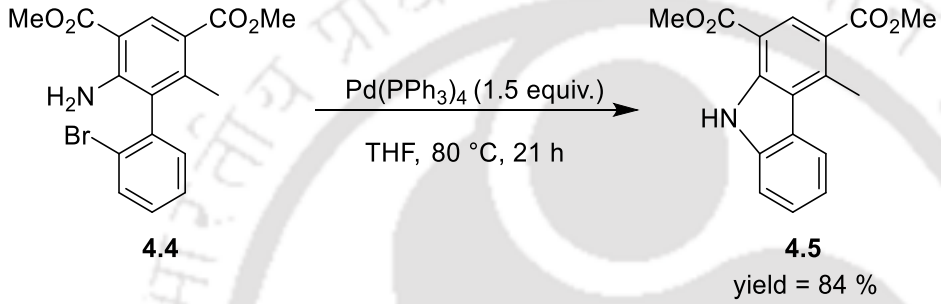

Scheme 4.2: Intramolecular C-N bond formation using Pd(0) complex reported by Boger and Panek [19]

After the decade that followed Migita's work, both Hartwig and Buchwald independently provided improvements and insight into Migita's work.[20-21] It has been demonstrated that the use of strong bases, such as KO^{t}Bu and LiHMDS, allowed C-N coupling using Pd.[22] Use of Pd-based catalyst in *N*-alkylation most often is limited by their moisture sensitivity and expensive nature. Buchwald first reported the use of $Ni(COD)_2$ (COD = 1,4 cyclooctadiene) in combination with 1,1′-*bis*(diphenylphosphino)ferrocene (dppf) or 1,10-phenanthroline for the synthesis of arylamines.[23] In 2002, Yves Fort and co-workers have reported the use of an *in-situ* generated colloidal Ni(0) for cross coupling methodology. The Ni(0)/SIPr.HCl [SIPr = 1,3-*bis*(2,6-diisopropylphenyl) dihydroimidazole-2-ylidiene] catalyst combined with NaO^{t}Bu proved to be efficient for the arylation of secondary cyclic or acyclic amines and anilines (Scheme 4.3).[24]

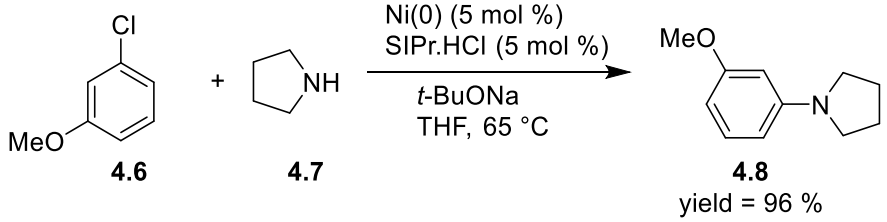

Scheme 4.3: Ni(0) catalyzed *N*-arylation reaction[24]

Alkylation reaction between amine and alkyl halide under basic condition can form C-N bonds. Recently, in 2015, Muthukumaran Nirmala explored C-N coupling reactions employing the air-stable complex of nickel(II) bearing *N*-heterocyclic carbene (NHC) ligand (Scheme 4.4).[25] Here alkyl halide is used as a substrate and HCl is generated as a byproduct.

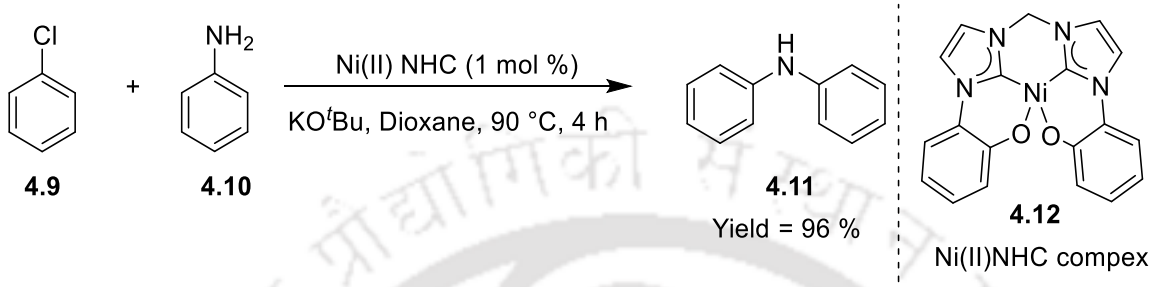

Scheme 4.4: C-N coupling reaction catalyzed by Ni(II) in the presence of a NHC ligand[25]

In 1903, Ullmann found that Cu could be used in the formation of C-N bonds.[26] In contrast with Buchwald and Hartwig's reaction, the Ullmann coupling reaction can proceed under milder conditions. In 2011, Wang *et al.* demonstrated an efficient Ullman reaction of aryl bromide and *N*-heterocycles catalyzed by the combination of CuI and acylhydrazine or acylhydrazone type of ligands (Scheme 4.5).[27]

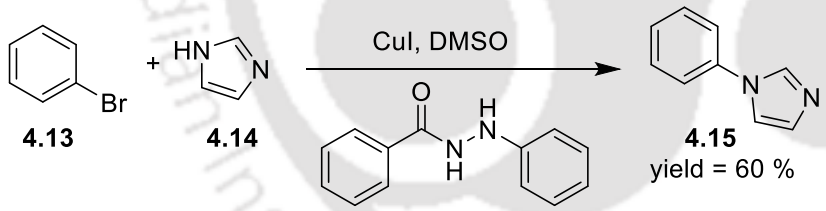

Scheme 4.5: An example of Ullman reaction leading to C-N bond formation that was reported by Wang[27]

The Weinreb group explored an efficient route for direct conversion of alcohols to protected higher-order amines. *N*-methyl *p*-toluenesulfonamide could be directly coupled with primary and secondary alcohols in presence of phosphorane reagent CMBP (cyanomethylenetributylphosphorne) under Mitsunobu conditions to afford various sulfonamide-protected amines (Scheme 4.6).[28]

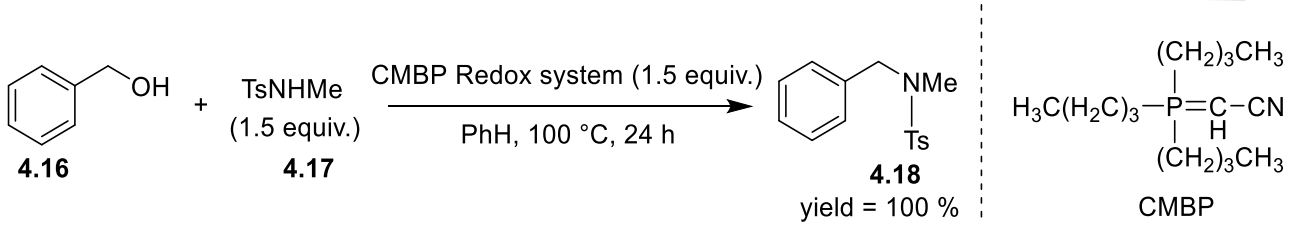

Scheme 4.6: Generation of sulfonamide-protected amines via the Mitsunobu reaction[28]

In 2017, Jun Yong Kang, with his coworkers achieved great success in *N*-alkylation by employing the Mitsunobu reaction condition. They reported C-N coupling with various cyclic amines in the presence of *N*-heterocyclic phosphine butane (NHP-butane) and an azo compound. Here benzyl alcohol and other aliphatic alcohols were used as substrates to give the corresponding *N*-alkylated products with more than 99% yield (Scheme 4.7).[29] This reaction procedure involves the dehydrogenative coupling of alcohols using a combination of a phosphine containing reducing agent and azo group that operates as an oxidizing agent.

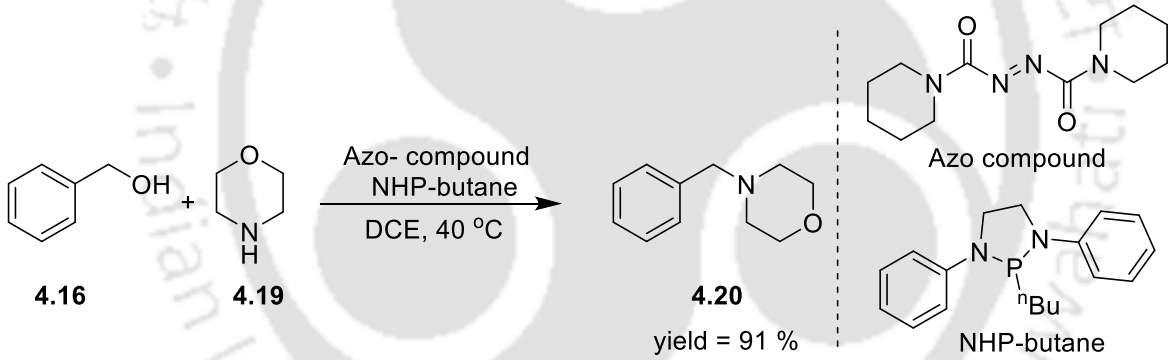

Scheme 4.7: *N*-alkylation by employing the Mitsunobu condition.[29]

The conversion of two secondary alcohol functionalities to corresponding alkyl azides can be achieved using Mitsunobu reaction condition. In 2001, Overman *et al.* exhibited a convenient route where these azides were subsequently reduced to primary amines and cyclized to desired bis-amidine functionalities (Scheme 4.8).[30]

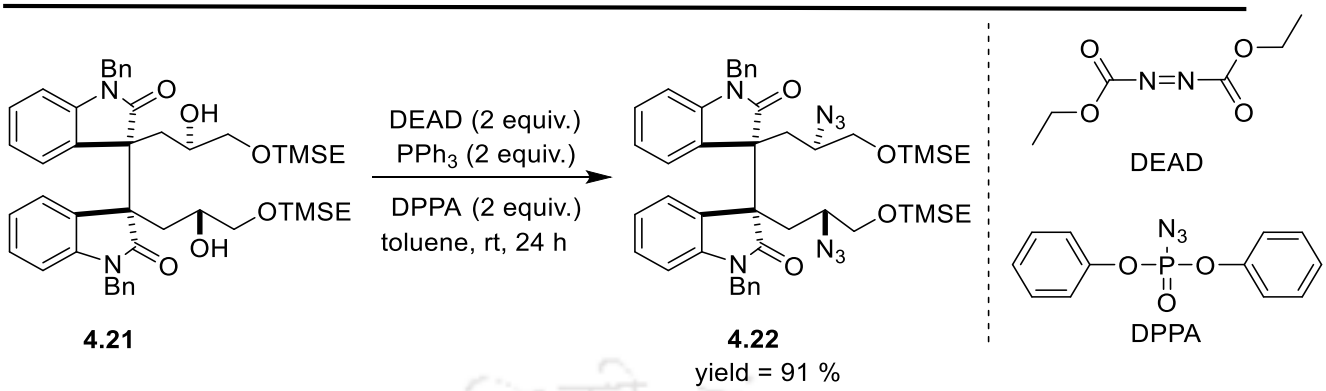

Scheme 4.8: Conversion of alcohol to azide under Mitsunobu reaction [30]

Though the Mitsunobu reaction offers interesting and efficient reactivity patterns, one of the major disadvantage is that this reaction requires more the stoichiometric amount of starting materials and regents such as alcohol, phosphine, azo compound, and an acid. Not surprisingly, the Mitsunobu reaction leads to several by-products such as phosphine oxide and biphenyl derivatives that are hard to separate from the desired product.

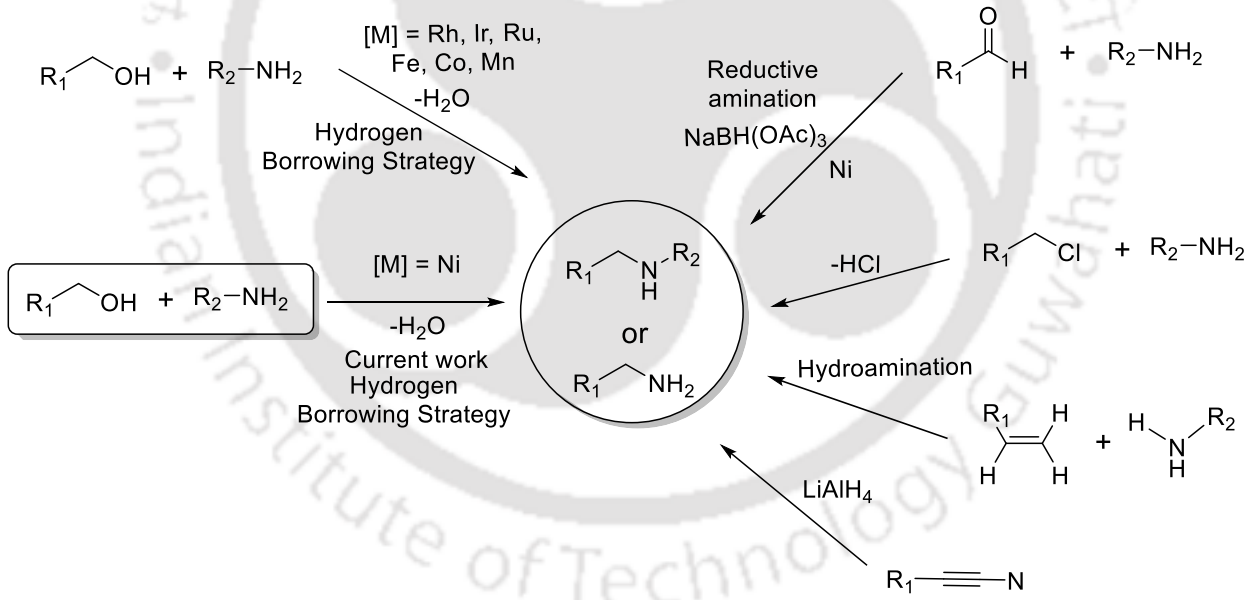

Figure 4.2: A few available methods for C–N bond formation

Most of the approaches to the *N*-alkylated amines that are discussed above (Figure 4.2) suffers from several limitations that include requirement of excess amounts of toxic halides along with generation of considerable amount of side products and waste. On the other hand, methods that accomplish the alkylation of primary amine with alcohol will generate higher-order amine with

water as a sole byproduct. This makes these methods environmental friendly as well as atom efficient (Figure 4.2). Besides, alcohols are more readily available and less hazardous starting materials compared to their corresponding halides. A generally accepted mechanism of this type of reaction involves "hydrogen borrowing".

The "hydrogen borrowing" approach, a term that was first coined by Williams,[31] is an efficient and greener approach for the preparation of amines. It involves the metal-catalyzed dehydrogenation of alcohol to generate a carbonyl compound, which subsequently reacts with the amine in an un-catalyzed step. The resulting imine is then hydrogenated *in-situ* to the amine while regenerating the transition metal catalyst.[32] This approach is green and atom-economical as water is the sole by-product. No additional external hydrogen source is needed because the parent alcohol itself acts as the hydrogen donor.

4.2 Known methods towards *N*-alkylation involving hydrogen borrowing approach

In 1981, Grigg[33] and Watanabe[34] independently reported for the first time, the homogeneous transition metal-catalyzed *N*-alkylation of amines.

Grigg and co-workers reported *N*-alkylation with several metal-phosphine complexes and showed $RhH(PPh_3)_4$ to be the most active catalyst.[33] They performed *N*-alkylation at ≤100 °C, and selective mono-alkylation of primary amines was observed (Scheme 4.9). Even heterocyclic rings could be obtained through intramolecular process.

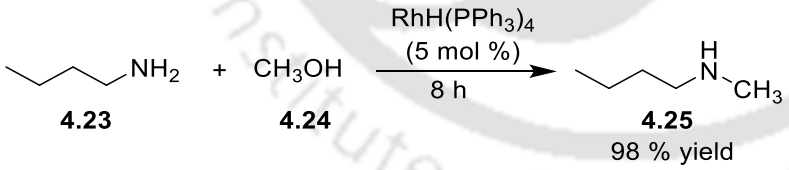

4.23 **4.24** **4.25**
98 % yield

Scheme 4.9: *N*-alkylation of amines with alcohols catalyzed by $RhH(PPh_3)_4$ [33]

In the same year, Watanabe and co-workers reported the formation of *N*-alkylaniline using aniline with saturated alcohol in presence of a ruthenium catalyst at 180 °C (Scheme 4.10).[34]

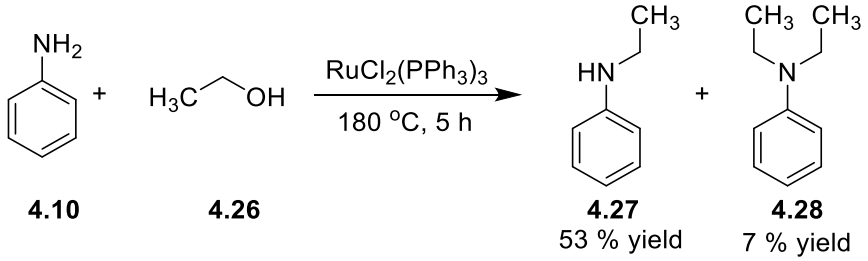

Scheme 4.10: Ru catalyzed *N*-alkylation of aniline with alcohols[34]

After five years, in 1986, Watanabe discovered that amines react with primary alcohols in the presence of Pt catalyst at 120-180 °C to give the corresponding *N*-alkylated product.[35] In the years that followed several homogeneous catalytic *N*-alkylation systems were reported by van Koten,[36] Milstein,[32] Beller[37], Martín-Matute[38] and Sabuj Kundu[39] among others.[40,41,45]

In 1998, van Koten observed that a Ru(II) complex containing a neutral terdentate donor of the type $[C_5H_3N(CH_2E)_2\text{-}2,6]$ (E = PPh_2 or NMe_2 in case of PNP and NNN respectively) were effective as catalyst in *N*-(cyclo)alkylation reactions of aromatic amines with diols $Y(CH_2CH_2OH)_2$ (Y= CH_2, NR).[36] These catalysts proved useful in the synthesis of *N*-phenylpiperidine in 85% yield starting from aniline and 1,5-pentanediol. The mono-alkylated product *N*-(5-hydroxypentyl) aniline, was formed in minor amounts. In 2010, Beller and Williams developed atom efficient and environmentally benign homogeneously catalyzed *N*-alkylation of indoles with alcohol.[37] In 2006, Baratta and co-workers, observed high TON (1.7×10^5) in the reduction of ketones under hydrogen transfer condition by using a CNN pincer-Ru(II) complex **4.30** (Scheme 4.11).[40] Employing the same catalyst in 2012, Belén Martín-Matute reported selective mono-alkylation of amines with high efficiency (Scheme 4.11).[38] They have shown that, by using catalyst loadings as low as 1 mol%, in presence of stoichiometric amounts of KO^tBu, the corresponding *N*-alkylated amines were obtained in quantitative yield. This pincer-Ru catalyzed *N*-alkylation has wide range of applicability. It catalyzes the selective monoalkylation of heteroaromatic amines with a wide range of primary alcohols, including heterocyclic ring substituents. In the presence of diamine substrates, *N*,*N*-dialkylation took place exclusively.

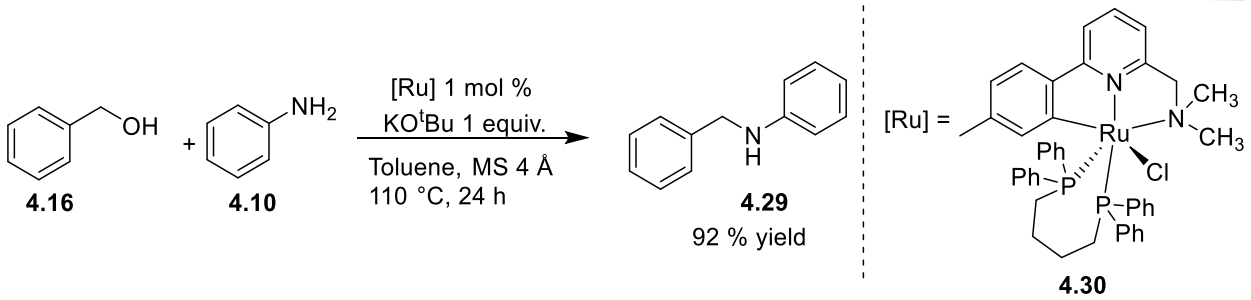

Scheme 4.11: Ru (II) CNN pincer catalyzed *N*-alkylation[38]

In 2018, Kundu and co-workers developed an air and moisture stable 2-hydroxypyridine based bi-functional ruthenium NNN-pincer complex to catalyze efficient (TON = 42,840) *N*-alkylation of amines under mild conditions (Scheme 4.12).[39]

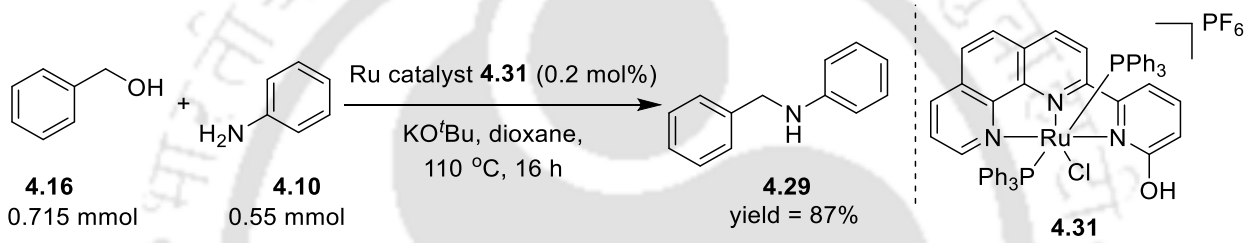

Scheme 4.12: NNN-Ru(II) catalyzed *N*-alkylation of amines[39]

In 2019, Kumar and co-workers demonstrated the use of NNN pincer-Ru complex for catalytic *N*-alkylation under neat conditions. Interestingly, for the first time the required base is generated *in-situ* from benzyl alcohol and sodium (Scheme 4.13).[41] The resulting sodium alkoxide reacts as a water scavenger. TON as high as 29,000 were observed for *N*-alkylation between aniline and cyclohexyl methanol using (^{tBu2}NNN)$RuCl_2PPh_3$ (0.002 mol %).

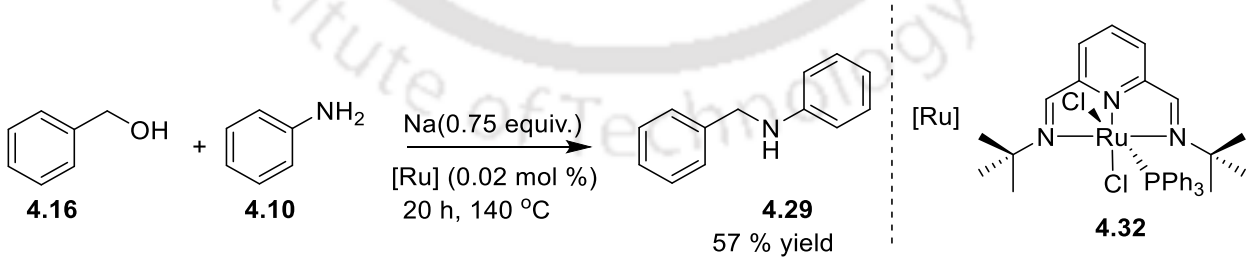

Scheme 4.13: NNN pincer-Ru(II) catalyzed *N*-alkylation[41]

Most common catalysts used for *N*-alkylation are based on precious metals, including Ru[37, 39, 42-44], Ir[45], Pd[17, 46-47], and Rh.[48] In general, Ir complexes are more reactive than Ru based catalysts.[33] In 2010, Kempe reported C-N alkylation by using iridium based catalysts at loadings as low as 0.1

mol % (Scheme 4.14).[49] Similar Ir-catalyzed amine alkylation utilizing the "hydrogen borrowing" strategy, have been developed into efficient synthetic methods by Beller,[50] Grigg[51], Fujita[52], Williams[53], and Kempe[49].

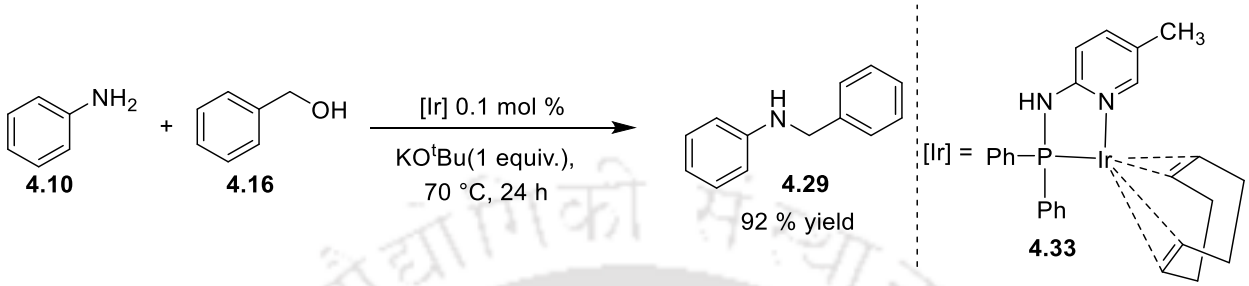

Scheme 4.14: Ir catalyzed *N*-alkylation [49]

In 2013, Ponnam Satyanarayana *et al.* reported the reaction between 4-methyl aniline and 4-methoxy benzyl alcohol in presence of $Rh(acac)_3$ to obtain 94 % of corresponding *N*-alkylated product (Scheme 4.15).

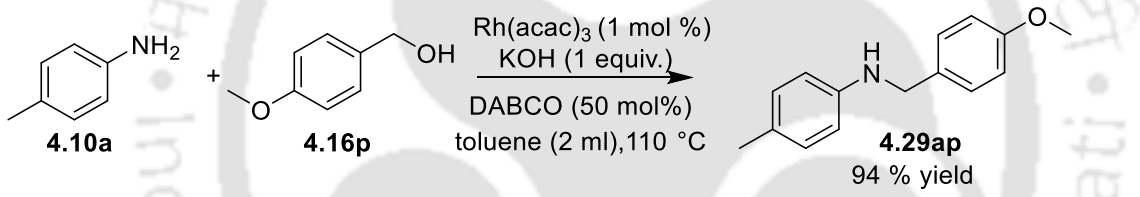

Scheme 4.15: *N*-alkylation using $Rh(acac)_3$ catalyst[48]

The group of Majeed Seayad reported *N*-alkylation of various primary and cyclic secondary amines using $PdCl_2$ in the presence of dppe (dppe = 1,2-*bis*(diisopropylphosphino)ethane) as ligand (Scheme 4.16).[54] Interestingly, more challenging secondary alcohols were used as alkylating agent to obtain *N*-alkylated product with good to moderate yield.

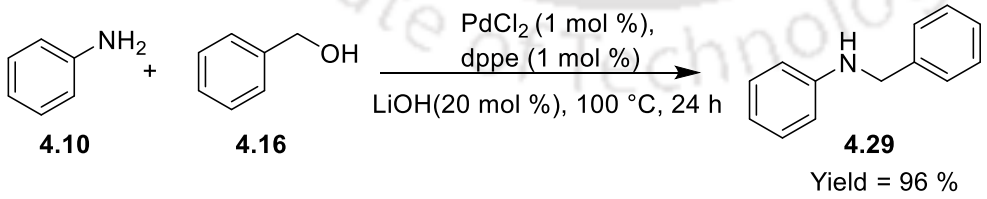

Scheme 4.16: *N*-alkylation catalyzed by a combination of a Pd(II) salt with dppe [54]

In homogeneous reactions, recovery, and reuse of expensive catalyst is challenging. On the other hand, heterogeneous catalysts have a lot of advantages, as they are easy to handle, are stable for a long time and can be securely disposed. Several heterogeneous catalysts have been developed for

alkylation of amines, which follows hydrogen borrowing methodology. Among them silica,[55] aluminum oxide,[56] Raney nickel,[57] copper (or copper oxide),[58] gold[59] have been used as heterogeneous catalysts. However, heterogeneous catalysts generally suffers from several limitations that include low turnover number (TON), limited scope, high catalyst loading and requirement of stoichiometric amounts of basic co-catalyst.

For the last few decades, researchers are interested in the search of more eco-friendly, inexpensive, and highly abundant metal catalysts for *N*-alkylation reaction. Rightly, there is a significant growth in research on catalysts based on most abundant metals such as Fe,[60] Mn,[61] Cu[62], Co[63-64] and Ni[65] for *N*-alkylation. However, considerable challenges remain as the first row transition metals tend to undergo one-electron changes in oxidation state and demonstrate radical reactions, which has limited their application as catalysts. In 2015, Zhang *et al.* observed *N*-alkylation of both aromatic and aliphatic amines by using a well-defined cobalt based PNP pincer complex (Scheme 4.17).

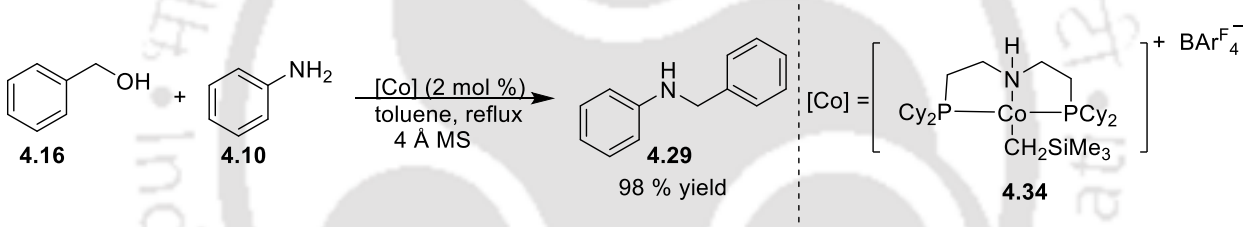

Scheme 4.17: Co-pincer catalyzed *N*-alkylation of aniline with benzyl alcohol[64]

Heterogeneous Ni catalyst which is easily recoverable as well as non-expensive is also reported for *N*-alkylation.[56, 66-67] In 2013, Shimizu and co-workers have obtained higher turnover number (ca. 800) in the *N*-alkylation of amines with *n*-octanol, catalyzed by Al_2O_3-supported Ni NPs (1 mol %) (NP = nano-particles) (Scheme 4.18).[66] However, there have been a very few reports on the use of homogeneous Ni[68-71] systems for catalytic *N*-alkylation.

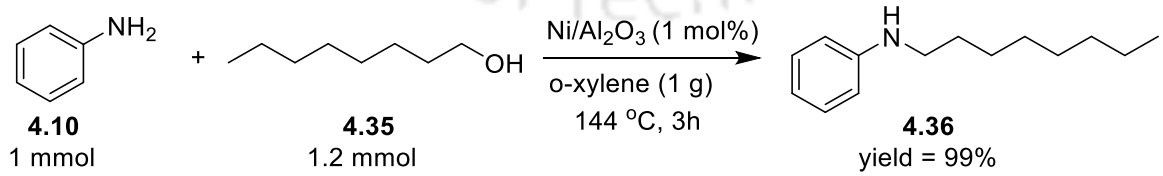

Scheme 4.18: *N*-alkylation of amine using Ni NPs[66]

In 2017, the Banerjee group demonstrated the use of $NiBr_2$ (10 mol%) in combination with 1,10 phenanthroline (20 mol%) to accomplish the *N*-alkylation of various amines with TON up to 10 in presence of stoichiometric amount of KO^{t}Bu (Scheme 4.19).[72]

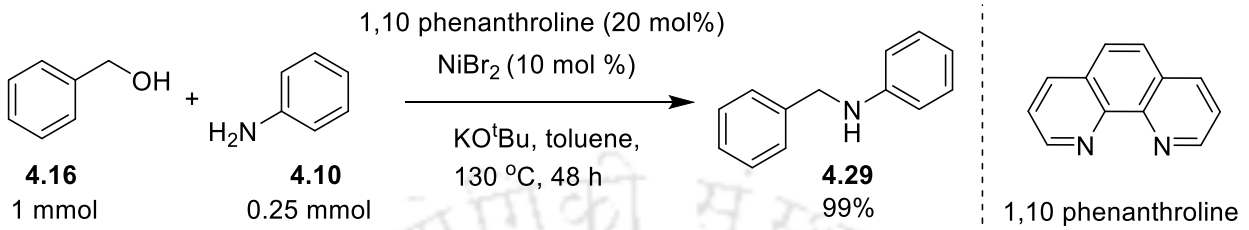

Scheme 4.19: *N*-alkylation of amine catalyzed by $NiBr_2$ in the presence of 1,10 phenanthroline[72]

Very recently, Kundu and co-workers revealed the use of the same catalytic system as reported by Banerjee[72] to produce a variety of substituted quinoxalines from the dehydrogenative coupling of vicinal diol with 1,2-diamines and 2-nitro-aniline derivatives (Scheme 4.20).[73] They observed that the reaction was not fully homogeneous and some heterogeneous Ni particles contributed to the catalytic activity.

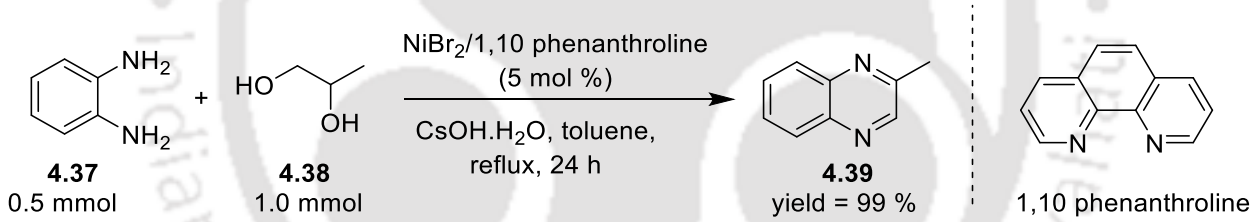

Scheme 4.20: Ni-catalyzed quinoxalines synthesis using dehydrogenative coupling strategy[73]

In 2018, the Sarkar group has reported the nickel catalyzed synthesis of poly-substituted quinolone.[74] The Barta group obtained a maximum of 28 TON in the $Ni(COD)_2$ (3 mol%) catalyzed *N*-alkylation of amines in the presence of KOH (30 mol%).[75] They attributed the catalytic activity to the Ni nano-particles that were formed *in-situ* under the reaction condition (Scheme 4.21).

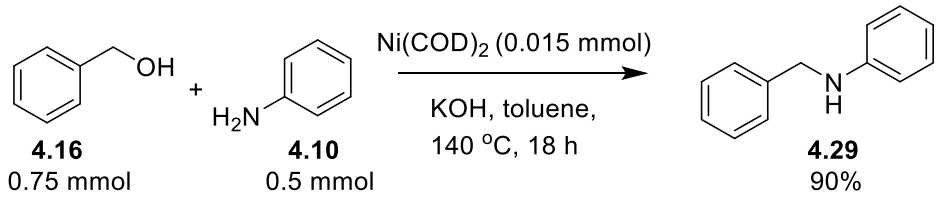

Scheme 4.21: *N*-alkylation of amine using $Ni(COD)_2$[75]

Very recently in 2019, Adhikari and co-workers have reported azophenolate ligand coordinated Ni catalyst for the efficient catalytic *N*-alkylation of amine with upto 92 % yield (Scheme 4.22).[69]

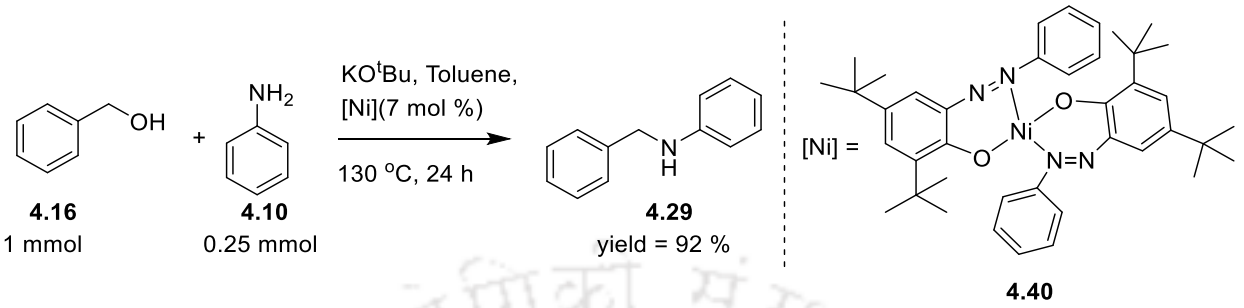

Scheme 4.22: Azophenolate ligand coordinated Ni catalyzed *N*-alkylation[69]

The Balaraman group have recently reported the use of NNN pincer-Ni complex **4.43** for the *N*-alkylation of aniline with secondary alcohols (Scheme 4.23).[68]

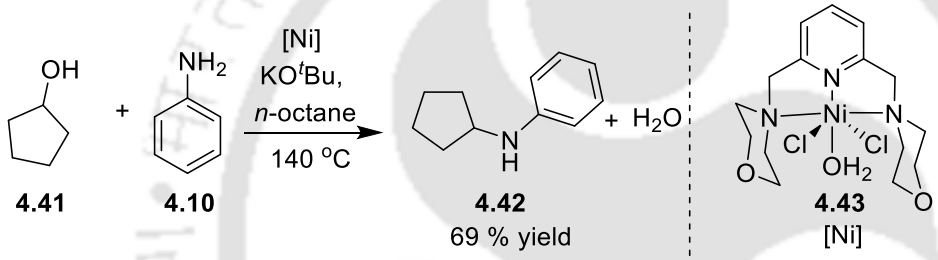

Scheme 4.23: NNN-Ni catalyzed *N*-alkylation of amine with secondary alcohol[68]

García and co-workers have utilized a catalytic system comprising of $Ni(COD)_2$ in presence of dippe (dippe = 1,2-*bis*(diisopropylphosphino)ethane) to accomplish the *N*-ethylation reaction of aniline(Scheme 4.24).[70]

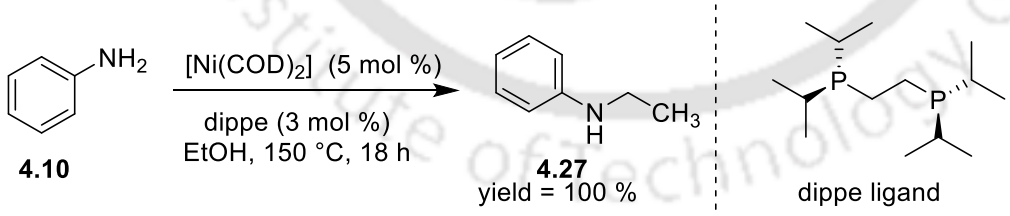

Scheme 4.24: *N*-alkylation of aniline catalyzed by a combination of $Ni(COD)_2$ with dippe[70]

Very recently, Ramesh demonstrated a highly sustainable catalytic protocol for the coupling of alcohol and amine to selectively yield monoalkylated amines using inexpensive NNO pincer-Ni(II) complexes (Scheme 4.25).[71]

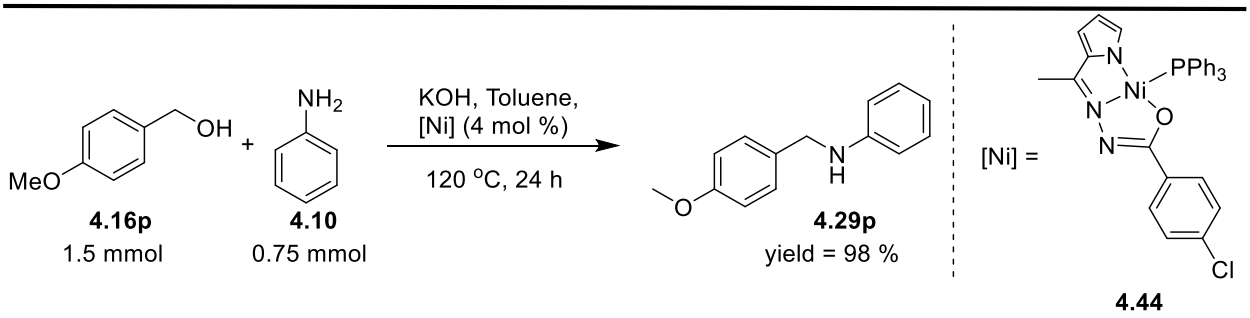

4.16p 1.5 mmol + **4.10** 0.75 mmol → **4.29p** yield = 98 %; [Ni] = **4.44**

Scheme 4.25: Ni(II)-NNO pincer catalyzed *N*-alkylation of amines with alcohol[71]

The studies on *N*-alkylation using homogeneous Ni catalysts are less explored and there have been no other reports on homogenous nickel catalytic systems for the alkylation of amines. In addition, there is no clear mechanistic understanding on these Ni catalyzed reactions. Accordingly, in this chapter, well-defined molecular pincer-Ni catalytic systems have been explored for *N*-alkylation reactions. Furthermore, a fundamental mechanistic understanding on the operative mechanism has been obtained both experimentally and theoretically.

4.3 Results & discussions

With an objective to work on environmental friendly pincer ligands as well as move away from precious metals, the reactivity of a well-defined molecular pincer-Ni(II)complex ($(^{iPr2}NNN)NiCl_2(NCCH_3)$ **4.45** (Scheme 4.26)[76 77] was studied towards *N*-alkylation.

4.3.1 Optimization of catalytic protocol

The 20-electron Ni pincer complex **4.45** catalyzes the *N*-alkylation between aniline and benzyl alcohol in presence of a base. Product conversion was suppressed significantly when a smaller amount of base was used (Table 4.1, Entries 8 and 9). Particularly, no product formation was

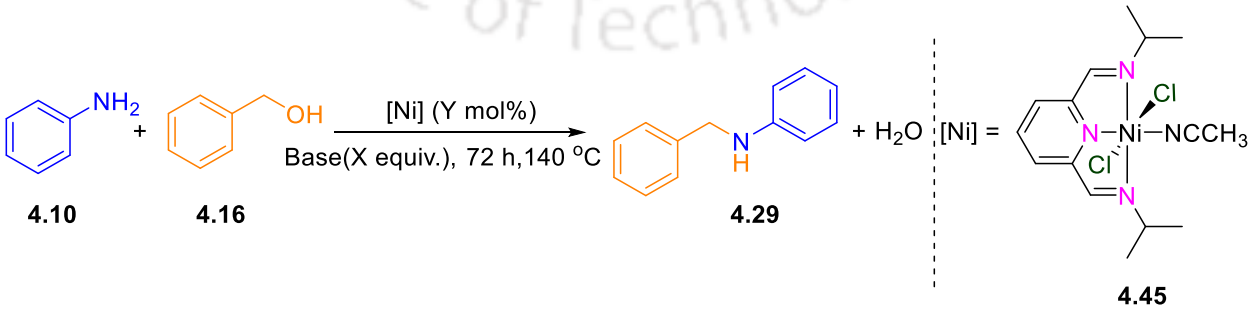

4.10 + **4.16** → **4.29** + H_2O; [Ni] = **4.45**

Scheme 4.26: $(^{iPr2}NNN)NiCl_2(NCCH_3)$ **4.45** catalyzed *N*-alkylation of aniline with benzyl alcohol

Table 4.1: Solvent-free *N*-alkylation of benzyl alcohol catalyzed by **4.45** under varying conditions[i]

Entry	Catalyst (Y mol %)	Base (X Equivalents)	Solvent	Yield[a] of **4.29** (%)	TON of **4.29**
1.	**4.45** (0.02)	-		0	0
2.	**4.45** (0.02)	NaOH (0.75)		2	70
3.	**4.45** (0.02)	KOH (0.75)		7	350
4.	**4.45** (0.02)	Na (0.75)		22	1080
5.	**4.45** (0.02)	KO^{t}Bu (0.75)		20	1010
6.	**4.45** (0.02)	NaH(0.75)		20	1000
7.	**4.45** (0.02)	NaO^{t}Bu (0.75)		43	2135
8.	**4.45** (0.02)	NaO^{t}Bu(0.50)		23	1135
9.	**4.45** (0.02)	NaO^{t}Bu(0.25)		15	765
10.	**4.45** (0.02)	NaO^{t}Bu(1.00)		47	2340
11.	**4.45** (4.0)	NaH (0.75)		40	10
12[b].	**4.45** (0.02)	NaO^{t}Bu (0.75)	toluene	42	2075
13[c].	**4.45** (0.02)	NaO^{t}Bu (0.75)	THF	12	622
14[d].	**4.45** (0.02)	NaO^{t}Bu (0.75)	dioxane	45	2250
15[e].	**4.45** (2.0)	NaO^{t}Bu (0.75)	dioxane	48	24
16[f].	**4.45** (2.0)	NaO^{t}Bu (0.75)	toluene	20 (15)[g]	10
17[h].	**4.45** (2.0)	NaO^{t}Bu (0.75)	toluene	60 (11)[g]	30
18[h].	**4.45** (4.0)	NaO^{t}Bu (0.75)	toluene	60 (30)[g]	15
19.	Ni(COD)$_2$(0.02)	KOH (0.3)		2	100
20.	[NiCl$_2$+ 2 phen] (0.02)	KO^{t}Bu (0.1)		25	1250

[a)] Yield determined via ^{1}H NMR using toluene as an internal standard. In all cases the remaining materials are unreacted starting material along with trace amount of the corresponding imine. [b)] 1 ml toluene is used as solvent. [c)] 1 ml THF is used as solvent. [d)] 1 ml Dioxane is used as solvent. [e)]Reaction condition: 1 mmol **4.10**, 1 mmol **4.16**, 0.75mmol of NaO^{t}Bu and 2 mol % of **4.45** in 1.8 ml of dioxane at 140 °C. [f)] Reaction condition: 1 mmol **4.10**, 1mmol **4.16**, 0.75mmol of NaO^{t}Bu and 2 mol % of **4.45** in 1.8 ml of toluene at 140 °C.[g)] the yield of corresponding imine is given in parenthesis. [h)] Reaction condition: 1 mmol **4.10,** 1 mmol **4.16**, 0.75 mmol of NaO^{t}Bu and Y mol % of **4.45** in 0.3 ml of toluene at 140 °C. [i)]Reaction condition unless specified otherwise: 4.8 mmol **4.10,** 4.8 mmol **4.16**, X equivalent of NaO^{t}Bu and Y mol % of **4.45** at 140 °C.

observed, when the reaction was performed without addition of base (Entry 1, Table 4.1) or in the absence of complex **4.45** (Entry 1, Table 4.2). Very poor results were obtained upon use of 0.75 equivalents of NaOH and KOH (Entry 2 and 3, Table 4.1). Further evaluation of different reaction parameters showed better result (upto 43 % yield) while performing the reaction with NaO^{t}Bu (0.75 equivalent) as base and a loading of 0.02 mol% of the catalyst **4.45** (Entry 7, Table 4.1). Interestingly, under these reaction conditions, the alkylation proceeds to give high turnover number (ca. TON 2132).

Notably, in no case *N, N*-alkylation was observed. While lowering the amount of NaO^{t}Bu resulted in poor turnover number, higher loading of NaO^{t}Bu (1 equivalent) increased the yield of *N*-alkylated product to 47 % (Entry 10, Table 4.1). As higher base loading decreases the homogeneity of reaction mixture, 0.75 equivalents of NaO^{t}Bu was used for further screening. Moreover, use of toluene and dioxane as solvents had a negligible effect on the turnover number, whereas using THF significantly lowered the yield. Upon increasing the catalyst loading from 0.02 to 4 mol % in presence of NaH, the yield of *N*-alkylated amine **4.29** increases from 20 % to 40 % (Entry 6 and 11, Table 4.1).

At higher catalyst concentrations, there is a chance of catalyst deactivation through cluster formation, which mainly occurs via the C-H activation of the isopropyl groups.[78-81] The deactivation through cluster formation could be minimized by operating at optimal dilutions. Particularly upon use of 4 mol % of catalyst **4.45** in presence of 0.3 ml of toluene, the total yield of amine and imine obtained was about 90 % (Entry 18, Table 4.1). The catalytic system reported by Barta[75] and Banerjee[72] gave poor results under the current reaction conditions (Entry 19 and 20, Table 4.1). The catalytic system screened in the current study also showed better efficiency from an atom-economy point of view and required 1:1 ratio of benzyl alcohol and aniline to yield the *N*-alkylated product, which is in stark contrast to previous reports[72, 75] where an excess (1.2-8 folds) of alcohol is used with respect to aniline.

With higher catalyst loading, the yield does not increase significantly. For instance, upon increasing the catalyst loading from 0.05 mol % to 0.1 mol %, the yield remains the same with decrease in TONs (Entry 4 and 5, Table 4.2). As TONs are significantly diminished with higher

catalyst loading, the studies were continued under low catalyst loading (≤0.02 mol %) in the presence of 0.75 equivalent of NaO^{t}Bu for most of the *N*-alkylation reactions.

Table 4.2: Solvent-free *N*-alkylation of aniline with benzyl alcohol using various Ni catalysts

Entry	Catalyst (mol %)	Base (X equivalents)	Yield[a] of **4.29**	TON
1.	-	NaO^{t}Bu (0.75)	2%	70
2.	$NiCl_2$ (0.02)	NaO^{t}Bu (0.75)	26%	1300
3.	$NiCl_2$(DME) (0.02)	NaO^{t}Bu (0.75)	42%	2100
4.	**4.45** (0.05)	NaO^{t}Bu (0.75)	46%	925
5.	**4.45** (0.1)	NaO^{t}Bu (0.75)	46%	460

Reaction condition: benzyl alcohol (4.8 mmol), aniline (4.8 mmol) at 140 °C in closed vessel. [a]Yield determined via ^{1}H NMR using toluene as an internal standard.

It should be noted that (entry 2-10, Table 4.1), the catalyst **4.45** was handled under inert (Ar) atmosphere and reaction mixture was homogenous and clear purple coloured which later turned into black colour that is indicative of the formation of Ni-H species.[72] Instead, if the catalyst **4.45** was handled under air, then the resulting reaction mixture quickly formed a clear colourless solution with black particulates leading to trace (<2%) product formation **4.29** after 72 h (Entry 1, Table 4.2).

While $NiCl_2$ gave moderate turnover number (Entry 2, Table 4.2), the turnover number obtained with 0.02 mol % of $NiCl_2$(DME) were comparable with NNN-Ni pincer complex **4.45** (Entry 3, Table 4.2). The high thermal stability of NNN-Ni pincer complex makes it a better catalyst towards *N*-alkylation at elevated temperature in comparison with $NiCl_2$(DME) (see Table 4.5). The TGA data for catalyst (^{iPr2}NNN)$NiCl_2(NCCH_3)$ **4.45** (Figure 4.3) indicates an initial loss of an acetonitrile molecule (12 % mass loss) at 83.7 ^{o}C following which the resulting species containing the two Cl^- ligands (which are key to catalysis) remained stable up to 260 °C. On the other hand, $NiCl_2$(DME) is relatively less stable and readily loses its Cl^- ligands.

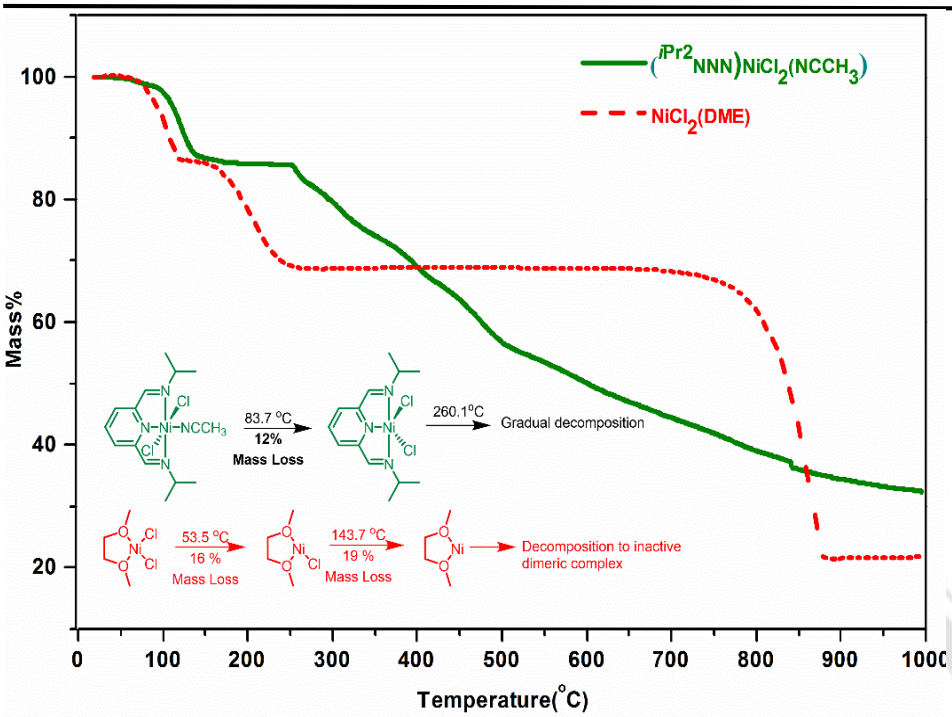

Figure 4.3: TGA data for catalyst (^{iPr2}NNN)$NiCl_2(NCCH_3)$ **4.45** and $NiCl_2$(DME)

4.3.2 Substrate scope

Having established the optimal reaction conditions for the effective *N*-alkylation of aniline with benzyl alcohol, the methodology was applied to other substrates i.e., various alcohols and amines. The reactions of benzyl alcohol with various aniline derivatives were tested under standard optimized reaction conditions (Entry 7, Table 4.1).

4.3.2.1 *N*-alkylation of various anilines with benzyl alcohol

Substrates bearing both electron-donating and electron-withdrawing substituents on the aryl ring of aniline were selectively alkylated to afford the *N*-monoalkylated anilines in good to moderate (typically 16 – 47 %) yields (Table 4.3). Amine with electron donating -OMe group (**4.29d**, Table 4.3), provided the corresponding mono-alkylated amines with 16 % yield. In contrast, strong electronegative substituent (-CF_3) at the para position of the aniline moiety did not proceed for *N*-alkylation reaction (**4.29b**, Table 4.3). Presence of strong electron donating methyl (-CH_3) substituent leads to corresponding product with 32 % yield (**4.29e**, Table 4.3).

Table 4.3: Solvent-free *N*-alkylation of various amines with benzyl alcohol catalyzed by **4.45** at 140 °C[f]

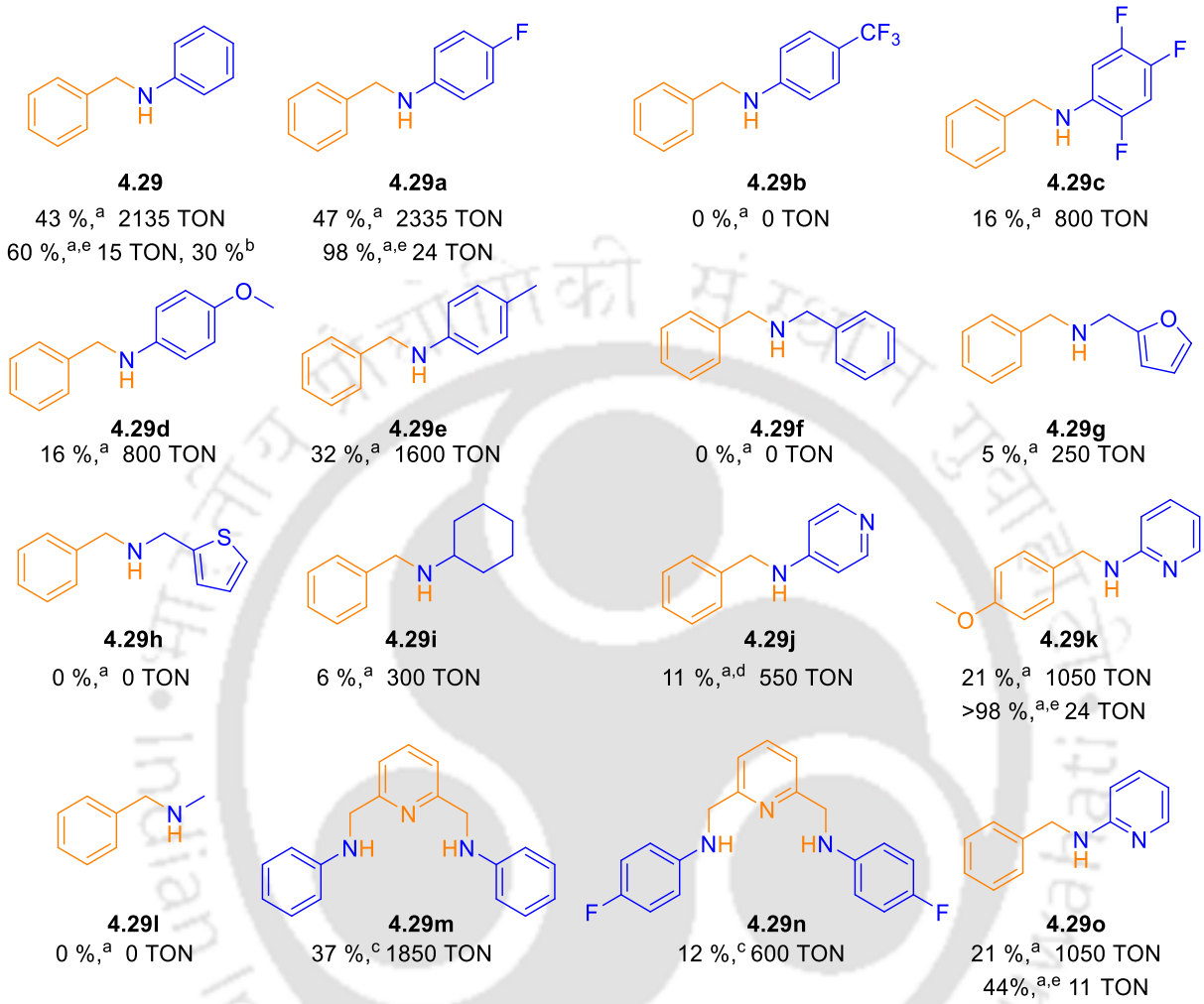

Table 4.3:[(a)]Yield is determined by ^{1}H NMR using toluene as an internal standard. In all cases remaining contain reacted starting material along with trace amount of the corresponding imine. [b)]yield of the corresponding imine, [c)] isolated yield, [d)] 1 ml of toluene was used as solvent, [e)] same condition as footnote h in Table 4.1 but with 4 mol % of **4.45**,[f)] Reaction condition: 4.8 mmol of **4.16a-p**, 4.8 mmol of **4.10a-p**, 3.6 mmol of NaO^{t}Bu, and 1 µmol of **4.45** at 140 °C in sealed vessel.

Hetero-aromatic amines led to the products (**4.29g** and **4.29h**, Table 4.3) in very poor yields (less than 5%). Reactions with methyl amine and benzyl amine (**4.29l** and **4.29f**, Table 4.3) did not proceed to yield *N*-alkylated amines. In the presence of cyclohexyl amine, only 6 % *N*-alkylated product was obtained (**4.29i**, Table 4.3). *N*-alkylation reaction between 2-amino-pyridine and benzyl alcohol gave 21 % yield and 1050 TON (**4.29o**, Table 4.3). Identical results were obtained

with *N*-alkylation of 2-amino pyridine with 4-methoxy benzyl alcohol (**4.29k**, Table 4.3). At higher catalyst (4 mol %) loading, very high yield (>98 %) of **4.29k** was obtained. The reaction of 4-amino pyridine with benzyl alcohol resulted in 11 % of the *N*-alkylated product with 550 TON (**4.29j**, Table 4.3). The reaction of pyridine-2, 6-dimethanol with 2 equivalents of aniline gave 37 % isolated yield of the corresponding bis-*N*-alkylated product (**4.29m**, Table 4.3). Similarly, 2, 6 pyridine di-methanol could also be alkylated with 2 equivalent of 4-fluoro aniline and the bis-alkylation product was isolated in 12% yield (**4.29n**, Table 4.3).

4.3.3.2 *N*-alkylation using (hetero)aromatic and aliphatic alcohols

It is noticed that strongly electron-donating 4-methoxy-derived benzylic alcohol is an excellent substrate for the reaction, affording the corresponding product in 48% yield and high TON 2420 (**4.29p**, Table 4.4), while electron-withdrawing substituents on the benzylic alcohol considerably decreased the yield of the desired secondary amine products to only 8% (**4.29q**, Table 4.4).

It is observed that the reaction of hetero-aromatic alcohols did not proceed well and provided the desired products in most cases with very low yields (less than 1%) (**4.29s** and **4.29t**, Table 4.4). Even in the presence of excess base, the yield did not increase satisfactorily. A secondary alcohol e.g., 4-fluro-α-methyl benzyl alcohol was tested for the reactions with aniline (**4.29r**, Table 4.4) and no coupling reactions were detected. Attempts were made to dehydrogenate methanol but *N*-methylation of amine was not observed (**4.29za**, Table 4.4). This is very different from the observation of Barta and co-workers who obtained moderately good yields of **4.29za** using Ni nanoparticles. This selectivity towards various alkylating agents is a signature of molecular catalysts and not nano-particles. In the presence of aliphatic amine such as cyclohexyl amine (**4.29v**, Table 4.4) *N*-alkylation reaction did not proceed well and corresponding yield is less than 10 %.

Pyridine 2-methanol and pyridine 4-methanol were also utilized as alkylating agents and the corresponding *N*-alkylated products were obtained with 39 % and 11% yield respectively (**4.29x**, **4.29w**, Table 4.4). *N*-alkylation between naphthalene-1-methanol and 2-amino pyridine provided the highest yield (around 90 %) and TON of 4500 (**4.29z**, Table 4.4). The reaction between naphthalene-1-methanol and aniline resulted in 1900 TON (**4.29y**, Table 4.4).

Table 4.4: The **4.45** catalyzed solvent-free *N*-alkylation of aniline with various alcohols[f]

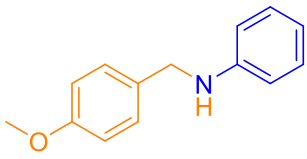

4.29p
48 %,[a] 2420 TON
28 %, [a,c] 1250 TON
60 %, [a,d]16 TON

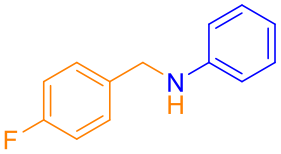

4.29q
8 %,[a] 400 TON
4%,[b] 200 TON

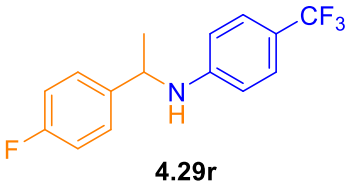

4.29r
0 %,[a] 0 TON

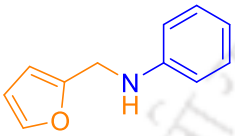

4.29s
0.5 %,[a] 50 TON

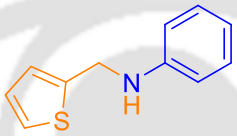

4.29t
0.7 %,[a] 50 TON

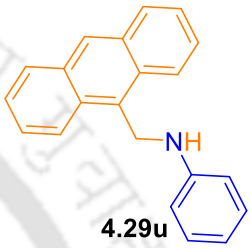

4.29u
8 %,[a] 400 TON

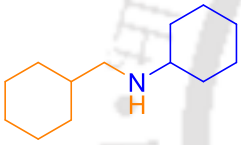

4.29v
9 %,[a] 450 TON
16 %,[b] 800 TON

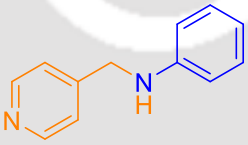

4.29w
39 %,[a] 1950 TON
55 %, [a,e] 14 TON

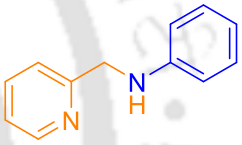

4.29x
39 %,[a] 1950 TON
60 %,[a,d] 15 TON

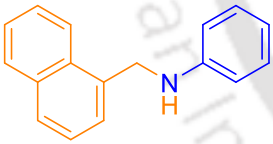

4.29y
38 %,[a] 1900 TON
50 %,[a,e] 13 TON

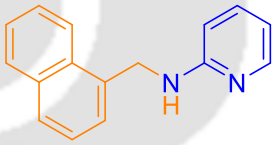

4.29z
90 %,[a] 4500 TON

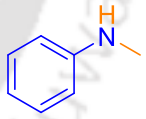

4.29za
0 %,0 TON

Table 4.4: [(a)]Yield is determined by ^{1}H NMR using toluene as an internal standard. In all cases remaining contain reacted starting material along with trace amount of the corresponding imine. [c)] NaH used as additive, [d)]NaH used as additive in presence of 4 mol % catalyst **4.45**, [e)] same condition as footnoteh in Table 1 but with 4 mol % of **4.45**, [f)] Reaction condition: 4.8 mmol of **4.16q-zb**, 4.8 mmol of **4.10q-zb**, 3.6 mmol of NaO^{t}Bu, and 1 µmol of **4.45** at 140 °C in sealed vessel.

Interestingly, upon lowering the catalyst loading, very high TON were obtained for few representative *N*-alkylation reactions at higher temperature 200 °C (Table 4.5). The *N*-alkylation at 200 °C of aniline with benzyl alcohol using $NiCl_2$(DME) resulted in lower TON (11,000 TON)

in comparison to the corresponding turnover obtained with NNN pincer-Ni **4.45** (17,500 TON) (**4.29**, Table 4.5). This difference is attributed to the high thermal stability of **4.45** when compared to $NiCl_2$(DME) (Figure 4.3). High TONs with moderate yields of *N*-alkylated products (**4.29w** and **4.29x**, Table 4.5) were obtained when 2-pyridinemethanol and 4-pyridinemethanol were used as alkylating agents. The best turnovers and yields were obtained for a combination of 2-amino pyridine with either benzyl alcohol (**4.29o**, Table 4.5) or 4-methoxy benzyl alcohol (**4.29k**, Table 4.5). Even TONs of the cyclohexyl amine *N*-alkylated products increased from 300 (**4.29i**, Table 4.3) to 6,500 (**4.29i**, Table 4.5), when performed under lower catalyst loading (0.002 mol %) and higher temperature (200 °C).

Table 4.5: Solvent-free *N*-alkylation of amines at 200 °C[c]

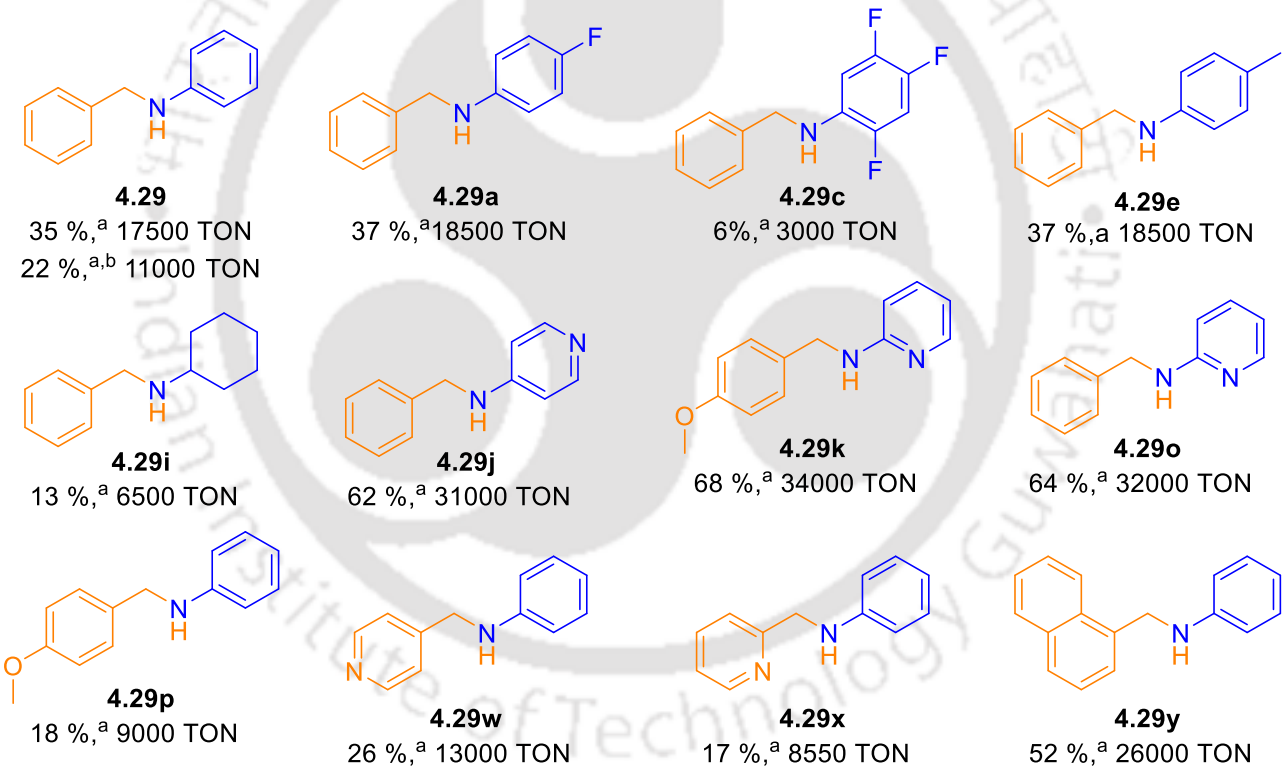

Table 4.5:[(a)]Yield determined from ^{1}H NMR using toluene as internal standard. [b)] Performed with 0.002 mol % of $NiCl_2$(DME). [c)] Reaction condition unless specified otherwise 4.8 mmol of **4.16a-z**, 4.8 mmol of **4.10a-z**, 3.6 mmol of NaO^tBu, and 0.1 µmol of **4.45** at 200 °C in sealed vessel.

4.3.3 Control experiments

To gain additional insight into coupling between benzyl alcohol and amine, mechanistic studies on the *N*-alkylation process was performed.

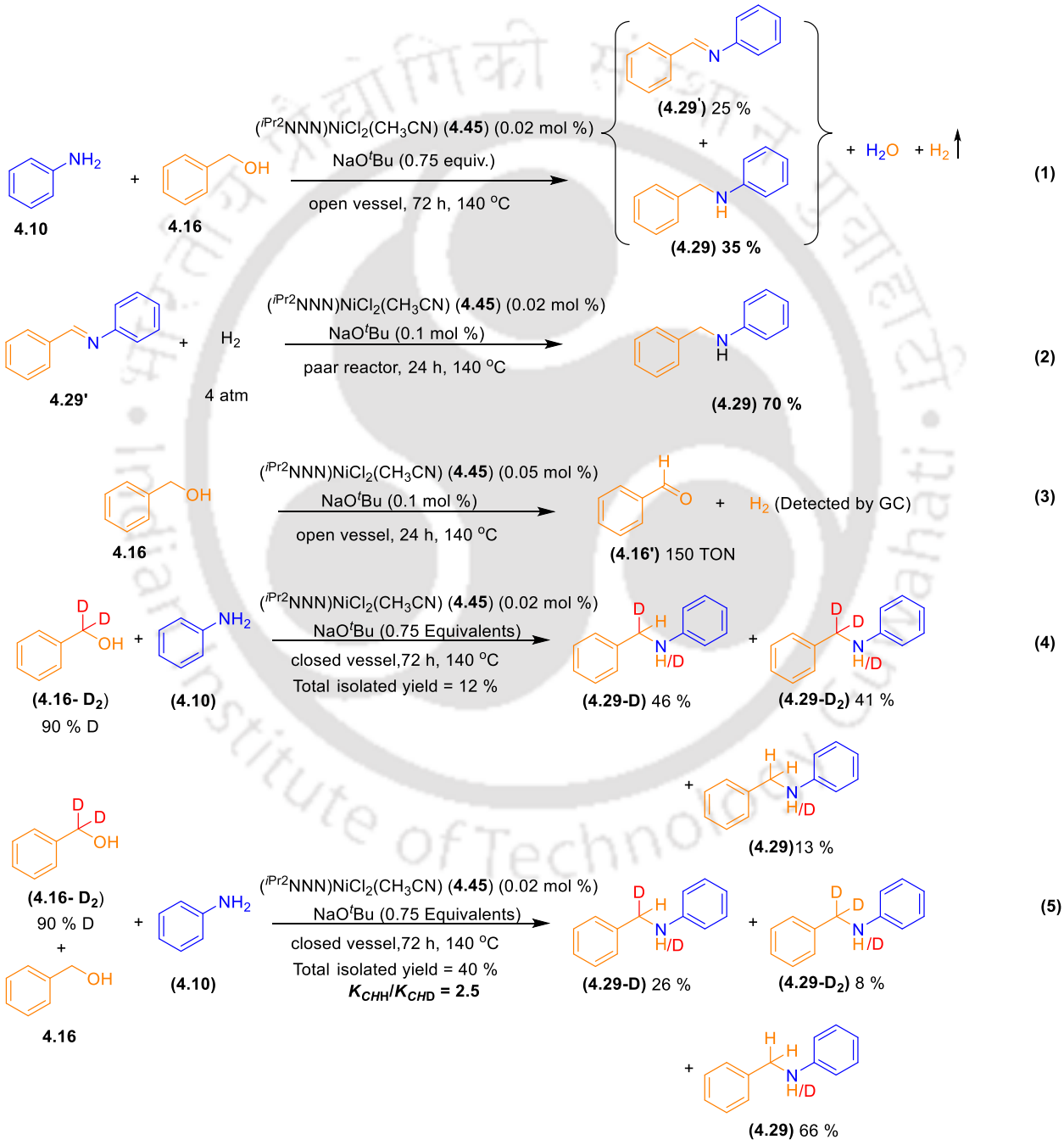

Scheme 4.27: Control experiments

The reaction of aniline **4.10** and benzyl alcohol **4.16** in the presence of catalytic amounts of NaO^{t}Bu (0.1 mol %) and **4.45** (0.02 mol %) in an open vessel lead to no reaction. It can be presumed that dehydrogenation of **4.16** is highly endothermic and the corresponding dehydrogenated product **4.16'** undergoes a facile reverse reaction rather than forming imine **4.29'** and water. To overcome this problem, the same reaction was performed in presence of 0.75 equivalents of NaO^{t}Bu under open vessel condition where the hydrogenated product *N*-benzyl aniline **4.29** (35 %) is obtained in addition to the expected **4.29'** (25 %) (Scheme 4.27, equation 1). The stoichiometric amount of base quenches water and pushes the equilibrium towards the forward direction. Stoichiometric amounts of base in reaction medium resulted in highly viscous reaction mixture, which consequently led to poor removal of H_2 and hence the formation of hydrogenated product **4.29** is observed even under open-vessel conditions.

On the other hand, under sealed-vessel conditions, hydrogenated product **4.29** is formed as a major product with only trace amounts (< 1%) of imine **4.29'** (Table 3.1). Additionally, under hydrogen atmosphere (4 atm) in a high-pressure reactor in presence of catalyst **4.45** (0.02 mol %), **4.29′** readily gets hydrogenated to *N*-benzyl amine **4.29** (Scheme 4.27, equation 2). When only benzyl alcohol was treated in presence of catalytic amount of base (0.1 mol % of NaO^{t}Bu) and 0.05 mol % of catalyst **4.45** at 140 ^{o}C for 24 h, benzaldehyde (150 TON) and benzyl benzoate (70 TON)[32, 47] were observed along with H_2 gas evolution (equation 3, Scheme 4.27, Figure 4.4).

From the previous discussions, it is already known that *N*-alkylation of benzyl alcohol and aniline in the presence of NaO^{t}Bu (0.075 equivalent) and **4.45** (0.02 mol %) in a closed vessel at 140 °C, resulted in the formation of **4.29** (Entry 7, Table 4.1, NMR yield = 43 % and isolated yield = 40 %). When this reaction was repeated with $C_6H_5CD_2OH$ (**4.16**-D_2) (90 % D), the products (**4.29-D**, **4.29-D$_2$**, **4.29**) were obtained in the ratio of 1.00:3.54:3.15 with an overall 29 % deuterium loss (equation 4, Scheme 4.27). The total isolated yield of *N*-alkylation of **2.16-D$_2$** is 12 % in comparison with **4.16**, which resulted in a 40 % isolated yield of **4.29**. Intermolecular competitive reactions between **4.16** and **4.16-D$_2$** with aniline in presence of NaO^{t}Bu (0.75 equivalent) and **4.45** (0.02 mol %) in a closed vessel at 140 °C lead to the formation of **4.29**, **4.29-D**, **4.29-D$_2$** in the ratio 8.25: 3.25: 1.00 (equation 5, Scheme 4.27). The ^{1}H NMR studies revealed k_{CHH}/k_{CHD} to be 2.5.[68-69, 72]

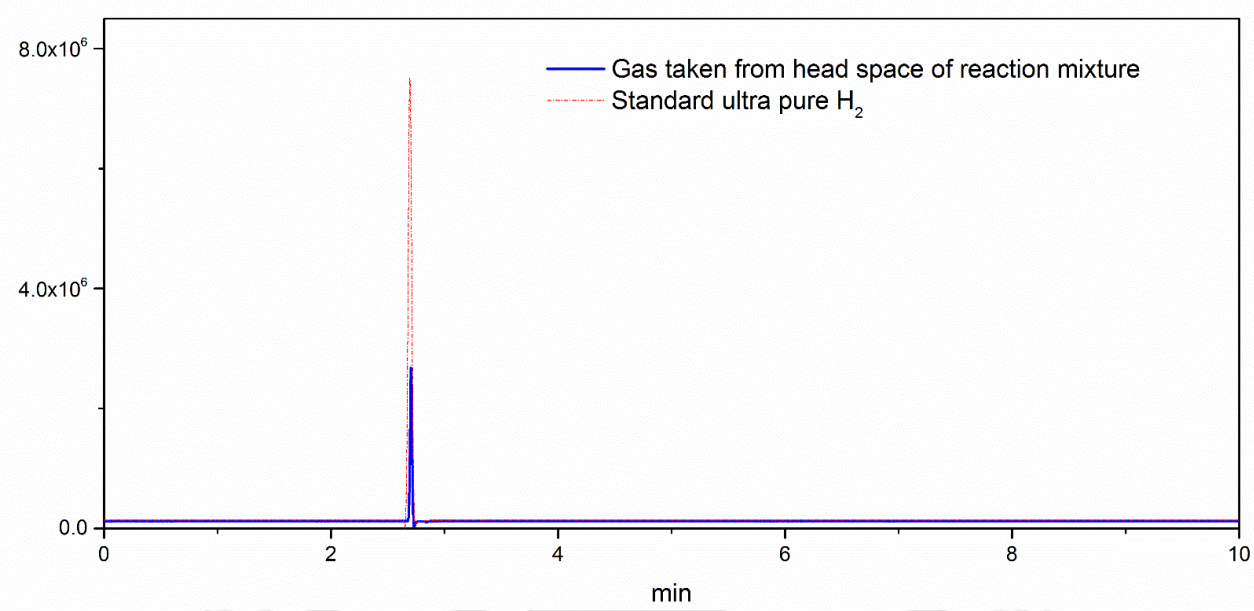

Figure 4.4: Evidence for H_2 evolution in the reaction of dehydrogenation of benzyl alcohol at 140 °C via GC analysis.

4.3.4 Mechanistic understanding

The plausible mechanism involved in *N*-alkylation is provided in Scheme 4.28. The first step in *N*-alkylation reaction involves the dissociation of acetonitrile from catalyst **4.45**. This is followed by the salt metathesis with $NaOCH_2Ph$ leading to the formation of **4.46**. For the sake of simplicity, the substitution of only one of two chlorides by benzyloxide in the transformation of complex **4.45** to **4.46** is represented. A *β*-hydride elimination from benzyloxide (OCH_2Ph) group in **4.46** results in the formation of Ni-hydride complex **4.48** along with the generation of benzaldehyde. The formation of Ni-hydride complex goes via TS **4.47**.

The hydride complex **4.48** can then readily react with another molecule of benzyl alcohol where it undergoes an σ-bond metathesis via TS **4.49** to regenerate **4.46** with the liberation of hydrogen molecule. This step completes the dehydrogenation cycle. An uncatalyzed reaction of benzaldehyde with aniline to give corresponding imine couples the dehydrogenation segment with the hydrogenation segment. In the hydrogenation segment, the first step involves the insertion of imine into the Ni-H bond in **4.48.** The insertion between Ni-hydride complex **4.48** and imine **4.29**'occurs through **TS 4.50** and results in the formation of complex **4.51**. The intermediate **4.51** then undergoes an σ-bond metathesis with H_2 via **TS 4.52** and extrudes the product *N*-benzyl amine with the regeneration of **4.48**.

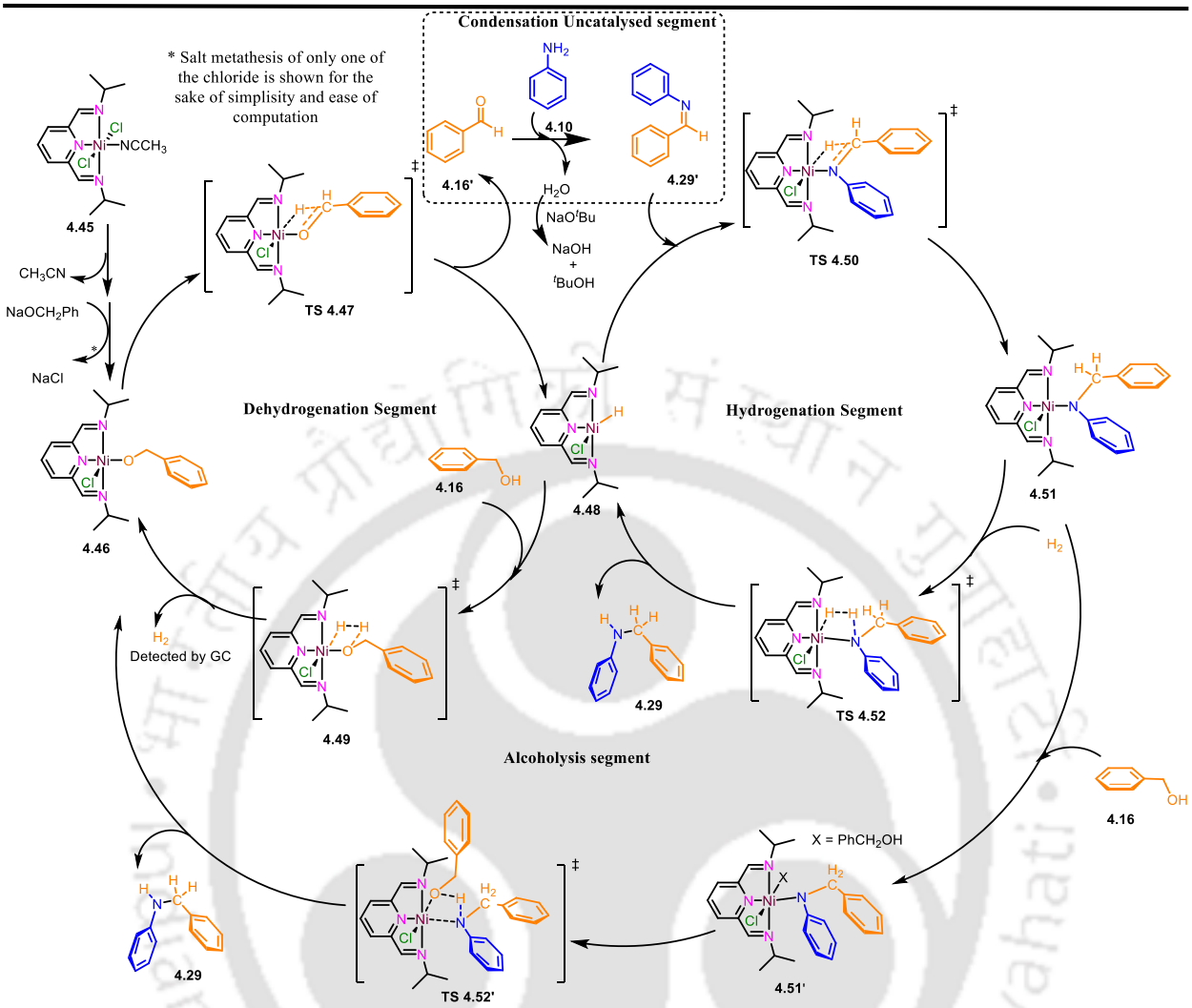

Scheme 4.28: Plausible mechanism involved in the ($^{i\text{Pr}2}$NNN)$NiCl_2(NCCH_3)$ catalyzed *N*-alkylation of amines

The *N*-alkylated amine could also form via an alternative path that involves alcoholysis without the requirement of H_2. In the alcoholysis segment, σ-bond metathesis occurs between Ni-N bond of **4.51'** and O-H bond of benzyl alcohol to yield the *N*-alkylated product. Notably here one would expect complete incorporation of deuterium in *N*-alkylated product upon use of deuteriated benzyl alcohol **4.16**-D_2. However, the observed overall 29 % deuterium loss, indicates a minor contribution from the hydrogenation segment.

At a higher catalyst loading (10 mol %) by keeping all other reaction conditions identical, the *N*-alkylation reaction was performed and the mixture was analyzed by HRMS (ESI). After 12 h of reaction at 140 °C, distinct peaks at m/z = 364.1815, m/z = 531.4092 and m/z = 712.4996 were observed which corresponds to [**4.45a**+H]$^+$, [**4.47a**+H+CH_3CN]$^+$, [**4.51a** +CH_3OH] (Figure 4.5).

HRMS also indicated the formation of imine **4.29'** (m/z = 182.0990) during the initial stages of the reaction. The formation of **4.45a** could possibly be attributed to the reaction of catalyst **4.45** with water formed during the uncatalyzed imine formation step of the reaction. In addition, it is likely that **4.47a** and **4.51a** are the resting species of the reaction (Figure 4.6-4.8; *vide infra*).

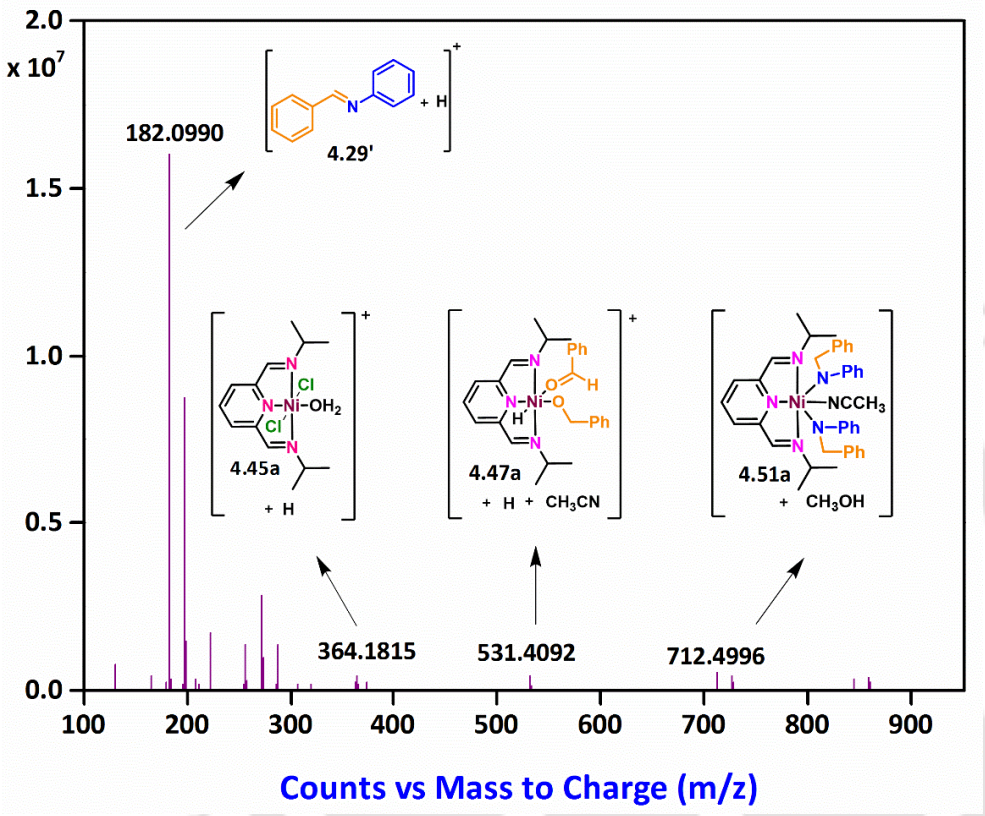

Figure 4.5: HRMS (ESI) plot of the reaction mixture obtained from the **4.45** (10 mol %) catalyzed reaction.

4.3.5 DFT studies

To understand the energetics of the various intermediates involved in the reaction, DFT studies were performed at the B3LYP/BSI level of theory. Both high spin and low spin states were optimized for all the complexes. Since the triplet state is lower in energy universally, it was selected for calculating the barrier.

The 20-electron Ni pincer catalyst (^{iPr2}NNN)NiCl$_2$(NCCH$_3$) **4.45**, will readily lose a molecule of acetonitrile to form either a 16-electron square-planar complex **4.46'** or an 18-electron trigonal-bipyramidal complex **4.46"** (Scheme 4.29). Generally, one might assume that formation of square planar complex **4.46'** would be much more favorable than trigonal bi-pyramidal complex **4.46"**. But, DFT calculations shows that the generation of 18-electron trigonal-bipyramidal complex

4.46'' is more exothermic by 23.16 kcal/mole compared to square planar complex **4.46'** (Scheme 4.29). Hence it can be assumed that, complex **4.46''** and the related trigonal-bipyramidal species are involved in the catalytic cycle rather than square-planar complexes analogous to **4.46'**.

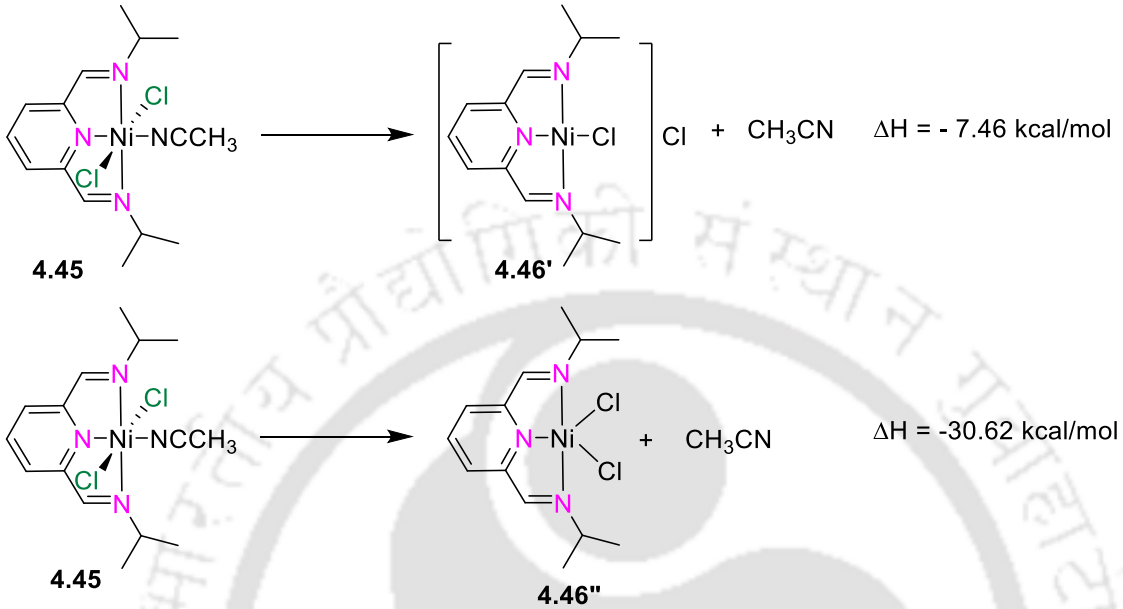

Scheme 4.29: Computed energetics for formation of trigonal bipyramidal and square planar complex

The free energies at 140 °C of various intermediates involved in the dehydrogenation segment and the corresponding hydrogenation segment (Scheme 4.28) are shown in Figure 4.6 and Figure 4.7 respectively. The *β*-hydride elimination from benzyloxide group in **4.46** and the associated extrusion of benzaldehyde to give **4.48** is computed to be thermodynamically uphill (ΔG_{140}= 7.66 kcal/mol) with a high barrier (**TS: 4.47**, $\Delta G^{\ddagger}_{140}$= 24.29 kcal/mol). The subsequent *σ*-bond metathesis is a downhill process (ΔG_{140}= - 13.35 kcal/mol) and proceeds with a lower barrier (**TS: 4.49**, $\Delta G^{\ddagger}_{140}$= 13.15 kcal/mol) (Figure 4.6).

The imine **4.29'** inserts into the Ni-H bond of **4.48** in a downhill process (ΔG_{140}= -11.73 kcal/mol) while crossing a barrier (**TS: 4.50**) of 31.34 kcal/mol (Figure 4.7). This is followed by a relatively uphill (ΔG_{140}= 5.75 kcal/mol) *σ*-bond metathesis of **4.51** with H_2 with a high energy barrier (**TS: 4.52**, $\Delta G^{\ddagger}_{140}$= 39.74 kcal/mol) (Figure 4.7). The alternative alcoholysis of **4.51** which involves initial coordination of benzyl alcohol **4.16** to Ni in **4.51** to yield **4.51'** is endothermic (ΔG_{140} = 11.30 kcal/mol). This is followed by *σ*-bond metathesis of Ni-N with O-H of **4.16** in **4.51'**, leading to product **4.29** with regeneration of **4.46**, which is exothermic (ΔG_{140} = -18.09 kcal/mol) and has a lower barrier (**TS: 4.52',** $\Delta G^{\ddagger}_{140}$ = 7.40 kcal/mol).

Alcoholysis (**4.51'→4.52'**, Figure 4.8) may not be the sole pathway to product (**4.29)** formation, though it has lower barrier than hydrogenation (**4.51→4.52**, Figure 4.7 and Figure 4.9). It should be noted that the lower barrier (**TS: 4.49**, $\Delta G^{\ddagger}_{140}$ = 13.15 kcal/mol) for the step **4.48→4.49** (Figure 4.6 and Figure 4.9) in comparison to the step **4.48→4.50** (Figure 4.7 and Figure 4.9) contributes to a significant amount of H_2 production. This corresponds to the fact that **4.51** can now react with either H_2 or **4.16**. Experimentally, it is observed that NNN-Ni pincer complex **4.45** can hydrogenate **4.29'** in presence of H_2 (equation 2, Scheme 4.27). In addition, deuterium loss (ca. 29%) is also observed in the *N*-alkylated product of reaction between **4.16-D$_2$** with **4.10** (equation 4, Scheme 4.27). All these observations indicate the evolution of H_2 and its reaction with **4.29'**.

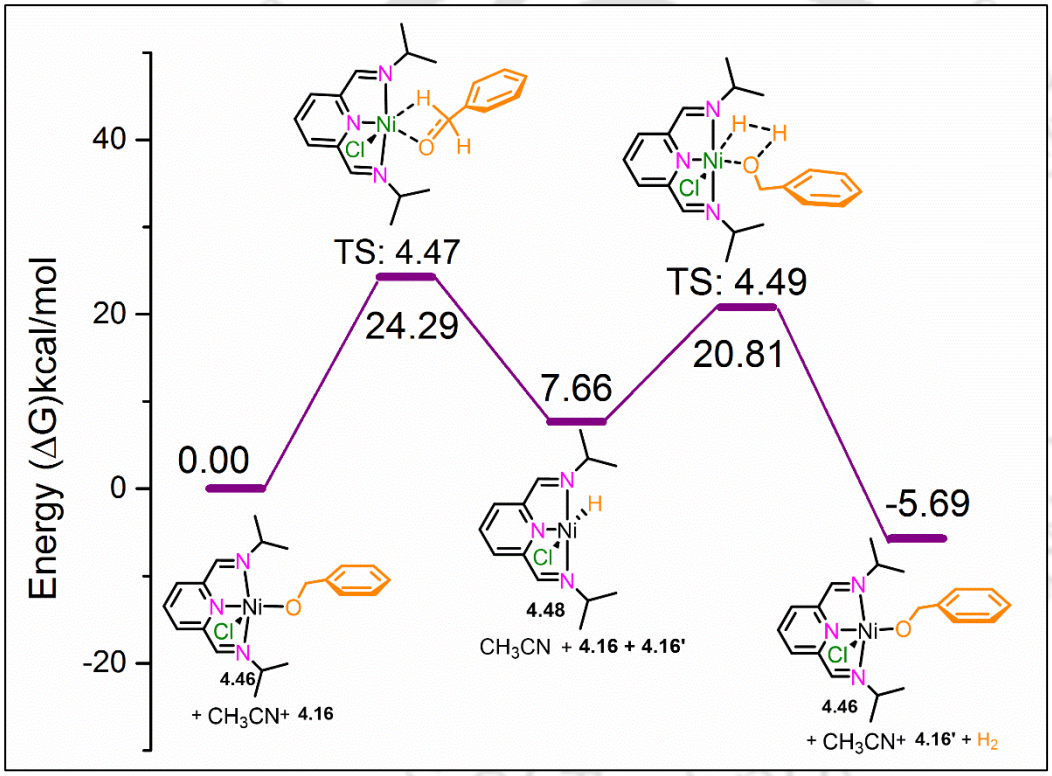

Figure 4.6: Relative free energies (140 °C) of intermediates involved in dehydrogenation of benzyl alcohol
DFT studies were carried out using B3LYP functional with SDD basis set for Ni and 6-311G(d) for all other atoms.

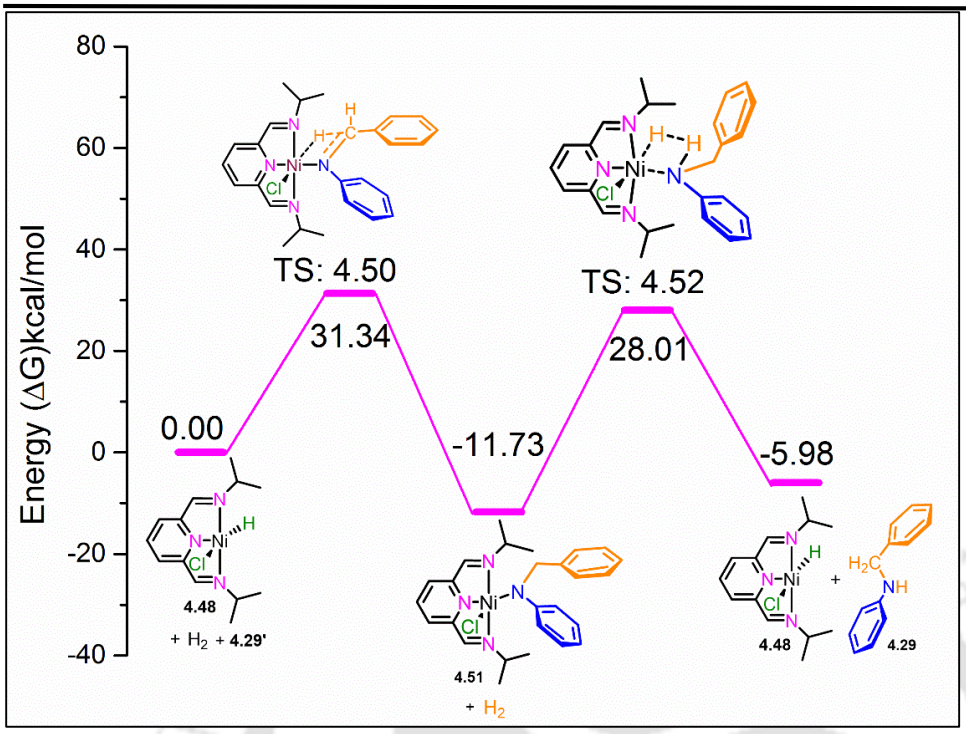

Figure 4.7: Free energy profile **4.45** catalyzed hydrogenation of aldimine
DFT studies were carried out using B3LYP functional with SDD basis set for Ni and 6-311G(d) for all other atoms.

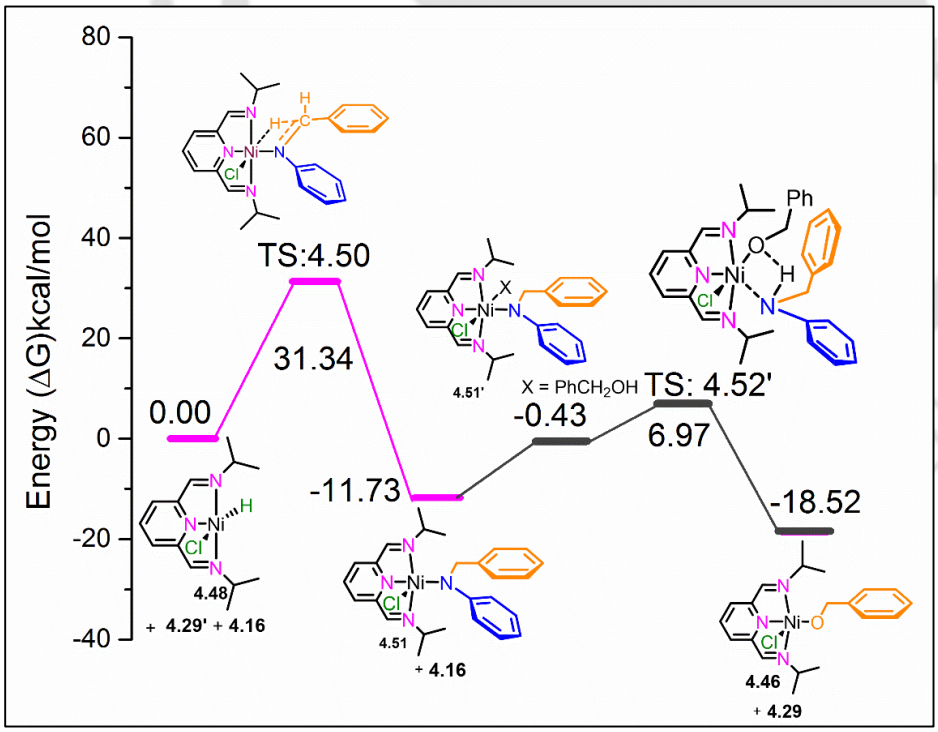

Figure 4.8: Free energy profile of the **4.45** catalyzed alcoholysis of aldimine **4.29**'
DFT studies were carried out using B3LYP functional with SDD basis set for Ni and 6-311G(d) for all other atoms.

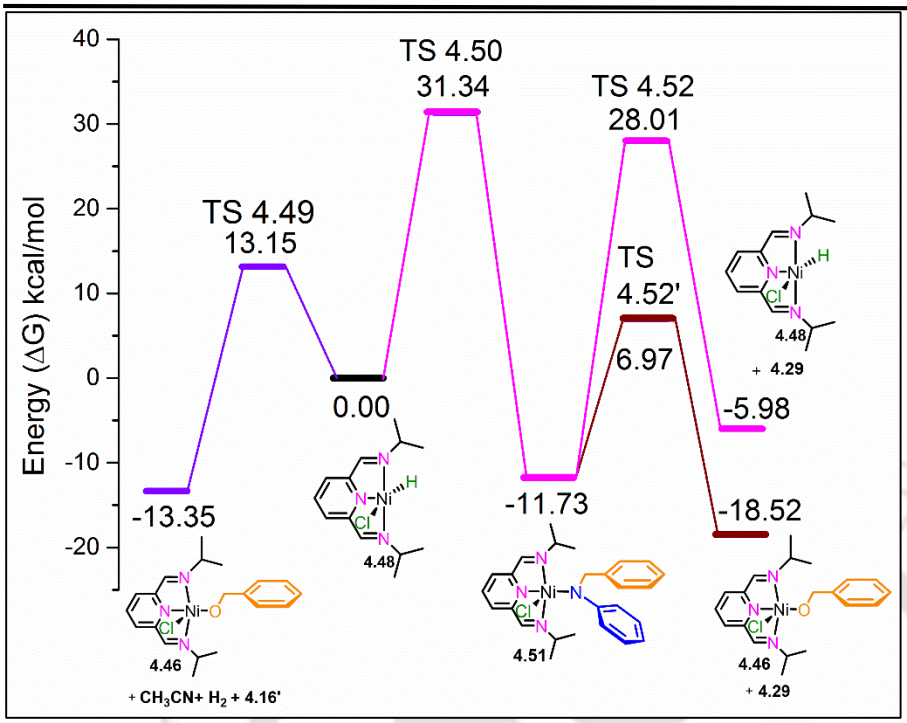

Figure 4.9: Comparison of free energies of species involved in various paths that are available for **4.48** and **4.51**. DFT studies were carried out using B3LYP functional with SDD basis set for Ni and 6-311G(d) for other atoms.

Computational studies indicate the lower barrier for alcoholysis (Figure 4.8 and Figure 4.9). These observations open up a possibility of the existence of both pathways (alcoholysis and hydrogenation) leading to formation of **4.29**. This bodes well for the formation of **4.29** under open-vessel conditions (equation 1, Scheme 4.27), which may now be attributed to not only poor H_2 removal but also an alternative alcoholysis path.

The *β*-hydride elimination is the rate-determining step (RDS) for dehydrogenation with **4.46** as the resting state. On the other hand, either for hydrogenation having a rate-determining *σ*-bond metathesis of **4.51** with H_2 or for alcoholysis with a rate-determining imine insertion step, **4.51** appears to be the resting state. This is in agreement with the HRMS (ESI) analysis (*vide supra*), where derivatives of both **4.46** and **4.51**are observed. As both the *β*-hydride elimination and imine insertion steps required for breaking and/or for forming of a C−H bond, further support of the claim of these two steps being rate determining is obtained from labeling studies that have been performed with use of **4.16- D_2**, where the k_{CHH}/k_{CHD} value of about 2.5 is obtained.

4.4 Introduction to the synthesis of benzimidazoles via dehydrogenative coupling

N-containing heterocyclic compounds are essential building blocks of numerous natural products such as α-amino acids, proteins, purines and biotin.[82] Besides this, they also find applications in organic or polymeric materials, optical brighteners for coating and thermally stable membranes for fuel cells.[83] In particular, benzimidazole derivatives are medicinally important bioactive scaffolds, having miscellaneous applications including anti-cancer, anti-viral, anti-bacterial, anti-tumor, anti-HIV, and related anti-fungal medicines (Figure 4.10).[84]

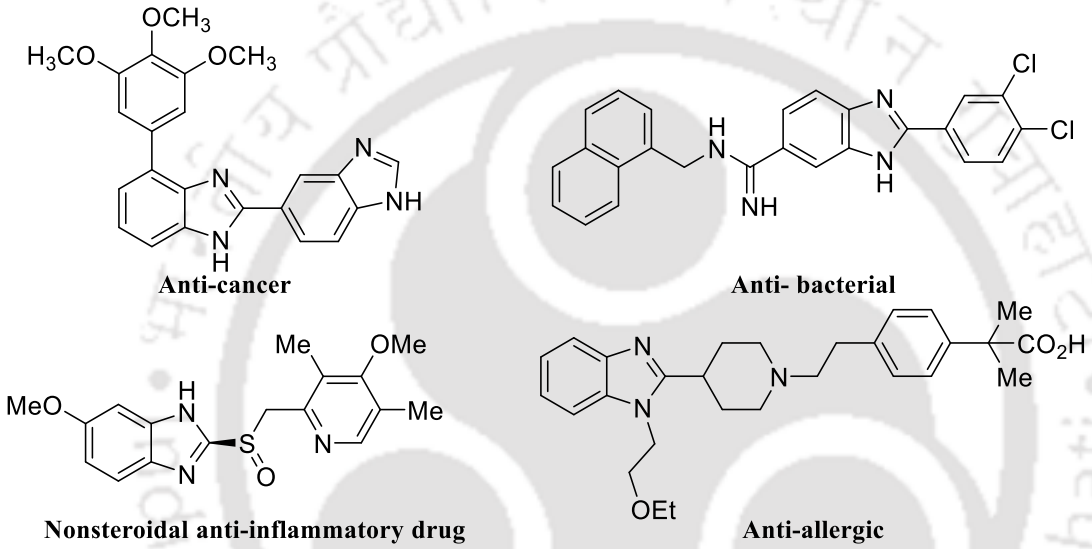

Figure 4.10: Drugs containing benzimidazole moiety

It is noteworthy that benzimidazole derivatives are important scaffolds and there are several synthetic strategies to generate this structure (Figure 4.11).[85-102]

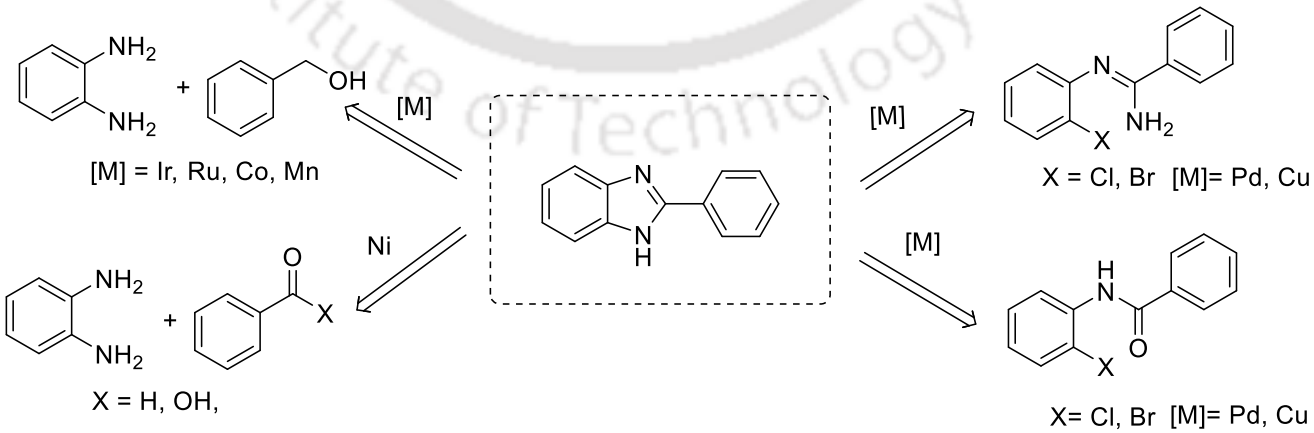

Figure 4.11: A few reported methods for benzimidazole synthesis

Intramolecular aryl-amination/cyclization is a one-step process to synthesize benzimidazoles. However, here along with the desired product, stoichiometric amounts of halide waste would be generated. In 2002, the Brain group developed a novel synthetic strategy to benzimidazoles via an palladium-catalyzed intramolecular *N*-arylation reaction starting from a (*o*-bromo-phenyl)amidine precursor (Scheme 4.30).[85]

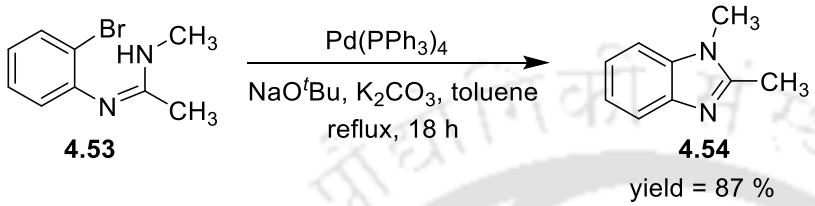

Scheme 4.30: Pd(0) catalyzed synthesis of benzimidazoles starting from amidines[85]

In 2009, Wang and co-workers developed a three component reaction for the synthesis of functionalized benzimidazoles by using *p*-toluene sulfonylazide, terminal alkynes and amino anilines (Scheme 4.31).[86] CuI undergoes oxidative addition with alkyne and azide **4.57** (Scheme 4.31) which is followed by nucleophilic addition of benzene-1,2-diamine to generate corresponding *N*-sulfonylamidine. Further intramolecular cyclization produces substituted benzimidazoles.[86]

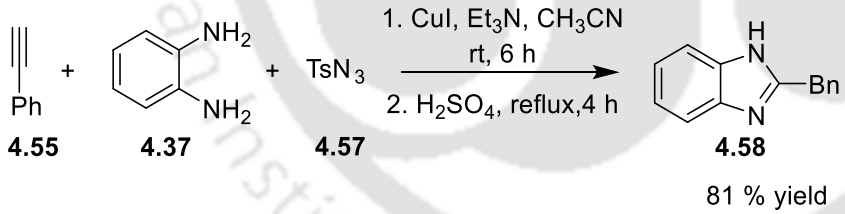

Scheme 4.31: The copper mediated three component cascade reaction to synthesize benzimidazoles[86]

One of the classical methods to synthesize 1,2-disubstituted benzimidazoles is the condensation reaction between 1,2-diaminoarene with benzaldehyde or its derivatives. Other than metal complexes several other mild reagents such as poly (*N*,*N*–dibromo-*N*-ethyl benzene-1,3-disulfonamide) (PBBS) or *N*,*N*,*N*,*N*-tetrabromobenzene-1,3-disulfonamide (TBBDA),[87] L-proline,[88] and $SiO_2/ZnCl_2$ (Scheme 4.32),[89] can be used to catalyze this reaction.

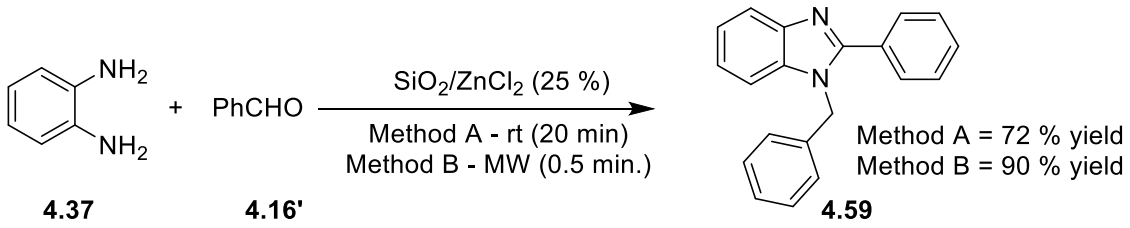

Scheme 4.32: Synthesis of 1, 2 disubstituted benzimidazoles catalyzed by $SiO_2/ZnCl_2$[89]

In 2009, Dang *et al.* generated phosphoric acid-containing benzimidazole moiety starting from 3-nitro-1,2-phenylene diamine and aldehyde as starting materials. The cyclization between these two reactants was catalyzed by using a combination of $FeCl_3/SiO_2$ (Scheme 4.33).[90]

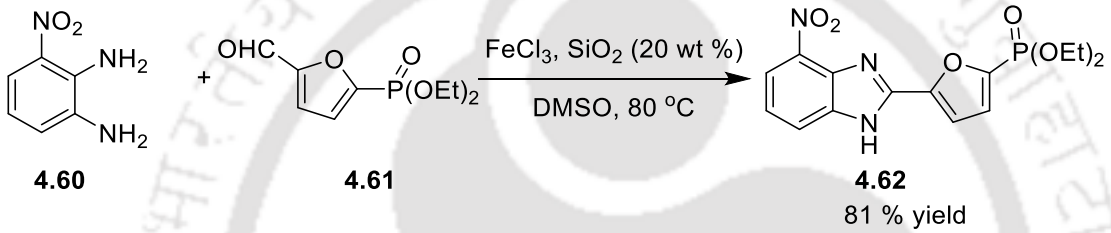

Scheme 4.33: Synthesis of phosphoric acid containing benzimidazoles[90]

Classical methods for the synthesis of functionalized benzimidazoles either generate stoichiometric amount of waste (because of the substrate leaving group or additive)[91-93] or are catalyzed by precious noble metal-based (Ir, Ru) catalyst[94-97]. Acceptorless dehydrogenative coupling (ADC) for the benzimidazole synthesis using highly abundant, less toxic and inexpensive base metal catalyst is a challenging task. This synthetic methodology attracts significant attention not only for avoiding multistep synthesis but also for being atom-economical. Dehydrogenative coupling between primary alcohols and derivatives of 1, 2-phenylenediamine is a useful synthetic pathway for benzimidazole formation, since here the only byproducts are stoichiometric amounts of water and two equivalents of valuable molecular hydrogen. In 2014, Kempe group reported that Ir catalyzed the benzimidazole synthesis via acceptorless dehydrogenative coupling of 1,2-benzene-diamines and aliphatic alcohols.[97] Here, KO^{t}Bu is needed for accelerating the oxidation step of alcohol. This dehydrogenative coupling is catalyzed by an Ir complex **4.64** which is stabilized by tridentate PNP pincer ligand (Scheme 4.34).

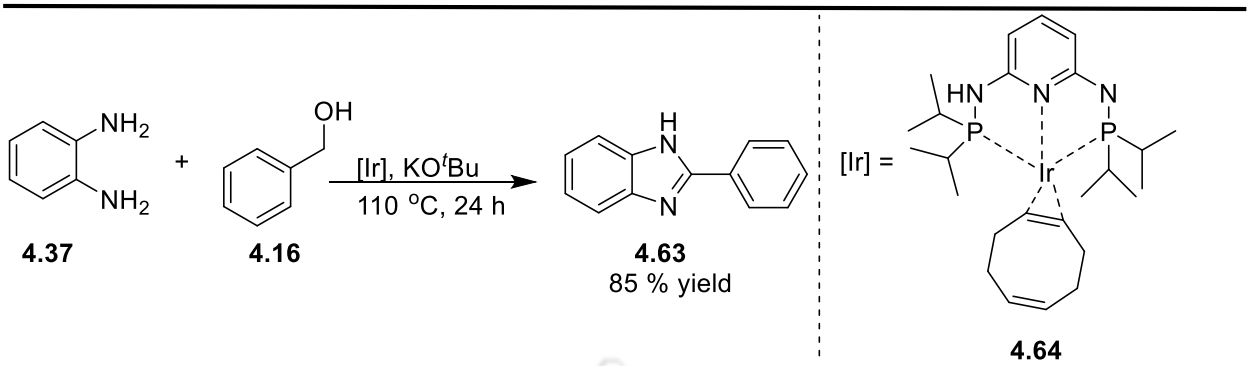

Scheme 4.34: Benzimidazole synthesis catalyzed by an PNP pincer-Ir complex[97]

In the same year, synthesis of benzimidazole was carried out by Ramachandran *et al*. in the presence of Ru(II) carbonyl complex **4.65** with phosphine functionalized PNS type thiosemicarbazone ligand (Scheme 4.35).[98] They also have shown the versatile catalytic activity of Ru(II) pincer towards both *N*-alkylation.

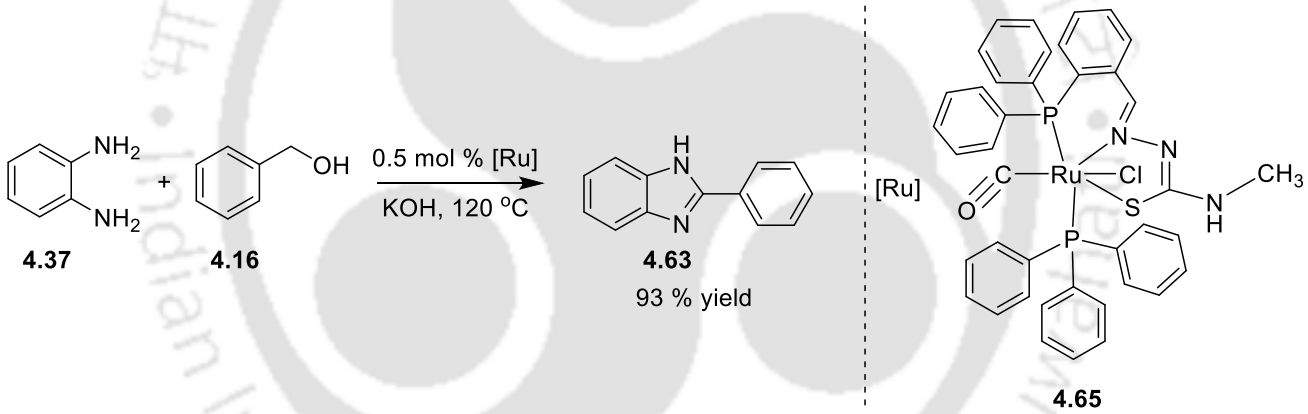

Scheme 4.35: Pincer-Ru(II) catalyzed benzimidazole synthesis[98]

In recent years, considerable efforts have been made towards the development of several different dehydrogenative reaction methodologies using first row transition metal complexes. Apart from precious transition metals such as Ir[97] and Ru[98], very recently non-toxic and earth-abundant Co[99] and Mn[100] have been revealed to act as a good catalysts for dehydrogenative coupling reactions.

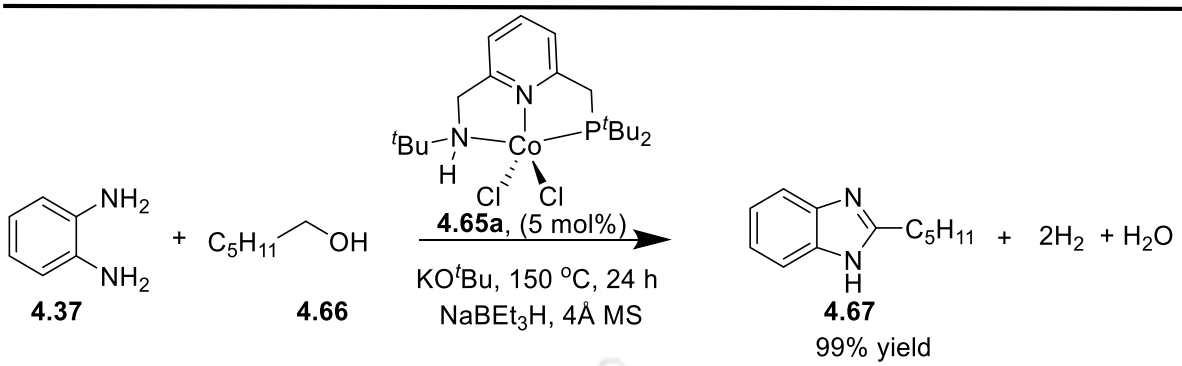

Scheme 4.36: Synthesis of functionalized benzimidazoles that are catalyzed by a PNN pincer-Co.[99]

In 2017, the Milstein group demonstrated the use of pincer-Co complex **4.65a** (5 mol %) to accomplish the dehydrogenative coupling between *ortho*-phenylene diamines and hexane-1-ol with TON up to 20 in presence of stoichiometric amount of KO^{t}Bu (Scheme 4.36).[99]

Very recently, in 2019, the Banerjee group demonstrated the use of $NiBr_2$ (2.5 mol %) in combination with 1,10 phenanthroline (3 mol %) to accomplish the synthesis of 1,2-disubstituted benzimidazoles in 91 % isolated yield in the presence of stoichiometric amount of KO^{t}Bu (Scheme 4.37).[101]

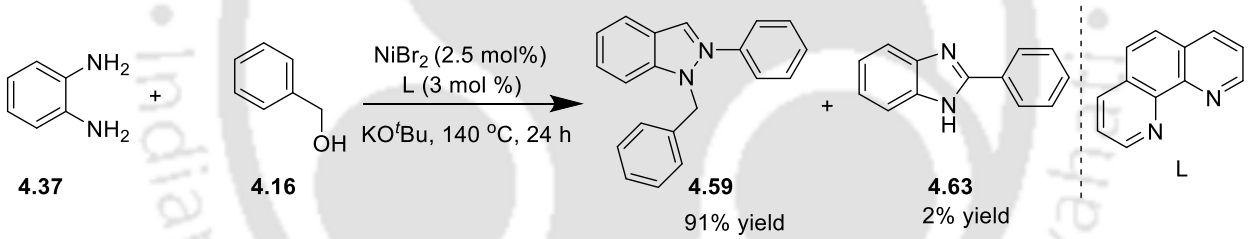

Scheme 4.37: Synthesis of 1,2-disubstituted benzimidazoles that is catalyzed by a combination of $NiBr_2$ and 1, 10-phenanthroline[101]

In 2019, Pathak and co-workers have demonstrated the use of pincer-nickel complexes for the synthesis of benzimidazoles using benzaldehydes and benzene diamines as precursors.[102] The NNN-Ni complex **4.45** reported in this chapter, efficiently catalyzes the dehydrogenation of benzyl alcohol to benzaldehyde. Hence, it would be interesting to see if **4.45** can be used to accomplish the synthesis of benzimidazole starting from benzyl alcohols rather than benzaldehyde.

4.5 Synthesis of benzimidazoles via dehydrogenative coupling catalyzed by ($^{i\text{Pr}2}$NNN)NiCl$_2$(NCCH$_3$)

To establish the synthetic potential of the pincer Ni system ($^{i\text{Pr}2}$NNN)NiCl$_2$(NCCH$_3$) **4.45** towards catalytic dehydogenative coupling as an alternative synthetic route to 2-phenyl-1*H*-

benzo[*d*]imidazole, the cyclization of 1,2-benzene diamine with benzyl alcohol was attempted under open vessel conditions (Scheme 4.38).

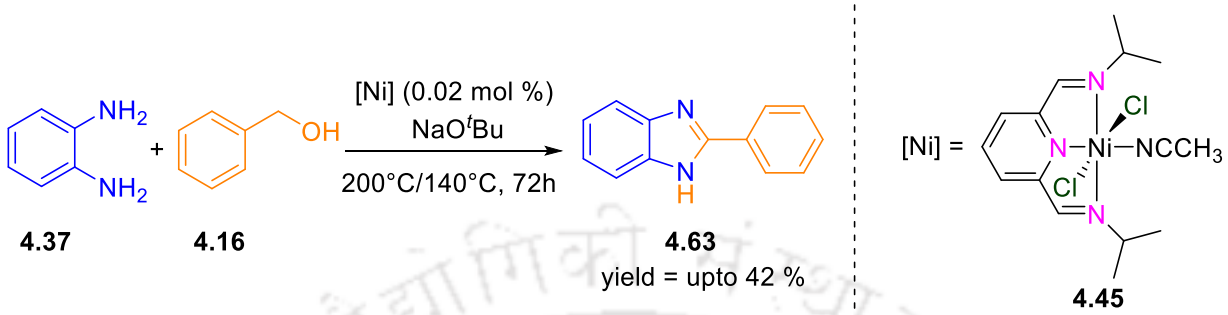

Scheme 4.38: Benzimidazole synthesis via dehydrogenative coupling catalyzed by (^{iPr2}NNN)NiCl$_2$(NCCH$_3$)

4.5.1 Optimization of the catalytic protocol

Table 4.6: Solvent-free benzimidazole synthesis catalyzed by **4.45** (0.02 mol %) under varying conditions.

Entry	Temperature	Base (loading)	Isolated yield
1.	200 °C	NaO^{t}Bu (0.75 equiv.)	35 %
2.	200 °C	NaO^{t}Bu (0.1 mol %.)	42 %
3.	140 °C	NaO^{t}Bu (0.1 mol %.)	10 %

Reaction condition: benzyl alcohol (4.8 mmol), 1, 2-benzene di-amine (4.8 mmol) at 200 °C in open vessel.

To generate the active Ni species, the use of minimal amount base (0.01 mol % of NaO^{t}Bu) was sufficient. It is observed that by use of (^{iPr2}NNN)NiCl$_2$(NCCH$_3$) catalyst **4.45** (0.02 mol %) without any solvent, in an open vessel, resulted in the formation of 2-phenyl-1H-benzo[d]imidazole (Entry 2, Table 4.6) with 42 % isolated yield at 200 °C after 72 h. Lowering the temperature to 140 °C resulted in a yield drop to 10 % (Entry 3 in Table 4.6).

4.5.2 Dehydrogenative coupling of 1,2-benzene diamine with various aromatic alcohols

Upon use of various functionalized aromatic alcohols, moderate yields of benzimidazoles were obtained with high turnovers in most of the cases. Alcohols based on five-membered heterocycles such as furfuryl alcohol (**4.63c**), thiophenyl alcohol (**4.63d**) gave the corresponding *N*-heterocyclic product with 4% and 6% yield respectively.

Table 4.7: The **4.45** catalyzed synthesis of various benzimidazoles at 200 °C

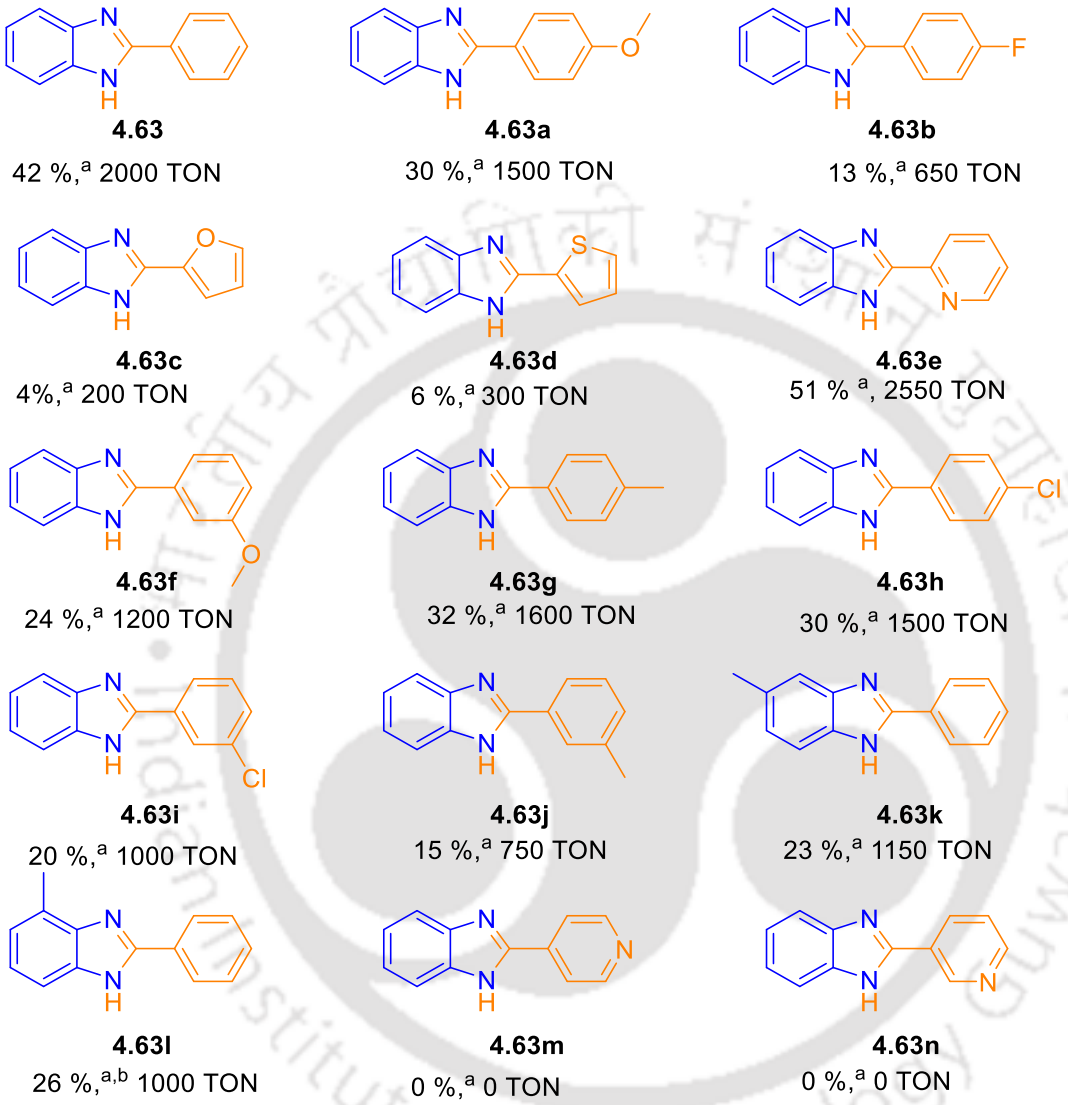

Reaction conditions: 4.6 mmol of **4.37a-z**, 4.6 mmol of **4.16a-z**, 4.62 µmol of NaO^{t}Bu and 0.9 µmol of **4.45** at 200 °C in an open vessel. [(a)]Isolated yield. [(b)]Mixture of isomers.

Dehydrogenative coupling reaction with six-membered heterocyclic compounds such as pyridine 4-methanol, pyridine 3-methanol (**4.63m** and **4.63n**, Table 4.7) did not lead to corresponding products. Alcohols with electron-withdrawing *p*-fluoro (**4.63b**) and with substituents at the *meta* positions such as 3-OMe (**4.63f**), 3-Cl (**4.63i**), 3-Me (**4.63j**, Table 4.7) gave slightly lower turnovers. Substituted diamines resulted in mixture of isomers (**4.63k** and **4.63l**, Table 4.7). The

highest TON (2550) is achieved for the dehydrogenative coupling of 1,2-benzene diamine with pyridine 2-methanol (**4.63e**, Table 4.7).

4.6 Conclusion

In one of the first reports, NNN pincer-nickel complex ($^{i\text{Pr}2}$NNN)$NiCl_2(NCCH_3)$ has been utilized as an efficient catalyst for the benign formation of C–N bonds. The pincer-nickel complex ($^{i\text{Pr}2}$NNN)$NiCl_2(NCCH_3)$ is highly thermally stable and proved to be versatile for both dehydrogenative coupling and hydrogen-transfer reactions at temperatures as high as 200 °C. The alkylation of various amines utilizing a variety of alcohols has been successfully catalyzed by ($^{i\text{Pr}2}$NNN)$NiCl_2(NCCH_3)$ in moderate yields (35% - 60%) but with good turnovers. Operating at lower catalyst loading (0.002 mol %) and elevated temperatures (200 °C) gave very high turnovers with the best results (ca. 68% yield and 34000 TON) obtained for a combination of 2-amino pyridine with 4-methoxy benzyl alcohol. It is also observed that ($^{i\text{Pr}2}$NNN)$NiCl_2(NCCH_3)$ efficiently catalyzes the dehydrogenative coupling of benzene-1,2-diamines with alcohols to yield benzimidazoles.

Quantum mechanical calculations provide valuable information on the operative mechanism. At 140 °C, the overall change in free energy for dehydrogenation is computed to be downhill with *β*-hydride elimination as the RDS. For the corresponding hydrogenation segment, the free energy change is also favorable but with *σ*-bond metathesis as the RDS. DFT studies are also in favor of the alcoholysis step for the formation of an *N*-alkylated product where the imine insertion appears to be the RDS. Control experiments are complementary to DFT calculations and provide strong evidence for the involvement of both hydrogenation and alcoholysis. The respective resting states of all the individual RDS have been identified by HRMS analysis. Labeling studies are in agreement with the DFT analysis and show the involvement of a benzylic C−H bond in the RDS. This is one of the first reports on the use of a pincer-nickel system for the *N*-alkylation of amines. This offers exciting opportunities for the design and development of pincer-Ni complexes for dehydrogenation and related reactions.

4.7 Experimental section

General procedure and materials

All manipulations were carried out under purified Ar using a standard double manifold. The nickel precursor, $NiCl_2$ was purchased from Sigma-Aldrich. Benzyl alcohol and aniline were purchased from MERCK and were dried according to literature procedure prior to experiment. Other chemicals were purchased from Sigma-Aldrich and used as such. All catalytic reactions were carried out with air and/or under argon atmosphere using dried glassware. The Pincer complex **4.45** was synthesized according to the literature procedure.[76, 77]

Physical measurements

^1H, $^{13}C(H)$and ^{19}F NMR were recorded either on a Bruker ASCEND 600 operating at 600 MHz for ^1H, 150 MHz for $^{13}C(H)$, and 565 MHz for ^{19}F or on a Bruker AVANCE 400 operating at 400 MHz for ^1H, 100 MHz for $^{13}C(H)$, 376 MHz for ^{19}F. Chemical shifts (δ) are reported in ppm, spin−spin coupling constant (J) are expressed in Hz, and other data are reported as follows: s = singlet, d = doublet, t = triplet, m = multiplet, q = quartet, and br s = broad singlet. HRMS measurements were done using an Agilent Accurate-Mass Q-TOF ESI–MS 6520. GC analysis (TCD detection) was performed on a Agilent 7820-GC instrument fitted with Agilent Front SS7 inlet N_2 HP5 column (30 m length x 0.32 mm ID) using the following method: Agilent 7820-GC Detector, Oven temperature 70 °C, Time at starting temp: 0 min, Hold time = 10 min, Flow rate (carrier): 5 mL/min (N_2), Split ratio: 50, Inlet temperature: 70 °C, Detector temperature: 250 °C.

General procedure for the pincer-nickel catalyzed *N*-alkylation of amine with alcohol.

To a 5 ml high pressure sealable Schlenk flask containing benzyl alcohol **4.16** (0.5 ml, 4.8 mmol), 0.75 equivalents of NaO^tBu (0.345 g, 3.6 mmol) was added under Ar atmosphere. The flask was closed and the contents were solubilized. The mixture was cooled to room temperature and to the resulting white slurry, aniline **4.10** (0.44 ml, 4.8 mmol) and $^{iPr2}NNNNiCl_2(NCCH_3)$ (0.3 mg, 0.7 µmol) were added respectively. The reaction mixture was heated at 200 ^oC for 72 hours. The reaction mixture was then cooled to room temperature followed by addition of toluene (100 µL) as an internal standard. An aliquot (21 mg) was withdrawn from the reaction mixture and NMR yield was determined by ^1H NMR using $CDCl_3$ (0.5 ml) as solvent. The rest of reaction mixture

was quenched with water followed by extraction of organic fraction with dichloromethane. The organic phase was separated and was dried over anhydrous Na_2SO_4. The solvent was removed from organic fraction under reduced pressure. Carrying out column chromatography using hexane-ethyl acetate mixture (0% - 5 %) as eluent gave product **4.29** in the pure form. The isolated product was characterized by NMR spectroscopy.

General procedure for the Pincer- Nickel catalyzed benzimidazole by dehydrogenation of amine with alcohol.

A mixture of 1, 2-diaminobenzene **4.37** (0.50 g, 4.62 mmol), benzyl alcohol **4.16** (0.48 ml, 4.62 mmol), NaO^{t}Bu (0.4 g), and **4.45** (0.9µmol) was stirred under neat condition at 200 °C for 20 h in open vessel under Ar atmosphere. After cooling, MeOH was added to dilute the mixture and filtered. The filtrate was concentrated under reduced pressure, and the residue was purified by silica gel column chromatography using 10% - 30% ethyl acetate in hexane as an eluent to get the benzimidazole derivative in the pure form.

Computational details

All the considered molecules were fully optimized using the Gussian 09 D.01 program package.[103] The B3LYP/BSI level of DFT was used for all the calculations (BSI is defined here as a basis set combination of SDD[104] for nickel atoms and 6-311G(d) for all other atoms). The level of calculation was selected on the basis of a previous report on Ni complexes.[105] Frequency calculations were also carried out to differentiate minima structures or transition states on the potential energy surface. Transition-state structures were further validated by following the reaction path using intrinsic reaction coordinate (IRC) calculations wherever necessary.[106] ΔG values were estimated by using the sum of electronic and thermal free energies. These values were computed at 140 °C to meet the experimental conditions.

N-benzylaniline (**4.29**)

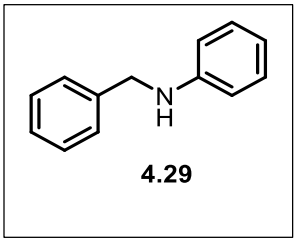

4.29

Yellow liquid (isolated yield = 42 %). ^{1}H NMR (400 MHz, $CDCl_3$) δ 7.44 – 7.35 (m, 4H), 7.31 (dd, J = 9.4, 4.3 Hz, 1H), 7.21 (t, J = 7.9 Hz, 2H), 6.75 (t, J = 7.3 Hz, 1H), 6.67 (d, J = 7.7 Hz, 2H), 4.36 (s, 2H), 4.05 (s, 1H). ^{13}C NMR (151 MHz, $CDCl_3$) δ 148.29, 139.57, 129.39, 128.76, 127.63, 127.35, 117.69, 112.97, 77.16, 48.45. HRMS (ESI): $[M+H]^+$calculated 184.1048, found 184.1151.

N-benzyl-4-fluoroaniline (**4.29a**)

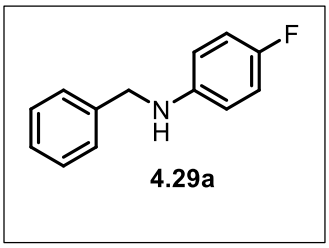

4.29a

Yellow liquid (isolated yield = 44 %) ^{1}H NMR (600 MHz, $CDCl_3$) δ 7.42 (d, J = 4.9 Hz, 4H), 7.35 (d, J = 5.2 Hz, 1H), 6.95 (t, J = 9.5 Hz, 2H), 6.61 (d, J = 12.5 Hz, 2H), 4.33 (s, 2H). ^{13}C NMR (151 MHz, $CDCl_3$) δ 156.72, 155.17, 144.58, 139.35, 128.77, 127.58, 127.41, 115.83, 115.69, 113.75, 113.70, 48.95. ^{19}F NMR (565 MHz, $CDCl_3$) δ -127.80.HRMS (ESI): $[M+H]^+$ calculated 202.2444, found 202.1081

N-benzyl-2,4,5-trifluoroaniline (**4.29c**)

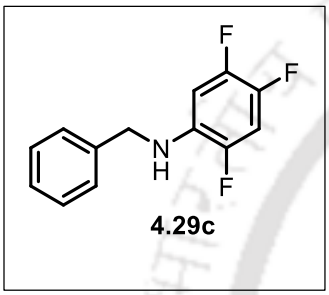

4.29c

Yellow liquid (isolated yield = 13 %) ^{1}H NMR (400 MHz, $CDCl_3$) δ 7.30 – 7.24 (m, 4H), 7.17 (s, 1H), 6.78 (td, J = 10.4, 7.2 Hz, 1H), 6.35 (dt, J = 12.1, 7.9 Hz, 1H), 4.22 (s, 2H). ^{13}C NMR (151 MHz, $CDCl_3$) δ 138.03, 128.86, 128.43, 127.67, 127.34, 104.81, 104.70, 104.55, 100.80, 100.71, 100.55, 100.52, 48.05. ^{19}F NMR (377 MHz, $CDCl_3$) δ -138.72 , -142.45 – -142.58 (m), -151.11.

N-benzyl-4-methoxyaniline (**4.29d**)

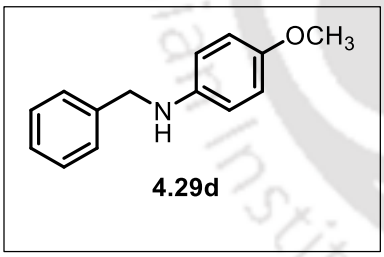

4.29d

^{1}H NMR (400 MHz, $CDCl_3$) δ 7.38 (t, *J* = 5.2 Hz, 4H), 7.29 (d, *J* = 6.9 Hz, 1H), 6.79 (d, *J* = 8.9 Hz, 2H), 6.62 (d, *J* = 8.9 Hz, 2H), 4.29 (s, 2H), 3.75 (s, 3H).^{1}H NMR (400 MHz, $CDCl_3$)δ 7.38 (t, *J* = 5.2 Hz, 4H), 7.29 (d, *J* = 6.9 Hz, 1H), 6.79 (d, *J* = 8.9 Hz, 2H), 6.62 (d, *J* = 8.9 Hz, 2H), 4.29 (s, 2H), 3.75 (s, 3H). HRMS (ESI): $[M+H]^+$calculated 214.1154, found 214.1285.

N-benzyl-4-methylaniline (**4.29e**)

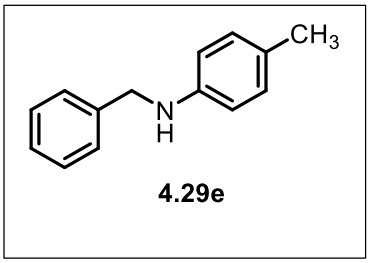

4.29e

^{1}H NMR (400 MHz, $CDCl_3$) δ 7.31 – 7.13 (m, 5H), 6.89 (d, J = 8.0 Hz, 2H), 6.46 (d, J = 8.2 Hz, 2H), 4.20 (s, 2H), 2.14 (s, 3H). ^{13}C NMR (151 MHz, $CDCl_3$) δ 145.94, 139.68, 129.78, 128.63, 127.53, 127.18, 126.77, 113.02, 48.66, 20.45. HRMS (ESI): $[M+H]^+$calculated 198.1204, found = 198.1299.

N-(4-methoxybenzyl)aniline (**4.29p**)

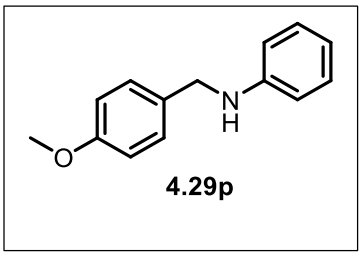

^{1}H NMR (600 MHz, $CDCl_3$) δ 7.35 (d, *J* = 8.6 Hz, 2H), 7.25 (s, 2H), 6.95 (d, *J* = 8.4 Hz, 2H), 6.81 – 6.77 (m, 1H), 6.69 (d, *J* = 7.9 Hz, 2H), 4.30 (s, 2H), 3.85 (s, 3H). ^{13}C NMR (151 MHz, $CDCl_3$) δ 158.86, 148.25, 131.45, 129.31, 128.86, 117.52, 114.05, 112.88, 55.33, 47.80. HRMS (ESI): $[M+H]^+$ calculated 214.1154, found 214.1247.

N,*N*′-(pyridine-2,6-diylbis(methylene))dianiline (**4.29m**)

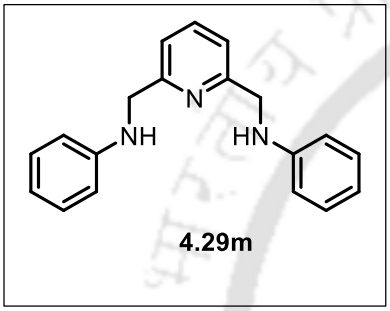

^{1}H NMR (600 MHz, $CDCl_3$) δ 7.60 (t, J = 7.7 Hz, 1H), 7.25 – 7.17 (m, 6H), 6.74 (s, 2H), 6.69 (d, J = 8.3 Hz, 4H), 4.48 (s, 4H). ^{13}C NMR (151 MHz, $CDCl_3$) δ 158.12, 147.93, 137.31, 129.30, 119.92, 117.68, 113.12, 49.28.HRMS (ESI): $[M+H]^+$calculated 290.1579, found = 290.1669.

N,*N*′-(pyridine-2,6-diylbis(methylene))bis(4-fluoroaniline) (**4.29n**)

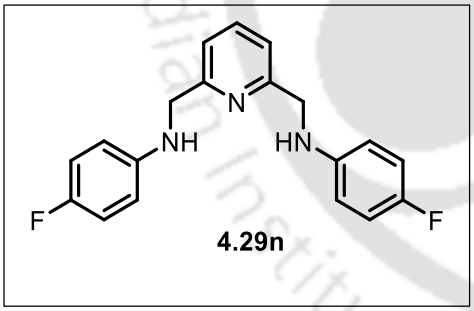

^{1}H NMR (600 MHz, DMSO-d_6) δ 7.66 (t, *J* = 7.7 Hz, 1H), 7.21 (d, *J* = 7.4 Hz, 2H), 6.89 (t, *J* = 8.5 Hz, 4H), 6.58 – 6.54 (m, 4H), 4.33 (s, 4H).^{13}C NMR (151 MHz, DMSO-d_6) δ 158.91, 155.15, 145.23, 137.16, 119.24, 115.21, 113.05, 49.00.^{19}F NMR (565 MHz, DMSO-d_6) δ -129.49 (s).HRMS (ESI): $[M+H]^+$calculated 326.1391, found = 326.1519.

N-(pyridin-4-ylmethyl)aniline (**4.29w)**

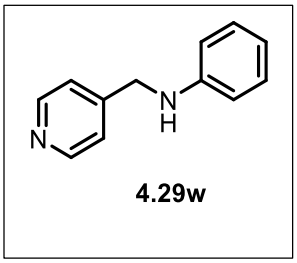

^{1}H NMR (600 MHz, $CDCl_3$) δ 8.54 (d, *J* = 5.9 Hz, 2H), 7.30 (d, *J* = 5.8 Hz, 2H), 7.17 (t, *J* = 7.9 Hz, 2H), 6.74 (t, *J* = 7.3 Hz, 1H), 6.58 (d, *J* = 7.7 Hz, 2H), 4.38 (s, 2H). ^{13}C NMR (151 MHz, $CDCl_3$) δ150.09, 149.11, 147.54, 129.48, 122.19, 118.22, 113.00, 47.21. HRMS (ESI): $[M+H]^+$calculated 185.1000, found = 185.1110.

N-benzylpyridin-2-amine (**4.29o**)

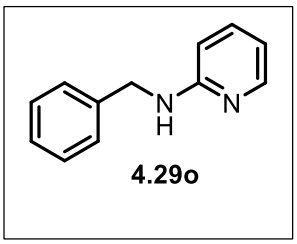

4.29o

^{1}H NMR (600 MHz, $CDCl_3$) δ 8.10 (d, *J* = 4.7 Hz, 1H), 7.44 – 7.31 (m, 5H), 7.28 (d, *J* = 7.0 Hz, 1H), 6.62 – 6.57 (m, 1H), 6.37 (d, *J* = 8.4 Hz, 1H), 4.90 (s, 1H), 4.51 (d, *J* = 5.8 Hz, 2H). ^{13}C NMR (151 MHz, $CDCl_3$) δ 158.77, 148.35, 139.32, 137.62, 128.78, 127.54, 127.39, 113.33, 106.95, 46.50 . HRMS (ESI): $[M+H]^+$calculated 185.1000, found 185.1135.

N-(pyridin-2-ylmethyl)aniline (**4.29x**)

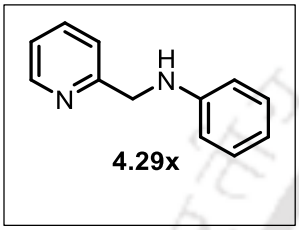

4.29x

^{1}H NMR (600 MHz, $CDCl_3$) δ 8.61 – 8.58 (m, 1H), 7.64 (td, *J* = 7.7, 1.8 Hz, 1H), 7.34 (d, *J* = 7.8 Hz, 1H), 7.21 – 7.16 (m, 3H), 6.73 (td, *J* = 7.3, 1.2 Hz, 1H), 6.70 – 6.65 (m, 2H), 4.47 (s, 2H). ^{13}C NMR (151 MHz, $CDCl_3$) δ 158.67, 149.33, 148.02, 136.73, 129.36, 122.19, 121.70, 117.72, 113.18, 49.44. HRMS (ESI): $[M+H]^+$calculated 185.1000, found = 185.1013.

N-(4-methoxybenzyl)pyridin-2-amine (**4.29k**)

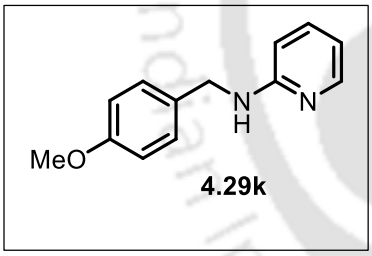

4.29k

^{1}H NMR (600 MHz, $CDCl_3$) δ 8.08 (s, 1H), 7.38 (s, 1H), 7.27 (d, *J* = 6.7 Hz, 2H), 6.86 (d, *J* = 6.7 Hz, 2H), 6.57 (s, 1H), 6.35 (d, *J* = 7.4 Hz, 1H), 4.87 (s, 1H), 4.41 (s, 2H), 3.78 (s, 4H). ^{13}C NMR (151 MHz, $CDCl_3$) δ 159.00, 158.78, 148.30, 137.58, 131.29, 128.82, 114.17, 113.20, 106.91, 55.41, 45.96. HRMS (ESI): $[M+H]^+$calculated 214.1106, found = 215.1225.

2-phenyl-1H-benzo[d]imidazole (**4.63**)

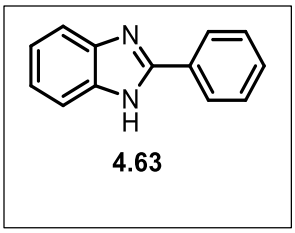

4.63

^{1}H NMR (600 MHz, DMSO-d_6) δ 12.93 (s, 1H), 8.19 (d, J = 8.3 Hz, 2H), 7.67 (d, J = 7.7 Hz, 1H), 7.59 – 7.48 (m, 4H), 7.21 (dt, J = 20.2, 6.8 Hz, 2H). ^{13}C NMR (151 MHz, DMSO-d_6) δ 151.66, 144.24, 135.44, 130.60, 130.31, 129.42, 126.88, 123.00, 122.13, 119.33, 111.78.HRMS (ESI): $[M+H]^+$calculated 195.0844, found = 195.0938.

2-(4-methoxyphenyl)-1H-benzo[d]imidazole (**4.63a**)

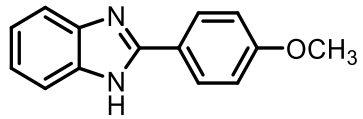

4.63a

^{1}H NMR (600 MHz, DMSO-d_6) δ 12.73 (s, 1H), 8.11 (s, 2H), 7.62 (d, *J* = 7.5 Hz, 1H), 7.49 (d, *J* = 7.4 Hz, 1H), 7.12 (d, *J* = 8.7 Hz, 4H), 3.85 (s, 3H). ^{13}C NMR (151 MHz, DMSO-d_6) δ 161.07 , 151.80 , 144.35 , 135.43 , 128.46 , 122.53 , 121.90 , 118.95 , 114.83 , 111.48 , 55.81 .HRMS (ESI): $[M+H]^+$ calculated 225.0950, found = 225.1052

2-(4-fluorophenyl)-1H-benzo[d]imidazole (**4.63b**)

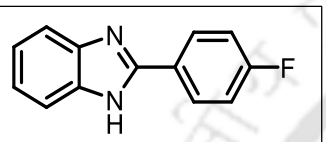

4.63b

^{1}H NMR (600 MHz, DMSO-d_6) δ 12.94 (s, 1H), 8.22 (dd, J = 8.7, 5.5 Hz, 2H), 7.66 (d, J = 4.4 Hz, 1H), 7.54 (d, J = 7.0 Hz, 1H), 7.42 (t, J = 8.8 Hz, 2H), 7.26 – 7.16 (m, 2H).^{13}C NMR (151 MHz, DMSO-d_6) δ 164.33, 162.69, 150.83, 129.20, 129.15, 127.27, 116.55, 116.41.^{19}F NMR (565 MHz, DMSO-d_6) δ -111.12 (d, J = 8.6 Hz).HRMS (ESI): $[M+H]^+$calculated 213.0750, found = 213.0883.

2-(furan-2-yl)-1H-benzo[d]imidazole(**4.63c**)

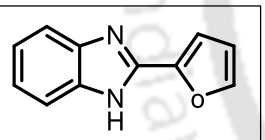

4.63c

^{1}H NMR (400 MHz, DMSO-d_6) δ 13.50 (s, 1H), 9.83 (s, 1H), 8.21 (s, 1H), 7.96 (s, 1H), 7.83 (d, J = 8.0 Hz, 1H), 7.65 (s, 2H), 7.31 (s, 2H).^{13}C NMR (151 MHz, DMSO-d_6) δ 144.50, 144.42, 131.67, 131.28, 129.70, 129.40, 124.70, 122.96, 120.31, 112.85. HRMS (ESI): $[M+H]^+$calculated 185.0637, found = 185.1098.

2-(thiophen-2-yl)-1H-benzo[d]imidazole(**4.63d**)

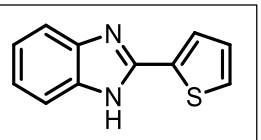

4.63d

^{1}H NMR (400 MHz, DMSO-d_6) δ 12.95 (s, 1H), 7.83 (d, J = 4.6 Hz, 1H), 7.73 (dd, J = 5.1, 1.2 Hz, 1H), 7.55 (d, J = 32.2 Hz, 3H), 7.25 – 7.16 (m, 3H). ^{13}C NMR (151 MHz, DMSO-d_6) δ 147.48, 134.06, 129.21, 128.72, 127.17.HRMS (ESI): $[M+H]^+$calculated 201.0408, found = 201.1046.

2-(pyridin-2-yl)-1H-benzo[d]imidazole (**4.63e**)

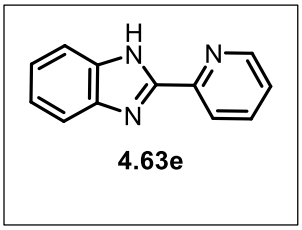

4.63e

^{1}H NMR (600 MHz, $CDCl_3$) δ 10.73 (s, 1H), 8.64 (d, J = 4.7 Hz, 1H), 8.44 (d, J = 7.9 Hz, 1H), 7.87 (t, J = 7.7 Hz, 2H), 7.50 (s, 1H), 7.41 – 7.36 (m, 1H), 7.31 (dd, J = 6.1, 2.8 Hz, 2H). ^{13}C NMR (151 MHz, $CDCl_3$) δ 150.89, 149.12, 148.52, 137.67, 124.74, 121.98.HRMS (ESI): $[M+H]^+$calculated 196.0796, found = 196.0890.

2-(3-methoxyphenyl)-1H-benzo[d]imidazole (**4.63f**)

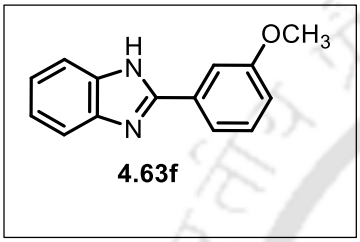

4.63f

^{1}H NMR (600 MHz, DMSO-d_6) δ 12.75 (s, 1H), 8.12 (d, *J* = 8.8 Hz, 2H), 7.62 (d, *J* = 7.5 Hz, 1H), 7.50 (d, *J* = 7.4 Hz, 1H), 7.17 (t, *J* = 8.3 Hz, 2H), 7.12 (d, *J* = 8.8 Hz, 2H), 3.84 (s, 3H). ^{13}C NMR (151 MHz, DMSO-d_6) δ 161.07 , 151.81 , 144.35 , 135.43, 128.47 , 123.17 , 122.53 , 121.90 , 118.95 , 114.83 , 111.48 , 55.81 . HRMS (ESI): $[M+H]^+$calculated 225.0950, found = 225.1069

2-(p-tolyl)-1H-benzo[d]imidazole (**4.63g**)

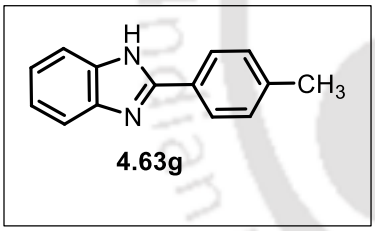

4.63g

^{1}H NMR (400 MHz, DMSO-d_6) δ 12.81 (s, 1H), 8.10 – 8.02 (m, 2H), 7.66 – 7.61 (m, 1H), 7.53 – 7.47 (m, 1H), 7.36 (d, J = 7.9 Hz, 2H), 7.19 (td, J = 6.6, 1.6 Hz, 2H), 2.39 (s, 3H). ^{13}C NMR (151 MHz, DMSO-d_6) δ 151.84 , 144.29, 140.01, 135.40 , 129.96 , 127.92 , 126.85 , 122.01 , 119.16 , 111.64 , 21.44 .HRMS (ESI): $[M+H]^+$ calculated 209.1000, found = 209.1118.

2-(4-chlorophenyl)-1H-benzo[d]imidazole (**4.63h**)

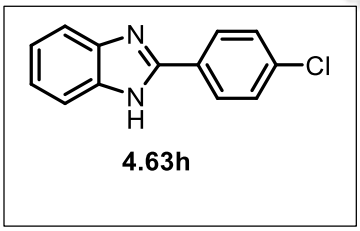

4.63h

^{1}H NMR (600 MHz, DMSO-d_6) δ 13.01 (s, 1H), 8.19 (d, *J* = 8.6 Hz, 2H), 7.64 (d, *J* = 8.6 Hz, 4H), 7.23 (s, 2H). ^{13}C NMR (151 MHz, DMSO-d_6) δ 151.66 , 144.24 , 135.44 , 130.60 , 130.31 , 129.42 , 126.88 , 123.00 , 122.13 , 119.33 , 111.78 . HRMS (ESI): $[M+H]^+$calculated 229.0454, found = 229.0530.

2-(3-chlorophenyl)-1H-benzo[d]imidazole (**4.63i**)

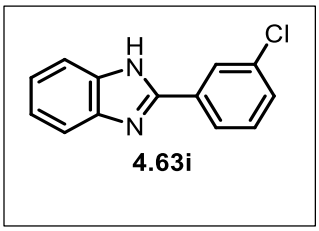

4.63i

^{1}H NMR (400 MHz, DMSO-d_6) δ 13.05 (s, 1H), 8.23 (s, 1H), 8.15 (d, J = 7.2 Hz, 1H), 7.57 (s, 4H), 7.24 (s, 2H).^{13}C NMR (151 MHz, DMSO-d_6) δ 150.19 , 134.23 , 132.66, 131.40 , 130.00 , 126.48 , 125.48 , 122.37 , 119.51 , 111.98 .HRMS (ESI): [M+H]$^{+}$calculated 229.0454, found = 229.0577.

2-(m-tolyl)-1H-benzo[d]imidazole (**4.63j**)

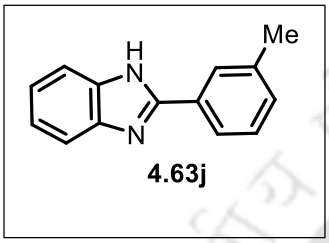

4.63j

^{1}H NMR (600 MHz, DMSO-d_6) δ 12.88 (s, 1H), 8.03 (s, 1H), 7.97 (d, J = 7.7 Hz, 1H), 7.66 (d, J = 7.4 Hz, 1H), 7.53 (d, J = 7.2 Hz, 1H), 7.44 (t, J = 7.6 Hz, 1H), 7.32 (d, J = 7.4 Hz, 1H), 7.24 – 7.17 (m, 2H), 2.42 (s, 3H). ^{13}C NMR (151 MHz, DMSO-d_6) δ 151.78 , 138.62 , 130.93 , 130.55 , 129.30 , 127.46 , 124.05 , 122.95 , 122.08 , 119.25 , 111.74 , 21.52 . HRMS (ESI): [M+H]$^{+}$calculated 209.1000, found = 209.1100.

5-methyl-2-phenyl-1H-benzo[d]imidazole(**4.63k**) and 6-methyl-2-phenyl-1H-benzo[d]imidazole (**4.63k**)

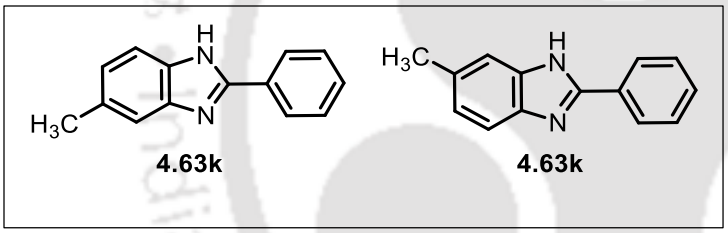

4.63k **4.63k**

^{1}H NMR (600 MHz, DMSO-d_6) δ 12.79 (s, 1H), 12.75 (s, 1H), 8.15(d, J = 7.5 Hz, 5H), 7.54 (t, J = 7.7 Hz, 7H), 7.51-7.45 (m, 4H), 7.41 (d, J = 8.1 Hz, 1H), 7.31 (s, 1H), 7.03 (dd, J= 21.1, 8.1 Hz, 3H), 2.44 (s, 4H), 2.42 (s, 3H). ^{13}C NMR (151 MHz, DMSO-d_6) δ 151.60, 150.82, 135.05, 130.78, 130.10, 129.36, 129.25, 127.16, 126.85, 123.56, 122.89, 122.21, 116.73, 109.23, 17.62, 17.13. HRMS (ESI): [M+H]$^{+}$calculated 209.1000, found = 209.1108.

4-methyl-2-phenyl-1,4-dihydrocyclopenta[d]imidazole and 6-methyl-2-phenyl-1,4-dihydrocyclopenta[d]imidazole (**4.63l**)

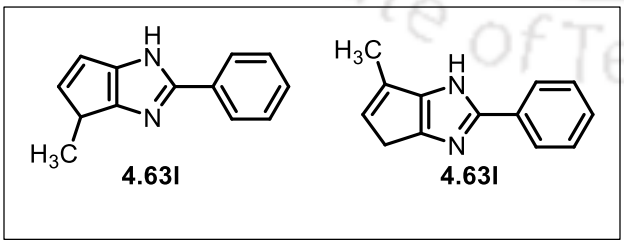

4.63l **4.63l**

^{1}H NMR (600 MHz, DMSO-d_6) δ 12.85 (s, 1H), 12.59(s, 1H), 8.25 (d, J = 7.3 Hz, 2H), 8.18 (d, J = 7.3 Hz, 3H), 7.56 (q, J = 7.3 Hz, 5H), 7.53-7.46 (d, J = 8.0 Hz, 1H), 713-7.07 (m, 3H), 7.00 (t, J= 7.4 Hz, 2H), 2.59 (s, 4H), 2.57 (s, 3H). ^{13}C NMR (151 MHz, DMSO-d_6) δ 151.17, 142.41, 130.14, 130.07, 126.79, 124.43, 123.70, 119.06, 119.81, 111.48, 111.29, 21.84, 21.75. HRMS (ESI): [M+H]$^{+}$calculated 209.1000, found = 209.1092.

Supporting information (containing NMR spectra of various compound and Cartesian coordinates of the computed complexes) for chapter 4 is available as appendix 3 and can be found at https://drive.google.com/file/d/1ihehIqPowud_sMY2RUiE8h3ZbLGq1vos/view?usp=sharing

4.8 References

1. Ghorai, S. K.; Gopalsamuthiram, V. G.; Jawalekar, A. M.; Patre, R. E.; Pal, S., *Tetrahedron* **2017**, *73* (14), 1769-1794.
2. Erden, I.; Alscher, P. E.; Keeffe, J. R.; Mercer, C., *J. Org. Chem.* **2005**, *70* (11), 4389-4392.
3. Lawrence, S., *There is no corresponding record for this reference*.
4. MOHRI, K.; SUZUKI, K.; Usui, M.; IsoBE, K.; TSUDA, Y., *Chem. Pharm. Bull.* **1995**, *43* (1), 159-161.
5. Mizuta, T.; Sakaguchi, S.; Ishii, Y., *J. Org. Chem.* **2005**, *70* (6), 2195-2199.
6. Huang, L.; Arndt, M.; Gooßen, K. t.; Heydt, H.; Goossen, L. J., *Chem. Rev.* **2015**, *115* (7), 2596-2697.
7. Vieira, T. O.; Alper, H., *Chem. Commun.* **2007**, *26*, 2710-2711.
8. Das, S.; Zhou, S.; Addis, D.; Enthaler, S.; Junge, K.; Beller, M., *Top. Catal.* **2010**, *53* (15-18), 979-984.
9. Junge, K.; Wendt, B.; Shaikh, N.; Beller, M., *Chem. Commun.* **2010**, *46* (10), 1769-1771.
10. Xu, Q.; Xie, H.; Zhang, E.-L.; Ma, X.; Chen, J.; Yu, X.-C.; Li, H., *Green Chem.* **2016**, *18* (14), 3940-3944.
11. Sperotto, E.; van Klink, G. P.; van Koten, G.; de Vries, J. G., *Dalton Trans.* **2010**, *39* (43), 10338-10351.
12. Magano, J.; Dunetz, J. R., *Chem. Rev.* **2011**, *111* (3), 2177-2250.
13. Nigh, W., *J. Chem. Educ.* **1975**, *52* (10), 670.
14. Heinonen, P.; Lönnberg, H., *Tetrahedron Lett.* **1997**, *38* (49), 8569-8572.
15. Hama, T.; Culkin, D. A.; Hartwig, J. F., *J. Am. Chem. Soc.* **2006**, *128* (15), 4976-4985.
16. Hartwig, J. F., *Angew. Chem. Int. Ed.* **1998**, *37* (15), 2046-2067.
17. Zhang, Y.; Qi, X.; Cui, X.; Shi, F.; Deng, Y., *Tetrahedron Lett.* **2011**, *52* (12), 1334-1338.
18. Kosugi, M.; Kameyama, M.; Migita, T., *Chem. Lett.* **1983**, *12* (6), 927-928.
19. Boger, L. D.; Panek, J. S., *Tetrahedron Lett.* **1984**, *25* (30), 3175-3178.
20. Guram, A. S.; Buchwald, S. L., *J. Am. Chem. Soc.* **1994**, *116* (17), 7901-7902.
21. Paul, F.; Patt, J.; Hartwig, J. F., *J. Am. Chem. Soc.* **1994**, *116* (13), 5969-5970.
22. Guram, A. S.; Rennels, R. A.; Buchwald, S. L., *Angew. Chem. Int. Ed. in English* **1995**, *34* (12), 1348-1350.
23. Wolfe, J. P.; Buchwald, S. L., *J. Am. Chem. Soc.* **1997**, *119* (26), 6054-6058.
24. Desmarets, C.; Schneider, R.; Fort, Y., *J. Org. Chem.* **2002**, *67* (9), 3029-3036.
25. Nirmala, M.; Prakash, G.; Ramachandran, R.; Viswanathamurthi, P.; Malecki, J. G.; Linert, W., *J. Mol. Catal. A Chem.* **2015**, *397*, 56-67.
26. Ullmann, F., *Ber. Dtsch. Chem. Ges.* **1903**, *36* (2), 2382-2384.
27. Li, L.; Zhu, L.; Chen, D.; Hu, X.; Wang, R., *Eur. J. Org. Chem.* **2011**, *2011* (14), 2692-2696.
28. Henry, J. R.; Marcin, L. R.; McIntosh, M. C.; Scola, P. M.; Harris Jr, G. D.; Weinreb, S. M., *Tetrahedron Lett.* **1989**, *30* (42), 5709-5712.
29. Huang, H.; Kang, J. Y., *J. Org. Chem.* **2017**, *82* (13), 6604-6614.
30. Overman, L. E.; Paone, D. V., *J. Am. Chem. Soc.* **2001**, *123* (38), 9465-9467.

31. Edwards, M. G.; Jazzar, R. F.; Paine, B. M.; Shermer, D. J.; Whittlesey, M. K.; Williams, J. M.; Edney, D. D., *Chem. Commun.* **2004**, *1*, 90-91.
32. Gunanathan, C.; Milstein, D., *Acc. Chem. Res.* **2011**, *44* (8), 588-602.
33. Grigg, R.; Mitchell, T.; Sutthivaiyakit, S.; Tongpenyai, N., *J. Chem. Soc., Chem. Commun.* **1981**, *12*, 611-612.
34. Watanabe, Y.; Tsuji, Y.; Ohsugi, Y., *Tetrahedron Lett.* **1981**, *22* (28), 2667-2670.
35. Tsuji, Y.; Takeuchi, R.; Ogawa, H.; Watanabe, Y., *Chem. Lett.* **1986**, *15* (3), 293-294.
36. Abbenhuis, R. A.; Boersma, J.; van Koten, G., *J. Org. Chem.* **1998**, *63* (13), 4282-4290.
37. Baehn, S.; Imm, S.; Mevius, K.; Neubert, L.; Tillack, A.; Williams, J. M.; Beller, M., *Chem. Eur. J.* **2010**, *16* (12), 3590-3593.
38. Agrawal, S.; Lenormand, M.; Martín-Matute, B., *Org. Lett.* **2012**, *14* (6), 1456-1459.
39. Maji, M.; Chakrabarti, K.; Paul, B.; Roy, B. C.; Kundu, S., *Adv. Synth. Catal.* **2018**, *360* (4), 722-729.
40. Baratta, W.; Bosco, M.; Chelucci, G.; Del Zotto, A.; Siega, K.; Toniutti, M.; Zangrando, E.; Rigo, P., *Organometallics* **2006**, *25* (19), 4611-4620.
41. Das, K.; Nandi, P. G.; Islam, K.; Srivastava, H. K.; Kumar, A., *Eur. J. Org. Chem.* **2019**, *40*, 6855-6866.
42. Guo, B.; Li, H. X.; Zhang, S. Q.; Young, D. J.; Lang, J. P., *ChemCatChem* **2018**, *10* (24), 5627-5636.
43. Derrah, E. J.; Hanauer, M.; Plessow, P. N.; Schelwies, M.; da Silva, M. K.; Schaub, T., *Organometallics* **2015**, *34* (10), 1872-1881.
44. Ye, X.; Plessow, P. N.; Brinks, M. K.; Schelwies, M.; Schaub, T.; Rominger, F.; Paciello, R.; Limbach, M.; Hofmann, P., *J. Am. Chem. Soc.***2014**, *136* (16), 5923-5929.
45. Fujita, K.-i.; Li, Z.; Ozeki, N.; Yamaguchi, R., *Tetrahedron Lett.* **2003**, *44* (13), 2687-2690.
46. Reyes-Rios, G.; García, J. J., *Inorg. Chim. Acta.* **2012**, *392*, 317-321.
47. Zhao, G.-M.; Liu, H.-l.; Huang, X.-r.; Yang, X.; Xie, Y.-p., *ACS Catal.* **2015**, *5* (10), 5728-5740.
48. Satyanarayana, P.; Reddy, G. M.; Maheswaran, H.; Kantam, M. L., *Adv. Synth. Catal.* **2013**, *355*,1859-1867.
49. Michlik, S.; Kempe, R., *Chem. Eur. J.* **2010**, *16* (44), 13193-13198.
50. Hollmann, D.; Bähn, S.; Tillack, A.; Parton, R.; Altink, R.; Beller, M., *Tetrahedron Lett.* **2008**, *49* (40), 5742-5745.
51. Löfberg, C.; Grigg, R.; Whittaker, M. A.; Keep, A.; Derrick, A., *J. Org. Chem.* **2006**, *71* (21), 8023-8027.
52. Fujita, K.-i.; Yamamoto, K.; Yamaguchi, R., *Org. Lett.* **2002**, *4* (16), 2691-2694.
53. Cami-Kobeci, G.; Williams, J. M., *Chem. Commun.* **2004**, *9*, 1072-1073.
54. Dang, T. T.; Ramalingam, B.; Shan, S. P.; Seayad, A. M., *ACS Catal.* **2013**, *3* (11), 2536-2540.
55. Brown, A.; Reid, E. E., *J. Am. Chem. Soc.* **1924**, *46* (8), 1836-1839.
56. Sun, J.; Jin, X.; Zhang, F.; Hu, W.; Liu, J.; Li, R., *Catal. Commun.* **2012**, *24*, 30-33.
57. Rice, R. G.; Kohn, E. J., *J. Am. Chem. Soc.* **1955**, *77* (15), 4052-4054.
58. Paul, B.; Maji, M.; Chakrabarti, K.; Kundu, S., *Org. Biomol. Chem.* **2020**, *18* (12), 2193-2214.
59. He, L.; Lou, X. B.; Ni, J.; Liu, Y. M.; Cao, Y.; He, H. Y.; Fan, K. N., *Chem. Eur. J.* **2010**, *16* (47), 13965-13969.
60. Cui, X.; Shi, F.; Zhang, Y.; Deng, Y., *Tetrahedron Lett.* **2010**, *51* (15), 2048-2051.

61. Elangovan, S.; Neumann, J.; Sortais, J.-B.; Junge, K.; Darcel, C.; Beller, M., *Nature Commun.* **2016**, *7*, 12641.
62. Martínez-Asencio, A.; Ramón, D. J.; Yus, M., *Tetrahedron Lett.* **2010**, *51* (2), 325-327.
63. Rösler, S.; Ertl, M.; Irrgang, T.; Kempe, R., *Angew. Chem. Int. Ed.* **2015**, *54* (50), 15046-15050.
64. Zhang, G.; Yin, Z.; Zheng, S., *Org. Lett.* **2015**, *18* (2), 300-303.
65. Winans, C. F.; Adkins, H., *J. Am. Chem. Soc.* **1932**, *54* (1), 306-312.
66. Shimizu, K.-i.; Imaiida, N.; Kon, K.; Hakim Siddiki, S. M. A.; Satsuma, A., *ACS Catal.* **2013**, *3* (5), 998-1005.
67. Su, H.; Gao, P.; Wang, M. Y.; Zhai, G. Y.; Zhang, J. J.; Zhao, T. J.; Su, J.; Antonietti, M.; Li, X. H.; Chen, J. S., *Angew. Chem. Int. Ed.* **2018**, *57* (46), 15194-15198.
68. Subaramanian, M.; Midya, S. P.; Ramar, P. M.; Balaraman, E., *Org. Lett.* **2019**, *21* (22), 8899-8903.
69. Bains, A. K.; Kundu, A.; Yadav, S.; Adhikari, D., *ACS Catal.* **2019**, *9* (10), 9051-9059.
70. Benitez-Medina, G. E.; García, J. J., *Dalton Trans.* **2019**, *48* (47), 17579-17587.
71. Balamurugan, G.; Ramesh, R.; Malecki, J. G., *J. Org. Chem.* **2020**, *85* (11), 7125-7135.
72. Vellakkaran, M.; Singh, K.; Banerjee, D., *ACS Catal.* **2017**, *7* (12), 8152-8158.
73. Shee, S.; Panja, D.; Kundu, S., *J. Org. Chem.* **2020**, *85* (4), 2775-2784.
74. Das, S.; Maiti, D.; De Sarkar, S., *J. Org. Chem.* **2018**, *83* (4), 2309-2316.
75. Afanasenko, A.; Elangovan, S.; Stuart, M. C.; Bonura, G.; Frusteri, F.; Barta, K., *Catal. Sci. Technol.* **2018**, *8* (21), 5498-5505.
76. Vinay Arora, Ph.D thesis work(on going), Indian Institute of Technology Guwahati.
77. Arora, V.; Dutta, M.; Das, K.; Das, B.; Srivastava, H. K.; Kumar, A., *Organometallics* **2020**, *39*, 2162-2176.
78. Das, K.; Kumar, A. *Adv. Organomet. Chem.*, Elsevier: 2019; Vol. 72, pp 1-57.
79. Kumar, A.; Bhatti, T. M.; Goldman, A. S., *Chem. Rev.***2017**, *117* (19), 12357-12384.
80. Kundu, S.; Choliy, Y.; Zhuo, G.; Ahuja, R.; Emge, T. J.; Warmuth, R.; Brookhart, M.; Krogh-Jespersen, K.; Goldman, A. S., *Organometallics* **2009**, *28* (18), 5432-5444.
81. Kumar, A.; Hackenberg, J. D.; Zhuo, G.; Steffens, A. M.; Mironov, O.; Saxton, R. J.; Goldman, A. S., *J. Mol. Catal. A Chem.* **2017**, *426*, 368-375.
82. Keri, R. S.; Hiremathad, A.; Budagumpi, S.; Nagaraja, B. M., *Chem. Biol. Drug. Des.* **2015**, *86* (1), 19-65.
83. Gürsel, S. A.; Gubler, L.; Gupta, B.; Scherer, G. G. In *Fuel cells I*, Springer: 2008; pp 157-217.
84. Horton, D. A.; Bourne, G. T.; Smythe, M. L., *Chem. Rev.* **2003**, *103* (3), 893-930.
85. Brain, C. T.; Brunton, S. A., *Tetrahedron Lett.* **2002**, *43* (10), 1893-1895.
86. She, J.; Jiang, Z.; Wang, Y., *Synlett* **2009**, *2009* (12), 2023-2027.
87. Ghorbani-Vaghei, R.; Veisi, H., *Mol. Divers.* **2010**, *14* (2), 249-256.
88. Varala, R.; Nasreen, A.; Enugala, R.; Adapa, S. R., *Tetrahedron Lett.* **2007**, *48* (1), 69-72.
89. Jacob, R. G.; Dutra, L. G.; Radatz, C. S.; Mendes, S. R.; Perin, G.; Lenardão, E. J., *Tetrahedron Lett.* **2009**, *50* (13), 1495-1497.
90. Dang, Q.; Kasibhatla, S. R.; Xiao, W.; Liu, Y.; DaRe, J.; Taplin, F.; Reddy, K. R.; Scarlato, G. R.; Gibson, T.; van Poelje, P. D., *J. Med. Chem.* **2009**, *53* (1), 441-451.
91. Carvalho, L. C.; Fernandes, E.; Marques, M. M. B., *Chem. Eur. J.* **2011**, *17* (45), 12544-12555.
92. Wright, J. B., *Chem. Rev.* **1951**, *48* (3), 397-541.

93. Preston, P., *Chem. Rev.* **1974**, *74* (3), 279-314.
94. Blacker, A. J.; Farah, M. M.; Hall, M. I.; Marsden, S. P.; Saidi, O.; Williams, J. M., *Org. Lett.* **2009**, *11* (9), 2039-2042.
95. Ramachandran, R.; Prakash, G.; Selvamurugan, S.; Viswanathamurthi, P.; Malecki, J. G.; Ramkumar, V., *Dalton Trans.* **2014**, *43* (21), 7889-7902.
96. Kondo, T.; Yang, S.; Huh, K.-T.; Kobayashi, M.; Kotachi, S.; Watanabe, Y., *Chem. Lett.* **1991**, *20* (7), 1275-1278.
97. Hille, T.; Irrgang, T.; Kempe, R., *Chem. Eur. J.* **2014**, *20* (19), 5569-5572.
98. Ramachandran, R.; Prakash, G.; Selvamurugan, S.; Viswanathamurthi, P.; Malecki, J. G.; Ramkumar, V., *Dalton Trans.* **2014**, *43* (21), 7889-7902.
99. Daw, P.; Ben-David, Y.; Milstein, D., *ACS Catal.* **2017**, *7* (11), 7456-7460.
100. Das, K.; Mondal, A.; Srimani, D., *J. Org. Chem.* **2018**, *83* (16), 9553-9560.
101. Bera, A.; Sk, M.; Singh, K.; Banerjee, D., *Chem. Commun.* **2019**, *55* (42), 5958-5961.
102. Agrahari, B.; Layek, S.; Ganguly, R.; Dege, N.; Pathak, D. D., *J. Organometal. Chem.* **2019**, *890*, 13-20.
103. G.W. T. M. J. Frisch, H. B. Schlegel, G. E. Scuseria, M. A. Robb, J. R. Cheeseman, G. Scalmani, V. Barone, B. Mennucci, G. A. Petersson, H. Nakatsuji, M. Caricato, X. Li, H. P. Hratchian, A. F. Izmaylov, J. Bloino, G. Zheng, J. L. Sonnenberg, M. Hada, M. Ehara, K. Toyota, R. Fukuda, J. Hasegawa, M. Ishida, T. Nakajima, Y. Honda, O. Kitao, H. Nakai, T. Vreven, J. A. Montgomery, Jr., J. E. Peralta, F. Ogliaro, M. Bearpark, J. J. Heyd, E. Brothers, K. N. Kudin, V. N. Staroverov, T. Keith, R. Kobayashi, J. Normand, K. Raghavachari, A. Rendell, J. C. Burant, S. S. Iyengar, J. Tomasi, M. Cossi, N. Rega, J. M. Millam, M. Klene, J. E. Knox, J. B. Cross, V. Bakken, C. Adamo, J. Jaramillo, R. Gomperts, R. E. Stratmann, O. Yazyev, A. J. Austin, R. Cammi, C. Pomelli, J.W. Ochterski, R. L. Martin, K. Morokuma, V. G. Zakrzewski, G. A. Voth, P. Salvador, J. J. Dannenberg, S. Dapprich, A. D. Daniels, O. Farkas, J. B. Foresman, J. V. Ortiz, J. Cioslowski, and D. J. Fox, *Gaussian 09, Revision D.01, Gaussian, Inc., Wallingford CT* **2013**.
104. Wang, C.; Wang, J.; Cai, Q.; Li, Z.; Zhao, H.-K.; Luo, R. *Comput. Theor. Chem.* 2**013**, *1024*, 34−44
105. Ghannam, J.; Al Assil, T.; Pankratz, T. C.; Lord, R. L.; Zeller, M.; Lee, W.-T. *Inorg. Chem.* **2018**, *57*, 8307−8316.
106. Gonzalez, C.; Schlegel, H. B. *J. Chem. Phys.* **1989**, *90*, 2154−2161.

Chapter 5

Computational Studies on the Pincer-Nickel Catalyzed Cyanomethylation of Benzaldehyde

5.1 Introduction

β-hydroxy nitrile is an important moiety which has a cyano moiety and a hydroxyl group attached to the same carbon atom. *β*-hydroxy nitrile is an useful biologically active intermediate used in the synthesis of *β*-hydroxy amides,[1] *β*-hydroxy esters,[2] *β*-amino alcohols,[3] *β*-hydroxy ketones,[4] *β*-hydroxy carboxylic acids[5] and *α*-hydroxy acids[6]. These compounds have several importance in producing fine-chemicals,[7] pharmaceuticals[8] and agrochemicals[9]. In addition, the hydroxyl group can generate new stereo-centers which would be used as chiral auxiliaries.

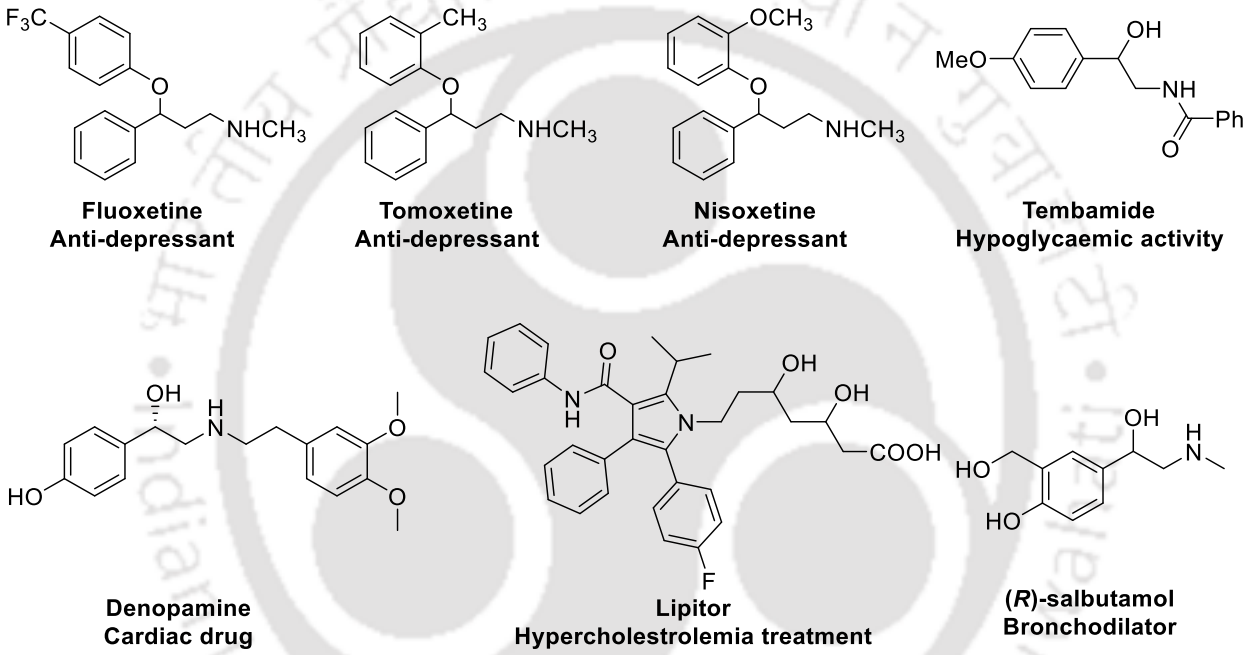

Figure 4.1: A few examples of *β*-hydroxy nitrile intermediates that are of pharmaceutical importance

5.2 History of cyanomethylation reaction

β-hydroxy nitrile can be prepared through several techniques. It can be directly obtained through ring-opening of 1,2 epoxide with HCN.[10] Better results can be obtained by the use of aqueous sodium cyanide in presence of 12-crown-4.[11]

A simple, efficient, regio- and stereo-selective method for the synthesis of *β*-hydroxy nitrile was demonstrated by the direct ring opening of 1, 2 epoxide with alkali metal cyanides in the presence of perchlorates (Scheme 5.1).[12]

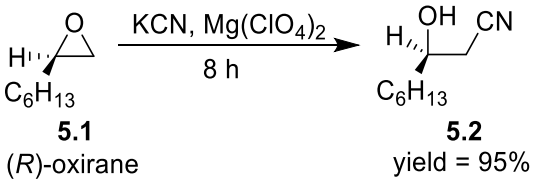

Scheme 5.1: Formation of *β*-Hydroxy nitriles by reaction of 1,2-epoxides with potassium cyanide[12]

LiCN can also be used for cyanation of epoxide.[13] *β*-hydroxy nitriles has been obtained by the regio-selective ring-opening of styrene oxide with NaCN in aqueous–alcoholic medium.[14] The presence of water in the reaction media not only facilitates the availability of the cyanide nucleophile but also assists the complete regioselective opening in good yields.

The cyanotrimethylsilane can be utilized as a versatile reagent for introduction of the cyano functionality to various electrophilic substrates. Reaction of Bu_3Yb, prepared from $YbCl_3$ and BuLi, smoothly proceeds with cyanotrimethylsilane to give $Yb(CN)_3$, which is the active species to produce a *β*-trimethylsiloxy nitrile from an oxirane (**5.3**) with excellent yield (Scheme 5.2).[15] Deprotection of trimethyl silyl ether to alcohol is easily achieved through several methods.[16]

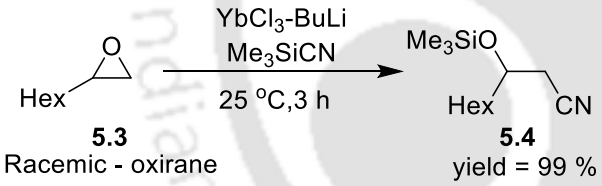

Scheme 5.2: Formation of nitriles mediated by $Yb(CN)_3$.[15]

Another technique to produce *β*-hydroxy nitrile is from the reaction between trimethylsilyl cyanide with epoxide in presence of aluminum chloride (Scheme 5.3). Initial reaction between Me_3SiCN with catalytic amounts of diethyl aluminium chloride gives diethyl aluminium cyanide and trimethyl chlorosilane. Diethyl aluminium cyanide then reacts with oxirane (**5.5**) to obtain ring opened product **5.5.1** which further reacts with additional trimethylsilyl cyanide to generate the desired product **5.6**.[17] There are several reports that use trimethyl silyl cyanide to afford *β*-hydroxy nitriles.[17-20]

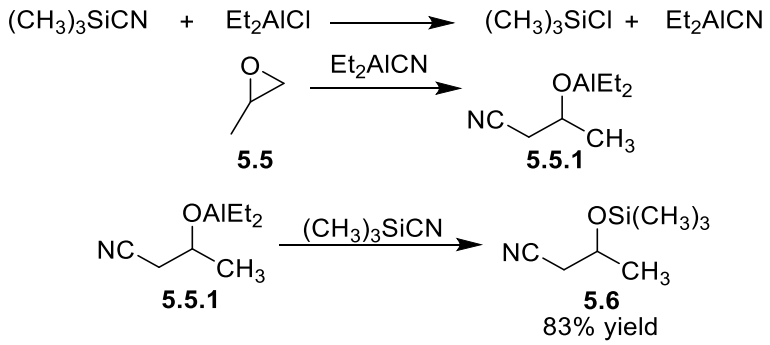

Scheme 5.3: Reactions of epoxides with trimethylsilyl cyanide to obtain nitrile species.[17]

Cyanide ion can also be generated from acetone cyanohydrin.[21] Acetone cyanohydrin in presence of stoichiometric amount of triethyl amine can open epoxides regio-specifically to give *β*-hydroxy nitriles (Scheme 5.4).[22]

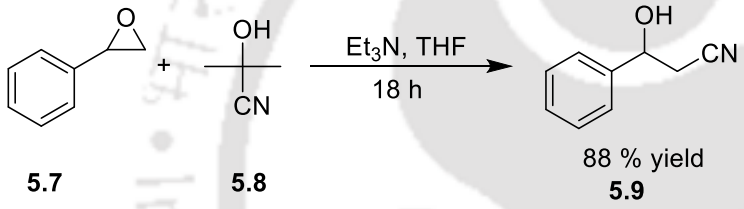

Scheme 5.4: Formation of *β*-hydroxy nitriles by ring opening of 1,2-epoxides with acetone cyanohydrin.[22]

N. Iranpoor and co-workers reported an efficient method for addition of cyanide to 1, 2 epoxide in presence of $Ce(OTf)_4$ to afford *β*-hydroxy nitriles in high yield (Scheme 5.5).[23] Here epoxides having both electron donating and withdrawing substituents can react with cyanide to obtain *β*-hydroxy nitriles as a major product through attack of cyanide ion on less substituted carbon atom.

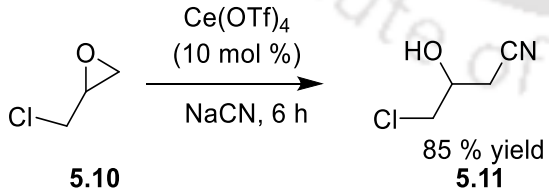

Scheme 5.5: Generation of *β*-hydroxy nitriles from ring opening of epoxides catalyzed by $Ce(OTf)_4$.[23]

Most of these methods suffer from limitations such as poor chemo-selectivity, use of volatile toxic substances and expensive reagents. In order to overcome these problems, a new practical method

for the preparation of *β*-hydroxy nitrile could be through the aldol-type cyanomethylation that involves the nucleophilic addition of *α*-cyano carbanions to carbonyl substrates.

Palomo and co-workers first reported the cyanomethylation by nucleophilic addition of *α*-cyano-carbanion generated from trimethylsilylacetonitrile ($TMSCH_2CN$). $TMSCH_2CN$ reacted with carbonyl compound in presence of catalytic amount of *tris*(dimethylamino)sulfonium diflurotrimethyl silicate (TSAF) to afford *β*-trimethylsiloxy nitrile in excellent yield.[24] Subsequently, the Shibasaki's group demonstrated Cu(I) catalyzed cyanomethylation of carbonyl substrates with trimethylsilylacetonitrile ($TMSCH_2CN$) in the presence of $(EtO)_3SiF$ (Scheme 5.6) [25]

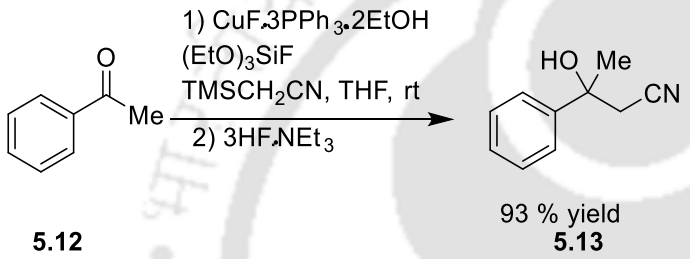

Scheme 5.6: CuF-catalyzed cyanomethylation of acetophenone using $TMSCH_2CN$[25]

Later Mukaiyama reported LiOAc catalyzed cyanomethylation of aldehydes and ketones in the presence of $TMSCH_2CN$ (Scheme 5.7).[26] Aromatic aldehydes having electron donating or withdrawing group reacted efficiently to afford cyanomethylated product in excellent yield.

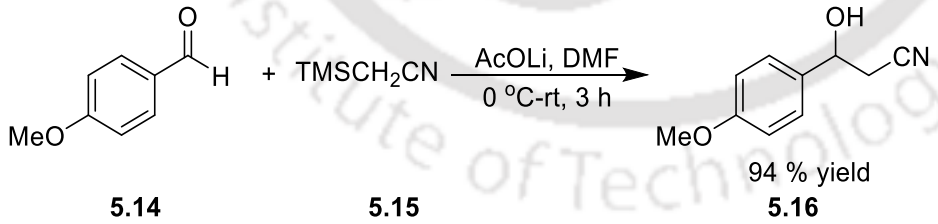

Scheme 5.7: Lewis base-catalyzed cyanomethylation of carbonyl compounds with $TMSCH_2CN$[26]

Trimethylsilyl acetonitrile ($TMSCH_2CN$) in presence of metal fluorides exhibited cyanomethylation of *N*-protected isatin to yield 3-hydroxy-3-cyanometyl oxindoles (Scheme 5.8).[27] Fluoride anion due to its high silicon-fluoride affinity can activate Si-C bond of

$TMSCH_2CN$ and generate the cyanomethylene anion *in-situ*. The CsF catalyzed aldol reaction was tested for a series of *N*-protected isatin derivatives at room temperature.

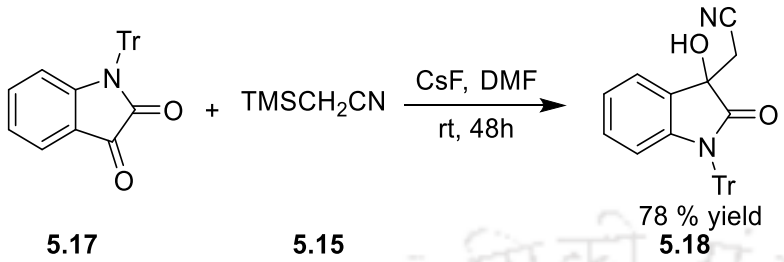

Scheme 5.8: Cyanomethylation of various *N*-trityl isatins with trimethyl-silyl acetonitrile[27]

Very recently, the cyanomethylation of ketone in the presence of α-alkylated (dimethylsilyl)acetonitrile using $MgCl_2$ or $CaCl_2$ has been reported.[28] Highly basic *tris*(2,4,6-trimethoxy phenyl)phosphine (TTMPP) catalyzes the cyanomethylation of carbonyl compound to give the corresponding product under metal-free condition (Scheme 5.9).[29]

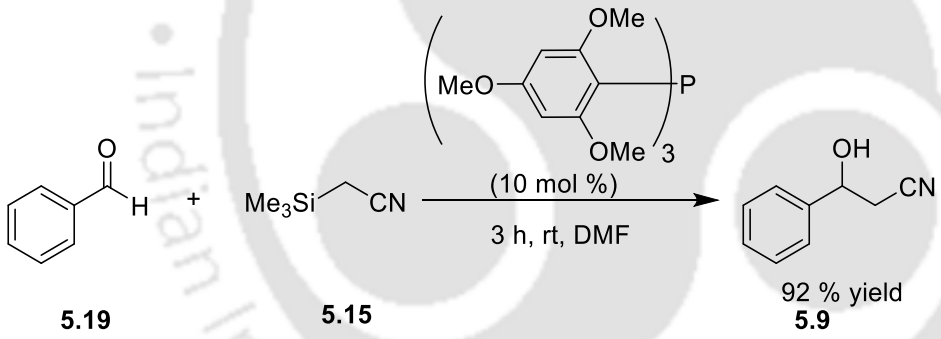

Scheme 5.9: TTMPP-catalyzed cyanomethylation of aldehyde[29]

Other than alkali metal cyanides and $TMSCH_2CN$, acetonitrile (CH_3CN) can also act as good nitrile source. In 2005, Suto *et al.* developed Cu alkoxide-chiral phosphine catalysts to generate enantio-selective β-hydroxy nitriles (Scheme 5.10).[30] Here chemo-selective activation and de-protonation of donor acetonitrile substrate occurred by soft metal alkoxide as Brönsted base. Lewis-acidic metal alkoxide center enhanced the catalytic activity. In metal alkoxides, the $d\pi$-$p\pi$ repulsion between an occupied metal *d*-orbital and the lone pair of oxygen, acts as an driving force for activation of CH_3CN.[31]

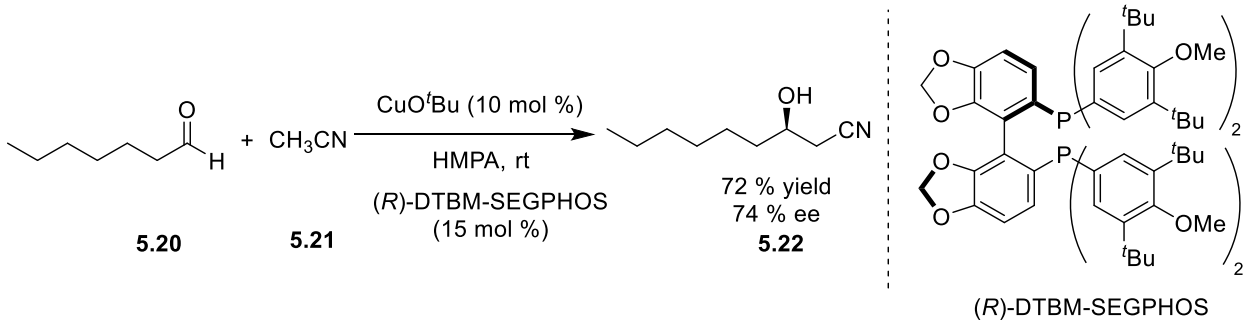

Scheme 5.10: Cu(I)-catalyzed aldol-type reaction of acetonitrile[30]

Transition metal catalyzed, base mediated deprotonaton of acetonitrile followed by a nucleophilic addition is an important strategy for the synthesis of *β*-hydroxy nitrile species. Shibasaki and co-workers reported [CpRu(PPh$_3$)(CH$_3$CN)$_2$]PF$_6$ as an effective catalyst for coupling of aldehyde and acetonitrile in presence of DBU (DBU = 1,8 diazabicyclo[5.4.0]undec-7-ene) as a base (Scheme 5.11).[32]

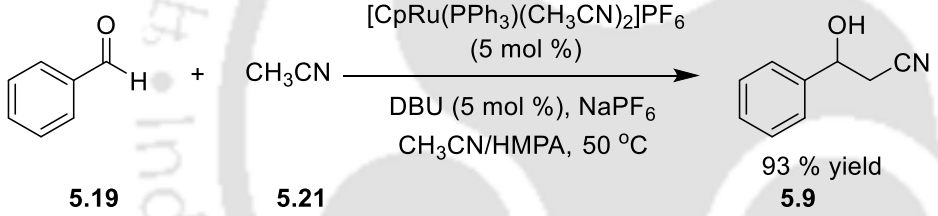

Scheme 5.11: Cationic ruthenium catalyzed cyanomethylation reaction[32]

Saito and co-workers reported cyanomethylation of aldehyde using Rh(I) under mild condition.[33] Here Rh(OMe)(COD)$_2$ catalyzed aldol type condensation of unactivated alkyl nitrile with aldehyde under mild conditions (Scheme 5.12). In 2011, the same group developed a straight forward method to provide *β*-hydroxy carboxamides from aldehyde, nitrile and water in an atom-economical fashion.[34]

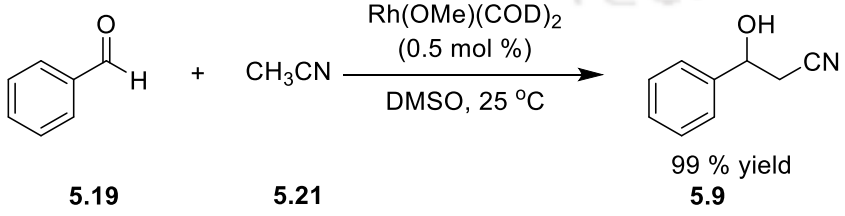

Scheme 5.12: Rh-catalyzed synthesis of *β*-hydroxy nitriles[33]

Among several methods, catalytic cyanomethylation using inexpensive, air and moisture stable Ni complexes have resulted in high yield and selectivity.[35-38] Ozerov group have developed an efficient catalytic system involving a cationic nickel complex supported by a diarylamido-based PNP pincer ligand (Scheme 5.13).[35] The cationic, base mediated Ni catalyzed reaction proceed through a Lewis acid mechanism. Analogous PNP pincer catalysts based on Pd and Pt were not as competent as Ni for the cyanomethylation reaction.[35]

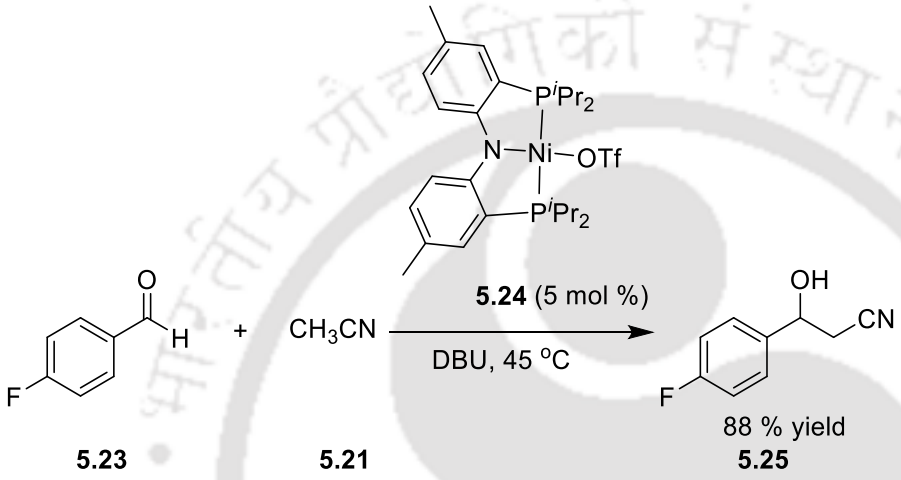

Scheme 5.13: Diarylamido-based PNP Ni catalyzed coupling of acetonitrile with aldehydes.[35]

In 2013, Guan and co-workers isolated an air and moisture stable cyanomethyl species (Ni-CH_2CN) that proved to be a highly active catalyst for the coupling between aldehyde and acetonitrile without an added base or additive (Scheme 5.14).[38] After the reaction with aldehyde, the $d\pi$-$p\pi$ repulsion between Ni and O orbital of the resulting Ni-alkoxide species facilitates the activation of acetonitrile followed by 1, 2 insertion of the aldehyde to generate Ni-C bond. Subsequent deprotonation of acetonitrile by nickel alkoxide would release the corresponding cyanomethylated product.[38] The main advantage of this reaction is that it proceeds without any added base. They also observed that the catalytic reaction is sensitive to steric effect of pincer ligand. Compare to ^{i}Pr substituent on the pincer ligand, bulky ^{t}Bu substituent gave poor result for the same reaction under similar condition.

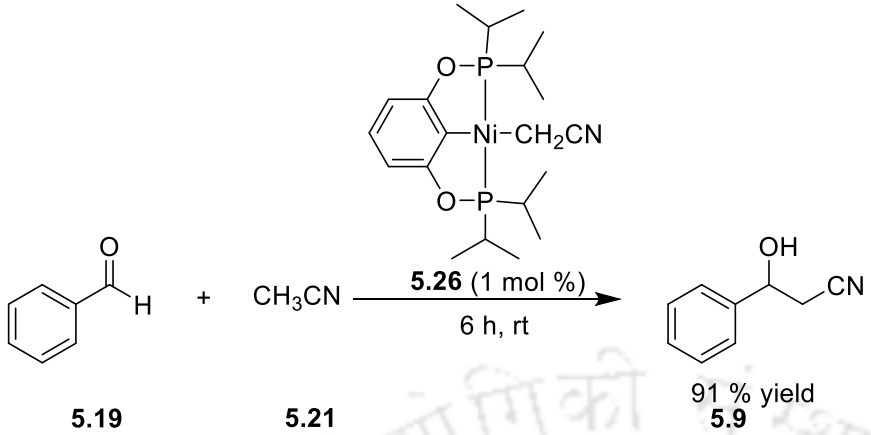

Scheme 5.14: Cyanomethylation of aldehydes catalyzed by a pincer-nickel catalyst under base-free conditions[38]

In 2015, the Miller group developed a new Ni catalyst supported by diethylamine or aza-crown-ether containing amino-phosphinate (NCOP) pincer ligands for catalyzing the insertion of benzaldehyde into a C-H bond of acetonitrile (Scheme 5.15).[36]

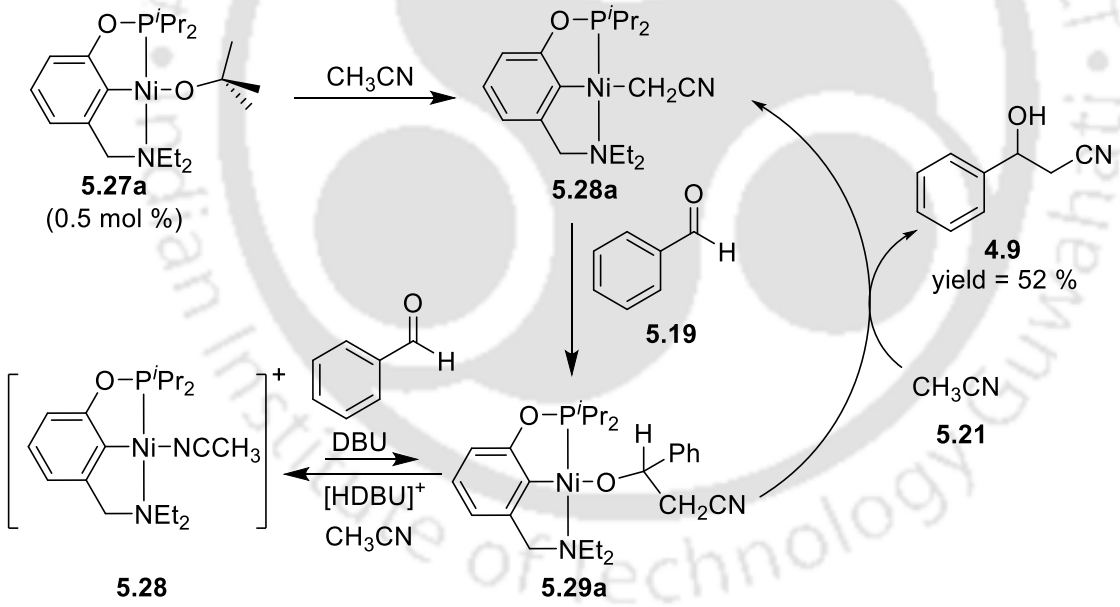

Scheme 5.15: Neutral and cationic pincer-nickel complexes reported for cyanomethylation reaction[36]

Miller proposed two distinct mechanistic pathways for pincer-Ni bound to a O^tBu^- group and for pincer-Ni bound to CH_3CN. The neutral (NCOP)Ni(O^tBu) complex can generate active catalyst without any added base, whereas the cationic complex $[(NCOP)Ni(NCCH_3)]^+$ slowly enter in the catalytic cycle in presence of base (Scheme 5.15). The area of Ni catalyzed cyanomethylation of

aldehydes offers exciting possibilities considering the mild conditions involved in the pincer-Ni catalyzed reactions in addition to the ready availability and inexpensive nature of Ni. In 2015, Ariafard *et al.* have computationally probed the mechanistic pathway of cyanomethylation of benzaldehyde with POCOP-Ni pincer catalyst **5.26** that was experimentally studied by chakraborty *et al*.[37,39] They have proposed that the exchange of alkoxide ligand with acetonitrile was highly energy demanding and presence of bulky pincer ligand prominently retards the exchange reaction which leads to catalyst deactivation. Similar observation was experimentally made by Guan.[38] While the effects of sterics around the Ni center is somewhat well-studied, the information on how electronics would affect the pincer-nickel catalyzed cyanomethylation is not available. The growing interest on pincer-Ni catalyzed cyanomethylation and the inherent subtle steric and electronic challenges that lead to significant changes in catalytic reactivity calls for systematic understanding on the operative mechanism. With this objective, a series of ten catalysts (**5.27b-5.27k**) (Figure 5. 2) were chosen with varying electronic demand and their cyanomethylation activity was computationally compared with the best catalyst (^{iPr2}POCCN^{Et2})NiO^{t}Bu (**5.27a**) that was reported by Miller. [36]

5.3 Results & discussions

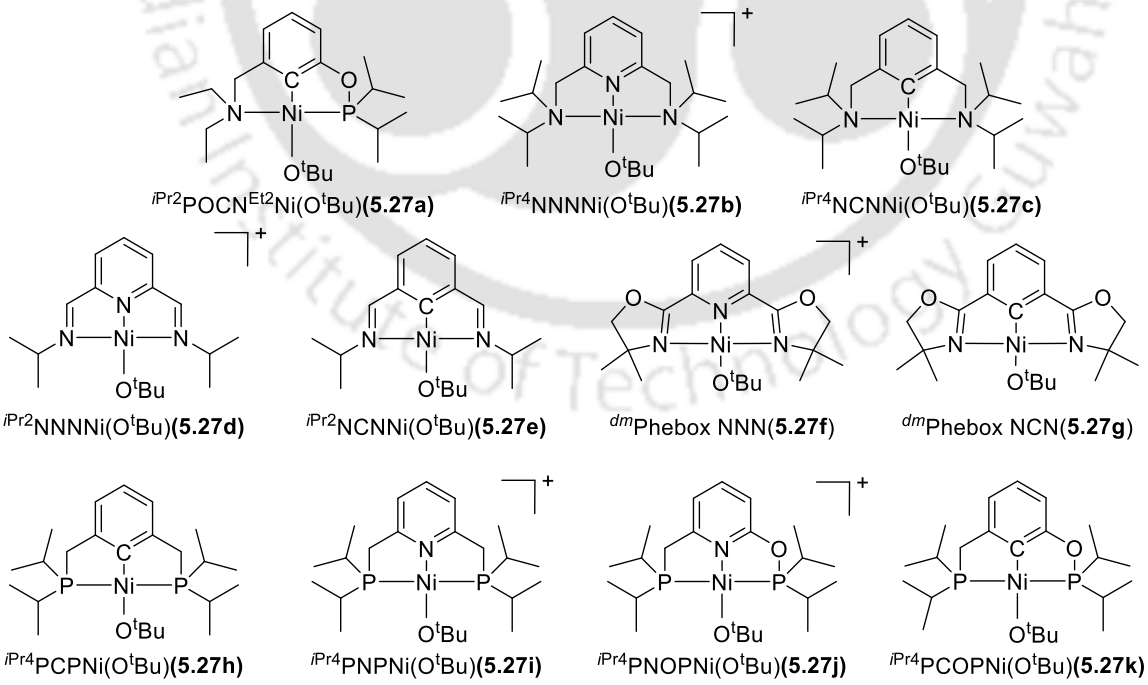

Figure 5.2: Pincer-Ni complexes (**5.27b-k**) screened for the DFT studies on cyanomethylation reaction.

In the current thesis, several pincer–nickel complexes have been tested by systematic variation of the ligating and linker atoms (Figure 5.2) on the active catalyst **5.27a** that was reported by Miller. The mechanism of cyanomethylation of benzaldehyde catalyzed by the Miller's system[36] is shown in Scheme 5.15. The catalyst precursor **5.27a** is readily generated by the treatment of corresponding nickel chloride with an equivalent of KO^{t}Bu. Complex **5.27a** upon reaction with acetonitrile leads to the formation of the catalytically active species **5.28a**. This is followed by the insertion of carbonyl group of benzaldehyde into the Ni-C bond giving rise to intermediate **5.29a**. Acetonitrile then reacts with **5.29a** to regenerate **5.27a** along with the formation of product **4.9** via an σ-bond metathesis reaction. One can anticipate similar catalytic intermediates in the corresponding cycles of **5.27b**-**5.27k**.

It was envisaged that a good start point for rational design would be to look at Ni complexes derived from ($^{i\text{Pr4}}$NNN)Ni(O^{t}Bu) **5.27b** and ($^{i\text{Pr4}}$NCN)Ni(O^{t}Bu) **5.27c**. Contrary to the mixed phosphine based systems, these amine systems not only offer greener reaction conditions but also are relatively easier to synthesize. With an objective to validate the choice of catalytic system and to compare it with the system ($^{i\text{Pr2}}$POCCN$^{\text{Et2}}$)NiCl already reported by the Miller group,[36] the energetics of the cyanomethylation reaction was computed using Gaussian 09 program package.[40] All the considered derivatives were fully optimized at room temperature (RT) by DFT (Density Functional Theory), using the hybrid three-parameter Becke-Lee-Yang-Parr (B3LYP) functional with 6-31G(d) basis set. All the obtained stationary points from frequency calculations characterize that they are minima on potential energy surface.

The barrier for the step **5.28→5.29**, starting with ($^{i\text{Pr4}}$NNN)Ni(CH$_2$CN) **5.28b** (TS **5.30b**; $\Delta G_{RT}^{\ddagger}$ = 68.85 kcal/mol) is higher than the corresponding barrier with either ($^{i\text{Pr2}}$POCN$^{\text{Et2}}$)Ni(CH$_2$CN) **5.28a** (TS **5.30a**; $\Delta G_{RT}^{\ddagger}$ = 37.61 kcal/mol) or ($^{i\text{Pr4}}$NNN)Ni(CH$_2$CN) **5.28c** (TS **5.30c**; $\Delta G_{RT}^{\ddagger}$ = 40.51 kcal/mol) (Figure 5.3a and Table 5.1). In comparison with **5.29a**, the barrier for the subsequent step **5.29→5.28**+**5.9** is unfavorable starting from both **5.29b** and **5.29c** by 24.82 kcal/mol and 10.98 kcal/mol respectively. The relatively higher barrier for the both the steps makes the catalysis by **5.28b** and **5.28c** unfavorable when compared to **5.28a**. The **5.28a-c** catalyzed reactions involves σ-bond metathesis of Ni–O in **5.29** with C–H of acetonitrile as the RDS. Repeating the calculations at a different level (BSI level, Figure 5.3b) and using a different method (PBEPBE, Figure 5.3c) provided a similar trend in energetics (Table 5.1)

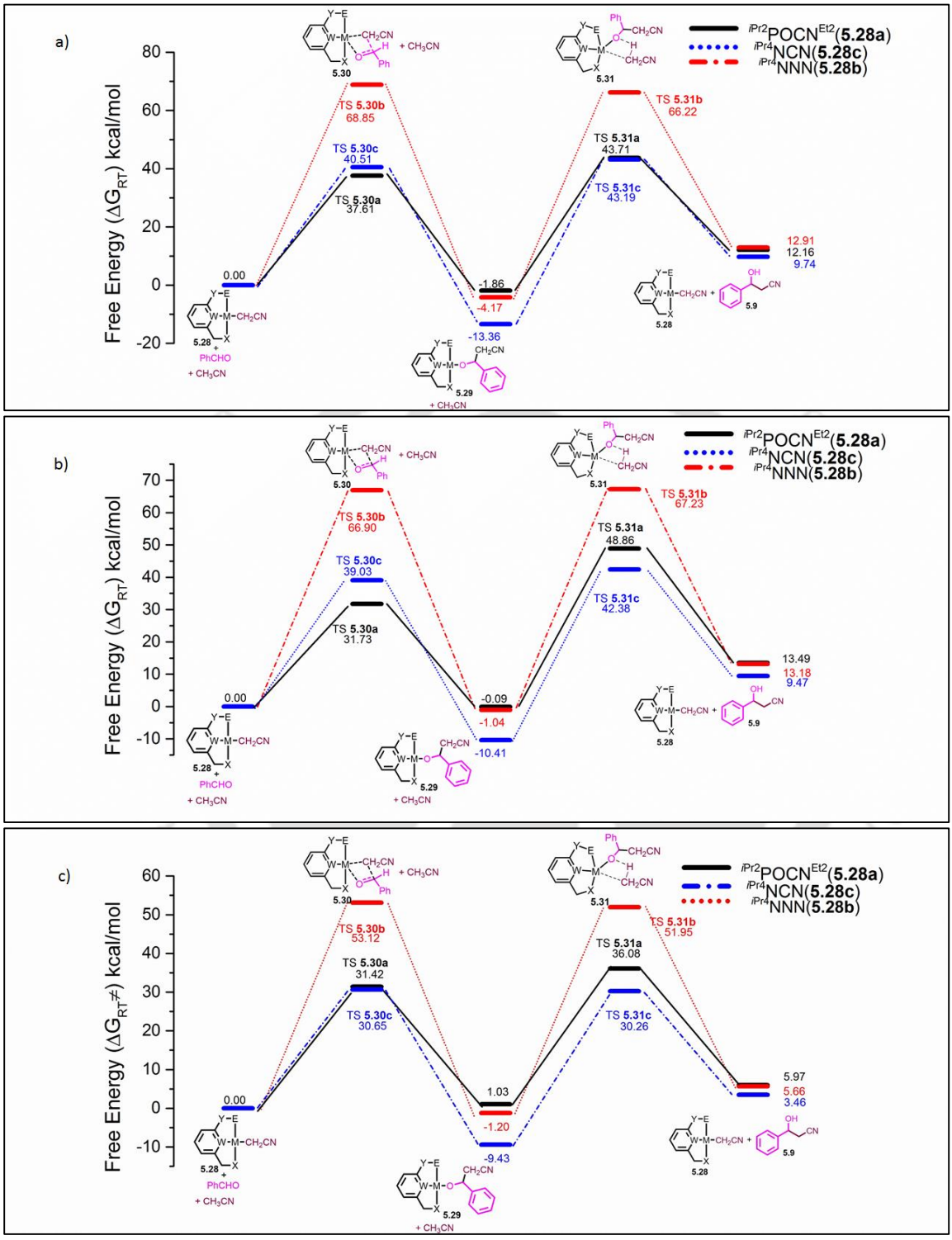

Figure 5.3: Relative free energy profile of **5.28a-c** catalyzed cyanomethylation determined from DFT studies carried out using (a) Hybrid three-parameter Becke-Lee-Yang-Parr (B3LYP) functional with 6-31G(d) basis set. (b) B3LYP/BSI level (BSI is defined here as a basis set combination of SDD basis set for Ni and 6-311G(d) for other atoms). (c) PBEPBE functional with the LANL2DZ basis set for Ni and 6-311G(d,p) for other atoms.

However, the barriers obtained with PBEPBE are much lower (Table 5.1) and more reasonable for a reaction occurring at room temperature. Apparently, the loss of reactivity of amine based pincers **5.28b**/**5.28c** in comparison with the mixed phosphine-amine system ($^{i\text{Pr}2}$POCN$^{\text{Et}2}$)Ni(O^{t}Bu) **5.28a** originates from the stronger σ-donating ability of amine ligands.

Table 5.1. Free energy barrier ($\Delta G_{RT}^{\ddagger}$) involved in the **5.28a**–**c** catalyzed cyanomethylation.

Entry	Catalyst	TS	$\Delta G_{RT}^{\ddagger}$ (kcal/mol)		
			B3LYP /6-31G(d)	B3LYP SDD for Ni, 6-311G(d) for all other atoms	PBEPBE LANL2DZ for Ni 6-311G(d,p) for all other atoms
1.	($^{i\text{Pr}2}$POCN$^{\text{Et}2}$)Ni(CH$_2$CN)	**5.30a**	37.61	31.73	31.42
	5.28a	**5.31a**	45.57	48.95	35.05
2.	($^{i\text{Pr}4}$NNN)Ni(CH$_2$CN)	**5.30b**	68.85	66.90	53.12
	5.28b	**5.31b**	70.39	68.27	53.15
3.	($^{i\text{Pr}4}$NCN)Ni(CH$_2$CN)	**5.30c**	40.51	39.03	30.65
	5.28c	**5.31c**	56.55	52.79	39.69

To reduce the amount of σ-donation, the energetics of the path involving imine based pincers ($^{i\text{Pr}2}$NNN)NiCl(CH$_2$CN) **5.28d** and ($^{i\text{Pr}2}$NCN)Ni(CH$_2$CN) **5.28e** were computed (Figure 5.4). At the B3LYP/6-31G(d) level of theory (Figure 5.4a), when compared to the catalysis by **5.28a**, the step **5.28→5.29** is more downhill with both **5.28d** and **5.28e** by 9.38 kcal/mol and 11.02 kcal/mol respectively (Figure 5.4a). Furthermore, the corresponding transition states (TSs) **5.30d** and **5.30e** are lower in energy by 10.15 kcal/mol and 13.67 kcal/mol (Figure 5.4a and Table 5.2). For the subsequent step **5.29→5.28**+**5.9**, while both **5.29a** and **5.29e** have similar barrier, the forward reaction with **5.29d** is kinetically unfavorable by 13.71 kcal/mol in comparison with **5.29a** (Figure 5.4a and Table 5.2). The trend in the relative free energy changes of the intermediates involved in the cyanomethylation reaction catalyzed by **5.28a**, **5.28d** and **5.28e** were very similar when the computations were repeated at a different level (Figure 5.4b) and with a different method (Figure 5.4c). Similar to **5.28a**, the reactions catalyzed by either **5.28d** or **5.28e** involve the σ-bond metathesis of Ni–O in **5.29** with C–H of acetonitrile is the RDS. Clearly, in comparison with **5.28a**, while the catalysis with **5.28d** is disfavored (entry 2, Table 5.2), the corresponding catalysis with **5.28e** is favorable (entry 3, Table 5.2). The complex ($^{i\text{Pr}2}$NCN)Ni(CH$_2$CN) **5.28e** based on phosphine–free and environmentally friendly ligands thus offers great promise.

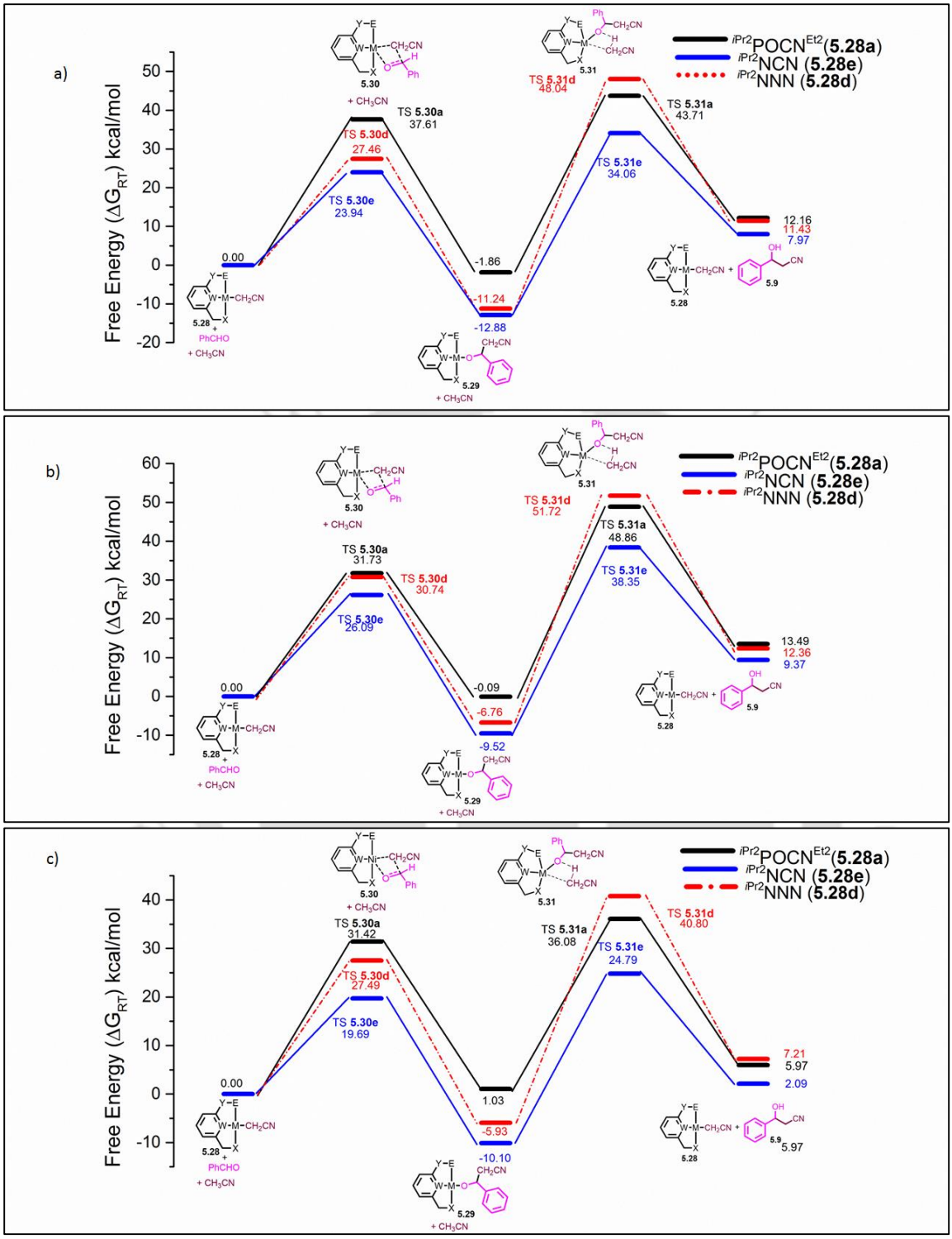

Figure 5.4: Relative free energy profile of **5.28a**, **5.28d**, **5.28e** catalyzed cyanomethylation determined from DFT studies carried out using (a) Hybrid three-parameter Becke-Lee-Yang-Parr (B3LYP) functional with 6-31G(d) basis set. (b) B3LYP/BSI level (BSI is defined here as a basis set combination of SDD basis set for Ni and 6-311G(d) for other atoms). (c) PBEPBE functional with the LANL2DZ basis set for Ni and 6-311G(d,p) for other atoms.

Table 5.2. Free energy barrier ($\Delta G_{RT}^{\ddagger}$) involved in the **5.28d**–**e** catalyzed cyanomethylation.

Entry	Catalyst	TS	$\Delta G_{RT}^{\ddagger}$ (kcal/mol)		
			B3LYP /6-31G(d)	B3LYP SDD for Ni, 6-311G(d) for all other atoms	PBEPBE LANL2DZ for Ni 6-311G(d,p) for all other atoms
1.	(^{iPr2}POCN^{Et2})Ni(CH$_2$CN)	**5.30a**	37.61	31.73	31.42
	5.28a	**5.31a**	45.57	48.95	35.05
2.	(^{iPr2}NNN)Ni(CH$_2$CN)	**5.30d**	27.46	30.74	27.49
	5.28d	**5.31d**	59.28	58.48	46.73
3.	(^{iPr2}NCN)Ni(CH$_2$CN)	**5.30e**	23.94	26.09	19.69
	5.28e	**5.31e**	46.94	47.87	34.89

The Phebox based NNN and NCN pincer complexes **5.28f** and **5.28g** demonstrated a very striking similarity in reactivity in comparison to their respective *bis*-imino pyridine based counterparts **5.28d** and **5.28e**. Accordingly, the σ-bond metathesis of Ni–O in **5.29** with C–H of acetonitrile is the RDS for catalytic cyanomethylation with both **5.28f** and **5.28g** (Figure 5.5, Table 5.3). Analogous to the *bis*-imino pyridine systems, the catalysis with Phebox based NNN **5.28f** is less favored (entry 2, Table 5.3) in comparison to the corresponding catalysis with Phebox based NCN **5.28g** (entry 3, Table 5.3). Interestingly, in the case of both *bis*-imino pyridine based and Phebox based complexes, the PBEPBE method provides the lowest barriers (Table 5.2 and 5.3) that are reasonable for a reaction that occurs at room temperature. Notably, the DFT studies indicate the possibility of Phebox based NCN pincer complex **5.28g** as another potential "green" catalyst (in addition to (^{iPr2}NCN)Ni(CH$_2$CN) **5.28e**) for cyanomethylation reactions.

Table 5.3. Free energy barrier ($\Delta G_{RT}^{\ddagger}$) involved in the **5.28d**–**g** catalyzed cyanomethylation.

Entry	Catalyst	TS	$\Delta G_{RT}^{\ddagger}$ (kcal/mol)		
			B3LYP /6-31G(d)	B3LYP SDD for Ni, 6-311G(d) for all other atoms	PBEPBE LANL2DZ for Ni 6-311G(d,p) for all other atoms
1.	(^{iPr2}POCN^{Et2})Ni(CH$_2$CN)	**5.30a**	37.61	31.73	31.42
	5.28a	**5.31a**	45.57	48.95	35.05
2.	(^{dm}Phebox NNN)Ni(CH$_2$CN)	**5.30f**	34.15	38.41	33.65
	5.28f	**5.31f**	58.1	59.09	43.55
3.	(^{dm}Phebox NCN)Ni(CH$_2$CN)	**5.30g**	30.38	28.48	23.07
	5.28g	**5.31g**	49.6	51.36	37.88

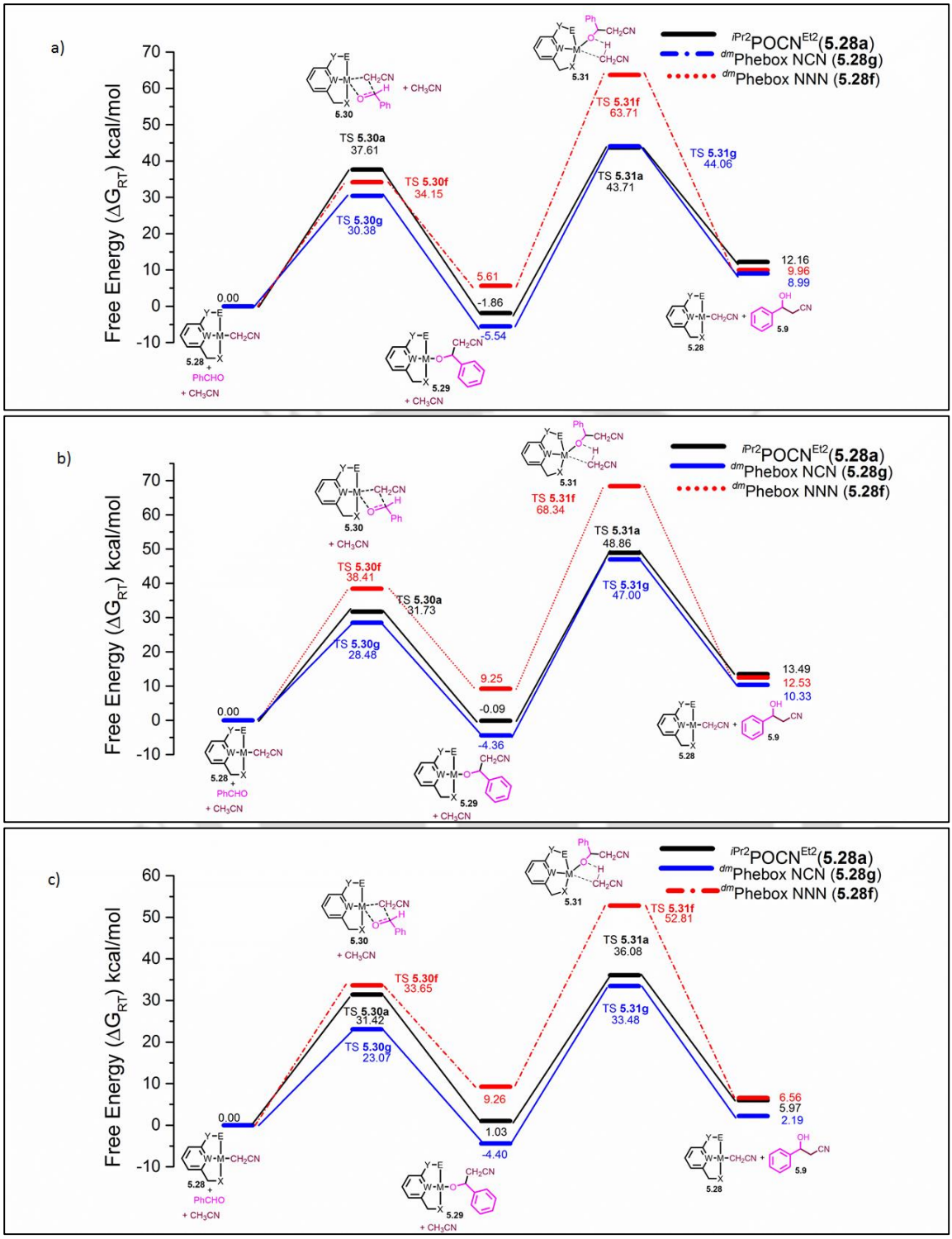

Figure 5.5: Relative free energy profile of **5.28a**, **5.28f**, **5.28g** catalyzed cyanomethylation determined from DFT studies carried out using (a) Hybrid three-parameter Becke-Lee-Yang-Parr (B3LYP) functional with 6-31G(d) basis set. (b) B3LYP/BSI level (BSI is defined here as a basis set combination of SDD basis set for Ni and 6-311G(d) for other atoms). (c) PBEPBE functional with the LANL2DZ basis set for Ni and 6-311G(d,p) for other atoms.

Thus, among the catalysts **5.28b-g** that were generated by the P for N substitutions in **5.28a**, the catalytic activity of complexes **5.28e** and **5.28g** were computed to be on par with that of the Millers system **5.28a**. It should be noted that with the best method (PBEPBE), the overall reaction (**5.28**+PhCHO+CH_3CN→**5.28**+**5.9**) catalyzed by **5.28e** and **5.28g** is uphill by 2.09 kcal/mol and 2.19 kcal/mol respectively that is in contrast to the Miller's system **5.28a** for which the cyanomethylation is uphill by 5.97 kcal/mol (Figure 5.4c, Figure 5.5c, Table 5.2 and Table 5.3). In comparison to **5.28a**, while the barrier for the insertion of benzaldehyde into the Ni–C bond in **5.28** was significantly lower for both **5.28e** and **5.28g** (Figure 5.4c, Figure 5.5c, Table 5.2 and Table 5.3), the barrier for the corresponding rate determining σ-bond metathesis was comparable.

The next task was to probe the effect of N for P substitutions. This was explored by employing Ni catalysts **5.28h** and **5.28i** based on the traditional PCP and PNP ligands. In comparison with the Miller's catalyst **5.28a**, the catalysts **5.28h** and **5.28i** had a slightly higher barrier (TS **5.30h**; $\Delta G_{RT}^{\ddagger}$ = 39.55 kcal/mol and TS **5.30i**; $\Delta G_{RT}^{\ddagger}$ = 43.51 kcal/mol respectively, Table 5.4) for the step **5.28** →**5.29** when B3LYP/6-31G(d) was used (Figure 5.6a and Table 5.4). The activation energy required for the subsequent step **5.29**→**5.28**+**5.9** was comparable for **5.28a** and **5.28h**. On the other hand, the corresponding barrier was about 19.19 kcal/mol higher when **5.28i** was used as catalyst. Among the different methods and basis sets employed, the calculations carried out with PBEPBE provided the lower barriers (Figure 5.6c). In all cases the σ-bond metathesis of Ni–O in **5.29** with C–H of acetonitrile is the RDS. The activity of **5.28a** and **5.28h** are comparable and the catalysis by **5.28i** is energetically unfavorable (Figure 5.6c and Table 5.4).

Table 5.4. Free energy barrier ($\Delta G_{RT}^{\ddagger}$) involved in the **5.28h**–**i** catalyzed cyanomethylation.

Entry	Catalyst	TS	$\Delta G_{RT}^{\ddagger}$ (kcal/mol)		
			B3LYP /6-31G(d)	B3LYP SDD for Ni, 6-311G(d) for all other atoms	PBEPBE LANL2DZ for Ni 6-311G(d,p) for all other atoms
1.	(^{iPr2}POCN^{Et2})Ni(CH_2CN)	**5.30a**	37.61	31.73	31.42
	5.28a	**5.31a**	45.57	48.95	35.05
2.	(^{iPr4}PCP)Ni(CH_2CN)	**5.30h**	39.55	33.52	35.15
	5.28h	**5.31h**	47.33	50.60	35.24
3.	(^{iPr4}PNP)Ni(CH_2CN)	**5.30i**	43.51	44.83	39.17
	5.28i	**5.31i**	64.76	62.90	48.15

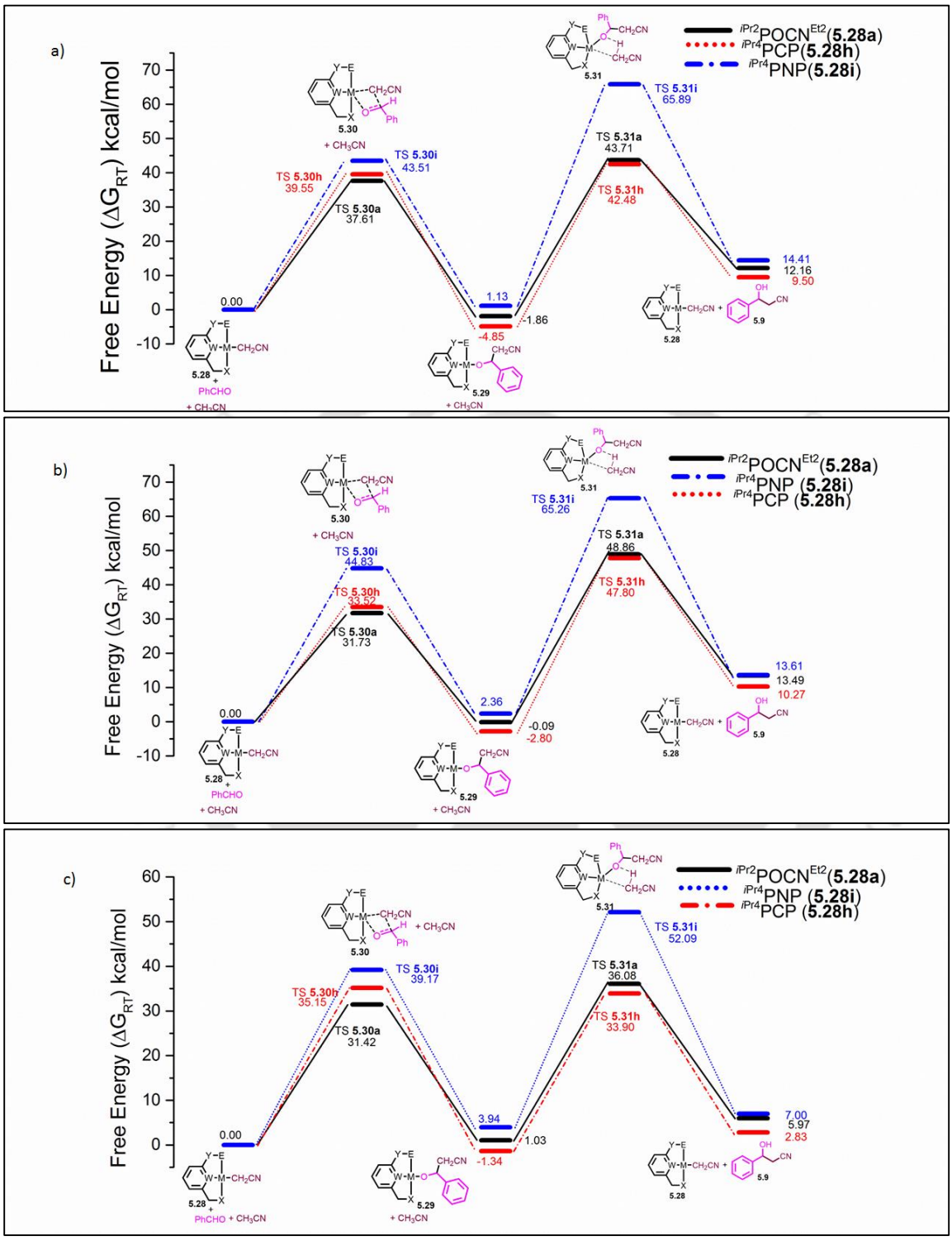

Figure 5.6: Relative free energy profile of **5.28a**, **5.28h**, **5.28i** catalyzed cyanomethylation determined from DFT studies carried out using (a) Hybrid three-parameter Becke-Lee-Yang-Parr (B3LYP) functional with 6-31G(d) basis set. (b) B3LYP/BSI level (BSI is defined here as a basis set combination of SDD basis set for Ni and 6-311G(d) for other atoms). (c) PBEPBE functional with the LANL2DZ basis set for Ni and 6-311G(d,p) for other atoms.

Subsequent studies involved the investigation on the effect of change in linker atoms. For this purpose the catalytic activity of asymmetric phosphine based complexes (^{iPr4}PNOP)Ni(CH_2CN) **5.28j** and (^{iPr4}PCOP)Ni(CH_2CN) **5.28k** were computed at the B3LYP/6-31G(d) level of theory (Figure 5.7a) and compared to **5.28a**. In stark contrast to **5.28a**, the first step **5.28 →5.29** is uphill for both **5.28j** and **5.28k** by 7.97 kcal/mol and 2.96 kcal/mol (Figure 5.7a). While the corresponding barriers **5.30** is lower by 2.89 kcal/mol upon starting from **5.28j**, the value is higher by 3.57 kcal/mol in the case of **5.28k** (Figure 5.7a, Table 5.5). For the next step **5.29→5.28**+**5.9**, the free energy of activation is higher for **5.28j** by 13.9 kcal/mol in comparison to **5.28a**. On the other hand, the barrier (**5.31**) is comparable with both **5.28a** and **5.28k**. Analogous to previous catalysts, the RDS involves the σ-bond metathesis of Ni–O in **5.29** with C–H of acetonitrile.

The barriers of the TSs calculated using the PBEPBE method (Figure 5.7c and Table 5.5) were lower than the corresponding barriers calculated using B3LYP. While **5.28j** the catalyzed reactions were clearly unfavourable due to both kinetic and thermodynamic reasons, the energetics involved in cyanomethylation catalyzed by **5.28k** were very much comparable to that of **5.28a**. Interestingly, in the PBEPBE method (Figure 5.7c and Table 5.5), while the σ-bond metathesis of Ni–O in **5.29** with C–H of acetonitrile is the RDS when **5.28a** is used (TS **5.31a**; $\Delta G_{RT}^{\ddagger}$ = 35.05 kcal/mol, Table 5.5), the insertion of benzaldehyde into the Ni–C bond is the RDS when **5.28k** is used as a catalyst with an very similar barrier (TS **5.30k**; $\Delta G_{RT}^{\ddagger}$ = 35.66 kcal/mol, Table 5.5).

Table 5.5. Free energy barrier ($\Delta G_{RT}^{\ddagger}$) involved in the **5.28j**–**k** catalyzed cyanomethylation.

Entry	Catalyst	TS	$\Delta G_{RT}^{\ddagger}$ (kcal/mol)		
			B3LYP /6-31G(d)	B3LYP SDD for Ni, 6-311G(d) for all other atoms	PBEPBE LANL2DZ for Ni 6-311G(d,p) for all other atoms
1.	(^{iPr2}POCN^{Et2})Ni(CH_2CN)	**5.30a**	37.61	31.73	31.42
	5.28a	**5.31a**	45.57	48.95	35.05
2.	(^{iPr4}PONP)Ni(CH_2CN)	**5.30j**	34.72	35.85	39.72
	5.28j	**5.31j**	59.47	56.34	43.01
3.	(^{iPr4}POCP)Ni(CH_2CN)	**5.30k**	41.18	40.37	35.66
	5.28k	**5.31k**	45.32	45.56	33.83

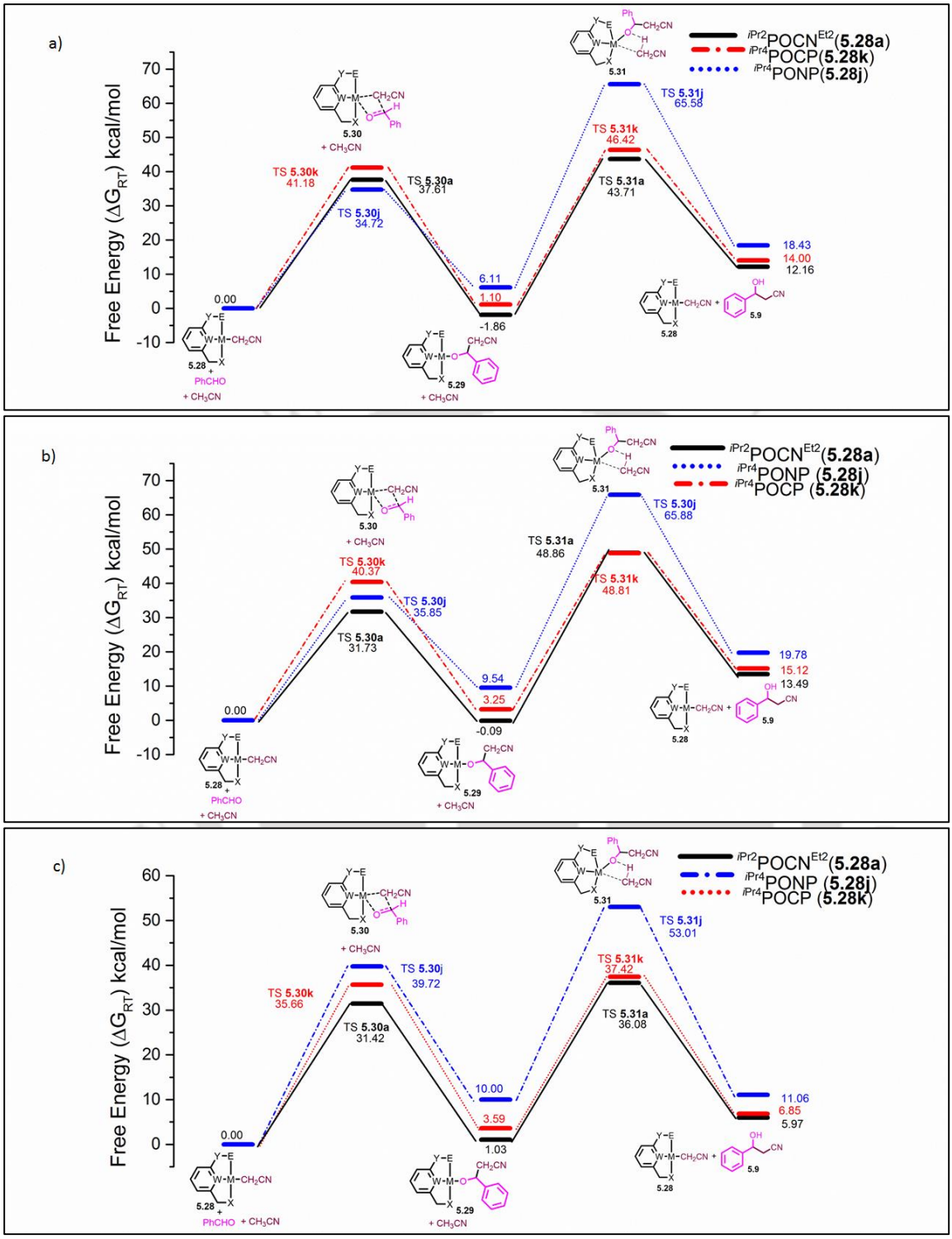

Figure 5.7: Relative free energy profile of **5.28a**, **5.28j**, **5.28k** catalyzed cyanomethylation determined from DFT studies carried out using (a) Hybrid three-parameter Becke-Lee-Yang-Parr (B3LYP) functional with 6-31G(d) basis set. (b) B3LYP/BSI level (BSI is defined here as a basis set combination of SDD basis set for Ni and 6-311G(d) for other atoms). (c) PBEPBE functional with the LANL2DZ basis set for Ni and 6-311G(d,p) for other atoms.

Upon comparison of the energetics of various species involved in the catalytic cycle, it is evident that complexes **5.27e**, **5.27g**, **5.27h** and **5.27k** that have strong *trans* influencing atom like C in the pincer central position assisted in reducing the barrier of rate determining σ-bond metathesis of Ni–O with C–H of acetonitrile (Table 5.1-5.5).[41, 42] On the other hand, complexes **5.27d**, **5.27f**, **5.27i** and **5.27j** having relatively weaker *trans* influencing N in the pincer central position had a significantly higher barrier for the σ-bond metathesis of Ni–O with C–H of acetonitrile (Table 5.1-5.5).

5.4 Conclusion

The PBEPBE method provides a reasonable energetics for the cyanomethylation reactions catalyzed by (^{iPr2}POCN^{Et2})Ni(CH$_2$CN) which is reported by Miller to experimentally accomplish this reaction at room temperature. Systematic computational studies have provided two potential leads into the possibility of a rational design of efficient phosphine free catalysts (^{iPr2}NCN)Ni(CH$_2$CN) and (^{dm}PheboxNCN)Ni(CH$_2$CN) based on *bis*(imino)pyridine and Phebox ligands. The catalytic efficiency is attributed to optimal σ-donating ability of imine based pincers that help not only in lowering the barrier but also in making the thermodynamics more favorable. The inability of amine based pincer nickel complexes (^{iPr4}NNN)Ni(CH$_2$CN) and (^{iPr4}NNN)Ni(CH$_2$CN) in catalyzing cyanomethylation reactions is attributed to their strong σ-donating nature. Among the phosphine based catalysts, while the efficiency of (^{iPr4}POCP)Ni(CH$_2$CN) and (^{iPr4}PCP)Ni(CH$_2$CN were comparable with (^{iPr2}POCN^{Et2})Ni(CH$_2$CN), the catalysis with (^{iPr4}PONP)Ni(CH$_2$CN) and (^{iPr4}PNP)Ni(CH$_2$CN) appears to be strongly disfavored. In most of the cases, the σ-bond metathesis of Ni–O with C–H of acetonitrile is the RDS. It is likely that having a strong *trans* influencing atom like C in the pincer central position will help in lowering barrier of the σ-bond metathesis of Ni–O with C–H of acetonitrile. On the other hand, a weaker *trans* influencing atom like N will not provide any such favorable assistance. Catalysts with improved efficiency can thus be computationally predicted by clever tuning of the ligand environment.

5.5 General procedure

Computational details

Gaussion-09 package (revision D.01) program package was used for all the calculation.[40] Geometries of all the considered molecules were fully optimized using generalized gradient corrected exchange and correlation functional PBEPBE.[43] The double-ζ quality LANL2DZ[44-46] basis set with effective core potential (ECP) was used for Ni atom and triple-ζ quality 6-311G basis set with polarization function (d,p) was used for all other atoms. Geometry optimization was performed at two more levels of DFT.One is the B3LYP/BSI level (BSI is defined here as a basis set combination of SDD[47] for nickel atoms and 6-311G(d) for all other atoms) and the other is B3LYP/6-31G(d,p) level[48]. The level of calculation was selected on the basis of a previous report on Ni complexes.[49] Frequency calculations at all three selected methods given above were performed to distinguish the obtained stationary points as minima structures or transition states on the potential energy surface. All the calculations were performed in the gas phase. ΔG values were estimated by using the sum of electronic and thermal free energies at room temperature.

Supporting information (containing Cartesian coordinates of the computed complexes) for chapter 5 is available as appendix 4 and can be found at https://drive.google.com/file/d/1ihehIqPowud_sMY2RUiE8h3ZbLGq1vos/view?usp=sharing

5.6 References

1. Kumar, A.; Ner, D. H.; Dike, S. Y., *Tetrahedron Lett.* **1991**, *32* (16), 1901-1904.
2. Boaz, N. W., *J. Org. Chem.* **1992**, *57* (15), 4289-4292.
3. Enders, D.; Haertwig, A.; Raabe, G.; Runsink, J., *Angew. Chem. Int. Ed. in English* **1996**, *35* (20), 2388-2390.
4. Zhang, S.-L.; Deng, Z.-Q., *Org. Biomol. Chem.* **2016**, *14* (30), 7282-7294.
5. Müller, H. M.; Seebach, D., *Angew. Chem. Int. Ed. in English* **1993**, *32* (4), 477-502.
6. Chauhan, S.; DiCosimo, R.; Fallon, R. D.; Gavagan, J. E.; Payne, M. S., Method for producing α-hydroxy acid from α-hydroxy nitrile using nitrilase. Google Patents: 2002.
7. Panke, S.; Held, M.; Wubbolts, M., *Curr. Opin. Biotech.* **2004**, *15* (4), 272-279.
8. Klieser, E.; Lehmann, E.; Heinrich, K., *Pharmacopsychiatry* **1995**, *28* (01), 14-19.
9. Brown, R. F.; Donohue, A. C.; Jackson, W. R.; McCarthy, T. D., *Tetrahedron* **1994**, *50* (48), 13739-13752.
10. Smith, J. G., *Synth.* **1984**, *08*, 629-656.

11. Yang, J.-C.; Shah, D. O.; Rao, N. U.; Freeman, W. A.; Soenovsky, G.; Gorenstein, D. G., *Tetrahedron* **1988**, *44* (20), 6305-6314.
12. Chini, M.; Crotti, P.; Favero, L.; Macchia, F., *Tetrahedron Lett.* **1991**, *32* (36), 4775-4778.
13. Ciaccio, J. A.; Stanescu, C.; Bontemps, J., *Tetrahedron Lett.* **1992**, *33* (11), 1431-1434.
14. Kamal, A.; Khanna, G. R.; Ramu, R., *Tetrahedron: Asymmetry* **2002**, *13* (18), 2039-2051.
15. Matsubara, S.; Onishi, H.; Utimoto, K., *Tetrahedron Lett.* **1990**, *31* (43), 6209-6212.
16. Saxena, I.; Deka, N.; Sarma, J. C.; Tsuboi, S., *Synth. Commun.* **2003**, *33* (23), 4185-4191.
17. Mullis, J. C.; Weber, W. P., *J. Org. Chem.* **1982**, *47* (15), 2873-2875.
18. Markandu, J.; Dondas, H. A.; Frederickson, M.; Grigg, R., *Tetrahedron* **1997**, *53* (38), 13165-13176.
19. Hayashi, M.; Tamura, M.; Oguni, N., *Synlett* **1992**, *8*, 663-664.
20. Sugita, K.; Ohta, A.; Onaka, M.; Izumi, Y., *Chem. Lett.* **1990**, *19* (3), 481-484.
21. Liotta, C. L.; Dabdoub, A.; Zalkow, L., *Tetrahedron Lett.* **1977**, *18* (13), 1117-1120.
22. Mitchell, D.; Koenig, T. M., *Tetrahedron Lett.* **1992**, *33* (23), 3281-3284.
23. Iranpoor, N.; Shekarriz, M., *Synth. Commun.* **1999**, *29* (13), 2249-2254.
24. Palomo, C.; Aizpurua, J. M.; López, M. C.; Lecea, B., *J. CHEM. SOC. PERKIN TRANS I* **1989**, 1693.
25. Suto, Y.; Kumagai, N.; Matsunaga, S.; Kanai, M.; Shibasaki, M., *Org. Lett.* **2003**, *5* (17), 3147-3150.
26. Kawano, Y.; Kaneko, N.; Mukaiyama, T., *Chem. Lett.* **2005**, *34* (11), 1508-1509.
27. Rao, V. B.; Kumar, K.; Singh, R. P., *Org. Biomol. Chem.* **2015**, *13* (38), 9755-9759.
28. Jinzaki, T.; Arakawa, M.; Kinoshita, H.; Ichikawa, J.; Miura, K., *Organic Lett.* **2013**, *15* (14), 3750-3753.
29. Matsukawa, S.; Kitazaki, E., *Tetrahedron Lett.* **2008**, *49* (18), 2982-2984.
30. Suto, Y.; Tsuji, R.; Kanai, M.; Shibasaki, M., *Org. Lett.* **2005**, *7* (17), 3757-3760.
31. Mayer, J. M., *Comment. Inorg. Chem.* **1988,** 8 (4), 125-135.
32. Kumagai, N.; Matsunaga, S.; Shibasaki, M., *J. Am. Chem. Soc.* **2004**, *126* (42), 13632-13633.
33. Goto, A.; Endo, K.; Ukai, Y.; Irle, S.; Saito, S., *Chem. Commun.* **2008**, *19*, 2212-2214.
34. Goto, A.; Naka, H.; Noyori, R.; Saito, S., *Chem. Asian. J.* **2011**, *6* (7), 1740-1743.
35. Fan, L.; Ozerov, O. V., *Chem. Commun.* **2005**, *35*, 4450-4452.
36. Smith, J. B.; Miller, A. J., *Organometallics* **2015**, *34* (19), 4669-4677.
37. Chakraborty, S.; Bhattacharya, P.; Dai, H.; Guan, H., *Acc. Chem. Res* **2015**, *48* (7), 1995-2003.
38. Chakraborty, S.; Patel, Y. J.; Krause, J. A.; Guan, H., *Angew. Chem. Int. Ed.* **2013**, *52* (29), 7523-7526.
39. Ariafard, A.; Ghari, H.; Khaledi, Y.; Hossein Bagi, A.; Wierenga, T. S.; Gardiner, M. G.; Canty, A. J., *ACS Catal.* **2015**, *6* (1), 60-68.
40. Frisch, M. J.; Trucks, G. W.; Schlegel, H. B.; Scuseria, G. E.; Robb, M. A.; Cheeseman, J. R.; Scalmani, G.; Barone, V.; Mennucci, B.; Petersson, G. A.; Nakatsuji, H.; Caricato, M.; Li, X.; Hratchian, H. P.; Izmaylov, A. F.; Bloino, J.; Zheng, G.; Sonnenberg, J. L.; Hada, M.; Ehara, M.; Toyota, K.; Fukuda, R.; Hasegawa, J.; Ishida, M.; Nakajima, T.; Honda, Y.; Kitao, O.; Nakai, H.; Vreven, T.; Montgomery, J. J. A.; Peralta, J. E. O., F.; Bearpark, M.; Heyd, J. J.; Brothers, E.; Kudin, K. N.; Staroverov, V. N.; Kobayashi, R.; Normand, J.; Raghavachari, K.; Rendell, A.; Burant, J. C.; Iyengar, S. S.; Tomasi, J.; Cossi, M.; Rega, N.; Millam, N. J.; Klene, M.; Knox, J. E.; Cross, J. B.; Bakken, V.; Adamo, C.; Jaramillo,

J.; Gomperts, R.; Stratmann, R. E.; Yazyev, O.; Austin, A. J.; Cammi, R.; Pomelli, C.; Ochterski, J. W.; Martin, R. L.; Morokuma, K.; Zakrzewski, V. G.; Voth, G. A.; Salvador, P.; Dannenberg, J. J.; Dapprich, S.; Daniels, A. D.; Farkas, Ö.; Foresman, J. B.; Ortiz, J. V.; Cioslowski, J.; Fox, D. J., Gaussian 09, Revision D.01, Gaussian, Inc., Wallingford, CT, 2009. See Supporting Information for the complete reference to Gaussian 09.

41. Wang, D. Y.; Choliy, Y.; Haibach, M. C.; Hartwig, J. F.; Krogh-Jespersen, K.; Goldman, A. S., *J. Am. Chem. Soc.* **2016**, *138* (1), 149-163.
42. Kumar, A.; Bhatti, T. M.; Goldman, A. S., *Chem. Rev.***2017**, *117* (19), 12357-12384.
43. Perdew, J. P.; Burke, K.; Ernzerhof, M., *Phys. Rev. Lett.* **1996**, *77* (18), 3865.
44. Wadt, W. R.; Hay, P. J., *J. Chem. Phy.* **1985**, *82* (1), 284-298.
45. Hay, P. J.; Wadt, W. R., *J. Chem. Phy.* **1985**, *82* (1), 299-310.
46. Hay, P. J.; Wadt, W. R., *J. Chem. Phy.* **1985**, *82* (1), 270-283.
47. Wang, C.; Wang, J.; Cai, Q.; Li, Z.; Zhao, H.-K.; Luo, R. *Comput. Theor. Chem.* 2**013**, *1024*, 34−44.
48. Curtiss, L. A.; Redfern, P. C.; Smith, B. J.; Radom, L., *J. Chem. Phy.* **1996**, *104* (13), 5148-5152.
49. Ghannam, J.; Al Assil, T.; Pankratz, T. C.; Lord, R. L.; Zeller, M.; Lee, W.-T. *Inorg. Chem.* **2018**, *57*, 8307−8316.

Summary &Outlook

भारतीय प्रौद्योगिकी संस्थान गुवाहाटी
Indian Institute of Technology Guwahati

Summary & Outlook

This thesis describes the application of NNN pincer complexes of ruthenium and nickel towards several catalytic reactions of great synthetic utility. All the probed reactions have been studied from a detailed mechanistic point of view.

Chapter 1 provides a brief introduction to organometallic complexes and how in recent times the pincer-metal chemistry has played a pivotal role in the success and applicability of organometallics. A historical perspective of the birth and growth of pincer-metal chemistry is provided with glimpses on their application in catalytic organic transformations. The chapter ends with a section that discusses on the scope of the current thesis.

Chapter 2 demonstrates the utility of NNN pincer-ruthenium complexes towards atom transfer radical addition (ATRA) or the Kharasch addition of polyhalogenated methanes to styrene in one of the first such reports for pincer-Ru. In particular, the complex (^{Cy2}NNN)$RuCl_2(PPh_3)$ [0.2 mM], catalyzed Kharasch addition of CCl_4 to styrene at 140 °C with very high turnovers (up to 5670) which is the highest reported hitherto either in the presence or in the absence of a co-catalyst radical initiator. The excellent activity of (^{Cy2}NNN)$RuCl_2(PPh_3)$ was attributed not only due to the easy generation of 5-coordinate 16-electron species but also owing to the ready oxidation of the Ru center. Detailed mechanistic studies point to the involvement of a benzylic radical in a path where the dissociation of PPh_3 is the rate determining step.

Chapter 3 discusses the application of NNN pincer-ruthenium complexes in catalytic transformation of glycerol to lactic acid. In a systematic mechanistic study, a rational explanation has been provided for the higher efficiency of pincer-ruthenium complexes based on less hindered 2,6-*bis*(benzimidazole-2-yl) pyridine ligands in comparison with the corresponding complexes based on *bis*(imino)pyridine. Interestingly the 2,6-*bis*(benzimidazole-2-yl) pyridine based pincer-ruthenium complexes had an optimal Ru-P bond energy that helped in easy generation of the catalytically active species. Furthermore, the favorable energetics that is attributable to lower steric encumbrance around the Ru center made the catalysis more conducive. On a synthetic front, the pincer-ruthenium complexes based on 2,6-*bis*(benzimidazole-2-yl) pyridine ligands were found to

be highly efficient in selectively (ca. 98%) transforming glycerol to lactic acid with up to 90 % yield and turnovers as high as 15,000.

Chapter 4 investigates the utility of phosphine-free pincer-nickel complexes in accomplishing catalytic *N*-alkylation of amines with alcohols in an attempt to move away from the use of catalysts derived from hazardous ligands and precious metals. The complex ($^{i\text{Pr}2}$NNN)NiCl$_2$(NCCH$_3$) was found to catalyze the *N*-alkylation with high yields (up to 90 %) and high TONs (up to 34000). under neat conditions. The labeling experiments provide evidence for the involvement of the benzylic C−H bond in the RDS with a k_{CHH}/k_{CHD} value of about 2.5. DFT studies are complementary and reveal that while *β*-hydride elimination is the RDS for alcohol dehydrogenation, the *N*-alkylated product can be formed either via alcoholysis that has imine insertion as the RDS or by hydrogenation with a rate-determining σ-bond metathesis. The corresponding resting states have been observed by HRMS (ESI) analysis. The studies have been extended to probe efficient dehydrogenative coupling (TONs up to 2550) of benzyl alcohols with benzene-1,2-diamines.

Chapter 5 dwells upon the efforts to computationally probe a phosphine-free pincer-nickel complex that would demonstrate an efficiency better than the reported phosphine based pincer-nickel complex ($^{i\text{Pr}2}$POCN$^{\text{Et}2}$)Ni(CH$_2$CN) for cyanomethylation reaction. For this purpose, the mechanism of cyanomethylation of benzaldehyde was studied quantum mechanically for a series of eleven pincer-nickel complexes. The energetics of various intermediates and transition states involved in the catalytic cycle for each catalyst was compared with the corresponding energetics of the Miller's catalyst ($^{i\text{Pr}2}$POCN$^{\text{Et}2}$)Ni(CH$_2$CN) that is reported to accomplish the cyanomethylation at room temperature. While pincer complexes ($^{i\text{Pr}4}$NNN)Ni(CH$_2$CN) and ($^{i\text{Pr}4}$NNN)Ni(CH$_2$CN) containing strong σ-donating amines were found to fare poorly, pincer-nickel complexes ($^{i\text{Pr}2}$NCN)Ni(CH$_2$CN) and (^{dm}PheboxNCN)Ni(CH$_2$CN) based on weaker σ-donating imines had energetics more favorable than the reported catalyst ($^{i\text{Pr}2}$POCN$^{\text{Et}2}$)Ni(CH$_2$CN). Furthermore, having strong *trans*-influencing C as the pincer central atom was found to be pivotal for lowering the kinetics of the reaction. On the other hand, presence

of a poor *trans*-influencing N proved to be detrimental on the overall energetics of the cyanomethylation reaction.

The ***current thesis*** has made an attempt to gain a systematic understanding on the mechanism of various pincer-Ru and pincer-Ni catalyzed organic transformations with an objective to help the rational design of future catalytic systems. It is gratifying to acknowledge that in recent years a significant amount of global research is focused on the versatile applications of pincer-chemistry. Not surprisingly, the current thesis also offers exciting leads which mainly includes but not limited to investigation of the asymmetric catalysis, development of sustainable and recyclable pincer-metal catalytic systems for synthesis of fuel, fine and value-added chemicals. These studies can be taken up for future investigations as they offer exciting possibilities.

~Curriculum Vitae~

Moumita Dutta
Ph.D. Student
Department of Chemistry
Indian Institute of Technology Guwahati
Guwahati – 781039, Assam, India
Email - moumita.dutta@iitg.ac.in
dutta.moumita.chem@gmail.com

Academic Qualifications

2009-2012 — **B.Sc.** Chemistry (Honours), Physics and Mathematics (Subsidiary)
Department of Chemistry
Visva-Bharati University, West Bengal, India
(Obtained *First class with Distinction*)

2012-2014 — **M.Sc.** in Chemistry
Department of Chemistry
Visva-Bharati University, West Bengal, India
(Obtained *First class with Distinction*)

2015-Present — **Ph.D.** in Organometallic Chemistry
Department of Chemistry
Indian Institute of Technology Guwahati,
Guwahati – 781039, Assam, India
Research Supervisor- Dr. Akshai Kumar A S
Thesis Tittle - Investigations on the Pincer-Ruthenium and Pincer-Nickel Catalyzed Organic Transformations

Area of Research

- Organometallics
- Catalysis
- Mechanistic Studies
- Computational Chemistry

List of Publications

1. Das, K.; **Dutta, M.**; Das, B.; Srivastava, H.; Kumar, A.,
   Highly Efficient Pincer-Ruthenium Catalysts for Kharasch Addition Reaction.
   Adv. Synth. Catal. **2019**, *361* (12), 2965-2980.

2. Arora, V.‖; **Dutta, M.**‖; Das, K.; Das, B.; Srivastava, H. K.; Kumar, A.,
   Solvent-Free N-Alkylation and Dehydrogenative Coupling Catalyzed by a Highly Active Pincer-Nickel Complex.
   Organometallics **2020**, *39*, 2162-2176. (‖Equal Contribution)

3. **Dutta, M.**; DAS, K.; Prathapa, S. J.; Srivastava, H. K.; Kumar, A.,
   Selective and High Yield Transformation of Glycerol to Lactic Acid Using NNN Pincer Ruthenium Catalysts.
   Chem. Commun. **2020**, *56*, 9886-9889.

4. Kumar, A.; **Dutta, M.**; Das, K.; Srivastava, H. K.
   A PROCESS FOR PRODUCTION OF LACTIC ACID FROM GLYCEROL,
   IN Patent Application; 202031021709, May 23, 2020; Indian Institute of Technology Guwahati.

5. **Dutta, M.**; Srivastava, H. K.; Kumar, A.,
   Computational Studies on Efficient Phosphine-Free Pincer-Nickel Catalytic Systems for Cyanomethylation of Benzaldehyde.
   Manuscript under preparation

6. **Dutta, M.**; Kumar, A.,
   Studies on the Unusual Chemistry of Diamine based Pincer-Nickel Complexes and their Catalytic Activity towards *N*-alkylation of Amines.
   Manuscript under preparation

Conferences Attended (2015-2020)

1. **Dutta, M.**; Kumar, Y.; Das, K.; Kumar, A*. Poster presentation in In-House Symposium CHEMCONVENE 2017 held at IIT Guwahati on **July 2017**.
   "Cyanomethylation of Aldehydes Catalyzed by Pincer-Based Nickel Complexes: An Experimental and Computational Study."

2. **Dutta, M.**; Das, K.; Srivastava, H. K.*; Kumar, A*. Poster presentation during FICS-2018, IIT Guwahati, **Dec 2018.**
   "Cyanomethylation of Aldehydes Catalyzed by Pincer-Based Nickel Complexes: An Experimental and Computational Study"

3. **Dutta, M.**; Das, K.; Srivastava, H. K.*; Kumar, A*. Poster presentation during Research Conclave-2019, IIT Guwahati, **March 2019**.
   "Cyanomethylation of Aldehydes Catalyzed by Pincer-Based Nickel Complexes: An Experimental and Computational Study".

4. **Dutta, M.**; Das, K.; Das, B.; Srivastava, H. K.*; Kumar, A*. Poster presentation during19th National Workshop on Catalysis-2019, IIT Delhi, **May 2019**.
   "Highly Efficient Pincer Ruthenium Catalysts for Atom Transfer Radical Additions".

5. Arora, V.; **Dutta, M.**; Das, K.; Das, B.; Srivastava, H. K.*; Kumar, A *. Poster presentation during Modern Trends in Inorganic Chemistry MTIC-XVIII, IIT Guwahati, **December 2019**.
   "Highly Efficient Pincer-Nickel Complex for Solvent-Free Catalytic N-Alkylation and Catalytic Dehydrogenative Coupling Reaction".